Seismic Retrofit of Squat Reinforced Concrete Shear Walls Using Shape Memory Alloys

By

Wilmar Leonardo Cortés Puentes

Thesis submitted to the
Faculty of Graduate and Postdoctoral Studies
in partial fulfillment of the requirements for the degree of
Doctor of Philosophy
in Civil Engineering *



uOttawa

Department of Civil Engineering
Faculty of Engineering
University of Ottawa

* The Doctor of Philosophy in Civil Engineering is a Joint Program with Carleton University, administrated by the Ottawa-Carleton Institute for Civil Engineering

© Wilmar Leonardo Cortés Puentes, Ottawa, Canada, 2017

Abstract

Squat reinforced concrete shear walls are stiff structural elements incorporated in buildings and other structures and are capable of resisting large seismic demands. However, when not properly designed, they are prone to shear-related brittle failure. To improve the seismic behaviour of these structural elements, a retrofitting bracing system incorporating superelastic Shape Memory Alloys (SMAs) was developed. Superelastic Shape Memory Alloys (SMAs) are smart materials with the ability to sustain and recover large pseudo-plastic deformations while dissipating energy. The SMA bracing system consists of tension-only SMA links coupled with rigid steel elements. The SMA links were designed to sustain and recover the elongation experienced by the bracing system, while the steel elements were designed to sustain negligible elastic elongations.

The SMA bracing system was installed on third-scale, 2000 mm × 2000 mm, shear walls, which were tested to failure under incremental reverse cyclic loading. The experimental results demonstrated that the tension-only SMA braces improve the seismic response of squat reinforced concrete walls. The retrofitted walls experienced higher strength, greater energy dissipation, and less permanent deformation. The re-centering properties of the SMA contributed to the reduction of pinching in the hysteretic response due mainly to the clamping action of the SMA bracings while recovering their original length. The walls were numerically simulated with the nonlinear finite element program VecTor2. The numerical simulations accurately captured the hysteretic response of both the original and the retrofitted walls. A parametric study was conducted to assess the effect of axial loading and size of the SMA braces.

Preface

This thesis is an original intellectual product of the author, W. Leonardo Cortés Puentes.

The thesis is written in an article-based format. It contains three article-based chapters that report and discuss the main findings of the doctoral research of the author. Chapter 3 corresponds to an article published in the journal Engineering Structures and Chapters 4 and 5 correspond to unpublished articles. The articles were written by the author, and reviewed and edited by Dr. Dan Palermo. The author recognizes the contributions of Dr. Dan Palermo.

The hysteretic constitutive model used in Chapters 3 and 5 for modelling SMA were developed by Dr. Alaa Abdulridha and Dr. Dan Palermo and implemented into program VecTor2 by Dr. Frank J. Vecchio.

Acknowledgements

The author would like to express his sincerest gratitude to Professor Dan Palermo for his support, guidance, patience, and encouragement throughout this research project. Professor Palermo provided critical evaluations of the research work that had a great impact on this thesis.

Special thanks are due to the technical and administrative staff of the Civil Engineering Department at the University of Ottawa. Thanks to Muslim Majeed for assisting in the setup for testing the walls, for installing the data acquisition system, and for operating the testing equipment; to Gamal Elnabelsya for providing valuable advice and helping to build the walls; to John Perrins and the staff of the machine shop for fabricating the SMA braces; and to the administrative officers and assistants for helping to prepare the paperwork.

The author gratefully acknowledges the financial support provided by the University of Ottawa, the Ontario Graduate Scholarship Program, the Canadian Seismic Research Network, Public Works and Government Services Canada, and the Colombian Administrative Department of Science, Technology and Innovation. Without the financial contribution from these institutions, the realization of this research work would not have been possible.

The author thankfully appreciates the collaboration of many graduate and undergraduate students. Special thanks to Alaa Abdulridha who was very enthusiastic in discussing and providing great advice for my research project. Thanks to Zaid, Amir, Mohammed, Mehdi, Jin, Greg, Rodrigo, Atylla, and Willian for contributing to the construction of the walls and preparing the setup for testing. Thanks to Pedro for assisting in the numerical analysis of the shear walls. Also,

thanks to all the friends in the faculty who shared a cup of coffee or a few minutes to chat about research and other interesting topics.

Profound thanks are extended to my family, especially to my wife, Yomara, and my son, Sebastián, whose love, support, and patience have inspired me to complete this academic journey. Thanks to my mother, my sisters, my grandmother, and my parents-in-law who have always believed in me. To all of them, I dedicate this work.

Table of Contents

Abstract ..... **ii**

Preface ..... **iii**

Acknowledgements ..... **iv**

Table of Contents ..... **vi**

List of Figures ..... **xi**

List of Tables ..... **xxvii**

Chapter 1 General Introduction **1**

1.1 Background 1

1.2 Novelty of Research 3

1.3 Research Significance 4

1.4 Research Methodology 5

1.5 Research Objectives 6

1.6 Thesis Layout 7

1.7 References 9

Chapter 2 Literature Review **10**

2.1 Introduction 10

2.2 Squat Shear Walls 10

2.3 Seismic Retrofit of Shear Walls 11

2.3.1 Injection of Cracks and Concrete Replacement 11

2.3.2 Replacement and Addition of Reinforcement 13

2.3.3 Attachment of External Steel Plates 16

2.3.4 Bonding of External Fibre Reinforced Polymers 18

2.3.5 Structural Weakening 25
2.4 Application of Shape Memory Alloys 26
2.4.1 Properties of NiTi Superelastic SMAs 27
2.4.2 Reinforcing of Concrete Structures 33
2.4.3 External Bracing of Concrete Structures 43
2.5 Summary 45
2.6 References 47

Chapter 3 SMA Tension Brace for Retrofitting Concrete Shear Walls 55
3.1 Introduction 56
3.2 Research Significance 59
3.3 Conceptual Design of SMA Retrofitting System 59
3.4 Design of Full-Scale SMA Retrofitting System 60
3.5 Testing of Third-Scale Retrofitting Systems 63
3.5.1 Properties of SMA and Steel Braces 65
3.5.2 Test Setup 68
3.5.3 Force-Elongation Response 70
3.6 Discussion of Results 73
3.6.1 Stress-Strain Response 73
3.6.2 Stiffness 74
3.6.3 Energy Dissipation 75
3.6.4 Residual Deformations 76
3.7 Numerical Analysis 77
3.7.1 Finite Element Modelling 77
3.7.2 Finite Element Analysis Results 79
3.8 Conclusions 89
3.9 Acknowledgments 91
3.10 References 91

Chapter 4 Seismic Retrofit of Concrete Shear Walls with SMA Tension Braces 95
4.1 Introduction 96
4.2 Research Significance 98
4.3 Experimental Program 99

4.4 Experimental Results 108
4.4.1 Response of Walls SQ1 and SQ1S 108
4.4.2 Response of Walls SQ2 and SQ2S 112
4.4.3 Response of SMA Braces 116
4.5 Discussion of Results 120
4.5.1 Damage and Failure Mechanism 121
4.5.2 Strength 121
4.5.3 Stiffness and Drift Capacity 123
4.5.4 Energy Dissipation 125
4.5.5 Displacement Recovery 126
4.5.6 Shear Distortion 127
4.6 Conclusions 130
4.7 Acknowledgments 132
4.8 References 132

Chapter 5 Modelling of Concrete Shear Walls Retrofitted with SMA Tension Braces 139
5.1 Introduction 140
5.2 Research Significance 142
5.3 Shear Walls 142
5.3.1 General Description 142
5.3.2 SMA Tension-Only Braces 143
5.3.3 Material Properties 145
5.3.4 Loading of Walls 147
5.4 Finite Element Modelling 148
5.4.1 Modelling of Concrete 148
5.4.2 Modelling of Reinforcing Steel 149
5.4.3 Modelling of SMA Braces 150
5.4.4 Finite Element Mesh 152
5.5 Numerical Analysis of Retrofitted Walls 160
5.5.1 Wall SQ1S 160
5.5.2 Wall SQ1aS 163
5.5.3 Wall SQ2S 165

5.6 Parametric Study 167
5.6.1 Effect of Axial Loading 168
5.6.2 Effect of Size of SMA Links 170
5.7 Conclusions 171
5.8 Acknowledgments 173
5.9 References 173

Chapter 6 General Conclusions 178
6.1 Overview 178
6.2 SMA Tension Brace for Retrofitting Concrete Shear Walls 178
6.3 Seismic Retrofit of Concrete Shear Walls with SMA Tension Braces 180
6.4 Modelling of Concrete Shear Walls Retrofitted with SMA Tension Braces 181
6.5 Final Remarks 182

Chapter 7 Future Work 183

Appendix A Development of an SMA Retrofitting System: Supplementary Material 186
A.1 Seismic Requirements 186
A.1.1 Design of the Original Wall 186
A.1.2 Seismic Assessment of the Original Wall 187
A.2 Design of the SMA Retrofit 189
A.2.1 Seismic Assessment of the Retrofitted Wall 189
A.3 SMA Braces 192
A.4 References 193

Appendix B Experimental Program: Supplementary Material 194
B.1 Construction of Shear Walls 194
B.1.1 Foundation Blocks 194
B.1.2 Shear Walls 197
B.1.3 SMA Bracing System 198
B.2 Material Properties 200
B.2.1 Concrete 200
B.2.2 Reinforcing Steel 201
B.2.3 Nickel-Titanium SMA 203

B.3 Instrumentation 203
B.3.1 Displacement Measurements 204
B.3.2 Strain Measurements 206
B.3.3 Force Measurements 208
B.4 Data Acquisition System 208
B.5 Loading Protocol 210
B.6 Test Results 211
B.6.1 Cracking 211
B.6.2 Displacement Response 227
B.6.3 Internal Reinforcement Strains 236
B.7 References 254

Appendix C Modelling of Shear Walls: Supplementary Material 255
C.1 Modelling of Prototype Walls 255
C.2 Calculated Response 257
C.3 Numerical Analysis of Third-Scale Walls 259
C.3.1 Sensitivity Study 259
C.3.2 Parametric Study 262
C.4 References 274

List of Figures

Figure 1-1 Stress-strain response of superelastic NiTi SMA.....2

Figure 1-2 Retrofit scheme with SMA braces.....4

Figure 2-1 Load-displacement response of shear walls (Lefas and Kotsovos 1990): (a) original Wall SW33; and (b) repaired Wall SW33R 12

Figure 2-2 Load-displacement response of flanged squat shear walls: (a) original Wall DP1 (Palermo and Vecchio 2002); and (b) repaired Walls DP1R and Wall DP2R (Vecchio et al. 2002).....13

Figure 2-3 Addition of diagonal reinforcement and replacement of concrete (Fiorato et al. 1983): (a) repair of Wall B11R; and (b) response of repaired Wall B11R.....14

Figure 2-4 Typical repaired pier wall (Haroun et al. 2000).....15

Figure 2-5 Response of repaired pier walls (Haroun et al. 2000): (a) original pier wall LU; and (b) repaired pier wall LU 16

Figure 2-6 Selective techniques for retrofitting shear walls (Elnashai and Pinho 1998): (a) strength-only; (b) stiffness-only; and (c) ductility-only.....17

Figure 2-7 Load-displacement response of squat shear walls with steel plates (Taghdi et al. 2000a): (a) original wall; and (b) retrofitted wall.....18

Figure 2-8 Retrofitting of shear wall with carbon fibre sheets (Lombard et al. 2000) 19

Figure 2-9 Response of shear walls retrofitted with carbon FRP (Lombard et al. 2000): (a) original wall; and (b) retrofitted wall.....20

Figure 2-10 Repair and retrofitting of shear walls with FRP (Antoniades et al. 2005) 21

Figure 2-11 Response of shear wall with height-to-length ratio of 1.5 (Antoniades et al. 2005): (a) original wall; and (b) retrofitted wall.....21

Figure 2-12 Retrofitting of squat shear walls with carbon FRP sheets (Khalil and Ghobarah 2005) 22

Figure 2-13 Force-displacement response of shear walls (Khalil and Ghobarah 2005): (a) control wall; and (b) retrofitted wall.....22

Figure 2-14 Squat shear walls retrofitted with FRP bands (Kobayashi 2005): (a) damage; and (b) force-displacement response of original (W03N) and retrofitted (W02R) walls.....23

Figure 2-15 Retrofitted squat wall with bi-diagonal carbon FRP strips (Hsiao et al. 2008): (a) tested wall; and (b) load-displacement response.....24

Figure 2-16 Retrofitted wall panel with diagonal and horizontal carbon FRP strips (El-Sokkary and Galal 2013): (a) tested wall; and (b) load-displacement response.....25

Figure 2-17 Structural weakening (Ireland et al. 2007): (a) horizontal cut; (b) vertical cut; and (c) response of retrofitted wall with horizontal cut 26

Figure 2-18 Stress-strain-temperature response of SMAs (DesRoches et al. 2004) 26

Figure 2-19 Typical stress-strain response of Nickel-Titanium SMA bars (ASTM 2014).....27

Figure 2-20 Stress-strain responses of NiTi wires tested at loading frequency of 0.1 Hz, 25ºC (solid line) and 35 ºC (dotted line), and different

strain amplitudes (Piedboeuf et al. 1998): (a) 2% strain; (b) 3% strain; and (c) 4% strain 28

Figure 2-21 Stress-strain responses of NiTi wires tested at 25ºC, 4% strain, and different loading frequencies (Piedboeuf et al. 1998): (a) 0.01 Hz; (b) 0.1 Hz; (c) 1 Hz; and (d) 10 Hz 29

Figure 2-22 Effect of ambient temperature on the hysteretic properties of superelastic NiTi wires (Dolce and Cardone 2001a): (a) energy loss per unit weight (hysteretic energy dissipation); and (b) equivalent damping 30

Figure 2-23 Stress-strain response of superelastic SMAs (DesRoches et al. 2004): (a) 1.8 mm-diameter wires; and (b) 25.4 mm-diameter bars 30

Figure 2-24 Energy dissipation and accumulated residual strain in repeated cycling loading (Nemat-Nasser and Guo 2006) 31

Figure 2-25 Stress-strain response of superelastic NiTi at 10^{-3}/s strain rate and different temperatures (Nemat-Nasser and Guo 2006) 32

Figure 2-26 Stress-strain response of superelastic NiTi bars (McCormick et al. 2007): (a) 19.1-mm diameter; and (b) 12.7-mm diameter 33

Figure 2-27 Column reinforced with NiTi SMA (Saiidi and Wang 2006): (a) column details; and (b) reverse cyclic response of SMA-reinforced column 34

Figure 2-28 Model for SMA (Tazarv and Saiidi 2015) 34

Figure 2-29 Beam reinforced with NiTi SMA (Saiidi et al. 2007) 35

Figure 2-30 Load-displacement response of beams (Saiidi et al. 2007) 36

Figure 2-31 Concrete beams reinforced with NiTi SMA (Abdulridha et al. 2013) 37

Figure 2-32 Response of SMA-reinforced (B6-NR) and steel-reinforced (B3-SR) beams (Abdulridha et al. 2013) 37

Figure 2-33 Simulation of SMA-reinforced beams (Abdulridha et al. 2013): (a) SMA tri-linear model with plastic offset; and (b) experimental and numerical responses of SMA-reinforced beam....38

Figure 2-34 Beam-column joint reinforced with superelastic SMA (Youssef et al. 2008): (a) reinforcement detail; and (b) SMA-steel coupling....39

Figure 2-35 Response of beam-column joints (Youssef et al. 2008): (a) steel reinforcement; and (b) SMA-steel reinforcement....39

Figure 2-36 Model for superelastic shape memory alloys (Auricchio and Sacco 1997)....40

Figure 2-37 Response of beam-column joints (Nehdi et al. 2010): (a) envelope of load-drift response; and (b) energy dissipation....41

Figure 2-38 Shear walls reinforced with hybrid SMA-steel reinforcement (Abdulridha and Palermo 2014): (a) detail of hybrid SMA-steel reinforcement; and (b) response of SMA-reinforced wall....42

Figure 2-39 Model for composite SMA-FRP bars (Zafar and Andrawes 2012)....43

Figure 2-40 SMA brace (Dolce et al. 2000): (a) braces installed in reinforced concrete frame; and (b) detail of re-centering device with superelastic NiTi wires....44

Figure 2-41 Shear wall reinforced with external SMA bars (Effendy et al. 2006): (a) damage of wall; and (b) load-displacement response of wall reinforced with superelastic SMA....45

Figure 3-1 Typical stress-strain response of superelastic nickel-titanium SMA....57

Figure 3-2 Retrofit with SMA: (a) retrofit scheme with SMA braces; and (b) expected response of SMA-retrofitted wall compared to original and steel-retrofitted walls.....59

Figure 3-3 Plan view of prototype building....60

Figure 3-4 Seismic assessment of retrofitted wall with SMA bracing....62

Figure 3-5 1/3rd-Scale shear wall SQ1, internal reinforcement layout 64

Figure 3-6 External retrofitting of Wall SQ1 with SMA and steel braces 65

Figure 3-7 Tension-only SMA link.....66

Figure 3-8 End of SMA links: (a) fixed end; and (b) free end.....67

Figure 3-9 Stress-strain responses of SMA rod and steel reinforcing bar.....68

Figure 3-10 Testing of bracing system 69

Figure 3-11 Instrumentation on SMA/steel braces 69

Figure 3-12 Force-elongation response of Brace SMA1 71

Figure 3-13 Force-elongation response of Brace SMA2 71

Figure 3-14 Typical force-elongation response of steel braces.....73

Figure 3-15 Envelope of stress-strain response of SMA and steel braces 74

Figure 3-16 Secant stiffness of braces 75

Figure 3-17 Cumulative energy dissipation of braces.....76

Figure 3-18 Finite element models: (a) control wall; and (b) retrofitted walls.....78

Figure 3-19 Predicted response of Wall SQ1.....80

Figure 3-20 Predicted response of Wall SQ1S.....80

Figure 3-21 Predicted response of Wall SQ1R 81

Figure 3-22 Envelope of force-displacement response of walls.....81

Figure 3-23 Comparison of SMA brace model with experimental response.....82

Figure 3-24 Comparison of steel brace model with experimental response 83

Figure 3-25 Cycle to 30 mm displacement: (a) SQ1; (b) SQ1S; and (c) SQ1R 84

Figure 3-26 Damage of shear walls at 30 mm: (a) Wall SQ1; (b) Wall SQ1S; and (c) Wall SQ1R 85

Figure 3-27 Cumulative energy dissipation of walls....87

Figure 3-28 Residual displacement of walls....88

Figure 3-29 Displacement recovery of walls....89

Figure 4-1 Detail of Walls SQ1 and SQ1S....99

Figure 4-2 Detail of Walls SQ2 and SQ2S....100

Figure 4-3 External retrofit of Walls SQ1S and SQ2S 101

Figure 4-4 SMA link 103

Figure 4-5 Rigid steel element....103

Figure 4-6 Connection of SMA link to rigid steel element....103

Figure 4-7 Stress-strain of 12.7-mm SMA rod 104

Figure 4-8 Force-elongation response of SMA brace....106

Figure 4-9 Test setup....107

Figure 4-10 Lateral load-displacement response of Wall SQ1....109

Figure 4-11 Lateral load-displacement response of Wall SQ1S 109

Figure 4-12 Damage of Wall SQ1 at ultimate....111

Figure 4-13 Damage of Wall SQ1S at ultimate....111

Figure 4-14 Lateral load-displacement response of Wall SQ2....113

Figure 4-15 Lateral load-displacement response of Wall SQ2S 113

Figure 4-16 Damage of Wall SQ2 at ultimate....115

Figure 4-17 Damage of Wall SQ2S at ultimate....116

Figure 4-18 Typical wall lateral load-elongation response of SMA braces in Wall SQ1S....117

Figure 4-19 Typical wall lateral load-elongation response of SMA links in Wall SQ1S....117

Figure 4-20 Typical wall lateral load-elongation response of SMA braces in Wall SQ2S....119

Figure 4-21 Typical wall lateral load-elongation response of SMA links in Wall SQ2S....120

Figure 4-22 Envelope of lateral load-displacement response of shear walls....122

Figure 4-23 Typical cycles prior to failure of Walls SQ1 and SQ1S....122

Figure 4-24 Typical cycles prior to failure of Walls SQ2 and SQ2S....123

Figure 4-25 Secant stiffness of walls (stiffness in logarithmic scale)....124

Figure 4-26 Cumulative energy dissipation of walls....126

Figure 4-27 Displacement recovery of walls....127

Figure 4-28 Shear distortion of walls....128

Figure 4-29 Typical net shear distortion response of Walls SQ2 and SQ2S at 30 mm displacement....130

Figure 5-1 Details of shear walls: (a) SQ1/SQ1S and SQ1a/SQ1aS; and (b) SQ2/SQ2S....143

Figure 5-2 External retrofit of Walls SQ1S and SQ2S....144

Figure 5-3 SMA Brace....144

Figure 5-4 Stress-strain response of SMA rod....146

Figure 5-5 Force-elongation response of SMA brace....147

Figure 5-6 Superelastic SMA brace constitutive model (Abdulridha et al. 2013) 151

Figure 5-7 Force-elongation response of SMA brace 152

Figure 5-8 Bond-link element (Cortés-Puentes and Palermo 2012) 153

Figure 5-9 Finite element model of Walls SQ1, SQ1a, and SQ1S (SMA braces only in SQ1S) 154

Figure 5-10 Finite element model of Walls SQ2 and SQ2S (SMA braces only in SQ2S) 155

Figure 5-11 Lateral load-displacement response of Wall SQ1 157

Figure 5-12 Damage of Wall SQ1 at 1.5% drift 157

Figure 5-13 Lateral load-displacement response of Wall SQ1a 158

Figure 5-14 Damage of Wall SQ1a at 2% drift 158

Figure 5-15 Lateral load-displacement response of Wall SQ2 159

Figure 5-16 Damage of Wall SQ2 at 1.5% drift 159

Figure 5-17 Lateral load-displacement response of Wall SQ1S 161

Figure 5-18 Damage of Wall SQ1S at -1.25% drift 162

Figure 5-19 Cycle to 20 mm, Wall SQ1S 163

Figure 5-20 Lateral load-displacement response of Wall SQ1aS 164

Figure 5-21 Damage of Wall SQ1aS at -2% drift 164

Figure 5-22 Lateral load-displacement response of Wall SQ2S 166

Figure 5-23 Cycle to 30 mm, Wall SQ2S 166

Figure 5-24 Damage of Wall SQ2S at -2% drift 167

Figure 5-25 Effect of axial loading, P: (a) lateral strength, V; (b) drift, D; (c) cumulative energy dissipation, E; and (d) displacement recovery, R 168

Figure 5-26 Effect of size of SMA links, ϕ: (a) lateral strength, V; (b) drift, D; (c) energy dissipation, E; and (d) displacement recovery, R.....170

Figure A-1 Graphical representation of hysteretic damping.....191

Figure A-2 SMA Brace and base anchor plate (all dimensions in mm).....192

Figure B-1 Cross section with reinforcement layout of foundation block 1.....195

Figure B-2 Cross section with reinforcement layout of foundation block 2.....195

Figure B-3 Steel cage of foundation block 1 196

Figure B-4 Casting of foundation block 1.....196

Figure B-5 Steel cage for Walls SQ2 and SQ2S 197

Figure B-6 Typical wood formwork and casting of walls 198

Figure B-7 FRP sheets on walls 199

Figure B-8 Detail of SMA brace connected to the walls.....199

Figure B-9 Typical stress-strain response of concrete used in walls.....200

Figure B-10 Typical stress-strain response of reinforcing steel 201

Figure B-11 Pullout test of 9.5-mm anchored reinforcing bars 202

Figure B-12 Typical stress-strain response of 9.5-mm anchored reinforcing bars 202

Figure B-13 Displacement sensors on control walls (letter C denotes cable transducer, and letter L denotes LVDT).....204

Figure B-14 Additional displacement sensors on retrofitted walls (letter C denotes cable transducer).....205

Figure B-15 Strain gauges on reinforcing steel of Walls SQ1, SQ1a, and SQ1S 207

Figure B-16 Strain gauges on reinforcing steel of Walls SQ2 and SQ2S 207

Figure B-17 Strain gauges on SMA braces (letter *s* denotes SMA) 208

Figure B-18 Flowchart of data acquisition system 209

Figure B-19 Loading protocol for the wall tests.....210

Figure B-20 Actual loading protocol for Wall SQ1 test.....210

Figure B-21 First cracking of Wall SQ1 at 0.6 mm displacement 211

Figure B-22 Cracking pattern of Wall SQ1 at 3.6 mm displacement.....212

Figure B-23 Cracking pattern of Wall SQ1 at 6.3 mm displacement.....212

Figure B-24 Cracking pattern of Wall SQ1 at -15.9 mm displacement.....213

Figure B-25 Cracking pattern of Wall SQ1 at 47.6 mm displacement.....213

Figure B-26 First cracking of Wall SQ1a at 0.6 mm displacement 214

Figure B-27 Cracking pattern of Wall SQ1a at 5.0 displacement 214

Figure B-28 Cracking pattern of Wall SQ1a at 10 mm displacement.....215

Figure B-29 Cracking pattern of Wall SQ1a at 20 mm displacement.....215

Figure B-30 Cracking pattern of Wall SQ1a at 40 mm displacement.....216

Figure B-31 Cracking pattern of Wall SQ1a at 50 mm displacement.....216

Figure B-32 First cracking of Wall SQ1S at 0.6 mm displacement.....217

Figure B-33 Cracking pattern of Wall SQ1S at 5.0 displacement.....217

Figure B-34 Cracking pattern of Wall SQ1S at 10 mm displacement.....218

Figure B-35 Cracking pattern of Wall SQ1S at 20 mm displacement.....218

Figure B-36 Cracking pattern of Wall SQ1S at 30 mm displacement.....219

Figure B-37 Cracking pattern of Wall SQ1S at 40 mm displacement.....219

Figure B-38 First cracking of Wall SQ2 at 0.3 mm displacement 220

Figure B-39 Cracking pattern of Wall SQ2 at 5.0 displacement 220

Figure B-40 Cracking pattern of Wall SQ2 at 10 mm displacement.....221

Figure B-41 Cracking pattern of Wall SQ2 at 20 mm displacement.....221

Figure B-42 Cracking pattern of Wall SQ2 at 30 mm displacement.....222

Figure B-43 Cracking pattern of Wall SQ2 at 40 mm displacement.....222

Figure B-44 First cracking of Wall SQ2S at 0.3 mm displacement.....223

Figure B-45 Cracking pattern of Wall SQ2S at 5.0 displacement.....223

Figure B-46 Cracking pattern of Wall SQ2S at 10 mm displacement.....224

Figure B-47 Cracking pattern of Wall SQ2S at 20 mm displacement.....224

Figure B-48 Cracking pattern of Wall SQ2S at 30 mm displacement.....225

Figure B-49 Cracking pattern of Wall SQ2S at 40 mm displacement.....225

Figure B-50 Cracking pattern of Wall SQ2S at 50 mm displacement.....226

Figure B-51 Cracking pattern of Wall SQ2S at -60 mm displacement.....226

Figure B-52 Lateral load-lateral displacement, sensor C4 in SQ1.....227

Figure B-53 Lateral load-vertical displacement, sensor C6 in Wall SQ1.....228

Figure B-54 Lateral load-diagonal displacement, sensor C8 in SQ1.....228

Figure B-55 Lateral load-lateral displacement response, sensor C2 in SQ1a.....229

Figure B-56 Lateral load-lateral displacement response, sensor C4 in SQ1a.....229

Figure B-57 Lateral load-vertical displacement response, sensor C6 in SQ1a 230

Figure B-58 Lateral load-diagonal displacement response, sensor C8 in SQ1a.....230

Figure B-59 Lateral load-lateral displacement response, sensor C4 in SQ1S 231

Figure B-60 Lateral load-vertical displacement response, sensor C6 in SQ1S.....231

Figure B-61 Lateral load-brace elongation response, sensor C16 in SQ1S.....232

Figure B-62 Lateral load-link elongation response, sensor C18 in SQ1S 232

Figure B-63 Lateral load-lateral displacement response, sensor C4 in SQ2.....233

Figure B-64 Lateral load-vertical displacement response, sensor C6 in SQ2.....233

Figure B-65 Lateral load-diagonal displacement response, sensor C8 in SQ2 234

Figure B-66 Lateral load-lateral displacement response, sensor C4 in SQ2S 234

Figure B-67 Lateral load-vertical displacement response, sensor C6 in SQ2S.....235

Figure B-68 Lateral load-brace elongation response, sensor C16 in SQ2S.....235

Figure B-69 Lateral load-link elongation response, sensor C18 in SQ2S 236

Figure B-70 Strain response of longitudinal reinforcement, strain gauge 4 in SQ1.....237

Figure B-71 Strain response of longitudinal reinforcement, strain gauge 5 in SQ1.....237

Figure B-72 Strain response of longitudinal reinforcement, strain gauge 6b in SQ1.....238

Figure B-73 Strain response of longitudinal reinforcement, strain gauge 13 in SQ1.....238

Figure B-74 Strain response of transverse reinforcement, strain gauge 20 in SQ1.....239

Figure B-75 Strain response of longitudinal reinforcement, strain gauge 4 in SQ1a.....239

Figure B-76 Strain response of longitudinal reinforcement, strain gauge 5 in SQ1a.....240

Figure B-77 Strain response of longitudinal reinforcement, strain gauge 6 in SQ1a....240

Figure B-78 Strain response of longitudinal reinforcement, strain gauge 8 in SQ1a....241

Figure B-79 Strain response of transverse reinforcement, strain gauge 20 in SQ1a....241

Figure B-80 Strain response of longitudinal reinforcement, strain gauge 4 in SQ1S....242

Figure B-81 Strain response of longitudinal reinforcement, strain gauge 5 in SQ1S....242

Figure B-82 Strain response of longitudinal reinforcement, strain gauge 6 in SQ1S....243

Figure B-83 Strain response of longitudinal reinforcement, strain gauge 9 in SQ1S....243

Figure B-84 Strain response of transverse reinforcement, strain gauge 20 in SQ1S....244

Figure B-85 Strain response of SMA link, strain gauge 1s in front brace in SQ1S....244

Figure B-86 Strain response of SMA link, strain gauge 2s in front brace in SQ1S....245

Figure B-87 Strain response of SMA link, strain gauge 3s in front brace in SQ1S....245

Figure B-88 Strain response of longitudinal reinforcement, strain gauge 1 in SQ2....246

Figure B-89 Strain response of longitudinal reinforcement, strain gauge 2 in SQ2....246

Figure B-90 Strain response of longitudinal reinforcement, strain gauge 3 in SQ2.....247

Figure B-91 Strain response of longitudinal reinforcement, strain gauge 4 in SQ2.....247

Figure B-92 Strain response of transverse reinforcement, strain gauge 23 in SQ2.....248

Figure B-93 Strain response of transverse reinforcement, strain gauge 25 in SQ2.....248

Figure B-94 Strain response of longitudinal reinforcement, strain gauge 1 in SQ2S.....249

Figure B-95 Strain response of longitudinal reinforcement, strain gauge 2 in SQ2S.....249

Figure B-96 Strain response of longitudinal reinforcement, strain gauge 3 in SQ2S.....250

Figure B-97 Strain response of longitudinal reinforcement, strain gauge 4 in SQ2S.....250

Figure B-98 Strain response of longitudinal reinforcement, strain gauge 5 in SQ2S.....251

Figure B-99 Strain response of transverse reinforcement, strain gauge 23 in SQ2S.....251

Figure B-100 Strain response of transverse reinforcement, strain gauge 25 in SQ2S.....252

Figure B-101 Strain response of SMA link, strain gauge 1s in front brace in SQ2S.....252

Figure B-102 Strain response of SMA link, strain gauge 2s in front brace in SQ2S.....253

Figure B-103 Strain response of SMA link, strain gauge 3s in front brace in SQ2S 253

Figure C-1 Finite element model of original wall 255

Figure C-2 Finite element model of SMA-retrofitted wall 256

Figure C-3 Predicted response of original wall 258

Figure C-4 Predicted response of SMA-retrofitted wall 258

Figure C-5 Predicted damage of walls: (a) original wall; and (b) SMA-retrofitted wall 259

Figure C-6 Response of Wall SQ1, medium mesh: (a) lateral load-displacement response; and (b) damage at 1.5% drift 259

Figure C-7 Response of Wall SQ1a, medium mesh: (a) lateral load-displacement response; and (b) damage at 2% drift 260

Figure C-8 Response of Wall SQ2, medium mesh: (a) lateral load-displacement response; and (b) damage at 1.5% drift 260

Figure C-9 Response of Wall SQ1, coarse mesh: (a) lateral load-displacement response; and (b) damage at 1.25% drift 261

Figure C-10 Response of Wall SQ1a, coarse mesh: (a) lateral load-displacement response; and (b) damage at 2% drift 261

Figure C-11 Response of Wall SQ2, coarse mesh: (a) lateral load-displacement response; and (b) damage at 1.5% drift 262

Figure C-12 Lateral load-displacement response of SQ1S, 0% axial load 262

Figure C-13 Lateral load-displacement response of SQ1S, 2% axial load 263

Figure C-14 Lateral load-displacement response of SQ1S, 5% axial load 263

Figure C-15 Lateral load-displacement response of SQ1S, 10% axial load 264

Figure C-16 Lateral load-displacement response of SQ1aS, 0% axial load 264

Figure C-17 Lateral load-displacement response of SQ1aS, 2% axial load.....265

Figure C-18 Lateral load-displacement response of SQ1aS, 5% axial load.....265

Figure C-19 Lateral load-displacement response of SQ1aS, 10% axial load.....266

Figure C-20 Lateral load-displacement response of SQ2S, 0% axial load.....266

Figure C-21 Lateral load-displacement response of SQ2S, 2% axial load.....267

Figure C-22 Lateral load-displacement response of SQ2S, 5% axial load.....267

Figure C-23 Lateral load-displacement response of SQ2S, 10% axial load.....268

Figure C-24 Lateral load-displacement response of SQ1S, 10-mm SMA link.....268

Figure C-25 Lateral load-displacement response of SQ1S, 13-mm SMA Link 269

Figure C-26 Lateral load-displacement response of SQ1S, 16-mm SMA Link 269

Figure C-27 Lateral load-displacement response of SQ1S, 19-mm SMA Link 270

Figure C-28 Lateral load-displacement response of SQ1aS, 10-mm SMA Link 270

Figure C-29 Lateral load-displacement response of SQ1aS, 13-mm SMA Link 271

Figure C-30 Lateral load-displacement response of SQ1aS, 16-mm SMA Link 271

Figure C-31 Lateral load-displacement response of SQ1aS, 19-mm SMA Link 272

Figure C-32 Lateral load-displacement response of SQ2S, 10-mm SMA Link 272

Figure C-33 Lateral load-displacement response of SQ2S, 13-mm SMA Link 273

Figure C-34 Lateral load-displacement response of SQ2S, 16-mm SMA Link 273

Figure C-35 Lateral load-displacement response of SQ2S, 19-mm SMA Link 274

List of Tables

Table 2-1 Properties of large diameter SMA bars at room temperature (Yin et al. 2015) 28

Table 3-1 Properties of braces 79

Table 3-2 Predicted response parameters of Walls SQ1, SQ1S, and SQ1R 86

Table 4-1 Concrete material properties....102

Table 4-2 Reinforcement material properties 102

Table 4-3 Behavioural parameters of walls....120

Table 5-1 Concrete material properties....145

Table 5-2 Reinforcement material properties 145

Table 5-3 Summary of finite element meshes in shear walls 156

Table 5-4 Experimental and numerical responses of control shear walls 156

Table 5-5 Experimental and numerical responses of retrofitted walls....160

Table B-1 Properties of concrete....201

Table B-2 Properties of Superelastic Nickel-Titanium SMA as provided by the manufacturer, SAES Smart Materials (2012) 203

Chapter 1

General Introduction

1.1 Background

Squat reinforced concrete shear walls with a height-to-length ratio of less than 2 are found in various low-rise structures such as parking structures, residential buildings, podiums of high-rise buildings, schools, hospitals, and bridges. These structural elements are very efficient in bracing buildings to control deformations associated with lateral loading. However, when not provided with adequate reinforcement, as prescribed by modern codes, squat shear walls may experience undesirable failure modes. Wide diagonal cracks and significant shear sliding, resulting from high intensity seismic loading, reduce the aggregate interlock and the corresponding contribution of concrete to shear resistance. This, in turn, reduces the ductility and energy dissipation capacity of the structure, triggering brittle failure. In response to these deficiencies, a number of retrofitting techniques have emerged to control shear damage and improve the seismic performance of existing squat reinforced concrete shear walls. Most existing retrofitting techniques have demonstrated satisfactory improvement of the seismic response in terms of strength and energy dissipation, while others have successfully improved the ductility capacity. Research, however, towards more comprehensive retrofitting strategies to enhance displacement recovery and reducing permanent deformation is lacking. Shape Memory Alloys (SMAs) are smart materials that can be implemented into retrofitting methodologies to address current deficiencies in retrofitting strategies.

Shape memory alloys possess recovery, damping, fatigue resistance, and corrosion resistance properties that have motivated the engineering community to

develop new reinforcing and retrofitting strategies for structures. Recovery of the material is the result of transformation of the internal crystalline structure between the martensite and the austenite phases. The material can recover the shape either by increasing the temperature (thermal shape-memory effect) or by releasing the applied stresses (superelasticity effect; also known as pseudo-elasticity). Nickel-Titanium (NiTi) SMA alloys, which are composed of approximately equal parts of Nickel and Titanium, are the most common type of shape memory alloys. The stress-strain curve for superelastic NiTi SMAs shows hysteresis loops with distinctive upper plateau stress, σ_{UP}, lower plateau stress, σ_{LP}, hysteretic damping, ξ_{eq}, and negligible residual strain, ε_r, when subjected up to 6% straining (Figure 1-1). The mechanical properties of superelastic NiTi are determined following the ASTM F2516-14 standard (ASTM 2014).

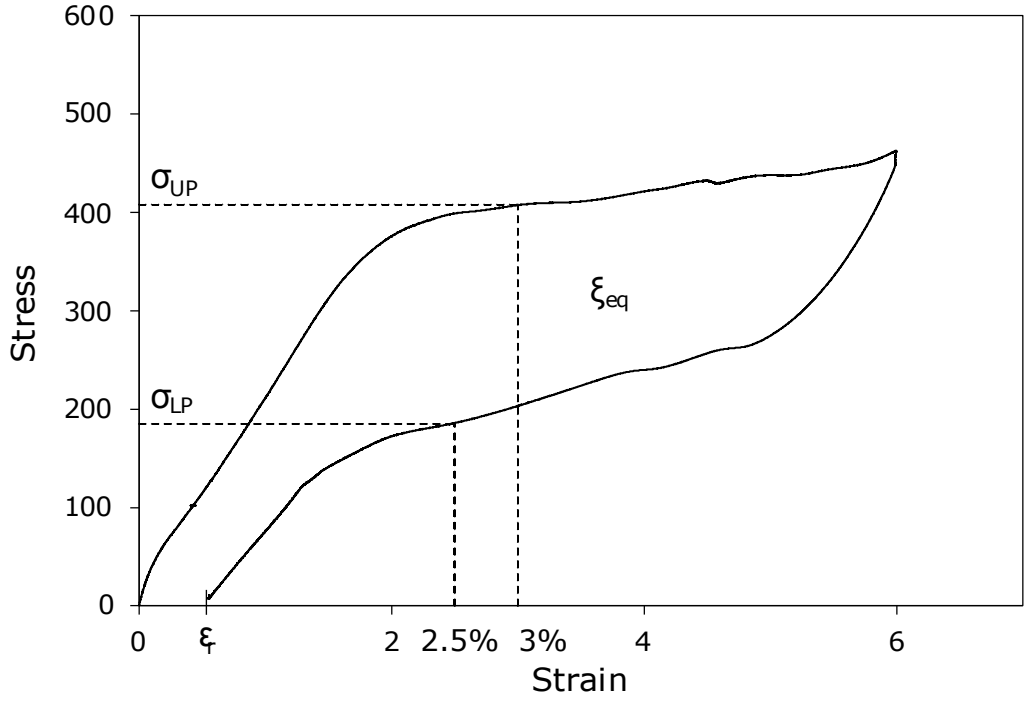


Figure 1-1 Stress-strain response of superelastic NiTi SMA

The flag-shape response of superelastic NiTi SMAs can potentially improve the seismic response of reinforced concrete structures and address deficiencies of existing retrofitting strategies. Strategies such as steel plates and Fibre Reinforced Polymers (FRP) can improve strength and ductility capacities; however, the shear associated

with the additional strength can trigger brittle failure of a shear wall before reaching its ultimate flexural capacity. Retrofitting strategies with shape memory alloys, on the other hand, can improve re-centering (minimize residual deformations) and control shear deformations, while improving strength, ductility and energy dissipation. This reduces damage and improves closure of cracks in the concrete, increasing aggregate interlock and mitigating shear-related failure.

1.2 Novelty of Research

Previous applications of SMAs on reinforced concrete shear walls have focused on the internal reinforcement of flexural walls (Abdulridha and Palermo 2014). Only one study, known by the author, have attempted the external application of SMAs as a replacement of internal reinforcement (Effendy et al. 2006). Long bi-directional SMA rods were connected to squat shear walls to increase the strength. The small deformations typical of squat walls and buckling of the SMA rods, however, limited the beneficial effect of the SMA to increase energy dissipation and improve re-centering. To address these shortcomings, the author developed an external tension-only SMA bracing system that incorporates optimized superelastic SMA elements that concentrate the recoverable non-linear damage (Figure 1-2). This is the first energy dissipater re-centering bracing system based on SMA that has been developed to improve the seismic performance of shear-critical reinforced concrete walls.

The braces consist of tension-only, NiTi SMA links coupled with rigid steel elements connected to the base and top of squat concrete shear walls through anchor plates, following a diagonal layout (Figure 1-2). The SMA links are designed as fuses where all the damage of the brace is concentrated (plastic deformations), while the rigid steel elements are designed to experience negligible deformations and remain in the elastic range. Furthermore, the SMA links are designed to recover large pseudo-plastic deformations, up to 6 %, while dissipating significant energy. The SMA brace functions as an external energy dissipater capable of improving the dynamic response of reinforced concrete shear walls. The braces were envisioned to increase strength and ductility, reduce permanent deformations, and mitigate damage in the walls. In addition, the braces are intended to be re-usable after a seismic event due to the re-

centering capabilities of the SMA link. The SMA braces are applicable for the retrofit of other reinforced concrete structural elements governed by shear deformations such as pier walls and shear deficient frames. The concept of diagonal, tension-only SMA links can improve the shear and flexural response of smaller structural elements such as coupling beams and short columns. The dissipative characteristics of SMAs may potentially benefit the response of reinforced concrete elements governed by flexure.

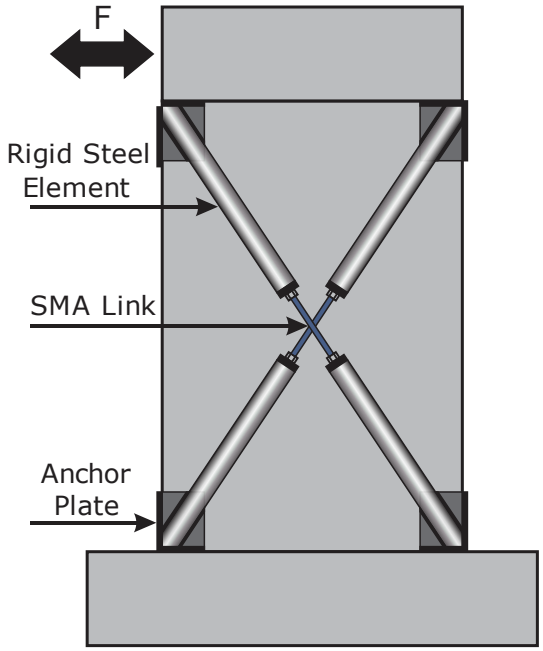


Figure 1-2 Retrofit scheme with SMA braces

1.3 Research Significance

Retrofitting seismically deficient reinforced concrete structures is the most viable and cost-effective solution to prevent catastrophic failures in the event of a significant earthquake. Therefore, detailed investigation of emerging retrofitting techniques is necessary. One of such techniques is the external application of superelastic shape memory alloys to improve strength and displacement recovery, reduce damage, and prevent brittle shear failure. Although there have been significant advances in the field of shape memory alloys, the application for civil engineering structures, specifically for retrofitting existing reinforced concrete structures, is in its infancy.

The results of this research will contribute to the Canadian Seismic Research Network (CSRN) and other government institutions in the development of seismic upgrading techniques to mitigate the effect of potentially significant earthquakes in Canada. The developed SMA bracing system will provide a novel retrofitting alternative that can be implemented by practicing engineers to improve resilience of existing structures. For the research community, the study will expand the knowledge frontier on seismic retrofit of shear-critical reinforced concrete structures and will motivate the development of new smart retrofitting techniques based on energy dissipation devises with re-centering capabilities.

1.4 Research Methodology

Experimental and numerical research on large-scale, squat reinforced concrete shear walls are conducted to study the effect of the proposed superelastic shape memory alloy retrofitting system on improving seismic response. The shear walls in this study are one-third scale specimens of a prototype buildings designed according to pre-1970s standards (NBCC-1965 and CSA A23.3-63). The following main phases describe the methodology employed during the course of this research.

Phase 1: Development of an SMA Retrofitting System

An SMA retrofitting system is developed using the performance-based design method and preliminary finite element simulations with the nonlinear program VecTor2. The performance-based design method assesses the capacity of the wall against the design seismic demand. Then, the designed retrofitting system is experimentally tested and numerically evaluated to demonstrate the performance and the potential improvement of response of seismically deficient squat reinforced concrete shear walls.

Phase 2: Experimental Program

This phase involves the design and testing of two types of squat shear walls. Original squat Walls SQ1 and SQ1a and their companion retrofitted Wall SQ1S are constructed with minimum web reinforcement without seismic detailing. Original

Wall SQ2 and its companion retrofitted Wall SQ2S are constructed with boundary zones with minimum detailing. Testing of the walls follows an incremental reverse cyclic loading protocol to simulate seismic loading.

Phase 3: Numerical Analysis

Numerical simulations using the finite element method are conducted to predict the response of squat concrete walls retrofitted with the proposed SMA bracing. The numerical tool (Program VecTor2) is validated by comparing numerical predictions of the walls with results from the experimental program. The aim is to select the input models that better capture the hysteretic response of original and SMA-retrofitted walls. Furthermore, the simulations are used to study the effect of axial loading and size of the SMA rods used in the braces on the behavioural response of the retrofitted walls. This phase of the study also provides guidance for modelling squat reinforced concrete shear walls retrofitted with SMAs.

1.5 Research Objectives

The main objective is to develop and assess an external SMA brace for retrofitting seismic deficient squat reinforced concrete shear walls. The SMA retrofitting system promises to enhance the performance of seismically deficient structural members. Following are detailed tasks geared towards achieving the main objective:

- Investigate the response of squat reinforced concrete shear walls designed according to pre-1970s building codes and design standards. Assess the seismic response of a prototype wall following performance-based methods and design a retrofit strategy using SMAs. Compare the response of prototype walls retrofitted with SMA and steel.

- Develop an SMA retrofitting system that can improve the seismic performance of squat reinforced concrete shear walls. Investigate the potential reusability of the SMA retrofitting system after the retrofitted structure experiences a seismic event.

- Design and test reinforced concrete shear walls to study the hysteretic response of seismically deficient and SMA-retrofitted walls. Provide experimental data to corroborate numerical methods for the analysis of SMA retrofitting systems.

- Assess and validate existing numerical simulation techniques based on the Finite Element Methods (FEMs) for predicting the response of SMA-retrofitted walls. Predict the response of the tested walls using the FEM and provide modelling guidance for numerical simulations. Conduct a parametric study using the FEM to assess the effect of axial loading and design of the SMA retrofitting system.

1.6 Thesis Layout

This thesis is written in an article-based format. It consists of seven chapters, three of them correspond to research articles. The thesis is organized as follows:

- Chapter 1, *General Introduction*, provides a general background on squat reinforced concrete shear walls and exposes the need to retrofit to improve seismic response. This chapter also presents the novelty of this study, research significance, the research methodology, the research objectives and scope, and the outline of the thesis.

- Chapter 2, *Literature Review*, describes the main seismic behavioural features of squat reinforced concrete walls, presents a comprehensive review of existing retrofitting techniques for squat reinforced concrete walls, and discusses the properties of superelastic SMAs and applications to reinforced concrete structures. This chapter extends the literature review presented in the articles.

- Chapter 3 (article 1), *SMA Tension Brace for Retrofitting Concrete Shear Walls*, presents the design of the SMA bracing system for the retrofit of third-scale concrete shear walls. This chapter includes testing of the SMA braces and preliminary numerical analyses of third-scale shear walls retrofitted with the proposed SMA braces and companion retrofitting strategies based on steel and

FRP. This chapter addresses Phase 1 of the research, *Development of SMA Retrofitting System*.

- Chapter 4 (article 2), *Seismic Retrofit of Concrete Shear Walls with SMA Tension Braces*, reports and discusses the results of the experimental program on four squat reinforced concrete shear walls: two control walls, SQ1 and SQ2, and two retrofitted walls with the SMA braces, SQ1S and SQ2S. This chapter corresponds to Phase 2 of the research, *Experimental Program*.

- Chapter 5 (article 3), *Modelling of Concrete Shear Walls Retrofitted with SMA Tension Braces*, reports finite element analyses of the squat shear walls tested in the experimental program. The analyses include a parametric study to assess the effect of axial loading and size of the SMA braces on the hysteretic response of the shear walls. This chapter corresponds to Phase 3 of the research, *Numerical Simulations*.

- Chapter 6, *General Conclusions*, integrates the material presented in previous chapters. It summarizes the findings and conclusions reported in the research articles.

- Chapter 7, *Future Work*, provides a list of recommendations for future work.

- Appendix A, *Development of an SMA Retrofitting System: Supplementary Material,* provides additional details for the development of the SMA retrofitting system. Specifically, it provides the seismic assessment of the original wall and the design of the SMA braces based on the seismic assessment of the retrofitted wall.

- Appendix B, *Experimental Program: Supplementary Material,* presents additional details of the experimental program, not reported in Chapter 4. It also presents the experimental results of the control wall, SQ1a.

- Appendix C, *Modelling of Shear Walls: Supplementary Material,* augments Chapter 3 by providing numerical predictions of the original and retrofitted prototype shear walls studied for the development of the SMA bracing system. In addition, this appendix presents additional predictions of the control and

retrofitted walls that complement the numerical and parametric studies reported in Chapter 5.

1.7 References

Abdulridha, A., and Palermo, D. (2014). "Response of a hybrid SMA reinforced concrete shear wall." *Tenth U.S. National Conference on Earthquake Engineering*, Network for Earthquake Engineering Simulation, Anchorage, AK, USA.

ASTM. (2014). *ASTM F2516-14 Standard test method for tension testing of nickel-titanium superelastic materials*. ASTM International, West Conshohocken, PA, USA.

Effendy, E., Liao, W. I., Song, G., Mo, Y. L., and Loh, C. H. (2006). "Seismic behavior of low-rise shear walls with SMA bars." *Earth & Space 2006*, American Society of Civil Engineers, Houston, TX, USA, 1–8.

Chapter 2

Literature Review

2.1 Introduction

Satisfactory seismic performance of existing buildings can be achieved by promoting the beneficial effects associated with flexural response of reinforced concrete shear walls, and maintaining and improving the seismic capacity of these critical elements. The seismic behaviour of shear walls can be improved through a number of retrofitting techniques ranging from simple techniques such as replacing of concrete to novel applications of superelastic Shape Memory Alloys (SMAs). The following is a review of the available research on existing retrofitting techniques for squat reinforced concrete shear walls.

2.2 Squat Shear Walls

Existing squat reinforced concrete shear walls with inadequate reinforcement and seismic detailing according to current provisions may lack sufficient strength, ductility, and energy dissipation capacity to survive earthquake events. Squat shear walls can exhibit high strength capacity due to high compressive stresses transferred to the base of the wall through diagonal compression struts and the contribution of the reinforcing steel in tension. Squat shear walls, however, are heavily governed by shear-related mechanisms, shear cracking (diagonal tension cracking) and sliding displacements, which results in a highly pinched hysteretic response with limited energy dissipation and ductility (Palermo and Vecchio 2002). In conventionally reinforced squat shear walls, the detrimental effect of shear increases with increases in the magnitude of shear stresses and reductions of axial loading and height-to-

length ratio (Paulay 1980). Horizontal and vertical reinforcement in the web control shear cracking when the lateral loading is distributed (Paulay 1975). For squat walls subjected to concentrated loads, however, it has been observed that distributed web reinforcement, specifically the horizontal reinforcement, has a slight effect on the shear capacity and failure mode. Arch action, resulting from concentrated loads, limits how the reinforcement engages when crossing diagonal cracks (Lefas et al. 1990). Sliding displacements, occurring along the base at construction joints due to load reversals, are responsible for significant reductions in stiffness and shear strength, particularly for low axial loading (Paulay et al. 1982; Sittipunt et al. 2001). The increase of axial loading increases the sliding resistance; therefore, the design of shear walls should not overestimate the axial loading. The use of diagonal reinforcement has proven effective in controlling shear cracking and sliding while increasing strength and ductility (Paulay et al. 1982). Conversely, additional vertical reinforcement increases the shear stresses that are associated with the increased flexural capacity, resulting in premature brittle shear failure.

2.3 Seismic Retrofit of Shear Walls

Seismic retrofit of shear walls refers to structural interventions aiming to improve the seismic performance. Proper selection of the retrofit strategy is crucial to achieve the target performance of the structure. This section presents research on traditional retrofitting techniques, including epoxy or grout injection of cracks, concrete replacement, addition of reinforcing steel, and external steel plates; and emerging techniques such as external bonding of Fibre Reinforced Polymers (FRP), and structural weakening. Section 2.4 reviews the behaviour and application of SMAs.

2.3.1 Injection of Cracks and Concrete Replacement

Epoxy or grout injection of cracks is a simple technique for repairing reinforced concrete. The technique forces a low viscosity epoxy or cement grout to fill cracks in damaged concrete. The effectiveness of the repair depends on the ability of the fill material to penetrate the cracks (Thermou and Elnashai 2006). When the concrete is heavily cracked, and injection is not sufficient to restore the initial capacity of the

structure, concrete replacement is necessary. This technique involves pouring, grouting, dry-packing, or spraying new concrete, typically with higher strength than the old concrete.

Lefas and Kotsovos (1990) conducted an experimental program on repaired reinforced concrete shear walls with a height-to-length ratio of 2 as part of an investigation on the effects of loading history and repair methods on behavioural features of reinforced concrete walls. The repair procedure followed two methods: one consisting of concrete replacement only, and another combining injection of cracks with replacement of concrete. Loading of the walls followed monotonic and reversed cyclic regimes. Injection of epoxy was applied for cracks greater than 0.2 mm in width. New concrete was used to repair one of the lower 150 mm × 100 mm compression toes. Buckled reinforcing bars were straightened during the concrete replacement stage. The repaired walls exhibited lower stiffness and reduced ductility than the original walls (Figure 2-1).

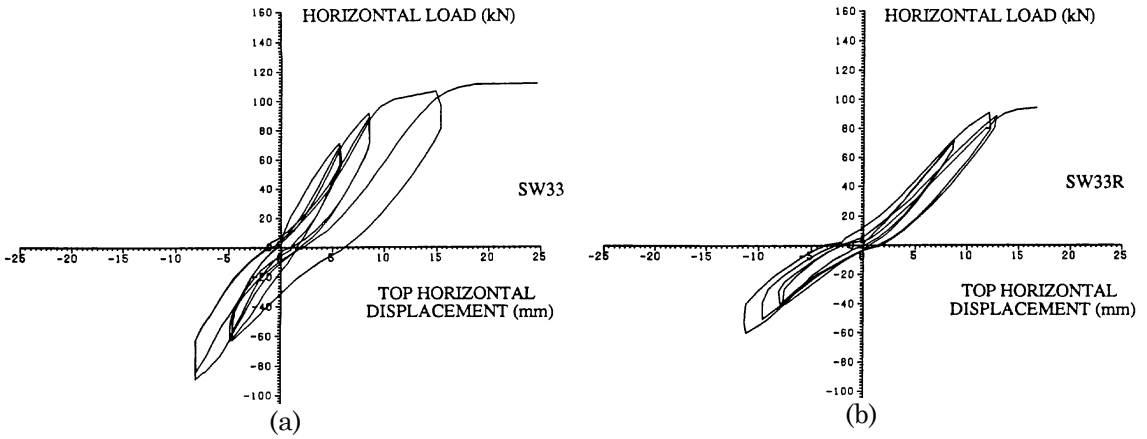


Figure 2-1 Load-displacement response of shear walls (Lefas and Kotsovos 1990): (a) original Wall SW33; and (b) repaired Wall SW33R

The experimental results from the tests conducted by Lefas and Kotsovos demonstrated that replacing the concrete in the damaged compression region restored the strength and shear resistance of the wall, while injection of cracks provided a slight improvement of the structural response of the repaired walls.

Vecchio et al. (2002) tested two large-scale repaired, wide-flanged, squat concrete shear walls subjected to incremental lateral loading and constant axial loading. The repair of the walls consisted of replacing concrete in the web and part of the flanges while keeping the reinforcement intact. Test results indicated that squat shear walls repaired by concrete replacement are capable of recovering strength, ductility, and energy dissipation (Figure 2-2).

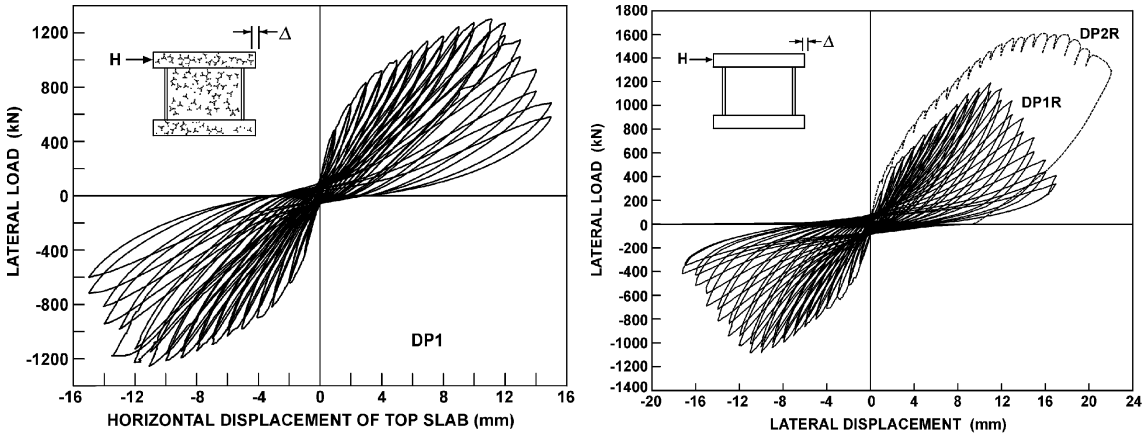


Figure 2-2 Load-displacement response of flanged squat shear walls: (a) original Wall DP1 (Palermo and Vecchio 2002); and (b) repaired Walls DP1R and Wall DP2R (Vecchio et al. 2002)

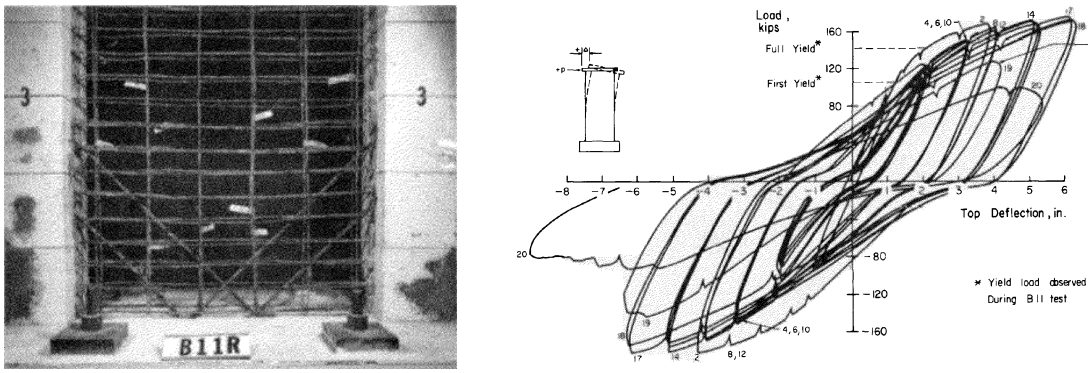
Vecchio et al. (2002) and Cortés-Puentes (2009) simulated the hysteretic response of the walls tested by Vecchio et al. with the nonlinear 2-D finite element program VecTor2 (Wong et al. 2013). The modelling approached followed an engaging-disengaging modelling technique proposed by Vecchio and Bucci (1999). The analyses captured failure in the form of shear sliding at the base of the wall; however, the strength and stiffness were slightly overestimated.

2.3.2 Replacement and Addition of Reinforcement

Replacement and addition of reinforcing bars, along with replacement of concrete, is a common seismic repair and retrofitting technique that aims to restore or improve strength, ductility, energy dissipation, and shear resistance of reinforced concrete shear walls. The design of the retrofitted structure should account for the extra shear

demand associated with the increase of flexural strength, which cannot exceed the wall's shear capacity.

Testing of repaired slender shear walls (Fiorato et al. 1983) demonstrated that replacement and addition of reinforcement combined with partial replacement of concrete are methods capable of restoring strength and controlling shear sliding (Figure 2-3). New bi-diagonal bars improved the strength, ductility, and shear capacity of the walls. Partial replacement of concrete, however, resulted in reduced stiffness. Cortés-Puentes and Palermo (2011) modelled the walls tested by Fiorato et al. using the nonlinear finite element program VecTor2. The simulations required disengaging of damaged reinforcing steel and engaging of the new reinforcing steel. The reinforcing steel was modelled with truss elements perfectly bonded to the concrete. In general, the predicted hysteretic responses of the walls were in good agreement with the observed responses. Behavioural features such as stiffness, strength, ductility, and energy dissipation were well predicted.



(a) (b)

Figure 2-3 Addition of diagonal reinforcement and replacement of concrete (Fiorato et al. 1983): (a) repair of Wall B11R; and (b) response of repaired Wall B11R

Haroun et al. (2000) tested six repaired half-scale bridge pier walls with a height-to-length ratio of 0.755 (Figure 2-4) to investigate retrofitting techniques with new reinforcement. The walls were tested under reversed cyclic loading in the out-of-plane direction and constant axial loading. Repair of the walls included replacing damaged concrete within the plastic hinge zone with an increased section of new concrete, adding of horizontal reinforcement around the existing vertical

reinforcement, and adding of cross-ties. Two types of cross-ties were investigated: double alternating 90- and 135-degree cross-ties and T-headed cross-ties. The repair techniques were effective in restoring the strength, ductility, and stiffness, specifically for walls with low to average vertical reinforcement ratios (Figure 2-5). The ductility of the repaired walls with higher vertical reinforcement ratio was in general lower than the corresponding non-retrofitted wall. Both types of cross-ties were effective in preventing buckling of vertical reinforcement and providing adequate confinement.

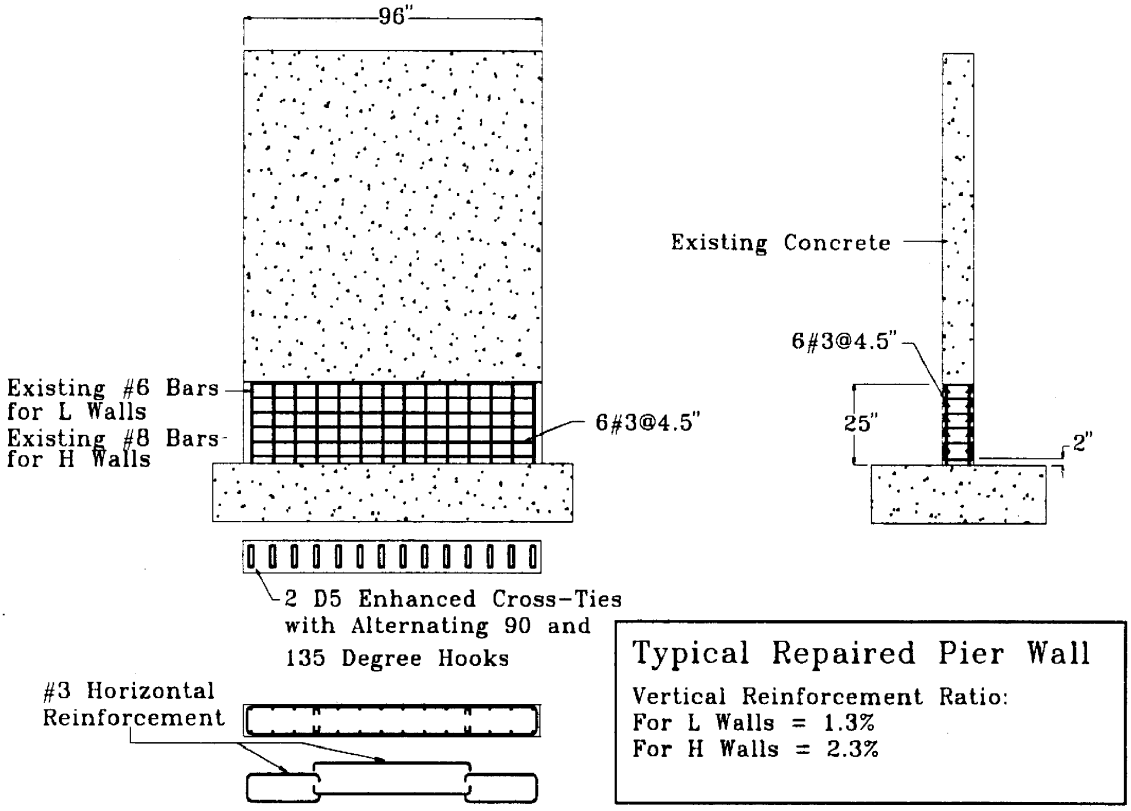


Figure 2-4 Typical repaired pier wall (Haroun et al. 2000)

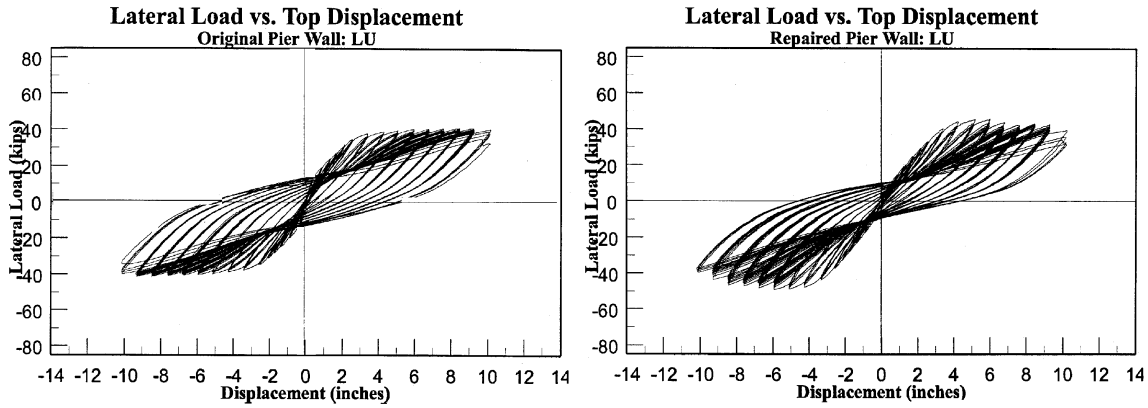


Figure 2-5 Response of repaired pier walls (Haroun et al. 2000): (a) original pier wall LU; and (b) repaired pier wall LU

2.3.3 Attachment of External Steel Plates

External steel plates are applied to enhance the seismic response of reinforced concrete shear walls. Specifically, steel plates are used to improve strength, stiffness, and ductility. The retrofitting requires proper bonding between the steel plates and the concrete to achieve composite action (Thermou and Elnashai 2006). Bonding and composite action are typically achieved by epoxy adhesive bonding or bolting of the steel plates to the concrete.

Elnashai and Pinho (1998) reported on reverse cyclic tests of reinforced concrete shear walls (600 mm in length × 1200 mm in height) seismically retrofitted with selective techniques using bonded steel plates (Figure 2-6). The retrofitting techniques were investigated to improve specific behavioural parameters such as strength, stiffness, and ductility. A strength-only technique consisted of external unbonded steel plates (Figure 2-6(a)), while stiffness-only (Figure 2-6(b)) and ductility-only (Figure 2-6(c)) techniques consisted of external bonded steel plates. The selective retrofitting methods effectively enhanced the response of shear walls according to the retrofit objectives.

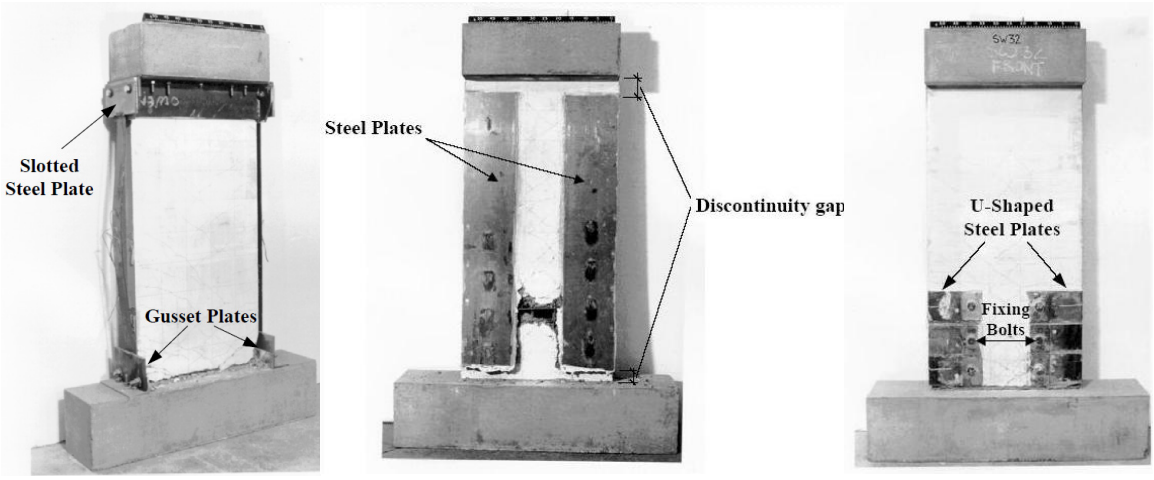


Figure 2-6 Selective techniques for retrofitting shear walls (Elnashai and Pinho 1998): (a) strength-only; (b) stiffness-only; and (c) ductility-only

Taghdi et al. (2000a) investigated the hysteretic behaviour of lightly reinforced squat concrete shear walls retrofitted with steel plates. The study comprised of testing 1800 mm high × 1800 mm long walls designed according to old seismic provisions. The retrofitting system consisted of diagonal and vertical steel strips attached to the walls with through-thickness bolts and connected to the foundation with stiff steel angles. The tests demonstrated that the retrofitting scheme was effective at improving the reverse cyclic response of squat lightly reinforced concrete shear walls, specifically in terms of strength, ductility, and energy dissipation (Figure 2-7). The monotonic response of the retrofitted walls was predicted with simple truss models that incorporated a lower bound theory of plasticity to estimate the ultimate strength (Taghdi et al. 2000b). The truss models captured the inelastic behaviour and the final failure mechanism. The analyses, however, did not accurately predict the ductility, the hysteretic stiffness, and the strength degradation.

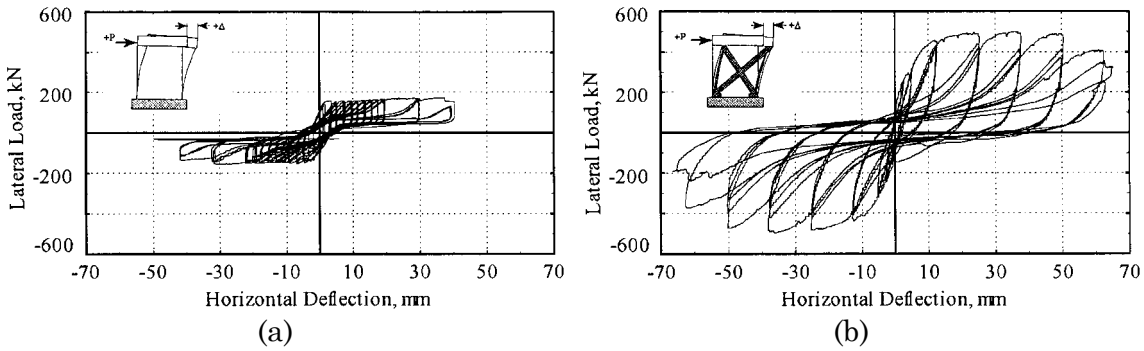


Figure 2-7 Load-displacement response of squat shear walls with steel plates (Taghdi et al. 2000a): (a) original wall; and (b) retrofitted wall

Cortés-Puentes and Palermo (2011, 2012) simulated, with program VecTor2, the retrofitting techniques investigated by Elnashai and Pinho (1998) and Taghdi et al. (2000a). Discrete truss elements connected to rectangular concrete elements were employed to model the steel plates. Bond-link elements were used to simulate bonding of the steel plates to the concrete, while perfectly bonded truss elements, directly connected to the concrete elements, simulated bolting of steel plates. The analyses satisfactorily simulated the hysteretic response of the retrofitted walls, including strength, displacement capacity, energy dissipation, and failure mode.

2.3.4 Bonding of External Fibre Reinforced Polymers

External bonding of Fibre Reinforced Polymer (FRP) composites is a versatile retrofitting technique that is suitable for seismic applications, specifically for reinforced concrete structures with limited space (Thermou and Elnashai 2006). The high strength-to-weight ratio of FRPs permits easy retrofitting applications that contribute to improvements in strength, ductility, and energy dissipation. In general, the quality of the retrofitting method is dependent on bonding of the FRP composite to the concrete surface.

Lombard et al. (2000) studied the effectiveness of externally bonded carbon FRP sheets to retrofit and repair reinforced concrete shear walls. Shear walls, 1795 mm in height × 1500 mm in length, were tested to failure following a reverse cyclic loading protocol. The retrofitting scheme consisted of vertically oriented carbon FRP

sheets bonded to each face of the wall and mechanically anchored to the foundation (Figure 2-8). Retrofitting with FRP improved stiffness, strength, ductility, and reduced pinching of the load-deflection response of the shear walls. (Figure 2-9). Reduction of pinching resulted in greater residual deflections. Cruz-Noguez et al. (2015) extended the study conducted by Lombard et al. by testing retrofitted shear walls with a height-to-length aspect ratio ranging from 0.68 to 1.2. The experimental results further demonstrated the benefits of externally bonded FRPs to improve the seismic performance of reinforced concrete shear walls and highlighted the importance of bonding between concrete and FRP. Companion numerical analyses incorporating link elements to model bond-slip of FRP, using finite element program VecTor2, captured the hysteretic response of the retrofitted shear walls. For shear walls with lap splices, however, the bond-slip models fell short in predicting displacement capacity and other behavioural features. Cortés-Puentes and Palermo (2012) followed a similar modelling approach in VecTor2, based on link elements and bond-slip models, to predict the response of one of the retrofitted wall tested by Lombard et al. In addition, link elements and a proposed bond-slip model simulated anchoring of FRP to the foundation. In general, the bond-slip models accurately predicted strength, ductility, and failure mode.

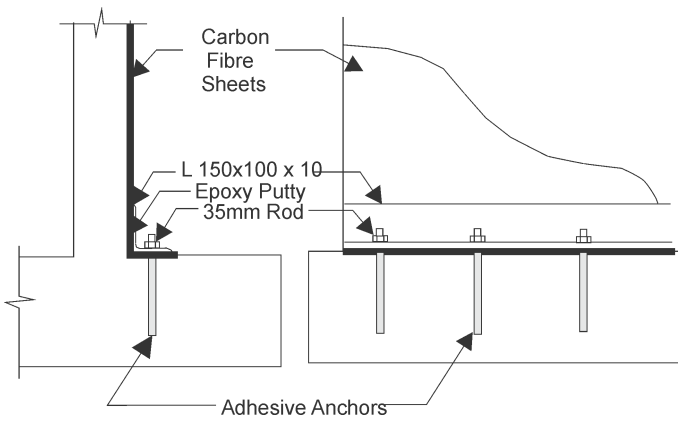
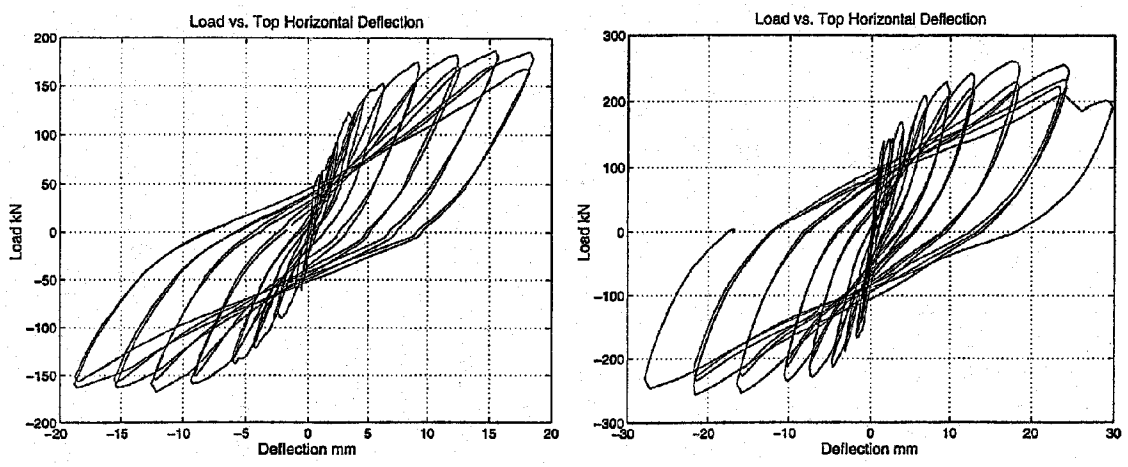


Figure 2-8 Retrofitting of shear wall with carbon fibre sheets (Lombard et al. 2000)



(a) (b)

Figure 2-9 Response of shear walls retrofitted with carbon FRP (Lombard et al. 2000): (a) original wall; and (b) retrofitted wall

Antoniades et al. (2003, 2005) conducted a series of tests on repaired and retrofitted reinforced concrete shear walls with a height-to-length ratio of 1 and 1.5 with different steel reinforcement configurations, including walls with inclined reinforcing bars at the base. The original walls were cyclically loaded to failure, and then repaired with new concrete and lap-welding of ruptured reinforcing steel, and retrofitted with externally bonded horizontal and vertical FRP sheets. Different systems were used to anchor the vertical FRP sheets to the foundation (Figure 2-10). The repair and retrofitting systems restored and improved the strength of the walls (Figure 2-11). Ductility and hysteretic response, however, were not restored, specifically in the post-peak range. Furthermore, the retrofitted walls dissipated less energy than the corresponding original wall. The most effective anchoring system consisted of U-shape FRP sheets and steel plates. Cortés-Puentes and Palermo (2011) predicted the response of the retrofitted walls with the finite element program VecTor2 using truss and link elements to simulate FRP sheets and epoxy, respectively. The numerical modelling was effective in predicting the strength-displacement response of the retrofitted reinforced concrete shear walls.

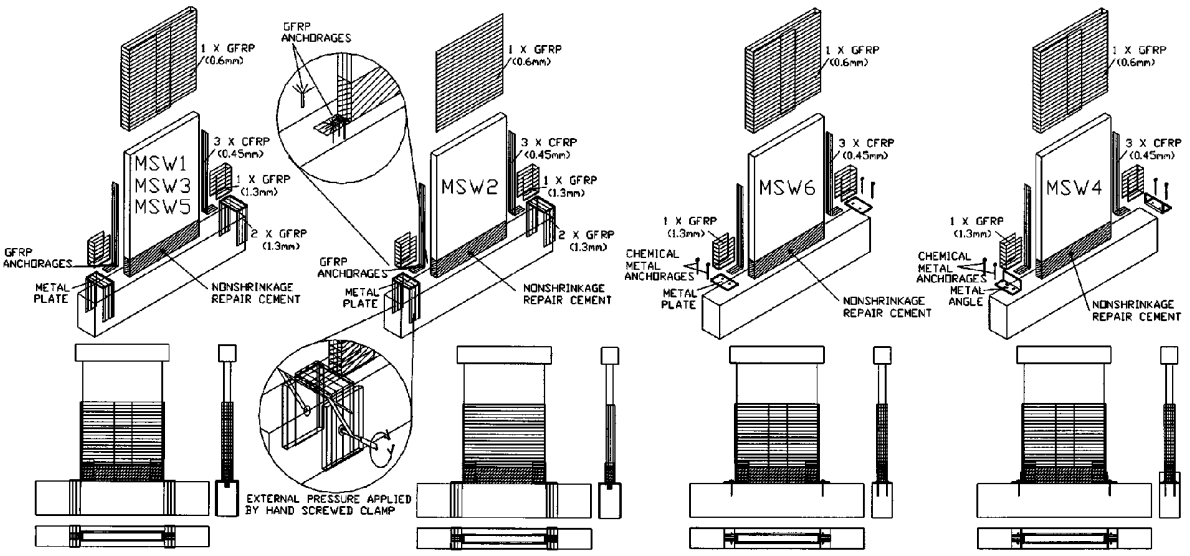


Figure 2-10 Repair and retrofitting of shear walls with FRP (Antoniades et al. 2005)

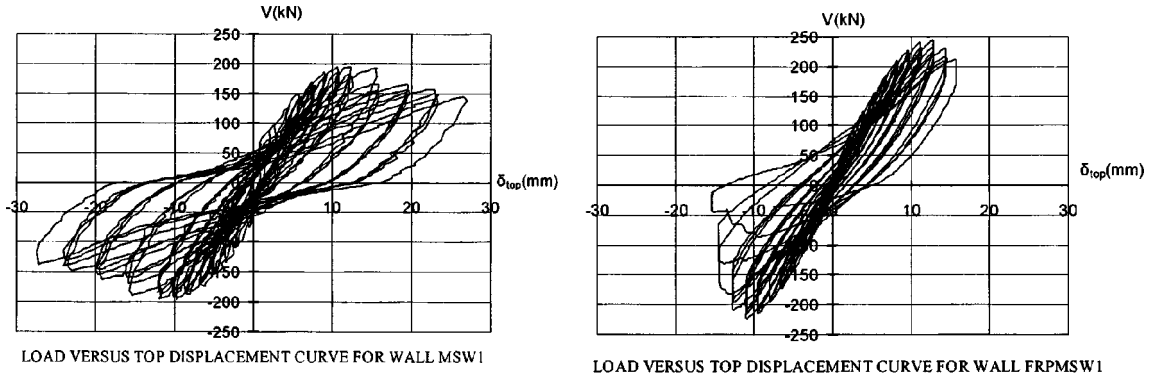


Figure 2-11 Response of shear wall with height-to-length ratio of 1.5 (Antoniades et al. 2005): (a) original wall; and (b) retrofitted wall

Khalil and Ghobarah (2005) conducted an experimental study on reinforced concrete shear walls with a shear span of 2.25 to investigate seismic retrofitting methods using FRPs. The retrofitting methods comprised of wrapping the shear walls with bi-directional carbon FRP sheets with the primary fibres oriented in the ±45° direction and horizontal unidirectional carbon FRP sheets to confine the ends of the walls (Figure 2-12). The test results demonstrated an increase in lateral load capacity, ductility, and energy dissipation (Figure 2-13) as a result of the increase in shear capacity and confinement.

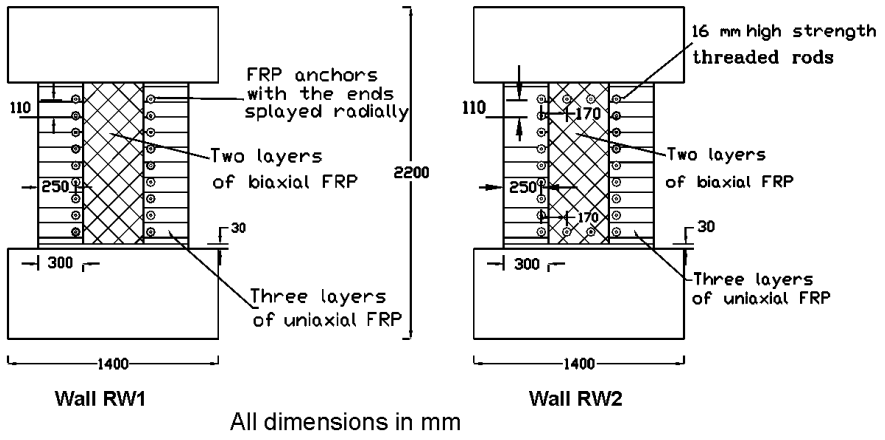


Figure 2-12 Retrofitting of squat shear walls with carbon FRP sheets (Khalil and Ghobarah 2005)

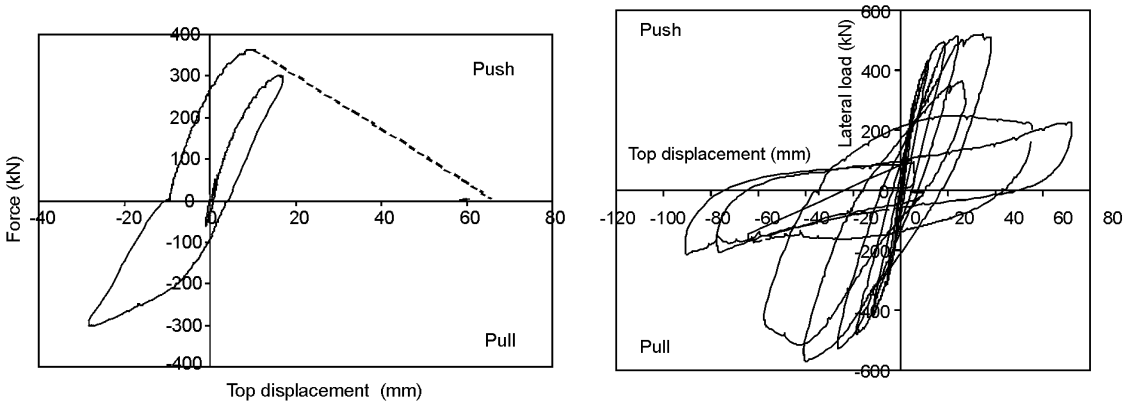


Figure 2-13 Force-displacement response of shear walls (Khalil and Ghobarah 2005): (a) control wall; and (b) retrofitted wall

Kobayashi (2005) proposed a retrofitting system with FRP bands sewed in a cross pattern onto 1000 mm long × 550 mm high squat concrete walls (Figure 2-14(a)). The FRP bands provided confinement that contributed to increases in strength and ductility of up to 24% and 83%, respectively (Figure 2-14(b)). The retrofitting system, however, did not mitigate damage in the post-peak range and the resulting stiffness and strength degradations.

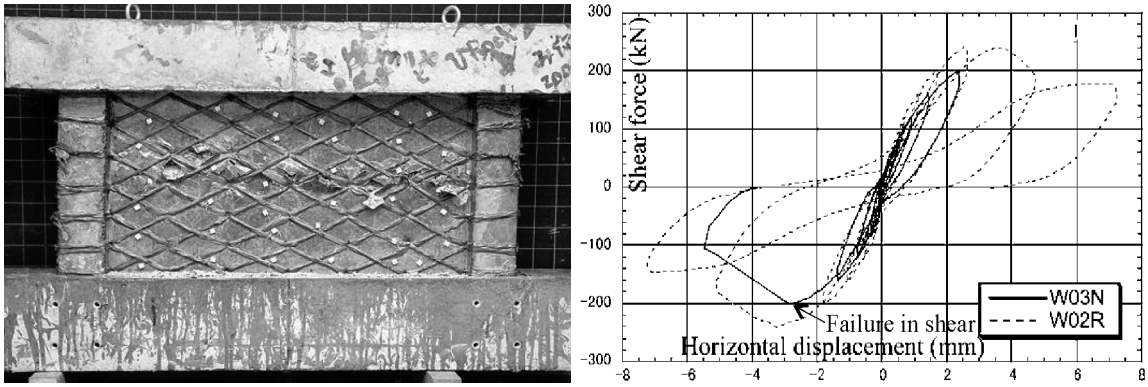


Figure 2-14 Squat shear walls retrofitted with FRP bands (Kobayashi 2005): (a) damage; and (b) force-displacement response of original (W03N) and retrofitted (W02R) walls

Hsiao et al. (2008) investigated a retrofitting scheme with bi-diagonal carbon FRP sheets externally bonded on reinforced concrete barbell-shaped squat shear walls (Figure 2-15(a)). The experimental program consisted of reverse cyclic testing of shear walls with a height-to-length ratio of 0.57 and 0.80. The FRP sheets were mechanically anchored to the foundation and top beam with steel angles and bolts. The results indicated that the retrofitting system increased the strength of the walls. However, for the walls with an aspect ratio of 0.80, the improvement in strength was negligible. Anchoring angles close to the boundary columns caused premature damage and reduced the ductility of the walls, specifically for those with a higher increase in strength. Separation of the anchoring angles from the boundary columns greatly improved the ductility. Pinching of the hysteretic response indicated significant shear degradation and limited energy dissipation of the retrofitted walls (Figure 2-15(b)).

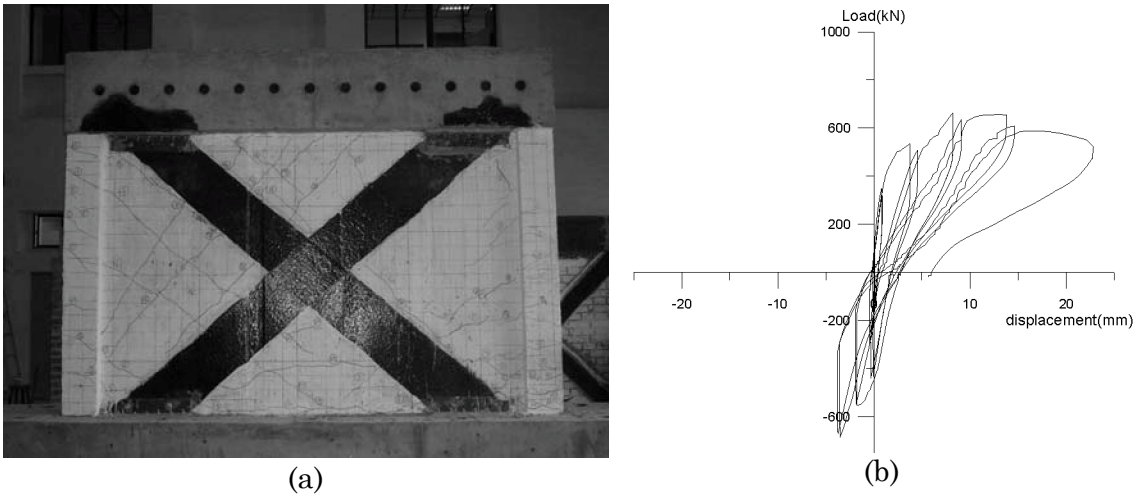
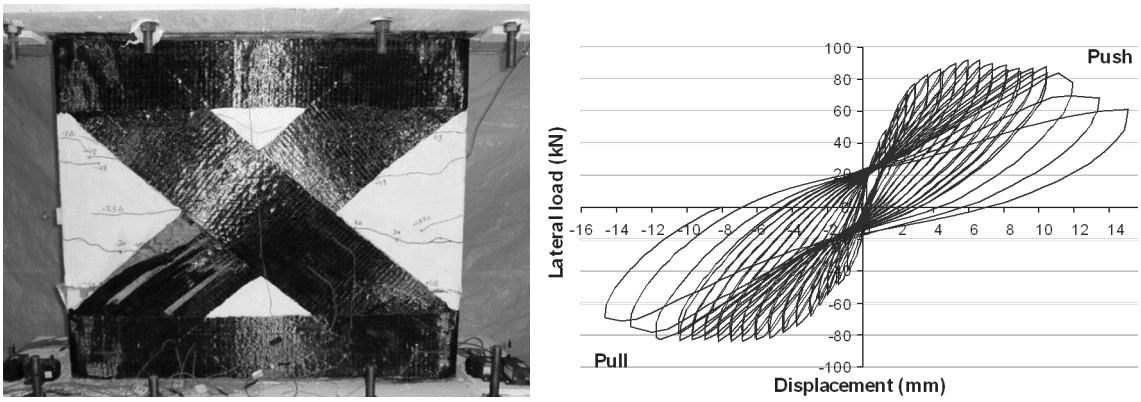


Figure 2-15 Retrofitted squat wall with bi-diagonal carbon FRP strips (Hsiao et al. 2008): (a) tested wall; and (b) load-displacement response

El-Sokkary and Galal (2013) conducted reversed cyclic tests on reinforced concrete shear wall panels retrofitted with carbon FRP composites. The wall panels represented the 6th-storey level of reduced-scale, 8-storey, FRP-retrofitted concrete shear walls previously tested under dynamic loading (El-Sokkary et al. 2013). The retrofitting scheme aimed to improve seismic response and mitigate damage of the shear walls. Two retrofitting layouts were studied: externally bonded vertical and horizontal FRP sheets, and externally bonded diagonal and horizontal FRP sheets (Figure 2-16(a)). The experimental results demonstrated the ability of the retrofitting schemes to increase the lateral strength of the wall panels (Figure 2-16(b)), and specifically for the scheme with diagonal FRP sheets, the beneficial effect of FRP composites to improve rotation capacity and flexural response. Retrofitting with the FRP composites, however, reduced the lateral displacement capacity and had marginal effect on the displacement recovery of the retrofitted wall panels.

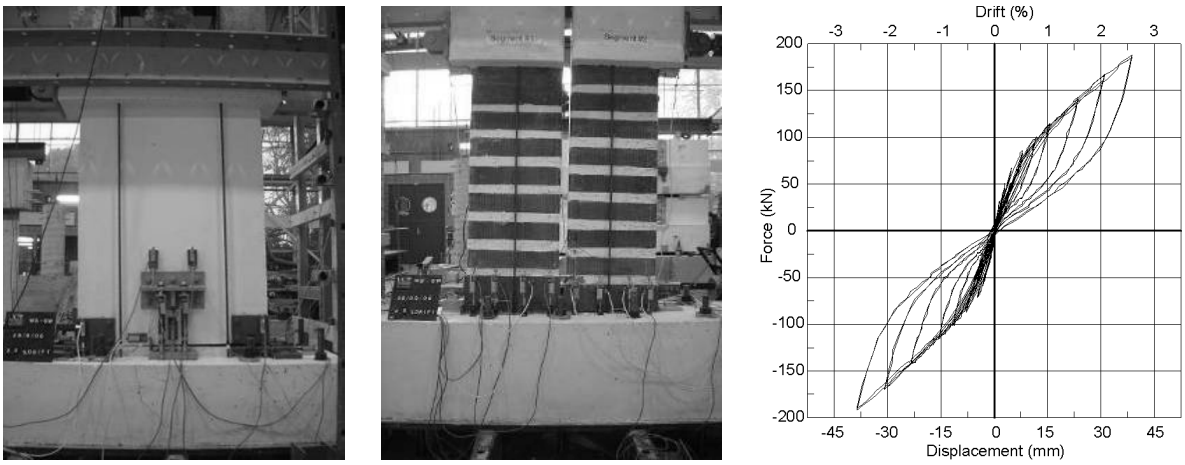


(a) (b)

Figure 2-16 Retrofitted wall panel with diagonal and horizontal carbon FRP strips (El-Sokkary and Galal 2013): (a) tested wall; and (b) load-displacement response

2.3.5 Structural Weakening

Ireland et al. (2007) examined weakening techniques for seismic retrofitting of low-rise shear walls incorporating energy dissipaters to promote flag-shape response with significant energy dissipation and minimal residual deformation. The study involved testing retrofitted reinforced concrete shear walls under reverse cyclic loading following two retrofitting approaches: horizontal cut with post-tensioning steel and external energy dissipaters (Figure 2-17(a)), and vertical cut with confinement of the resulting wall segments and post-tensioning steel (Figure 2-17(b)). The weakening techniques improved the flexural response and reduced damage in the shear walls. Specifically for the horizontal cut, retrofitting of the walls increased strength and introduced re-centering characteristics, while providing significant energy dissipation (Figure 2-17(c)). The resulting flag-shaped hysteretic response is capable of improving seismic response in comparison to elastic-plastic hysteretic systems (Christopoulos et al. 2002).



(a) (b) (c)

Figure 2-17 Structural weakening (Ireland et al. 2007): (a) horizontal cut; (b) vertical cut; and (c) response of retrofitted wall with horizontal cut

2.4 Application of Shape Memory Alloys

Shape Memory Alloys (SMAs) are materials that can recover deformations due to shape memory and superelastic effects (Figure 2-18). SMAs with shape memory effect recover deformations with an increase of temperature as the polycrystalline structure of the material transforms from the martensite phase at lower temperatures to the austenite phase at higher temperature. Superelastic SMAs recover deformations through phase transformations resulting from the release of stresses at relatively high temperatures.

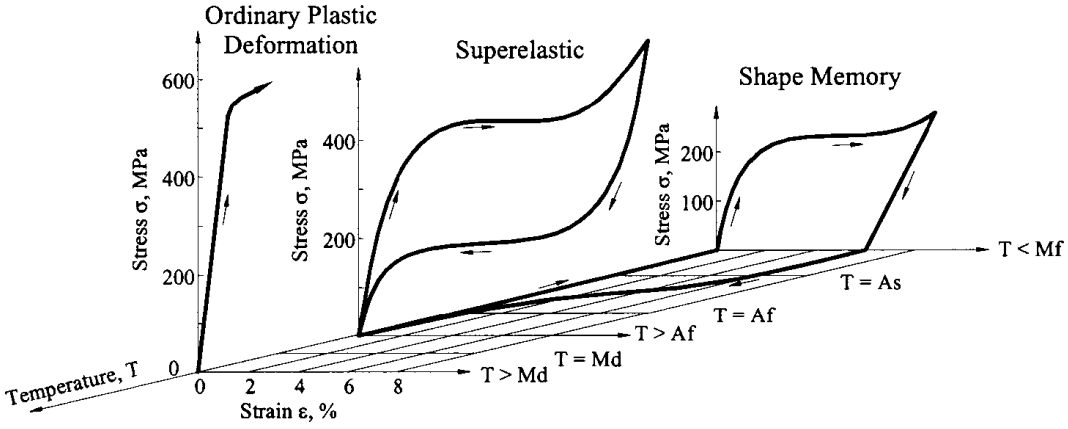


Figure 2-18 Stress-strain-temperature response of SMAs (DesRoches et al. 2004)

Both shape memory and superelastic SMAs are applicable to retrofitting of reinforced concrete structures. Specifically, Nickel-Titanium (NiTi) superelastic SMAs are attractive for seismic retrofitting due to pseudo-yielding properties (stress plateau), strain hardening, large strain capacity, excellent displacement recovery, and good hysteretic damping (DesRoches et al. 2004). Furthermore, NiTi SMAs exhibit excellent fatigue properties (Van Humbeeck 1991), low temperature sensitivity (Melton 1990), and high resistance to corrosion (Melton and Harrison 1994).

2.4.1 Properties of NiTi Superelastic SMAs

The typical stress-strain response of superelastic NiTi SMAs is illustrated in Figure 2-19. The main properties of superelastic NiTi SMAs are upper plateau stress, *UPS*; lower plateau stress, *LPS*; initial elastic modulus, E_i; residual elongation, El_r; ultimate elongation, El_u; and equivalent viscous damping, ξ_{eq} (based on area under the hysteretic cycles). Table 2-1 lists the typical mechanical properties of commercially available large diameter NiTi SMA bars at room temperature (Yin et al. 2015). The mechanical properties of superelastic NiTi SMAs make the material an attractive choice for seismic applications in civil engineering structures (Dolce and Cardone 2001b; Yin et al. 2015).

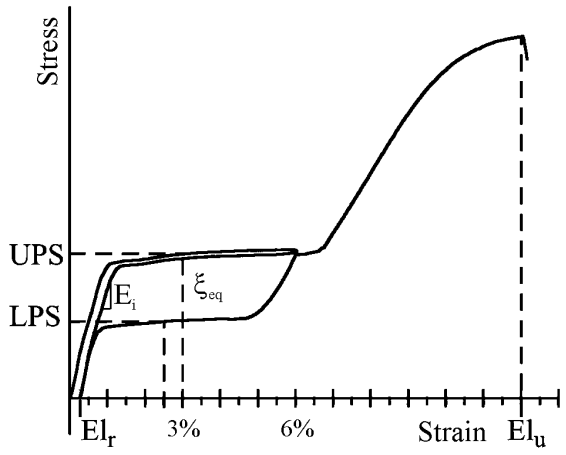


Figure 2-19 Typical stress-strain response of Nickel-Titanium SMA bars (ASTM 2014)

Table 2-1 Properties of large diameter SMA bars at room temperature (Yin et al. 2015)

Property	Value
Upper plateau stress	400-550 MPa
Elastic modulus	40-75 GPa
Ultimate tensile stress	1100-1400 MPa
Ultimate elongation	15-20%

Piedboeuf et al. (1998) conducted thermo-mechanical analyses to investigate the effect of loading frequency, strain amplitude, and temperature on the hysteretic energy dissipation and damping of superelastic NiTi SMA wires. Experimental results demonstrated that increases in temperature, specifically ambient temperatures, has a small effect on hysteretic energy dissipation, but it slightly increases damping of superelastic NiTi SMAs (Figure 2-20). Increases in strain amplitude increased hysteretic energy and damping of the wires (Figure 2-20). Both hysteretic energy and damping decreased with increase of loading frequency due to the change of temperature during the phase transformation (Figure 2-21). Piedboeuf et al. developed a model, based on a Fourier sine series, to determine the dynamic response of NiTi SMAs, including hysteretic energy and damping. The input parameters of the model are loading frequency, strain amplitude, and temperature.

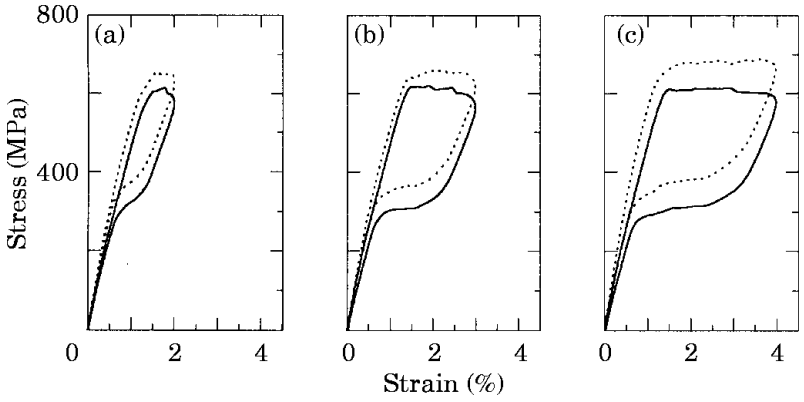


Figure 2-20 Stress-strain responses of NiTi wires tested at loading frequency of 0.1 Hz, 25ºC (solid line) and 35 ºC (dotted line), and different strain amplitudes (Piedboeuf et al. 1998): (a) 2% strain; (b) 3% strain; and (c) 4% strain

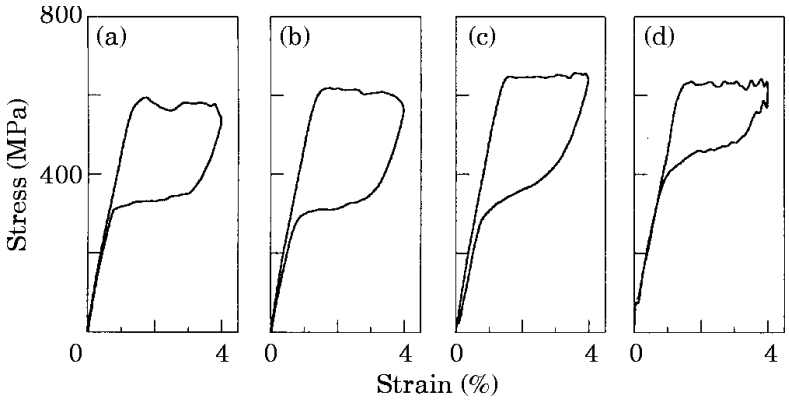


Figure 2-21 Stress-strain responses of NiTi wires tested at 25°C, 4% strain, and different loading frequencies (Piedboeuf et al. 1998): (a) 0.01 Hz; (b) 0.1 Hz; (c) 1 Hz; and (d) 10 Hz

Dolce and Cardone (2001a; b) tested NiTi SMAs to study the mechanical behaviour of NiTi SMAs and the potential use for seismic applications. Wires and bars with sizes ranging from 1 mm to 30 mm in diameter and different physical characteristics were subjected to cycling loading with variable strain rate and amplitude, temperature, and cyclic repetition. Superelastic NiTi bars experienced stable and repeatable cyclic behaviour, specifically after the initial cycle to a determined strain amplitude, with low equivalent damping in the range of 5% to 6% and negligible residual deformation. The experimental results corroborated the findings of Piedboeuf et al. (1998) in regards to the effect of strain rate, strain amplitude, and temperature on the energy dissipation capacity and equivalent damping of NiTi SMAs. Dolce and Cardone stated that although the change of ambient temperature on the mechanical properties of NiTi SMAs is significant (Figure 2-22), specifically on equivalent damping, temperature sensitivity is comparable to that of other materials used for seismic devices.

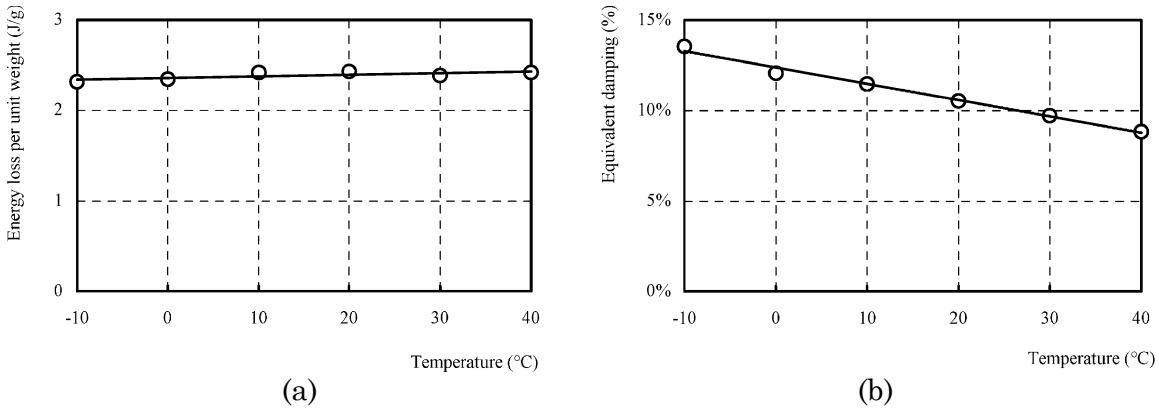


Figure 2-22 Effect of ambient temperature on the hysteretic properties of superelastic NiTi wires (Dolce and Cardone 2001b): (a) energy loss per unit weight (hysteretic energy dissipation); and (b) equivalent damping

DesRoches et al. (2004) evaluated the properties of superelastic NiTi wires and bars for the use in seismic applications. The experimental program consisted of cyclic testing of 1.8 mm-diameter wires and 25.4 mm-diameter bars. Both wires and bars experienced superelastic behaviour with well-defined upper and lower plateaus and excellent strain recovery when loading up to 6% strain (Figure 2-23). The stress-strain response of the wires displayed wider hysteretic loops with corresponding greater energy dissipation. The wires and bars experienced damping of 2% and 8%, respectively. Straining beyond 6% strain reduced re-centering and damping. The results suggested that despite the low damping, the re-centering and the energy dissipation properties make superelastic NiTi SMAs suitable for seismic applications.

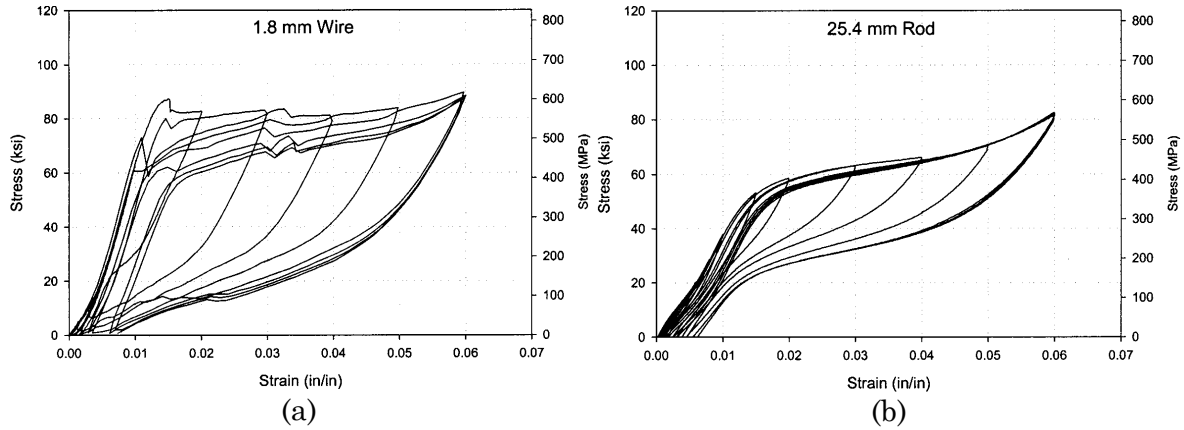


Figure 2-23 Stress-strain response of superelastic SMAs (DesRoches et al. 2004): (a) 1.8 mm-diameter wires; and (b) 25.4 mm-diameter bars

Nemat-Nasser and Guo (2006) further investigated the thermo-mechanical characteristics of superelastic NiTi SMAs. Quasi-static (cyclic) and dynamic compressive testing of cylindrical samples demonstrated the effect of temperature and loading strain rate on the behaviour of superelastic NiTi. The stress-strain response was dependent on the annealing temperature, which is an important factor for the manufacture and engineering of the material. Higher annealing temperatures resulted in less superelasticity. Repetitions of cyclic loading lead to stable superelastic response with minimum energy dissipation and maximum residual strain (Figure 2-24). This effect was smaller for repeated dynamic loading. Increases in temperature resulted in increased upper stress plateau and residual strain. The superelasticity behaviour, however, remained unchanged for ambient temperatures, from 296K (23ºC) to 326K (53ºC) (Figure 2-25). For strain rates in the order of 10^{-3}/s to 2100/s, the stress-strain material displayed well-defined superelasticity properties, specifically the shape of the loading branch. [Note that typical strain rates due to seismic loading are within this range (Riisgaard et al. 2007).] At higher strain rates, the material tends to lose superelasticity and behave as common austenite metals with non-recoverable plastic response.

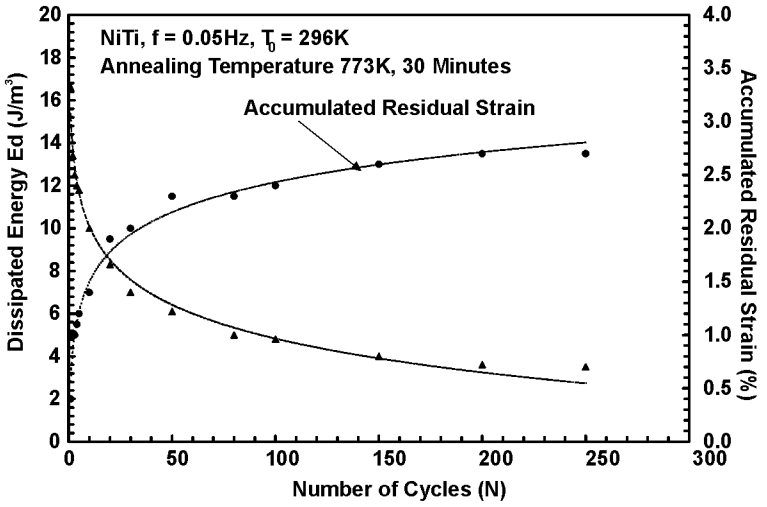


Figure 2-24 Energy dissipation and accumulated residual strain in repeated cycling loading (Nemat-Nasser and Guo 2006)

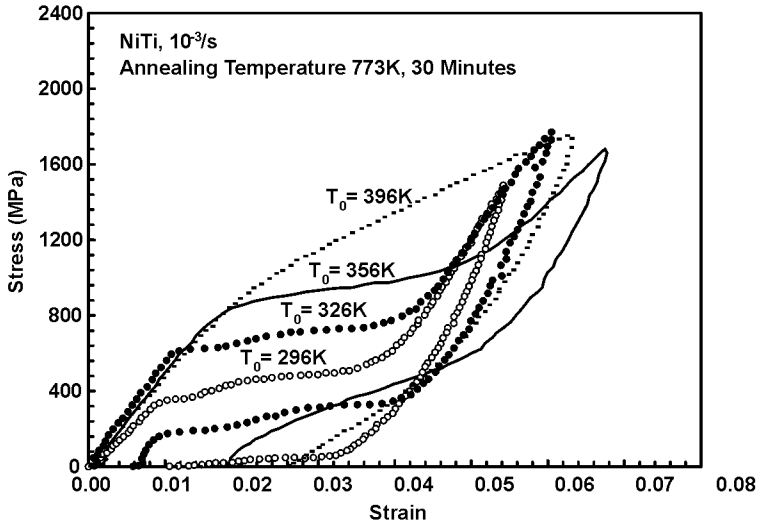


Figure 2-25 Stress-strain response of superelastic NiTi at 10^{-3}/s strain rate and different temperatures (Nemat-Nasser and Guo 2006)

Tyber et al. (2007) and McCormick et al. (2007) conducted a study on NiTi SMA bars with different diameters (12.7 mm, 19.1 mm, and 31.8 mm), length scales, and heat treatments (annealing). The study focused on the effects on crystal structure, thermal transformation behaviour, and mechanical performance. The results demonstrated important behavioural trends (Figure 2-26). Transformation stresses and hardness were dependent on the heat treatment. Forward transformation stress decreased with increase of the repetitions of cyclic loading. The thermo-mechanical properties were not affected by the size of the bars. Re-centering capabilities and equivalent damping, however, decreased with increase of bar size. Furthermore, full-scale specimens experienced lower upper plateau stress, larger residual strain, and less equivalent damping than reduced-area specimens. McCormick et al. suggested that low equivalent damping (below 7%) limits SMA bars for pure damping applications.

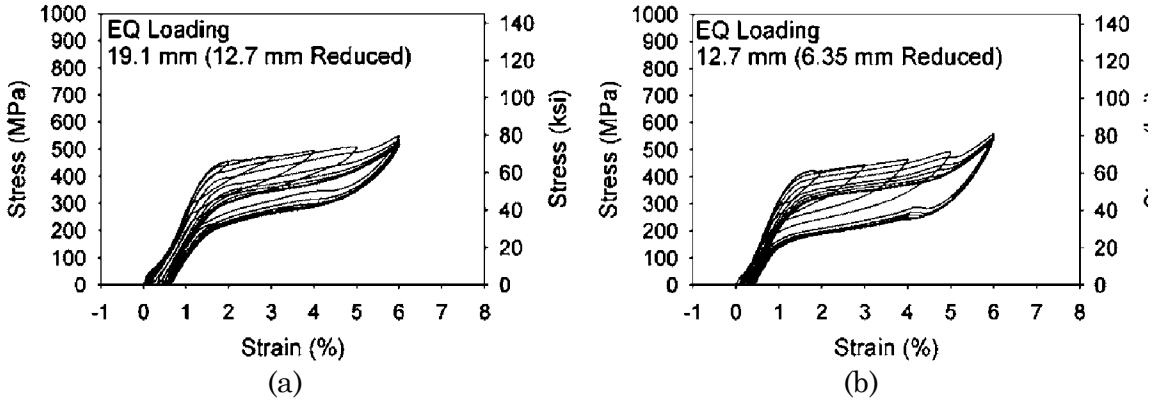


Figure 2-26 Stress-strain response of superelastic NiTi bars (McCormick et al. 2007): (a) 19.1-mm diameter; and (b) 12.7-mm diameter

2.4.2 Reinforcing of Concrete Structures

Numerous research and field projects have implemented SMAs in civil engineering structures (Alam et al. 2007; Janke et al. 2005; Song et al. 2006). The applications include damping, isolation, active control, bracing, restraining, reinforcing and post-tensioning, pre-stressing of fibres in concrete, re-centering and self-rehabilitation, and sensing of new and existing structures. Among these applications, the use of superelastic NiTi SMAs as a reinforcing alternative to improve seismic behaviour of reinforced concrete structures constitutes a major area of research. Research on the retrofit of reinforced concrete structures is in the early stages.

2.4.2.1 Concrete Columns

Saiidi and Wang (2006) and Nakashoji and Saiidi (2014) investigated superelastic NiTi SMAs rods and Engineered Cementitious Composites (ECC) to reduce the residual displacement in columns. Quarter-scale concrete columns were tested under dynamic loading (Figure 2-27). The experimental results demonstrated that reinforcing with SMA rods improved recovery of the plastic deformations and that repairing with ECC reduced the damage of concrete. The columns were governed by the response of the SMA, resulting in a curvilinear envelope response that fit a tri-linear force-displacement relationship. A proposed tri-linear hysteretic model, incorporated in program SAP2000, predicted the monotonic and dynamic responses of

the columns. The predictions were in good agreement with the experimental results. Further analyses were conducted with the finite element program OpenSees (Tazarv and Saiidi 2015). A hysteretic relationship, based on tri-linear loading-unloading envelopes with constant loading and unloading stiffness and zero residual strain, was implemented to model the SMA rods (Figure 2-28). Pushover analyses captured the envelope of the force-displacement response of the columns but not the residual displacements.

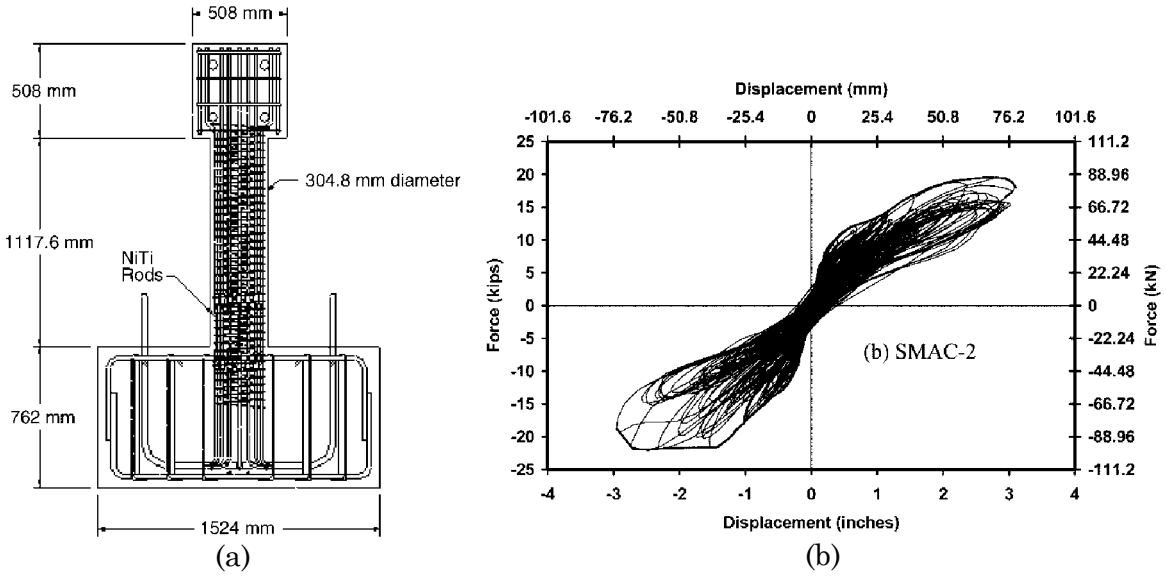


Figure 2-27 Column reinforced with NiTi SMA (Saiidi and Wang 2006): (a) column details; and (b) reverse cyclic response of SMA-reinforced column

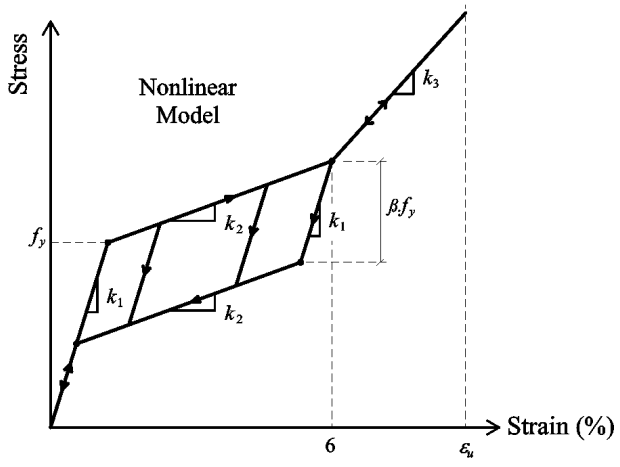


Figure 2-28 Model for SMA (Tazarv and Saiidi 2015)

2.4.2.2 Concrete Beams

Saiidi et al. (2007) tested concrete beams reinforced with superelastic NiTi SMA rods under cycling loading. The flexural reinforcement of the beams consisted of external, 254 mm-long NiTi rods coupled to steel rods with stiff steel plates at the centre of beams (Figure 2-29). The beams reinforced with NiTi SMA rods experienced less than one-fifth of the residual displacement experienced by companion beams reinforced with steel. Reinforcing with SMA, however, resulted in lower stiffness. Proposed hybrid reinforcement alternatives combining SMA with ductile steel and SMA with FRP were analytically investigated to assess improvements in the stiffness of SMA-reinforced beams. The analyses predicted the monotonic response of the beams based on the moment-curvature of the cross-section. The analytical results suggested that beams with hybrid reinforcement could experience partial displacement recovery while sustaining strength and stiffness comparable to those of steel-reinforced beams (Figure 2-30).

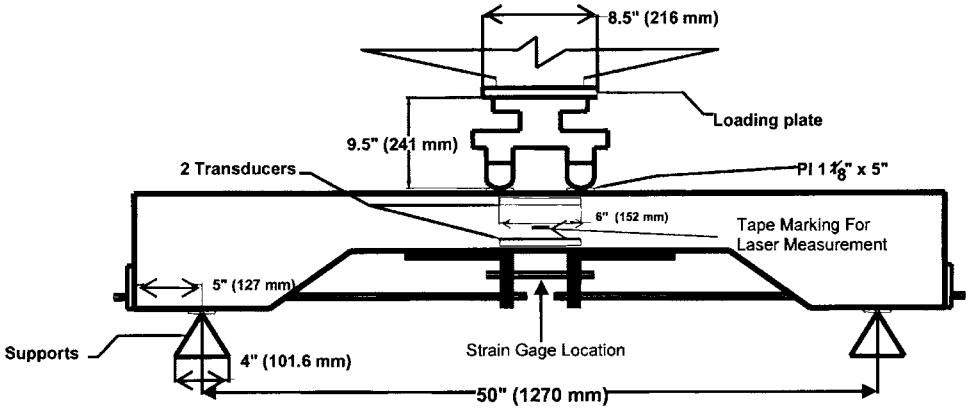


Figure 2-29 Beam reinforced with NiTi SMA (Saiidi et al. 2007)

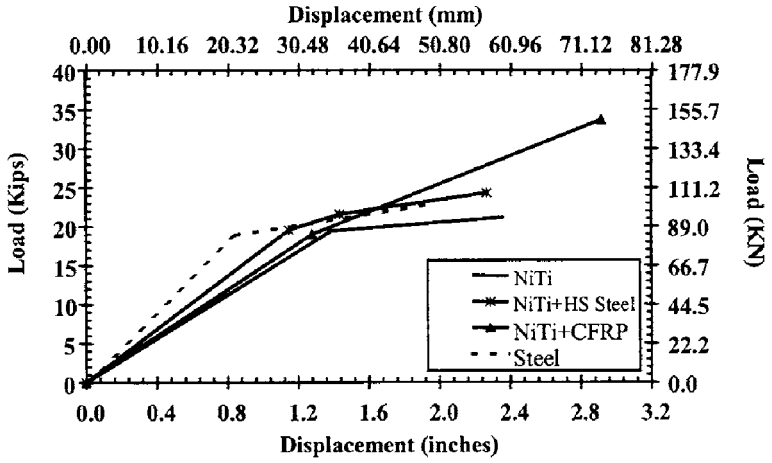


Figure 2-30 Load-displacement response of beams (Saiidi et al. 2007)

Abdulridha et al. (2013) tested concrete beams reinforced with a hybrid reinforcing system combining superelastic NiTi SMA and ductile steel (Figure 2-31). Testing of the beams followed monotonic, cyclic, and reversed cyclic loading regimes. 12.7-mm-diameter SMA rods with a length of 600 mm were placed at the mid-span, in the plastic hinge region, and were coupled to 15M (diameter of 16 mm) deformed steel reinforcing bars using hexagonal threaded mechanical couplers. The SMA rods were reshaped to a diameter of 9.5 mm to ensure pseudo-yielding and rupture away from the couplers. The strength and ductility of the beams reinforced with SMA were comparable to steel-reinforced beams, while the residual displacements were significantly smaller (Figure 2-32). Smaller residual displacement, however, resulted in reduced energy dissipation. The response of the beams was satisfactorily simulated with the finite element program VecTor2 using a tri-linear SMA model with plastic offset (Figure 2-33).

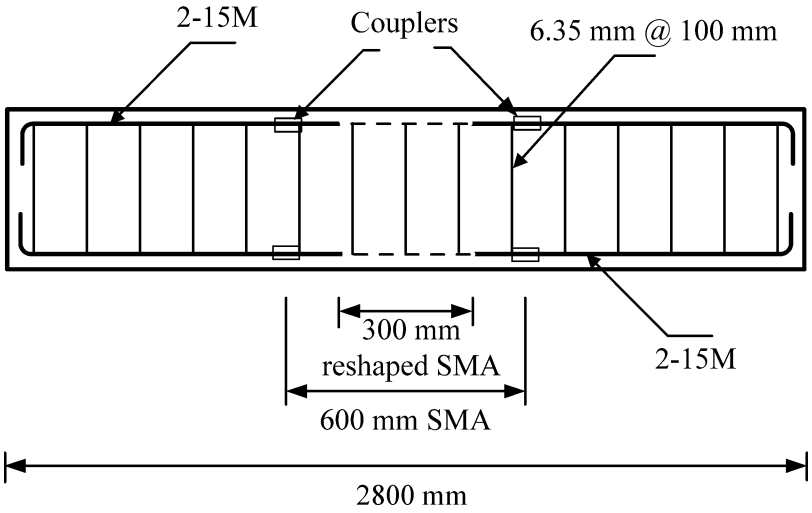


Figure 2-31 Concrete beams reinforced with NiTi SMA (Abdulridha et al. 2013)

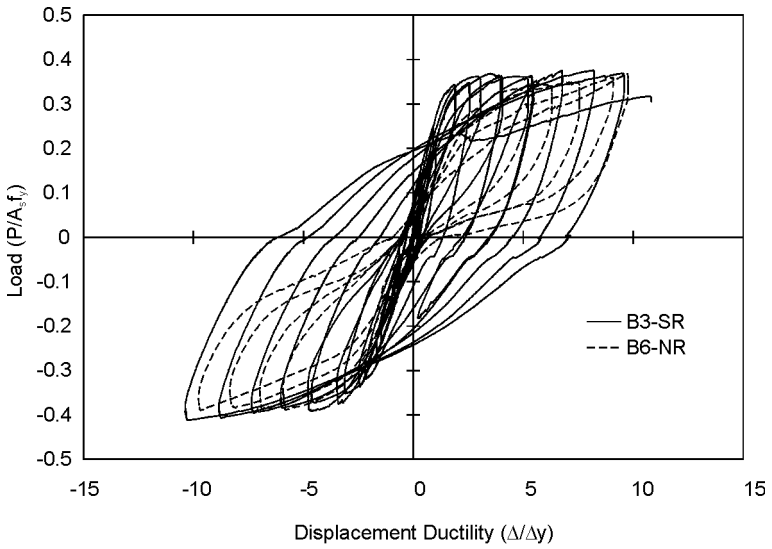


Figure 2-32 Response of SMA-reinforced (B6-NR) and steel-reinforced (B3-SR) beams (Abdulridha et al. 2013)

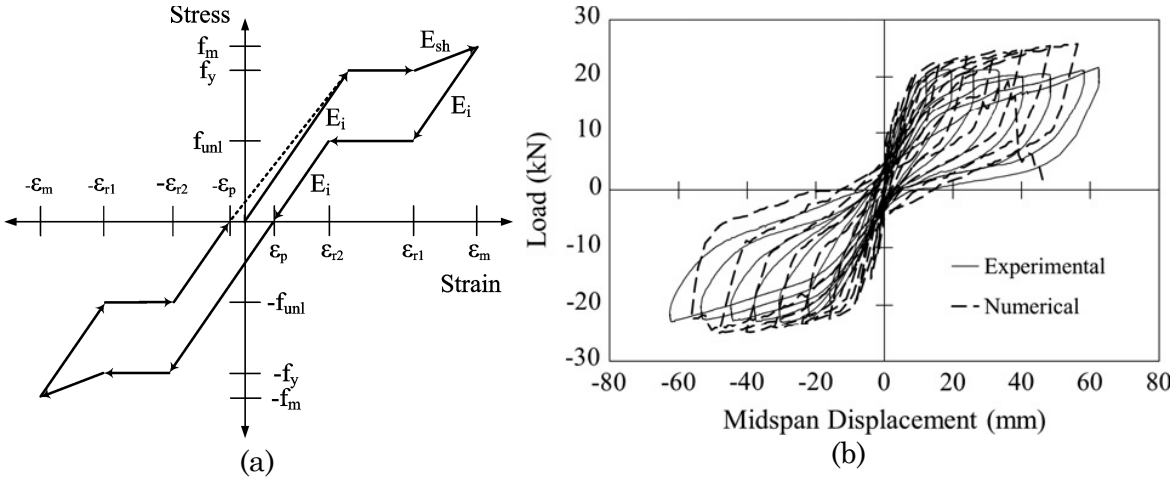
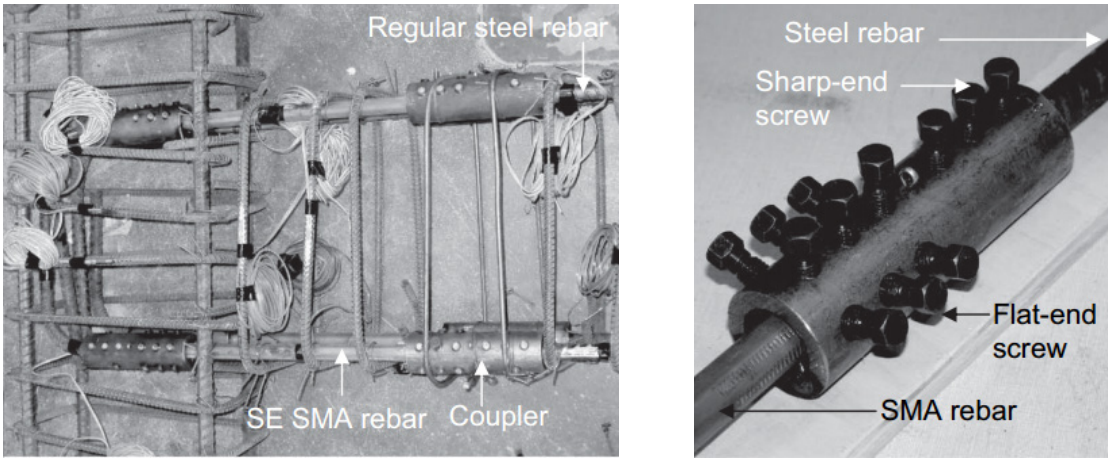


Figure 2-33 Simulation of SMA-reinforced beams (Abdulridha et al. 2013): (a) SMA tri-linear model with plastic offset; and (b) experimental and numerical responses of SMA-reinforced beam

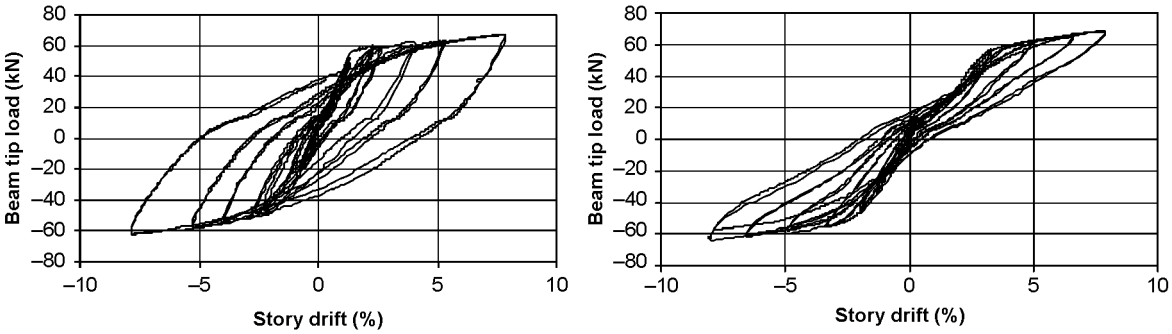
2.4.2.3 Concrete Beam-Column Joints

Youssef et al. (2008) tested a large-scale beam-column joint reinforced with an SMA-steel hybrid reinforcing system. Superelastic NiTi SMA bars coupled to reinforcing steel bars, using bar-lock couplers, reinforced the beams over the plastic hinge (Figure 2-34). Comparison of the experimental results with a companion steel-reinforced joint with comparable strength capacities demonstrated the benefits of using superelastic SMAs in concrete structures (Figure 2-35). The beam-column joint reinforced with SMA experienced less residual deformations than the companion beam-column joint reinforced with reinforcing steel. The energy dissipation, however, was less for the joint with the SMA. Low modulus of elasticity of the SMA bars (62.5 GPa) resulted in low initial stiffness, delay of yielding, and an increase of rotation of the beam. Furthermore, the SMA reinforcement promoted localized cracking away from the column face instead of the distributed cracking observed in steel-reinforced joints.



(a) (b)

Figure 2-34 Beam-column joint reinforced with superelastic SMA (Youssef et al. 2008): (a) reinforcement detail; and (b) SMA-steel coupling



(a) (b)

Figure 2-35 Response of beam-column joints (Youssef et al. 2008): (a) steel reinforcement; and (b) SMA-steel reinforcement

Alam et al. (2008) conducted nonlinear dynamic analyses of the beam-column joints tested by Youssef et al. (2008). Finite element models based on the fibre approach modelled the cross-section of the joints. A stress-strain relationship developed by Auricchio and Sacco (1997) modelled the NiTi SMA reinforcing bars (Figure 2-36). The SMA model is defined by the phase transformation stresses, the range of full recoverable strains, and the modulus of elasticity of the SMA. It accounts for differences in behaviour in tension and compression and considers full strain recovery. The analyses captured the response of the joints reinforced with SMA.

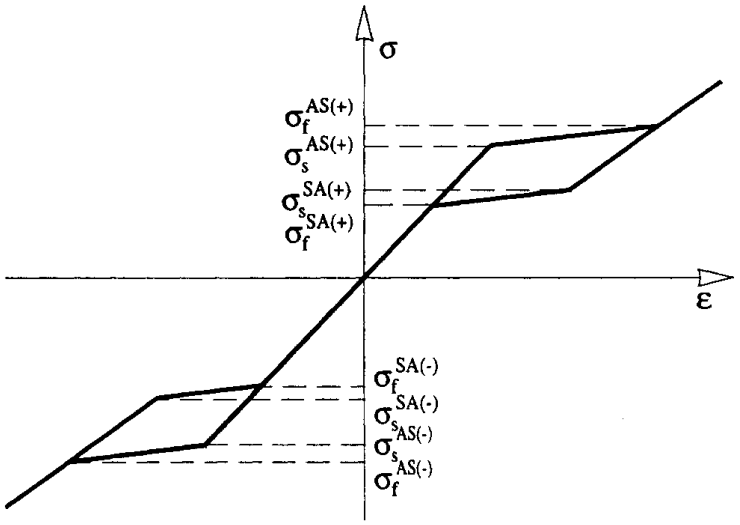


Figure 2-36 Model for superelastic shape memory alloys (Auricchio and Sacco 1997)

Nehdi et al. (2010) proposed a corrosion resistant hybrid SMA-FRP system for reinforcing beam-column joints. A beam-column joint incorporating the proposed reinforcing system was constructed with the same dimensions and similar material properties to the joints tested by Youssef et al. (2008). The joint was tested under reversed cyclic loading. The hybrid reinforcement consisted of superelastic NiTi SMA bars connected to FRP bars using a coupling device that combined single barrel bar-lock couplers (attached to the SMA) and epoxy-filled stainless steel pipes (attached to the FRP). The response of the joint compared well with that of a control joint reinforced with conventional steel, specifically the strength, the drift, and the energy dissipation (Figure 2-37). Re-centering, however, was not achieved due to significant slip of the SMA and FRP bars inside the couplers. The authors of this study acknowledged that a better SMA-FRP coupling system is necessary to improve the re-centering of the joint.

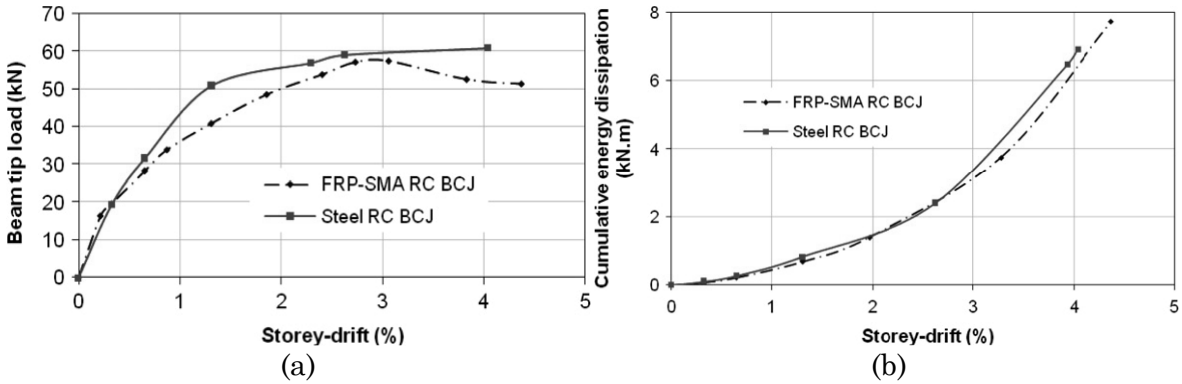


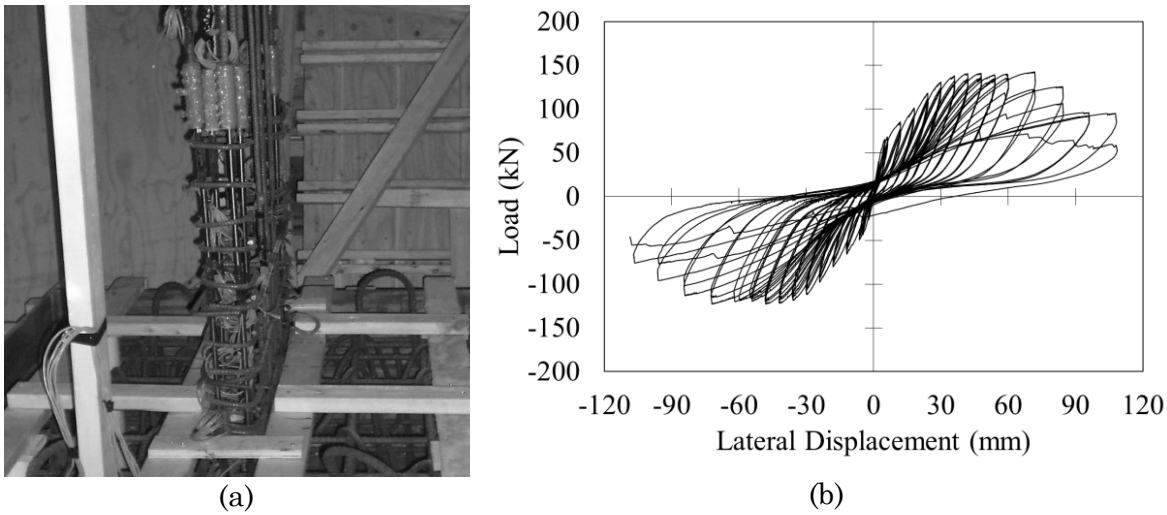
Figure 2-37 Response of beam-column joints (Nehdi et al. 2010): (a) envelope of load-drift response; and (b) energy dissipation

Billah and Alam (2012) conducted nonlinear dynamic analyses of beam-column joints reinforced with hybrid SMA-steel and SMA-FRP reinforcement. The stress-strain relationships for the hybrid reinforcement followed the model developed by Auricchio and Sacco (1997) (Figure 2-36). The analyses predicted reductions of residual drifts of up to 87% and considerable energy dissipation. The hybrid reinforcement with steel dissipated more energy than the reinforcement incorporating FRP.

2.4.2.4 Concrete Shear Walls

Abdulridha and Palermo (2014) tested a slender reinforced concrete shear wall reinforced with hybrid SMA-steel in the boundary columns (Figure 2-38). The SMA was concentrated within the plastic hinge, while reinforcing steel was placed in the remainder of the boundary zones. Bar-lock couplers connected the SMA to the reinforcing steel. Longitudinal and transverse deformed reinforcing bars were used to reinforce the web region. Loading of the wall followed a reversed cyclic regime. The wall sustained strength and ductility similar to that of a companion wall reinforced only with steel reinforcement. The SMA-reinforced wall experienced less residual deformation than the steel-reinforced wall. Wider and more localized cracking appeared as a result of limited bonding between the SMA rods and the concrete. The recovery properties of the SMA improved closing of the cracks. Stiffness prior to

yielding, however, was lower in the wall reinforced with SMA as a result of the lower modulus of elasticity of the SMA (approximately 60 GPa).



(a) (b)

Figure 2-38 Shear walls reinforced with hybrid SMA-steel reinforcement (Abdulridha and Palermo 2014): (a) detail of hybrid SMA-steel reinforcement; and (b) response of SMA-reinforced wall

2.4.2.5 Concrete Frames

A few researches have conducted numerical studies on concrete frames reinforced with superelastic NiTi SMAs. Alam et al., (2009) and Youssef and Elfeki (2012) conducted dynamic analyses of concrete frame buildings reinforced with SMA rods along the plastic hinges at the interfaces of beams at columns. Modelling of the SMA bars conformed to a simplified superelastic SMA model developed by Auricchio and Sacco (1997) (Figure 2-36). Alam et al. considered SMA reinforcement in all the plastic hinges, while Youssef and Elfeki assessed seven SMA reinforcement layouts at critical sections. Zafar and Andrawes (2012) simulated the dynamic response of frames reinforced with composite bars consisting of SMA and FRP. A parallel material model, which combines a flag-shape response with zero residual strain for the SMA with a linear elastic response for the FRP, simulated the composite reinforcement in the finite element program OpenSees (Figure 2-39). In general, the numerical simulations demonstrated that frames reinforced with SMA sustained less inter-storey and top-storey residual drifts than comparable frames reinforced with steel.

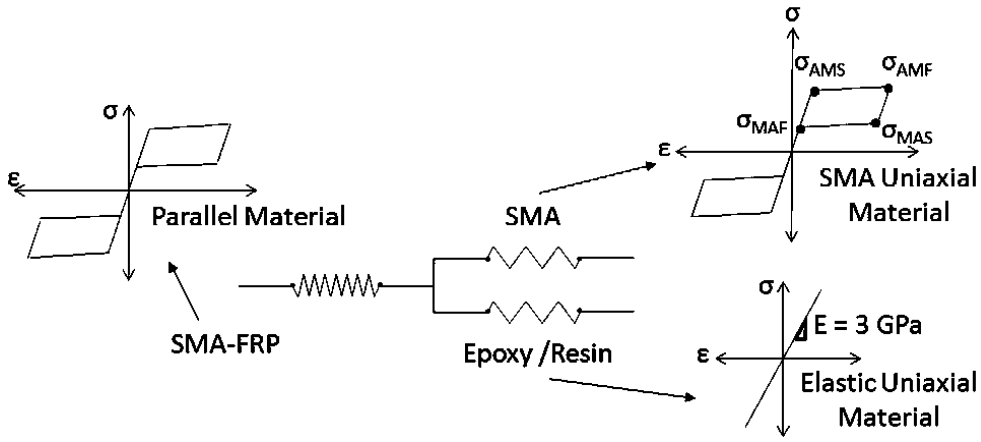


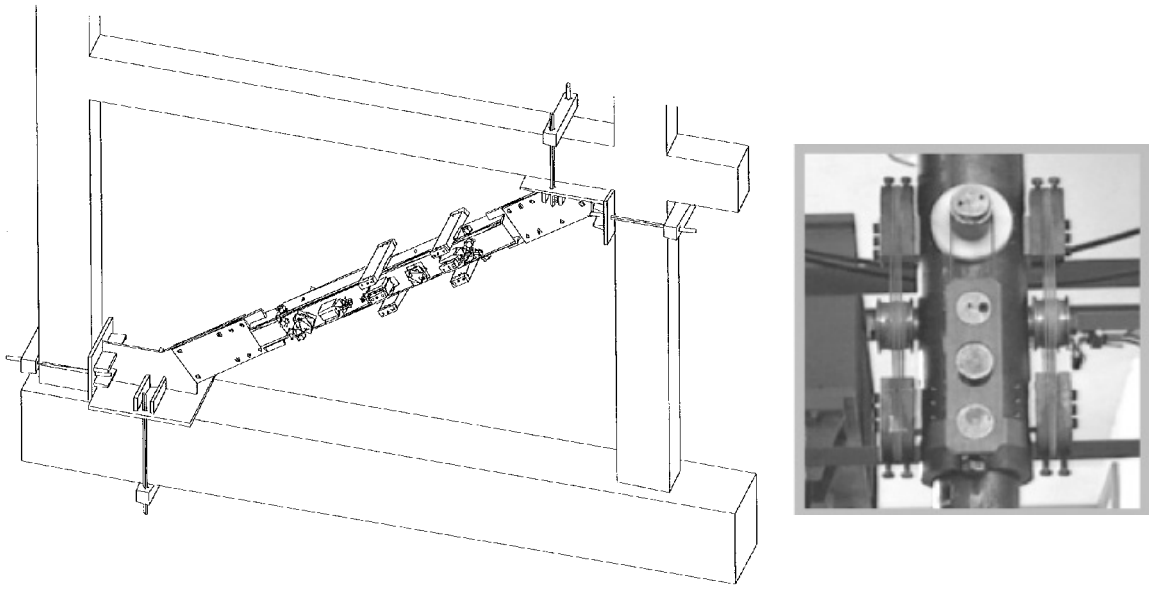
Figure 2-39 Model for composite SMA-FRP bars (Zafar and Andrawes 2012)

2.4.3 External Bracing of Concrete Structures

Bracing systems based on superelastic SMAs are feasible alternatives for active control of frame structures. Studies on steel frames have revealed that superelastic SMA braces increase stiffness, energy dissipation, and re-centering of structures (Lafortune et al. 2007; Salichs et al. 2001). Due to the hysteretic response with satisfactory energy dissipation and associated damping, SMA braces are very effective in controlling vibrations, specifically at large vibration amplitudes. Experimental and numerical results have indicated that SMA braces may exceed the energy dissipation capabilities of viscous dampers (Salichs et al. 2001). The re-centering effect of superelastic SMA braces increases with increase of elongations. Therefore, a strategy for increasing re-centering and energy dissipation of the structure is to pre-stress the braces (Lafortune et al. 2007). Another strategy for inducing larger strains on SMA braces, and therefore achieve greater re-centering benefits, is to shorten the SMA in the brace (Auricchio et al. 2006; McCormick et al. 2006). In addition to improvement in performance, optimization of the SMA substantially reduces the cost of the braces. Given the benefits of SMAs, few studies have proposed superelastic SMA bracing systems based on NiTi wires and bars for the retrofit and external reinforcement of reinforced concrete structures.

Dolce et al. (2000) developed heavy re-centering SMA braces based on tension-only NiTi SMA wires (Figure 2-40). The braces were designed to increase strength,

stiffness, and energy dissipation while improving re-centering of frame structures. Superelastic SMA wires provided re-centering and energy dissipation, while shape-memory-effect SMA bars provided energy dissipation only. Three configurations of the SMA components with different levels of pre-straining produced flag-shaped responses with variable displacement recoveries and energy dissipation capacities. This feature permits unique adjustments of response to specific retrofitting needs. The SMA braces reduced the inter-storey drifts and the shear forces in the columns of three-storey concrete frames tested under dynamic loading (Dolce et al. 2005).



(a) (b)

Figure 2-40 SMA brace (Dolce et al. 2000): (a) braces installed in reinforced concrete frame; and (b) detail of re-centering device with superelastic NiTi wires

Effendy et al. (2006) investigated the effect of external SMA reinforcement on squat barbell-shaped shear walls subjected to reverse cyclic loading. Shear walls were externally reinforced with bi-diagonal shape memory effect and superelastic SMA bars that replaced internal steel reinforcement (Figure 2-41(a)). The SMA bars improved the strength capacity and re-centering, specifically for the walls reinforced with superelastic SMA (Figure 2-41(b)). Ductility was approximately the same as that of a control wall reinforced with conventional internal steel. The SMA-reinforced walls, however, experienced post-peak stiffness and strength degradation associated with an increase of flexural capacity. The long diagonal SMA bars buckled during

testing, limiting the performance of the shear walls and the benefit of the SMA in terms of energy dissipation and damage reduction (Figure 2-41(a)).

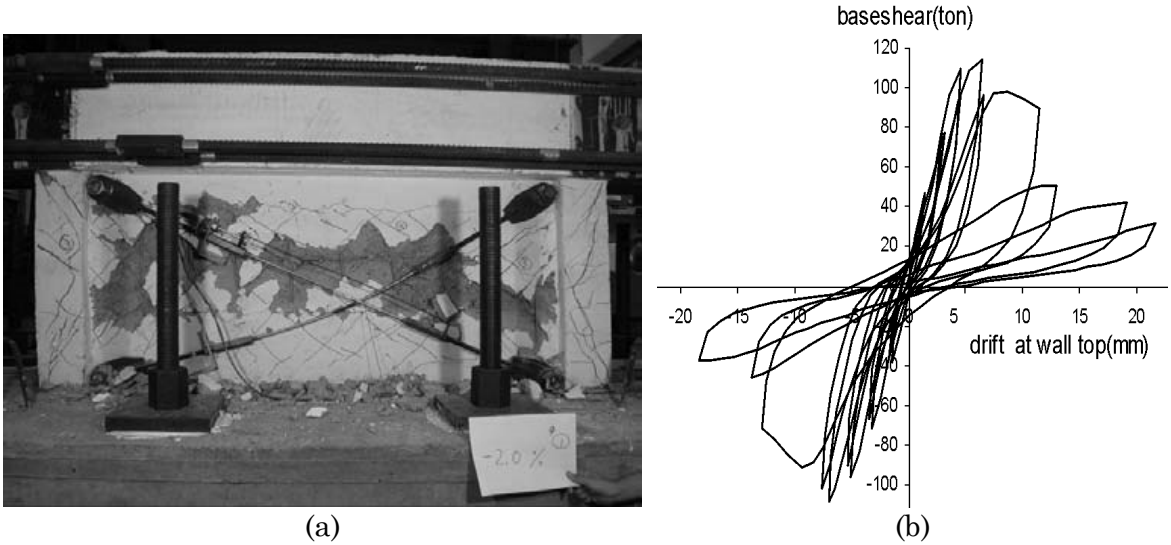


Figure 2-41 Shear wall reinforced with external SMA bars (Effendy et al. 2006): (a) damage of wall; and (b) load-displacement response of wall reinforced with superelastic SMA

2.5 Summary

Shear walls highly contribute to strength, stiffness, and drift control of buildings. Given these benefits, numerous studies have focused on the seismic performance of these structural elements. For deficient buildings, retrofitting of shear walls is a viable strategy to improve seismic performance. The available techniques range from simple concrete replacement to the addition of emerging materials such as Shape Memory Alloys (SMAs).

The performance of retrofitted squat shear walls depends on the retrofitting technique. Replacement of concrete and addition of reinforcing steel results in restoring of strength and ductility capacities but do not typically restore initial stiffness. External steel plates are effective in restoring specific parameters such as stiffness, strength, and ductility; however, yielding of the steel at large displacement demands results in extensive damage and permanent deformations. Retrofitting with steel plates requires heavy steel sections with lack of corrosion resistance. In recent years, steel plates have been gradually replaced by external bonding of Fibre

Reinforced Polymers (FRP). The advantage of FRP is the high tensile strength of very thin and light layers of the material and the longer durability. FRP retrofitting strategies can improve strength, as long as adequate bonding is ensured. The contribution to ductility and energy dissipation is minimal due to the linear stress-strain response of FRP. Given the thin layers of the material used for retrofit, FRP applications are not suitable for restoring stiffness. Similar to retrofitting strategies with steel plates, shear walls retrofitted with FRP sustain significant damage and permanent residual deformations. Other retrofitting techniques aim to improve the seismic response through a flag-shaped hysteretic response with sufficient strength, ductility, energy dissipation capacity, and recovery. One such technique is structural weakening in which shear walls are cut and supplied with ductile elements. Flag-shaped response is also realized with smart Shape Memory Alloys (SMAs) capable of recovering deformations.

Shape memory alloys have been used as internal reinforcement for new concrete elements. Experimental and numerical studies have demonstrated that superelastic NiTi SMAs improve re-centering and provide adequate energy dissipation while mitigating residual damage. Application of SMAs on squat reinforced concrete shear walls, however, is limited. The only documented study was focused on external reinforcement with diagonal braces based on long SMA bars. In this application, small straining of the long bars did not engage the full benefit of the SMA in terms of energy dissipation and re-centering. Other applications have involved the use of large-scale bracing systems based on NiTi SMA wires and bars. The implementation of wires required complex tension-compression mechanisms that impose difficulties in fabrication and installation in the field. Braces based on bars considered reduced-length slender SMA elements to optimize the material and exploit the strain range of full recovery. These SMA elements are prone to reduced strength capacity due to buckling.

The SMA lightweight bracing system proposed herein addresses deficiencies of existing retrofitting techniques for squat reinforced concrete shear walls. In addition to increases in strength and ductility, the bracing system improves re-centering and energy dissipation capacity, while mitigating shear-related damage. The bracing

system incorporates optimized superelastic SMA components with reduced length and large strain capacity that overcome current technical and economic challenges in the design and construction of SMA braces. These SMA components are envisioned as replaceable and resettable fuses that can retrofit a range of structural elements.

Few researchers have conducted numerical studies on retrofitting of squat reinforced concrete shear walls using truss models and the finite element method (FEM) to predict the force-displacement response. The truss models have performed well in predicting the strength and failure mode, but have been inadequate in satisfactorily predicting other salient features such as ductility and hysteretic response. The FEM has successfully captured salient features of hysteretic response, including progressive damage. Phenomenological superelastic SMA models with full strain recovery capacity and plastic strain offset have been able to simulate the behaviour of SMA bars and predict the response of SMA-reinforced concrete structures. Therefore, the FEM is a reliable tool for the design and development of the proposed retrofitting system based on superelastic NiTi SMAs.

2.6 References

Abdulridha, A., and Palermo, D. (2014). "Response of a hybrid SMA reinforced concrete shear wall." *Tenth U.S. National Conference on Earthquake Engineering*, Network for Earthquake Engineering Simulation (distributor), Anchorage, AK, USA.

Abdulridha, A., Palermo, D., Foo, S., and Vecchio, F. J. (2013). "Behavior and modeling of superelastic shape memory alloy reinforced concrete beams." *Engineering Structures*, 49, 893–904.

Alam, M. S., Nehdi, M., and Youssef, M. A. (2009). "Seismic performance of concrete frame structures reinforced with superelastic shape memory alloys." *Smart Structures and Systems*, 5(5), 565–585.

Alam, M. S., Youssef, M. A., and Nehdi, M. (2007). "Utilizing shape memory alloys to enhance the performance and safety of civil infrastructure: a review." *Canadian Journal of Civil Engineering*, 34(9), 1075–1086.

Alam, M. S., Youssef, M. A., and Nehdi, M. (2008). "Analytical prediction of the seismic behaviour of superelastic shape memory alloy reinforced concrete elements." *Engineering Structures*, 30(12), 3399–3411.

Antoniades, K. K., Salonikios, T. N., and Kappos, A. J. (2003). "Cyclic tests on seismically damaged reinforced concrete walls strengthened using fiber-reinforced polymer reinforcement." *ACI Structural Journal*, 100(4), 510–518.

Antoniades, K. K., Salonikios, T. N., and Kappos, A. J. (2005). "Tests on seismically damaged reinforced concrete walls repaired and strengthened using fiber-reinforced polymers." *Journal of Composites for Construction*, 9(3), 236–246.

ASTM. (2014). *ASTM F2516-14 Standard test method for tension testing of nickel-titanium superelastic materials*. ASTM International, West Conshohocken, PA, USA.

Auricchio, F., Fugazza, D., and DesRoches, R. (2006). "Earthquake performance of steel frames with Nitinol braces." *Journal of Earthquake Engineering*, 10(spec01), 45–66.

Auricchio, F., and Sacco, E. (1997). "A superelastic shape-memory-alloy beam model." *Journal of Intelligent Material Systems and Structures*, 8(6), 489–501.

Billah, A. H. M. M., and Alam, M. S. (2012). "Seismic performance of concrete columns reinforced with hybrid shape memory alloy (SMA) and fiber reinforced polymer (FRP) bars." *Construction and Building Materials*, 28(1), 730–742.

Christopoulos, C., Filiatrault, A., and Folz, B. (2002). "Seismic response of self-centring hysteretic SDOF systems." *Earthquake Engineering & Structural Dynamics*, 31(5), 1131–1150.

Cortés-Puentes, W. L. (2009). "Nonlinear modelling and analysis of repaired and retrofitted shear walls." M.Sc. Thesis, Dept. of Civil Engineering, University of Ottawa, Ottawa, ON, Canada.

Cortés-Puentes, W. L., and Palermo, D. (2011). "Modelling seismically repaired and retrofitted reinforced concrete shear walls." *Computers and Concrete*, 8(5), 541–561.

Cortés-Puentes, W. L., and Palermo, D. (2012). "Modeling of RC shear walls retrofitted with steel plates or FRP sheets." *Journal of Structural Engineering*, 138(5), 602–612.

Cruz-Noguez, C. A., Lau, D. T., Sherwood, E. G., Hiotakis, S., Lombard, J., Foo, S., and Cheung, M. (2015). "Seismic behavior of RC shear walls strengthened for in-plane bending using externally bonded FRP sheets." *Journal of Composites for Construction*, 19(1), 04014023.

DesRoches, R., McCormick, J., and Delemont, M. (2004). "Cyclic properties of superelastic shape memory alloy wires and bars." *Journal of Structural Engineering*, 130(1), 38–46.

Dolce, M., and Cardone, D. (2001a). "Mechanical behaviour of shape memory alloys for seismic applications 1. Martensite and austenite NiTi bars subjected to torsion." *International Journal of Mechanical Sciences*, 43(11), 2631–2656.

Dolce, M., and Cardone, D. (2001b). "Mechanical behaviour of shape memory alloys for seismic applications 2. Austenite NiTi wires subjected to tension." *International Journal of Mechanical Sciences*, 43(11), 2657–2677.

Dolce, M., Cardone, D., and Marnetto, R. (2000). "Implementation and testing of passive control devices based on shape memory alloys." *Earthquake Engineering & Structural Dynamics*, 29(7), 945–968.

Dolce, M., Cardone, D., Ponzo, F. C., and Valente, C. (2005). "Shaking table tests on reinforced concrete frames without and with passive control systems." *Earthquake Engineering & Structural Dynamics*, 34(14), 1687–1717.

Effendy, E., Liao, W. I., Song, G., Mo, Y. L., and Loh, C. H. (2006). "Seismic behavior of low-rise shear walls with SMA bars." *Earth & Space 2006: Engineering, Construction, and Operations in Challenging Environment*, American Society of Civil Engineers, Houston, TX, USA, 1–8.

Elnashai, A. S., and Pinho, R. (1998). "Repair and retrofitting of RC walls using selective techniques." *Journal of Earthquake Engineering*, 2(4), 525–568.

El-Sokkary, H., and Galal, K. (2013). "Seismic behavior of RC shear walls strengthened with fiber-reinforced polymer." *Journal of Composites for Construction*, 17(5), 603–613.

El-Sokkary, H., Galal, K., Ghorbanirenani, I., and Léger, P. (2013). "Shake table tests on FRP-rehabilitated RC shear walls." *Journal of Composites for Construction*, 17(1), 79–90.

Fiorato, A. E., Oesterle, R. G., and Corley, W. G. (1983). "Behavior of earthquake resistant structural walls before and after repair." *ACI Journal*, 80(5), 403–413.

Haroun, M., Pardoen, G., Bhatia, H., Shahi, S., and Kazanjy, R. (2000). "Structural behavior of repaired pier walls structural behavior of repaired pier walls." *ACI Structural Journal*, 97(2), 259–267.

Hsiao, F. P., Wang, J. C., and Chiou, Y. J. (2008). "Shear strengthening of reinforced concrete framed shear walls using CFRP strips." *The 14th World Conference on Earthquake Engineering*, Beijing, China.

Ireland, M. G., Pampanin, S., and Bull, D. (2007). "Experimental investigations of a selective weakening approach for the seismic retrofit of R.C. walls." *The NZSEE 2007 Annual Conference*, Palmerston North, New Zealand.

Janke, L., Czaderski, C., Motavalli, M., and Ruth, J. (2005). "Applications of shape memory alloys in civil engineering structures - Overview, limits and new ideas." *Materials and Structures*, 38(279), 578–592.

Khalil, A., and Ghobarah, A. (2005). "Behaviour of Rehabilitated Structural Walls." *Journal of Earthquake Engineering*, 9(3), 371–391.

Kobayashi, K. (2005). "Innovative application of FRPs for seismic strengthening of RC shear wall." *SP-230: 7th International Symposium on Fiber-Reinforced (FRP) Polymer Reinforcement for Concrete Structures*, American Concrete Institute, Kansas City, MO, USA, 1269–1288.

Lafortune, P., McCormick, J., DesRoches, R., and Terriault, P. (2007). "Testing of superelastic recentering pre-strained braces for seismic resistant design." *Journal of Earthquake Engineering*, 11(3), 383–399.

Lefas, I. D., and Kotsovos, M. D. (1990). "Strength and deformation characteristics of reinforced concrete walls under load reversals." *ACI Structural Journal*, 87(6), 716–726.

Lefas, I. D., Kotsovos, M. D., and Ambraseys, N. N. (1990). "Behavior of Reinforced Concrete Structural Walls: Strength, Deformation Characteristics, and Failure Mechanism." *ACI Structural Journal*, 87(1), 23–31.

Lombard, J., Lau, D. T., Humar, J. L., Foo, S., and Cheung, M. S. (2000). "Seismic strengthening and repair of reinforced concrete shear walls." *12th World Conference on Earthquake Engineering*, Auckland, New Zealand, 2032–1–2032–8.

McCormick, J., DesRoches, R., Fugazza, D., and Auricchio, F. (2006). "Seismic vibration control using superelastic shape memory alloys." *Journal of Engineering Materials and Technology*, 128(3), 294–301.

McCormick, J., Tyber, J., DesRoches, R., Gall, K., and Maier, H. J. (2007). "Structural engineering with NiTi. II: mechanical behavior and scaling." *Journal of Engineering Mechanics*, 133(9), 1019–1029.

Melton, K. N. (1990). "Ni-Ti based shape memory alloys." *Engineering Aspects of Shape Memory Alloys*, Butterworth-Heinemann, 21–35.

Melton, K. N., and Harrison, J. D. (1994). "Corrosion of NiTi based shape memory alloys." *1st International Conference on Shape Memory and Superelastic Technologies*, ASM International, Pacific Grove, CA, USA.

Nakashoji, B., and Saiidi, M. S. (2014). *Seismic performance of square nickel-titanium reinforced ECC columns with headed couplers*. Report, University of Nevada, Reno, NV, USA.

Nehdi, M., Alam, M. S., and Youssef, M. A. (2010). "Development of corrosion-free concrete beam–column joint with adequate seismic energy dissipation." *Engineering Structures*, 32(9), 2518–2528.

Nemat-Nasser, S., and Guo, W.-G. (2006). "Superelastic and cyclic response of NiTi SMA at various strain rates and temperatures." *Mechanics of Materials*, Shape Memory Alloys, 38(5–6), 463–474.

Palermo, D., and Vecchio, F. J. (2002). "Behavior of three-dimensional reinforced concrete shear walls." *ACI Structural Journal*, 99(1), 81–89.

Paulay, T. (1975). "Design aspects of shear walls for seismic areas." *Canadian Journal of Civil Engineering*, 2(3), 321–344.

Paulay, T. (1980). "Earthquake-resisting shearwalls - New Zealand design trends." *ACI Journal*, 77(3), 144–152.

Paulay, T., Priestley, M. J. N., and Synge, A. J. (1982). "Ductility in Earthquake Resisting Squat Shearwalls." *ACI Journal*, 79(4), 257–269.

Piedboeuf, M. C., Gauvin, R., and Thomas, M. (1998). "Damping behaviour of shape memory alloys: strain amplitude, frequency and temperature effects." *Journal of Sound and Vibration*, 214(5), 885–901.

Riisgaard, B., Ngo, T., Mendis, P., Georgakis, C., and Stang, H. (2007). "Dynamic increase factors for high performance concrete in compression using split Hopkinson pressure bar." *Fracture Mechanics of Concrete and Concrete Structures*, Catania, Italy.

Saiidi, M. S., Sadrossadat-Zadeh, M., Ayoub, C., and Itani, A. (2007). "Pilot study of behavior of concrete beams reinforced with shape memory alloys." *Journal of Materials in Civil Engineering*, 19(6), 454–461.

Saiidi, M. S., and Wang, H. (2006). "Exploratory study of seismic response of concrete columns with shape memory alloys reinforcement." *ACI Structural Journal*, 103(3), 436–443.

Salichs, J., Hou, Z., and Noori, M. (2001). "Vibration suppression of structures using passive shape memory alloy energy dissipation devices." *Journal of Intelligent Material Systems and Structures*, 12(10), 671–680.

Sittipunt, C., Wood, S. L., Lukkunaprasit, P., and Pattararattanakul, P. (2001). "Cyclic behavior of reinforced concrete structural walls with diagonal web reinforcement." *ACI Structural Journal*, 98(4), 554–562.

Song, G., Ma, N., and Li, H.-N. (2006). "Applications of shape memory alloys in civil structures." *Engineering Structures*, 28(9), 1266–1274.

Taghdi, M., Bruneau, M., and Saatcioglu, M. (2000a). "Seismic retrofitting of low-rise masonry and concrete walls using steel strips." *Journal of Structural Engineering*, 126(9), 1017–1025.

Taghdi, M., Bruneau, M., and Saatcioglu, M. (2000b). "Analysis and design of low-rise masonry and concrete walls retrofitted using steel strips." *Journal of Structural Engineering*, 126(9), 1026–1032.

Tazarv, M., and Saiidi, M. S. (2015). "Reinforcing NiTi superelastic SMA for concrete structures." *Journal of Structural Engineering*, 141(8), 04014197, 1–10.

Thermou, G. E., and Elnashai, A. S. (2006). "Seismic retrofit schemes for RC structures and local-global consequences." *Progress in Structural Engineering and Materials*, 8(1), 1–15.

Tyber, J., McCormick, J., Gall, K., DesRoches, R., Maier, H. J., and Maksoud, A. E. A. (2007). "Structural engineering with NiTi. I: basic materials characterization." *Journal of Engineering Mechanics*, 133(9), 1009–1018.

Van Humbeeck, J. (1991). "Cycling effects, fatigue and degradation of shape memory alloys." *Le Journal de Physique IV*, 01(C4), C4-189-C4-197.

Vecchio, F. J., and Bucci, F. (1999). "Analysis of repaired reinforced concrete structures." *Journal of Structural Engineering*, 125(6), 644–652.

Vecchio, F. J., Haro de la Peña, O. A., Bucci, F., and Palermo, D. (2002). "Behavior of repaired cyclically loaded shearwalls." *ACI Structural Journal*, 99(3), 327–334.

Wong, P. S., Vecchio, F. J., and Trommels, H. (2013). *VecTor2 and Formworks user's manual: second edition*. Manual, Dept. of Civil Engineering, University of Toronto, Toronto, ON, Canada.

Yin, W., Sczerzenie, F., Long, M., Belden, C., Manjeri, R. M., and Lafond, R. (2015). "Structure and properties of large diameter hot rolled NiTi bars for seismic applications." Presentation, New Hartford, NY, USA. Retrieved from http://www.memry.com/sites/default/files/documents/Weimin%20SMST2015%20Seismic%20Bars.pdf.

Youssef, M. A., Alam, M. S., and Nehdi, M. (2008). "Experimental investigation on the seismic behavior of beam-column joints reinforced with superelastic shape memory alloys." *Journal of Earthquake Engineering*, 12(7), 1205–1222.

Youssef, M. A., and Elfeki, M. A. (2012). "Seismic performance of concrete frames reinforced with superelastic shape memory alloys." *Smart Structures and Systems*, 9(4), 313–333.

Zafar, A., and Andrawes, B. (2012). "Incremental dynamic analysis of concrete moment resisting frames reinforced with shape memory composite bars." *Smart Materials and Structures*, 21(2), 025013, 1–14.

Chapter 3

SMA Tension Brace for Retrofitting Concrete Shear Walls

Authors: W. Leonardo Cortés-Puentes, Dan Palermo

Reference: Cortés-Puentes, W. L., and Palermo, D. (2017). "SMA tension brace for retrofitting concrete shear walls." Engineering Structures, 140, 177-188, DOI: 10.1016/j.engstruct.2017.02.045

Abstract

A Shape Memory Alloy (SMA) tension brace was developed as a retrofit device to improve the seismic response of deficient reinforced concrete squat shear walls. Three, tension-only SMA braces and two, companion tension-only steel braces were built and subjected to cyclic loading. The braces consisted of SMA and reinforcing steel links, respectively, placed at the centre of the bracing system and connected to rigid hollow structural steel members. A total of four links were utilized for testing: two SMA links and two reinforcing steel links. A superelastic, nickel-titanium rod, capable of recovering large nonlinear strains was used for one SMA link; while a nickel-titanium, shape-memory rod lacking the capacity to recover strains after the removal of load was used in the other SMA link. Deformed reinforcing steel bars that experience significant residual strains during the inelastic range of loading were incorporated into the steel links. Testing illustrated that the pseudo-yield and ultimate strengths, and energy dissipation capacity of the SMA braces were comparable to the steel braces. Furthermore, the SMA braces experienced superior elongation recovery. Testing and retesting of the SMA braces illustrated their potential to act as resettable

braces. Complementary nonlinear finite element analyses were conducted to assess the application of the braces to enhance the seismic response of reinforced concrete shear walls. The analyses demonstrated that the SMA braces can improve the lateral strength capacity, energy dissipation, and re-centering of reinforced concrete shear walls, while reducing strength and stiffness degradation associated with shear-related damage. [Supplementary details of the development of the SMA tension braces are presented in Appendix A.]

Keywords

Shape Memory Alloy; Tension-Only Braces; Seismic Retrofitting; Reinforced Concrete; Shear Walls; Testing; Numerical Analysis.

3.1 Introduction

A large stock of existing buildings designed and constructed prior to the enactment of seismic provisions that appeared in building codes during the 1970s and 80s lack sufficient reinforcement detailing. As a result, these buildings are vulnerable to current design-level earthquakes. Pre-1970s shear walls, therefore, may require retrofitting to improve the response to current seismic demands and to mitigate the potential damage. An emerging retrofit strategy, as suggested herein, incorporates Shape Memory Alloys (SMAs). SMAs are smart materials that recover their original shape (negligible residual deformations) with the application of heat or the removal of stress due to two-way, forward-reverse, transformation of the internal crystalline structure (DesRoches et al. 2004). Transformation due to heat is known as the shape memory effect, and transformation due to stress is known as the superelasticity effect. Both shape memory and superelastic SMAs have been investigated for civil engineering applications (Alam et al. 2007; Janke et al. 2005; Song et al. 2006). Superelastic SMAs are appealing as reinforcement and passive control due to the loading-unloading nature of earthquakes that benefits re-centering. In comparison to black carbon steel, superelastic SMAs recover substantially larger deformations, while sustaining similar stress levels. Superelastic SMAs, specifically nickel-titanium SMAs (Figure 3-1), typically recover up to 6% deformation, while carbon steels recover

only approximately 0.2%. The potential benefits of retrofitting concrete walls with superelastic SMAs include: increases in lateral strength, drift, and energy dissipation capacities; improvement in re-centering (reduction of permanent deformation); reduction of shear stresses; and mitigation of damage.

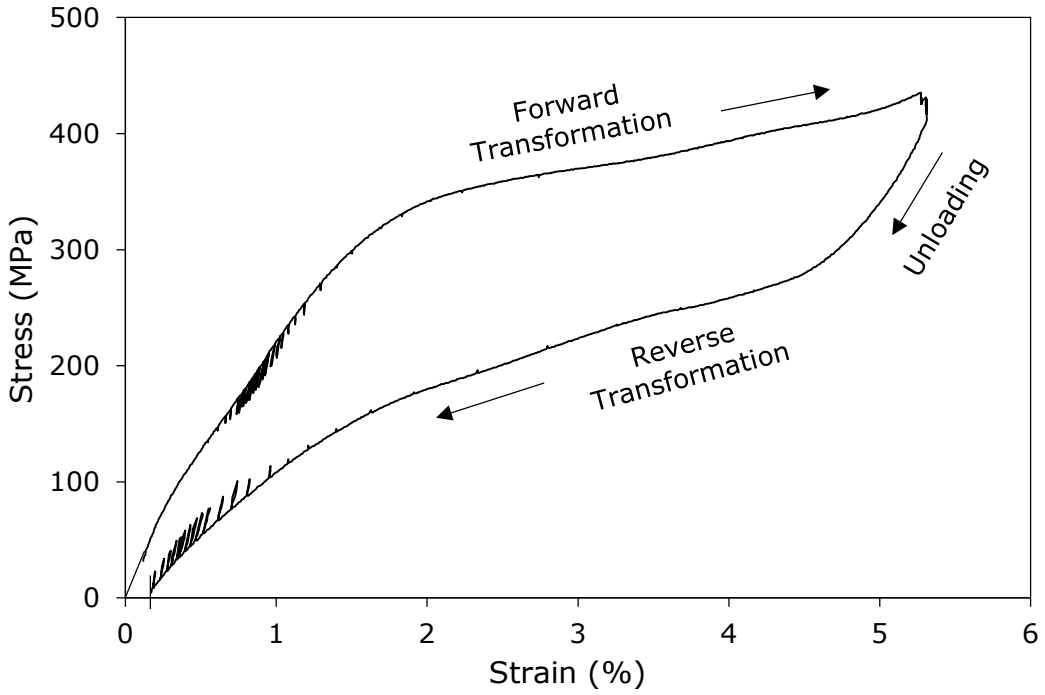


Figure 3-1 Typical stress-strain response of superelastic nickel-titanium SMA

Applications of superelastic SMAs in reinforced concrete structures have focused on implementing the alloy as internal reinforcement for new structures, while limited research has been documented on external applications for seismic retrofitting of existing concrete structures. Testing of concrete structural elements reinforced with superelastic SMAs has demonstrated the re-centering capacity of SMAs. Nickel-Titanium SMA rods have been experimentally studied as alternative reinforcement for concrete beams (Abdulridha et al. 2013; Saiidi et al. 2007), concrete columns (Saiidi et al. 2009; Saiidi and Wang 2006), concrete beam-column joints (Nehdi et al. 2010; Youssef et al. 2008), concrete frames (Dolce et al. 2005), and concrete shear walls (Abdulridha and Palermo 2014). In each of these studies, the SMA rods contributed to reductions of permanent deformations and damage of the concrete relative to companion elements reinforced with black carbon reinforcing steel. Furthermore,

testing has demonstrated that the flag-shaped stress-strain response with low modulus of elasticity, typical of nickel-titanium SMAs, results in concrete elements with reduced initial stiffness and energy dissipation capacity. However, the reduced energy dissipation does not necessarily imply a deficiency in the SMA material. Christopoulos et al. (2002) demonstrated that flag-shaped hysteretic behaviours can match or improve the seismic response in comparison to elastic-plastic hysteretic behaviours. Further applications of SMAs have been studied numerically, including concrete columns (Billah and Alam 2012; Tazarv and Saiidi 2015), concrete beam-column joints (Alam et al. 2008), and concrete frames (Alam et al. 2009; Youssef and Elfeki 2012; Zafar and Andrawes 2012). The analyses have highlighted that SMA rods and SMA-based composite materials possess the capability to increase strength and drift, while reducing damage and permanent deformations.

The only experimental study, known by the authors, on the external application of superelastic SMA rods to reinforce concrete structures was conducted by Effendy et al. (2006). SMA rods were externally connected to barbell-shaped squat shear walls in a bi-diagonal pattern as replacement of internal reinforcement. In comparison to a companion reinforced wall, the SMA retrofitted walls were stronger, less ductile, and exhibited narrower hysteretic response with less energy dissipation. The long SMA rods, in addition to the relatively small lateral deformation of the walls, limited the straining experienced by the SMA and, therefore, reduced the re-centering effect. Furthermore, the long SMA rods buckled during testing. SMA bracing concepts have also been considered in other studies. Auricchio et al. (2006) numerically modelled steel frames braced with reduced-length superelastic SMA elements, while Dolce et al. (2005) tested reinforced concrete frames with SMA bracing devices. The braces studied by Auricchio et al. consisted of SMA elements assumed to resist compressive forces without buckling. These braces, however, may not achieve the full-recovery strain of the SMA before buckling given the probable high compressive stresses at large lateral displacements of the frames. The braces tested by Dolce et al. incorporated a device with SMA wires (some of them pre-strained), capable of sustaining tensile and compressive stresses. Although effective for improving the response of structures, the braces require specialized fabrication that may not be feasible for field applications.

3.2 Research Significance

To address challenges with the application of long SMA rods as external reinforcement for concrete shear walls, an optimized external, SMA tension-only bracing system is proposed, where the length of SMA rods is sized to fully utilize the range of deformation recovery. In addition, buckling is eliminated in the brace through a mechanism that releases compressive stresses. The proposed tension-only SMA brace is a simple, easy to construct, retrofitting element capable of improving the seismic response of structures subjected to large displacements. The brace system is scalable and can be utilized for retrofitting a wide range of structures, including reinforced concrete or steel frames, and reinforced concrete shear walls. Furthermore, the braces are designed such that the SMA rods can be removed and replaced, while the bracing system remains in place.

3.3 Conceptual Design of SMA Retrofitting System

The proposed tension-only SMA bracing system consists of nickel-titanium SMA links, coupled with rigid hollow structural steel elements that are connected with anchor plates to the base and top of a shear wall (Figure 3-2(a)).

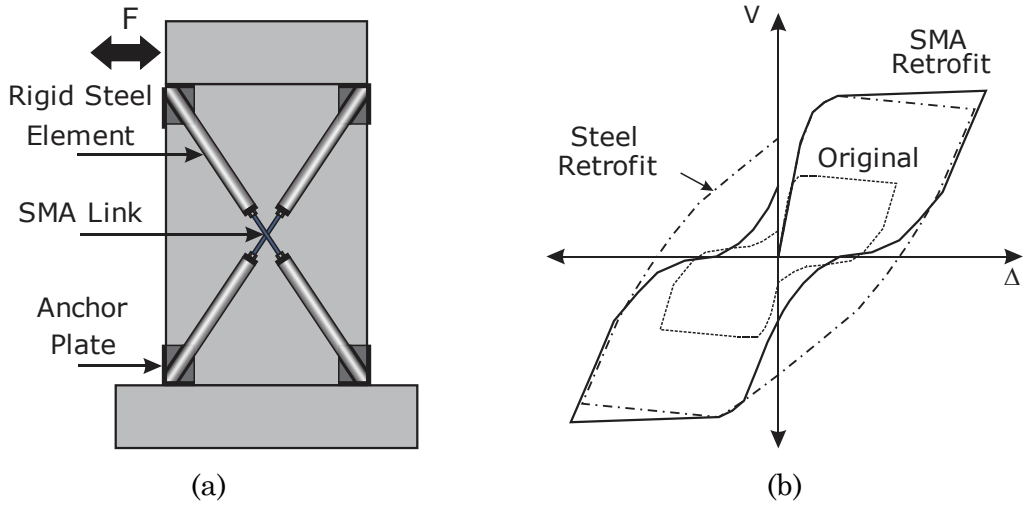


Figure 3-2 Retrofit with SMA: (a) retrofit scheme with SMA braces; and (b) expected response of SMA-retrofitted wall compared to original and steel-retrofitted walls.

The SMA braces act as flag-shaped energy dissipaters that, in addition to increasing lateral strength, can potentially improve drift, energy dissipation, and re-centering (Figure 3-2(b)). In comparison to a similar steel retrofitting system, the SMA bracing is expected to reduce damage, improve closing of cracks during load reversals, reduce permanent deformations, and promote more stable hysteretic cycles with reduced strength and stiffness degradation.

3.4 Design of Full-Scale SMA Retrofitting System

The proposed SMA braces were first conceived at full-scale as a retrofitting system to improve the seismic response of a 6000 mm-long × 6000 mm-high × 300 mm-thick shear wall of a two-storey prototype building subjected to the demands corresponding to the high seismic region of Western Canada (Figure 3-3).

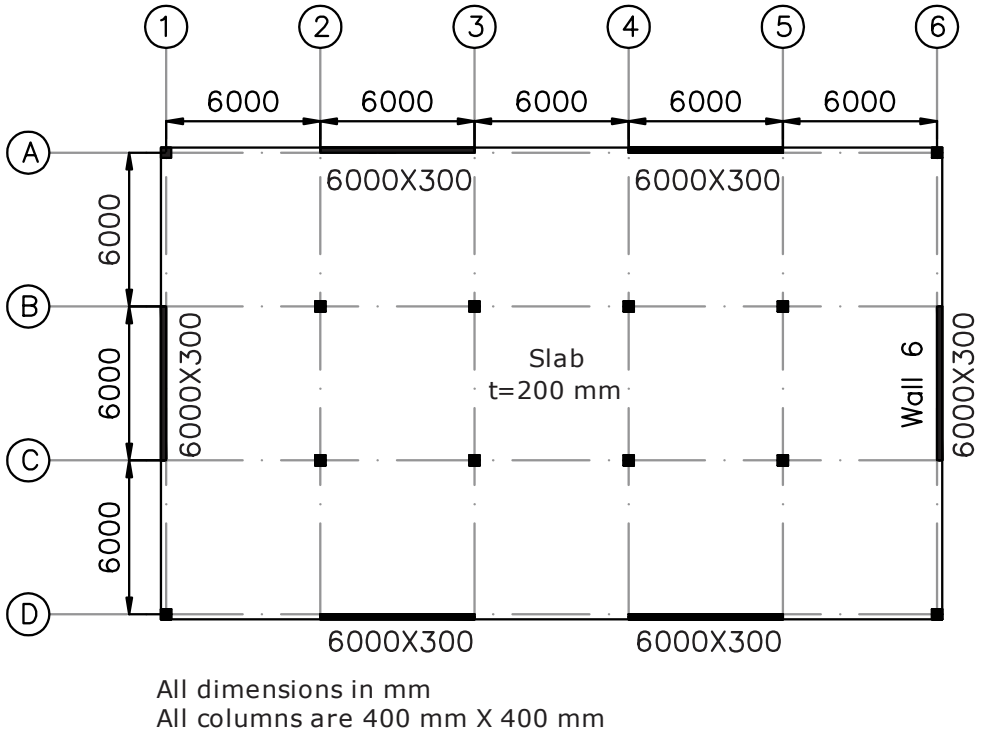


Figure 3-3 Plan view of prototype building

The shear walls were designed following the 1965 edition of the National Building Code of Canada, NBCC-1965 (NRC 1965), assuming material properties that were representative of construction practices of the 1960s: cylinder compression

strength of concrete and yield stress of reinforcing steel equal to 21 MPa and 280 MPa, respectively. The design of the prototype wall resulted in minimum reinforcement in the longitudinal (0.18%) and transverse (0.21%) directions. Seismic detailing such as confinement and anti-buckling reinforcement was not prescribed in the NBCC-1965.

The capacity spectrum method of ATC-40 (ATC 1996) and FEMA 440 (ATC 2005) was used to assess the performance of the retrofitted wall (Figure 3-4). The capacity curves of the original and retrofitted walls were established from the envelope of the lateral load-displacement hysteretic responses predicted with program VecTor2 (Wong et al. 2013). The capacity curves were converted to spectral coordinates by dividing the top displacement by a factor of 1.23, which was calculated from the product of the first modal participation factor and the first modal roof displacement based on a fundamental triangular modal distribution. The reduced elastic demand curve was based on the Uniform Hazard Spectrum (UHS) for the location of the building, as prescribed in the NBCC-2010 (NRC 2010), and reduction factors SR_A (plateau) and SR_V (descending branch) calculated with the Newmark and Hall (1982) formulations using effective damping, β_{eff}. The reduction factors were calculated as follows.

$$SR_A = \left[3.21 - 0.68\ln\left(100\beta_{eff}\right)\right]/2.12; \quad SR_V = \left[2.31 - 0.41\ln\left(100\beta_{eff}\right)\right]/1.65 \tag{3-1}$$

$$\beta_{eff} = \beta_o + k\beta_{eq}; \ \beta_{eq} = \left(1/4\pi\right)\left(E_D/E_{So}\right) \tag{3-2}$$

The effective damping is a combination of the inherent elastic viscous damping of the structure, β_o, and the equivalent viscous damping of the hysteretic loops, β_{eq}. The equivalent damping was calculated based on the energy dissipated by hysteretic damping, E_D, and the maximum strain energy, E_{So}, at the target displacement.

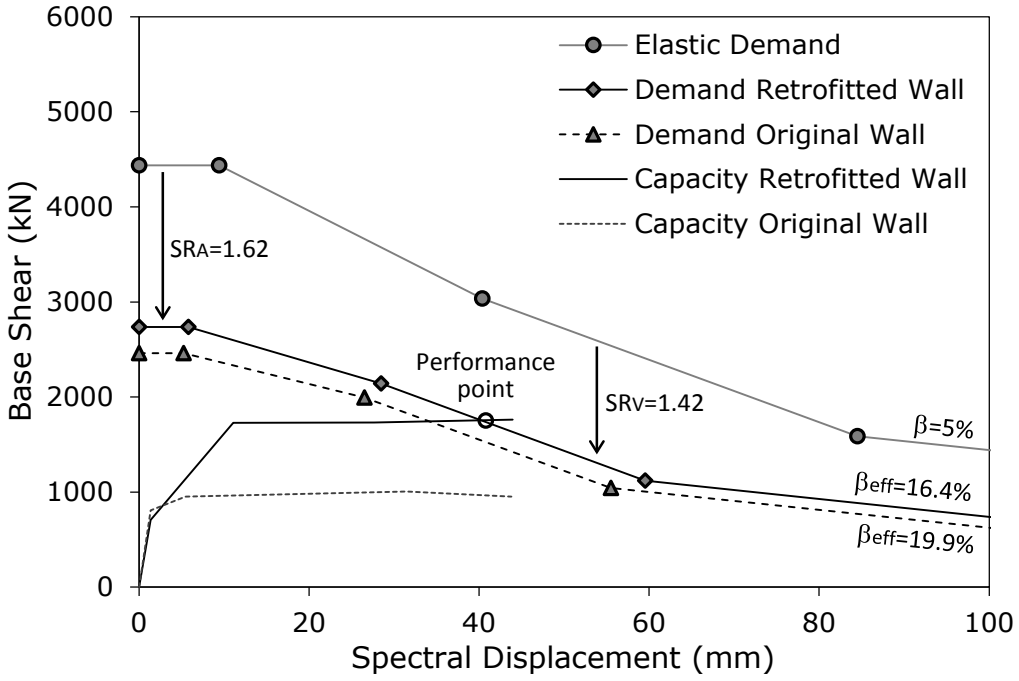


Figure 3-4 Seismic assessment of retrofitted wall with SMA bracing

The analysis of the original wall predicted a peak lateral strength capacity of 1124 kN and corresponding top displacement of 54 mm (43.9 mm spectral displacement). This response fell below the reduced elastic demand curve (Figure 3-4), illustrating that the original wall was deficient. The retrofitting system was continuously redesigned (the area and the length of the SMA link) until the capacity curve intersected the demand curve, which defined the performance point (Figure 3-4). The objective for this study was for the performance point to match the collapse prevention performance level as defined by ASCE 41-06 (ASCE 2007): *"The building remains standing, but only barely; any other damage or loss is acceptable."* The collapse performance level corresponded to the ultimate displacement of the retrofitted wall, which was 54 mm at a lateral strength capacity of 1760 kN based on the analysis with VecTor2. [Details of the modelling of the retrofitted wall are presented in Appendix C.] The final SMA retrofitting system was achieved at a spectral displacement of 40.7 mm, corresponding to 50 mm of top lateral displacement, defining the performance point (Figure 3-4). Note that this is approximately equal to the ultimate displacement of 54 mm. The tension-only SMA braces consisted of 670

mm-long (approximately 1/12 of the length of the brace), superelastic nickel-titanium SMA link rods with a diameter of 38 mm (cross-sectional area of 1140 mm^2) with pseudo-yield (upper plateau) stress capacity of 420 MPa. The total length of the SMA braces was 8060 mm; therefore, the remaining length of 7390 mm corresponded to the steel sections, whose cross-section was designed to limit the working stress to 25% of the yield stress of the steel (75 MPa for Grade 300W). The braces were designed to sustain recoverable damage in the SMA links but not exceed 6% strain at the performance point, while the connecting rigid structural steel elements remain in the elastic range. This ensures that the SMA links are resettable fuses that can experience large deformations ranging between pseudo-yielding and full recovery. At the performance point, the SMA links experienced 4.9% strain. Therefore, the design process ensured that the area of the SMA was optimized for the selected performance level.

3.5 Testing of Third-Scale Retrofitting Systems

The conceptual SMA braces were scaled and fabricated to retrofit a 2000 mm-long × 2000 mm-high × 100 mm-thick shear wall (Wall SQ1) that forms part of an experimental program to study SMA retrofitting techniques for reinforced concrete shear walls. Wall SQ1 is a 1/3rd-scale specimen of the prototype wall described in Figure 3-3. The wall complied with scaling laws related to geometry and reinforcement ratios, but did not conform to the scaled size and spacing for the reinforcing bars due to constraints in constructability. The horizontal and vertical reinforcement consisted of 9.5 mm-diameter bars spaced at 360 mm and 450 mm, respectively. Figure 3-5 provides dimensional and reinforcement details of the wall. Further details of the scaled walls can be found elsewhere (Cortés-Puentes and Palermo 2015).

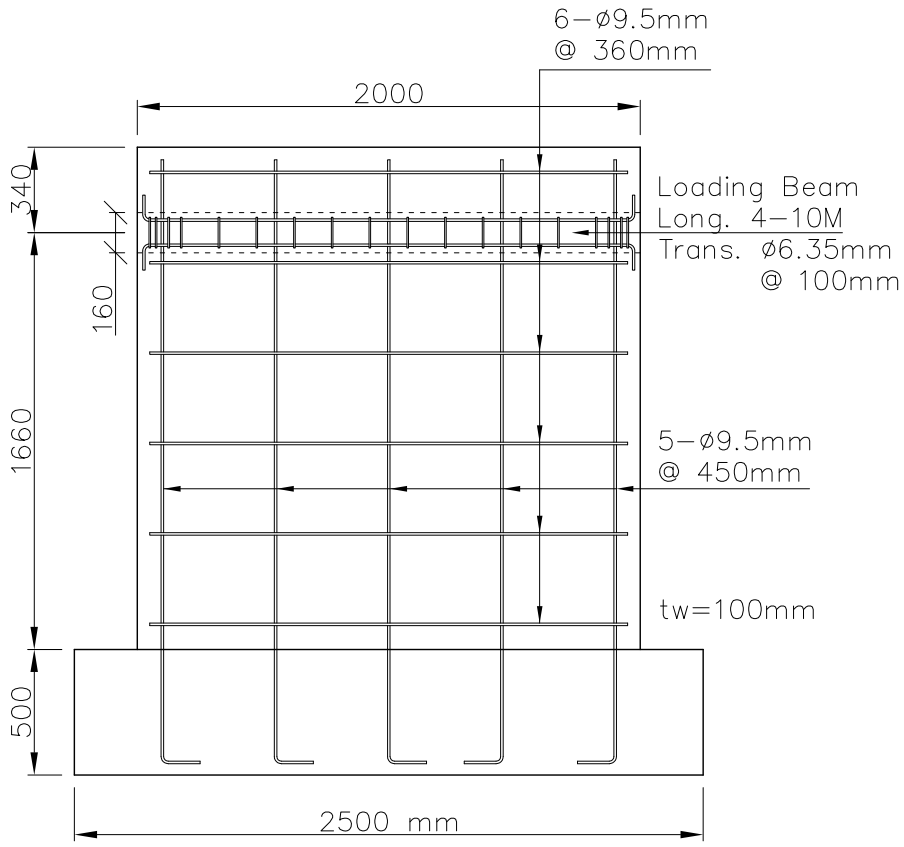


Figure 3-5 1/3rd-Scale shear wall SQ1, internal reinforcement layout

The 2540 mm-long braces to retrofit Wall SQ1 consisted of 635 mm-long SMA links. The length of the SMA links were optimized to ensure the braces were capable of experiencing forward transformation (upper stress plateau) and maximum axial elongation of 38 mm (6% strain). Achieving forward transformation permitted the deformation recovery action of the brace, while not exceeding the superelastic strain limit of 6% permitted reuse of the SMA braces. The performance point of the retrofitted SQ1 wall corresponded to 37 mm of top lateral displacement (drift of 1.85%) following the same capacity spectral method used for the design of the retrofitting system for the prototype wall. The corresponding strain of the SMA links at the performance point was 4.2%.

Two, tension-only, superelastic SMA and two, tension-only, steel braces were fabricated and cyclically tested to validate the design and verify the performance of the brace components, and to establish the cyclic response of the braces. The two SMA

braces made use of only one link. The first SMA brace was tested to a maximum strain of 5.5% and, thereafter, it was retested to failure (second SMA brace). The objective of retesting was to evaluate the reusability of the retrofitting system. An additional SMA brace that incorporated a half-length, shape-memory-effect, SMA link was tested to assess a modification of the design to improve the ductility of the brace. The two steel braces made used of one steel link each. Figure 3-6 provides a schematic drawing of the retrofitting components of the SMA and steel braces for retrofitting Wall SQ1.

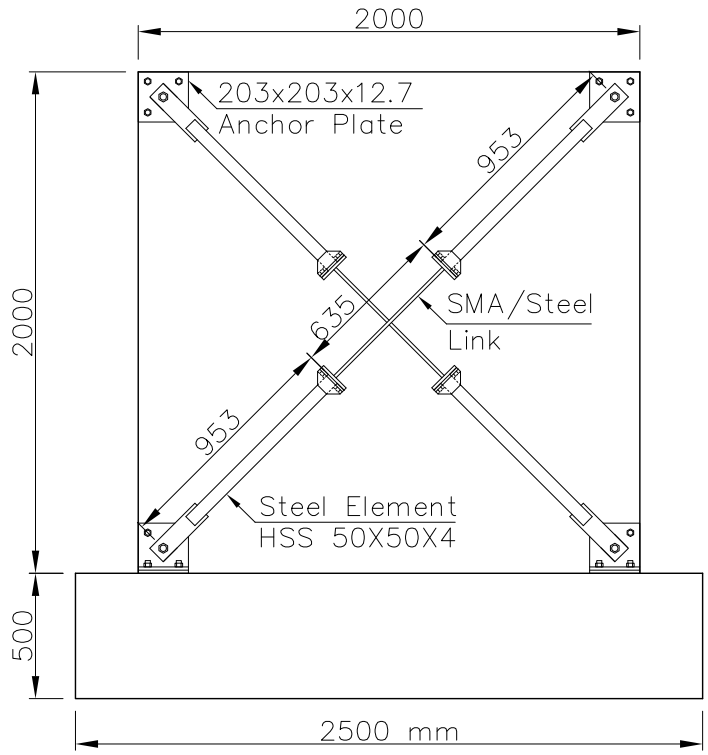


Figure 3-6 External retrofitting of Wall SQ1 with SMA and steel braces

3.5.1 Properties of SMA and Steel Braces

The SMA links (Figure 3-7) incorporated 12.7 mm-diameter superelastic Nitinol (Nickel-Titanium) SMA rods (126 mm^2 cross sectional area), and the steel links consisted of 10M steel reinforcing bars (100 mm^2 cross sectional area). The bar size of the steel link was selected such that the yield strength of the steel braces was comparable to the upper plateau strength (pseudo-yield strength) of the SMA braces.

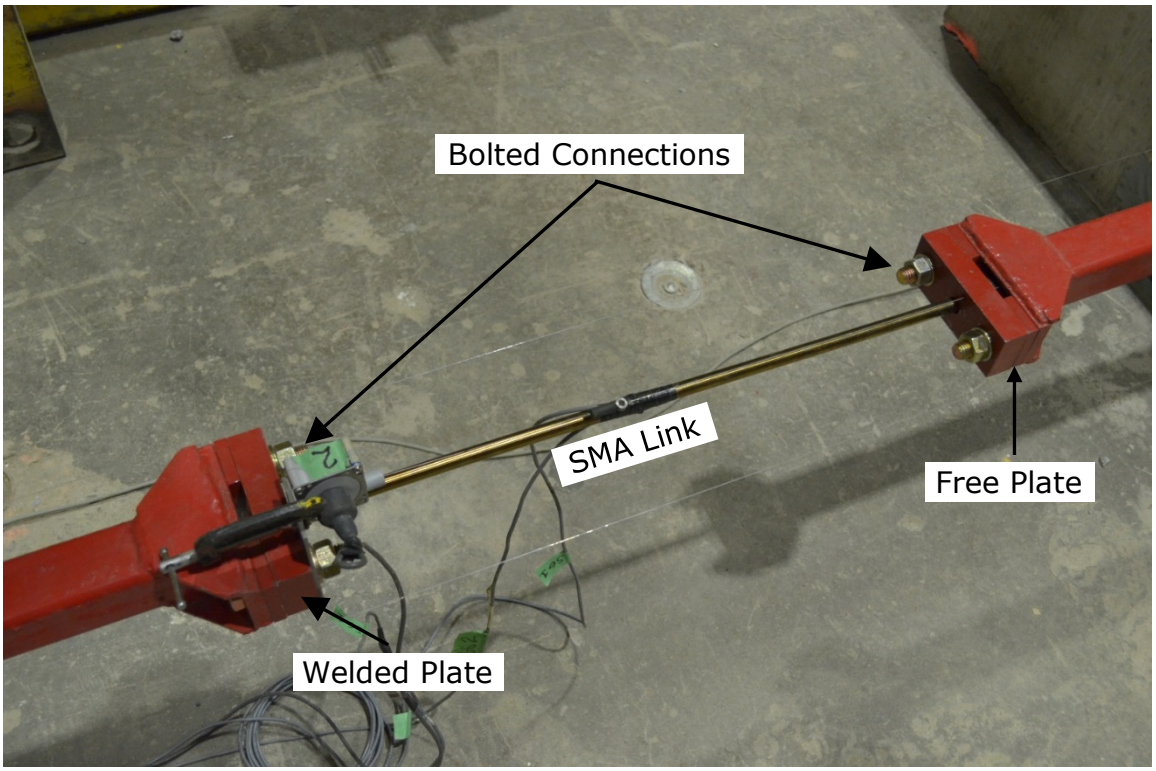
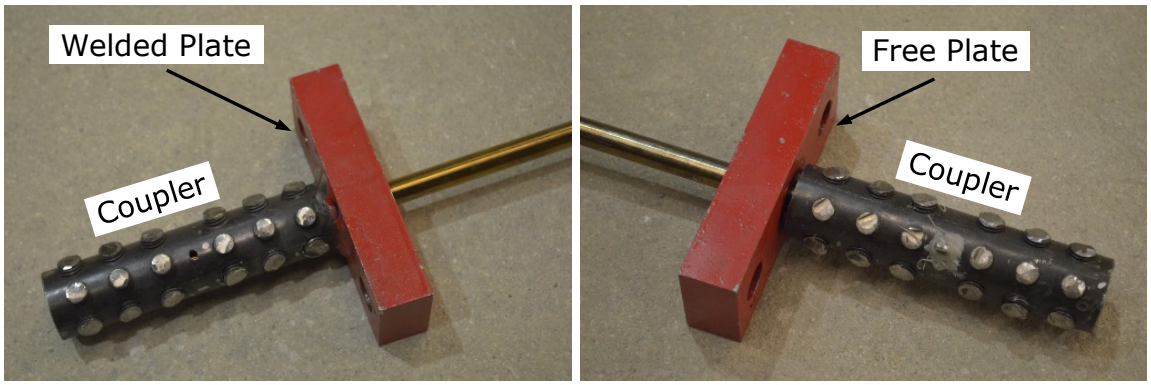


Figure 3-7 Tension-only SMA link

The links included two Bar-Lock couplers, one at each end of both the SMA rod and steel bar. 25.4-mm thick steel plates were positioned at the head of the couplers for the SMA links, through which 5/8" (15.9 mm) grade 8 bolts were used to connect to the rigid steel elements constructed from 50 mm × 50 mm × 4 mm Hollow Structural Sections (HSS). The rigid steel elements were designed to sustain a maximum stress of 25% of the yield stress (approximately 80 MPa), ensuring they remained within the elastic range and experienced negligible deformations. To ensure tension-only stresses in the links, one of the couplers was welded to the steel plate (Figure 3-8(a)), while the other was free to move and slide into the hollow section (Figure 3-8(b)). Eighteen, shear-off bolts, tightened to a torque of 50 ft-lb (67.8 N-m), were used with the couplers, preventing slip of the SMA rods. The steel link was constructed with thinner steel plates (12.7-mm thick) and smaller Bar-Lock couplers that required only 4 bolts. Due to the smoothness of the SMA rods, the SMA links required longer couplers with additional bolts to prevent slip. Furthermore, thicker steel plates were used for the SMA links to eliminate bending that was observed during testing of the steel braces.



(a) (b)

Figure 3-8 End of SMA links: (a) fixed end; and (b) free end

The specified Austenite start temperature, A_s, of the Nitinol SMA rods was -30˚C and the specified Austenite finish temperature (fully annealed temperature), A_f, was -10˚C. Mechanical properties of the SMA rods were established from the stress-strain response of an SMA rod following the test protocol specified by the ASTM F2516-14 (ASTM 2014) standard (Figure 3-9): upper plateau stress (pseudo-yield stress) of 407 MPa at 3% strain; lower plateau stress of 186 MPa at 2.5% strain, ultimate stress (rupture) of 1054 MPa at 19.8%; and residual strain of 0.6% for the cycle to 6% strain. [Note that the upper and lower strength plateaus were determined at the strains prescribed by the ASTM F2516-14 standard.] Similarly, the mechanical properties of the 10M steel reinforcing bars were determined from the stress-strain response of a bar following the ASTM A615M-16 standard (ASTM 2016): yield strength of 460 MPa at corresponding yield strain of 0.3%; ultimate stress of 664 MPa; and rupture strain of 16% (Figure 3-9).

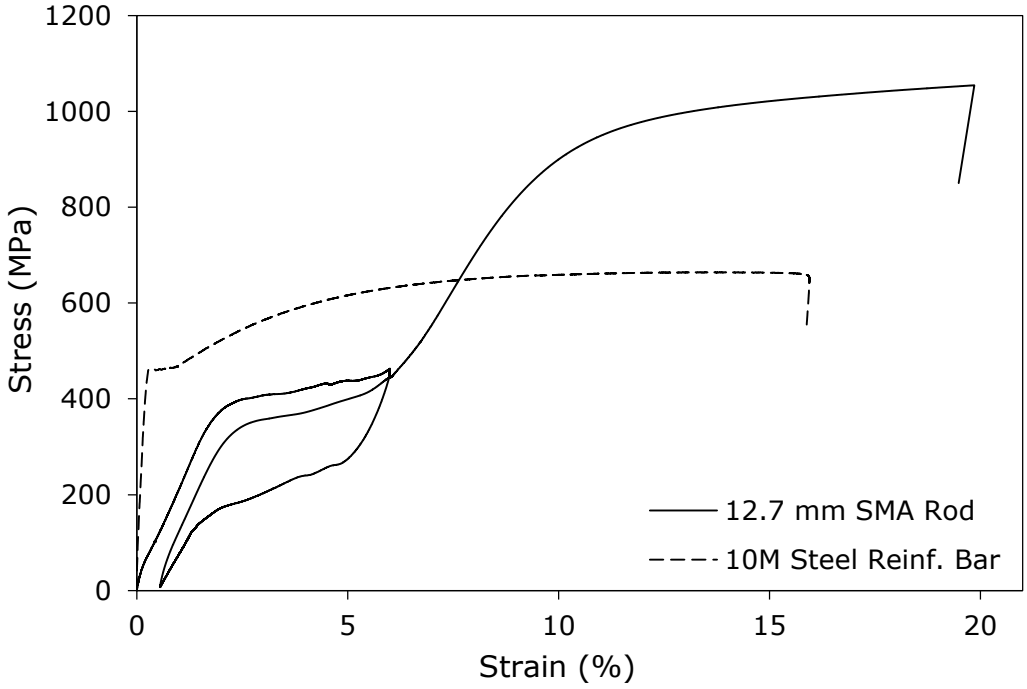


Figure 3-9 Stress-strain responses of SMA rod and steel reinforcing bar

3.5.2 Test Setup

The axial loading imposed on the braces was applied in displacement-controlled mode using an actuator positioned between a reaction frame and the braces. The braces were placed in the horizontal position and pin-connected at one end to the actuator and at the other end to a reinforced concrete block (Figure 3-10). One or two Strain Gauges (SGs) were bonded to the SMA or steel links (Figure 3-11) to measure localized strain, and four Displacement Transducers (DTs) were placed at different locations to measure axial deformations in the braces and links (Figure 3-11). DT1 measured the elongation of the entire brace from center to center of the pin connections, DT2 measured the elongation of the SMA/steel links, DT3 measured the elongation of the brace from the actuator to the concrete block, and DT4 monitored the displacement of the pin connection on the concrete block.

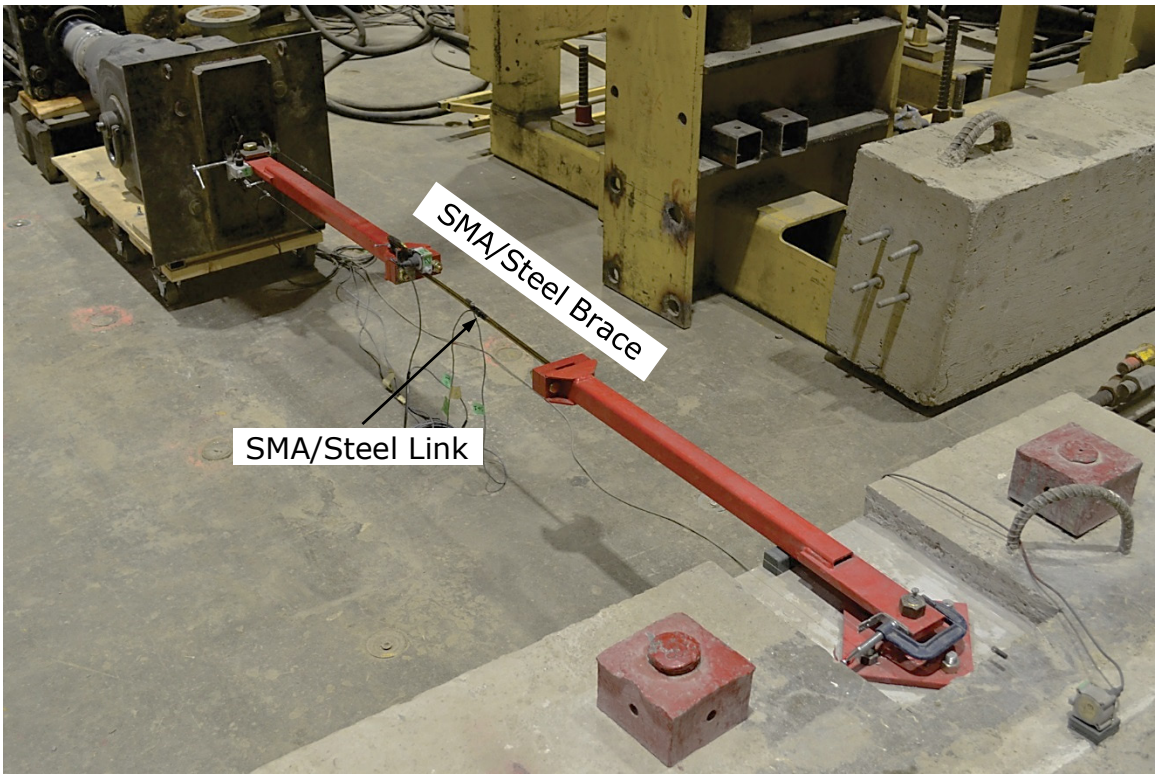


Figure 3-10 Testing of bracing system

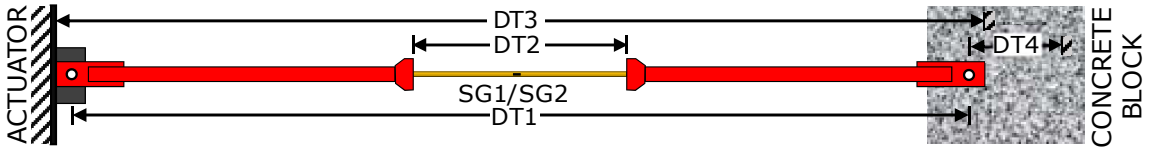


Figure 3-11 Instrumentation on SMA/steel braces

The braces were tested following the quasi-static testing protocol recommended by FEMA 461 (ATC 2007). Two repetitions of loading were applied at each displacement level. The displacement amplitudes were linked to the expected elongation of the braces during testing of the retrofitted wall. The loading protocol consisted of an initial stage prior to yielding, a damage stage to the target elongation of 35 mm (1.4% strain in the brace, corresponding to 5.5% strain in the link), and a final stage to failure. The target elongation of 35 mm corresponded to the displacement level prior to exceeding the full recovery limit of the SMA link.

3.5.3 Force-Elongation Response

Brace SMA1 was tested to the target elongation of 35 mm, and then retested to failure (Brace SMA2). The responses of the SMA braces, measured with cable transducer DT1, were governed by the behaviour of the SMA link as demonstrated by the flag-shaped force-elongation responses (Figure 3-12 and Figure 3-13). This indicates satisfactory performance of the braces in which damage was concentrated in the links. The upper plateau strength, measured at 3% elongation of the SMA links (0.75% strain in the SMA braces), corresponded to 45.5 kN and 47.2 kN (361MPa and 375 MPa) for Braces SMA1 and SMA2, respectively. The lower plateau strengths, measured at 2.5% elongation of the SMA links (0.625% strain in the SMA braces), were approximately 41% and 53% of the upper plateau strengths, 18.6 kN (148 MPa) and 24.8 kN (197 MPa) for Braces SMA1 and SMA2, respectively. The sharp decrease of approximately 10 kN in strength at the initiation of unloading corresponded to the elastic response of the steel plates connecting the link to the brace. At the end of unloading, the response was linear to the residual elongation. For the range of imposed elongations, the SMA braces had the capacity to return approximately to their original length. The cumulative residual deformation was only 2.5 mm (0.1% strain) for both braces. The strength of the braces at the target elongation of 35 mm was 52.1 kN and 54.3 kN (413 MPa and 431 MPa) for Braces SMA1 and SMA2, respectively. The SMA link in Brace SMA2 ruptured at 41 mm of elongation (1.61% strain in the brace, and 6.45% strain in the link), corresponding to 66.1 kN (525 MPa). Rupture initiated at the location of the coupler due to the plane of weakness introduced by the sharp-end bolts used to connect the coupler to the SMA rod. The similarities in response between Brace SMA1 and SMA2 illustrate that the SMA brace is resettable provided the SMA link remains within the superelastic recovery range (6%).

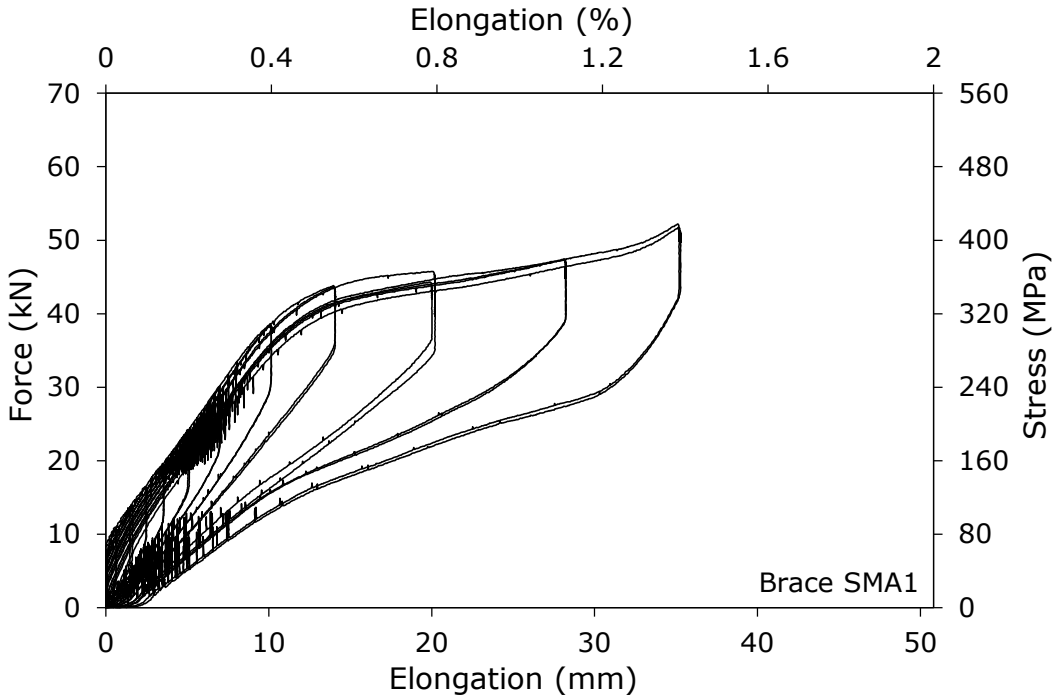


Figure 3-12 Force-elongation response of Brace SMA1

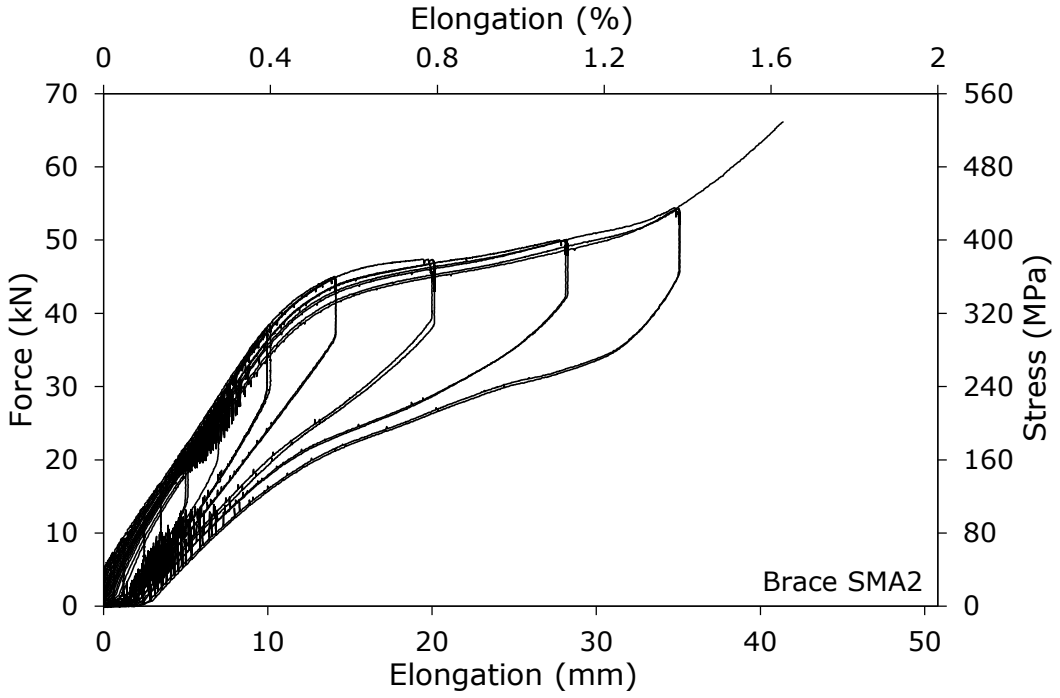


Figure 3-13 Force-elongation response of Brace SMA2

An additional SMA brace, Brace SMA3, with a 317.5 mm-long SMA link (half the length of the 635 mm SMA links) was built with 12.7 mm-diameter shape-

memory-effect nickel-titanium SMA, which lacked the re-centering properties due to superelasticity. The cross sectional area was reduced by 13% (110 mm^2) for a length of 200 mm along the centre portion of the link between the couplers. The objective of this test was to improve the deformation capacity of the SMA links by shifting failure from the location of the couplers to the centre of the links by reducing the cross-sectional area. The shape-memory SMA was used for this brace given the similar hardness and smoothness as the superelastic SMAs of the other braces. Testing demonstrated that reshaping of the SMA rods increased the strain in the brace and link to 2.2% and 8.8%, respectively, at fracture, corresponding to 75 kN (682 MPa). Failure shifted from the coupler to the transition zone from the original size of the SMA to the reduced section. As a result, the 635 mm-long SMA links to be used in future tests will incorporate SMA rods with reduced area of 110 mm^2 along the central 500 mm of the link. The redesigned SMA links are expected to provide additional reserve displacement capacity, and ensure that failure initiates at the intended location in the bracing system.

The companion steel braces experienced ductile behaviour governed by the response of the steel links (Figure 3-14). The envelope of the cyclic response provides a typical stress-strain curve with an initial elastic branch, followed by a yield plateau, and finally strain hardening. The maximum elongations of the steel braces and steel links were similar; therefore, damage was sustained by the steel links, while the rigid steel elements experienced negligible deformations. Yield strengths of 43 kN and 47 kN (430 MPa and 470 MPa) were recorded for Braces STL1 and STL2, respectively. Rupture at the centre of the steel links occurred at 82 mm and 90 mm of elongation for Braces STL1 and STL2, respectively. Both steel links ruptured at a strength of approximately 65 kN (650 MPa). The significant drop of strength of approximately 40 kN at the onset of unloading was a result of deformation of the steel components. The steel plates that connected the steel links to the rigid elements experienced deformations of approximately 1.5 mm.

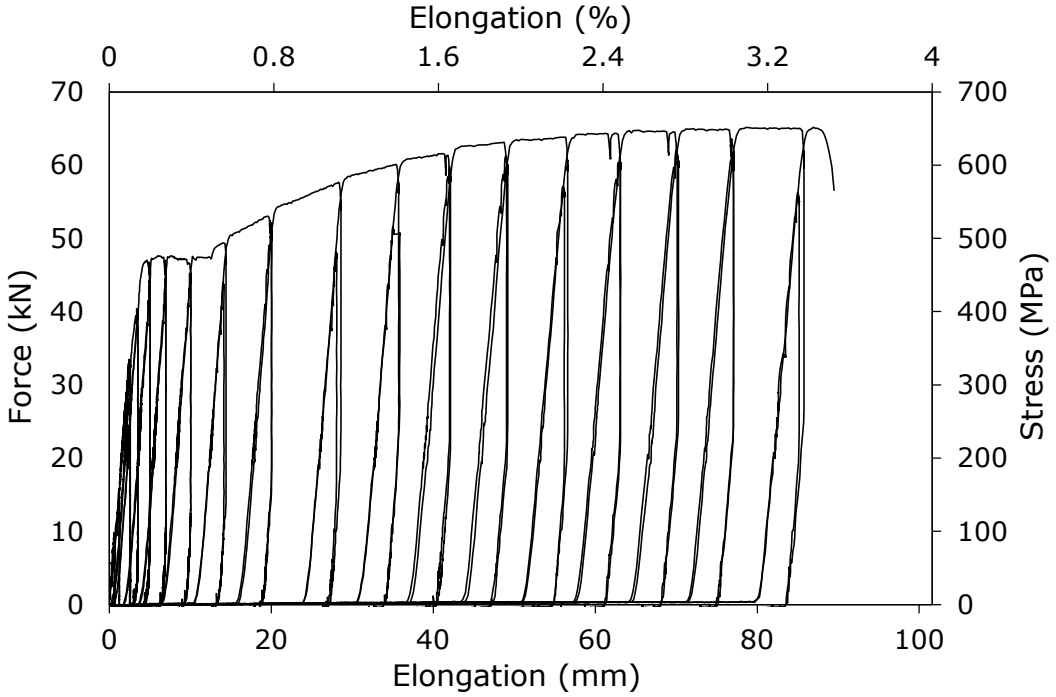


Figure 3-14 Typical force-elongation response of steel braces

3.6 Discussion of Results

The results in this section are based on Braces SMA2 and STL2, which provide typical responses for each type of brace.

3.6.1 Stress-Strain Response

The SMA and the steel braces experienced comparable strengths as demonstrated in Figure 3-12, Figure 3-13, and Figure 3-14. The average pseudo-yield strength of the SMA braces was 46.4 kN (368 MPa), and the average yield strength of the steel braces was 45 kN (450 MPa). The rupture strength of Brace SMA2 (66.1 kN, 525 MPa) was slightly greater than the rupture strength of Brace STL2 (64.6 kN, 646 MPa). Although the steel reinforcing bar had smaller cross-sectional area, the steel braces experienced slightly greater strength than the SMA braces up to 35 mm elongation, thereafter the SMA braces experienced greater strength. Negligible strength degradation was observed between first and second repetitions of loading of the SMA braces. In the post-yield range, the strengths between first and second repetitions of

loading for the steel braces differed by up to 5%. The rupture strains of the SMA and steel braces were 1.63% and 3.55%. Therefore, both the SMA and the steel braces exceeded the target elongation of 35 mm (corresponding strain of 1.38%). The envelopes of the first repetitions of the stress-strain responses for the SMA and steel braces are presented in Figure 3-15.

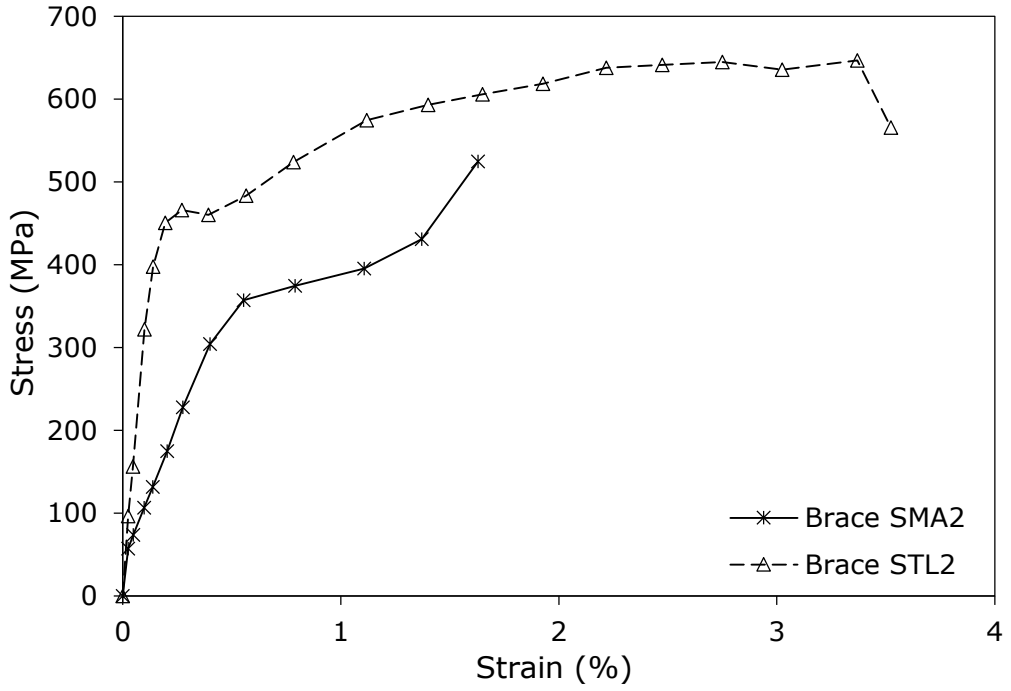


Figure 3-15 Envelope of stress-strain response of SMA and steel braces

3.6.2 Stiffness

The initial stiffness was based on the limit of proportionality of the responses of the braces (10 mm elongation, 0.39% strain, for the SMA braces; and 3.6 mm elongation, 0.14% strain, for the steel braces). The SMA braces experienced an average initial stiffness of 76 GPa, while the steel braces experienced an average initial stiffness of 286 GPa. As a result of the reduced stiffness, the pseudo-yield strength of the SMA braces was attained at a larger elongation relative to the steel braces. A benefit of the low stiffness of the SMA braces is an increase of strength of the retrofitted structure without significantly increasing the seismic demand. Conversely, the stiffer steel braces result in an increase in the stiffness of the retrofitted structure, reducing

ductility and increasing the seismic force demands. The variation of the secant stiffness of the SMA and steel braces with respect to the axial strain for the first repetition of loading is illustrated in Figure 3-16.

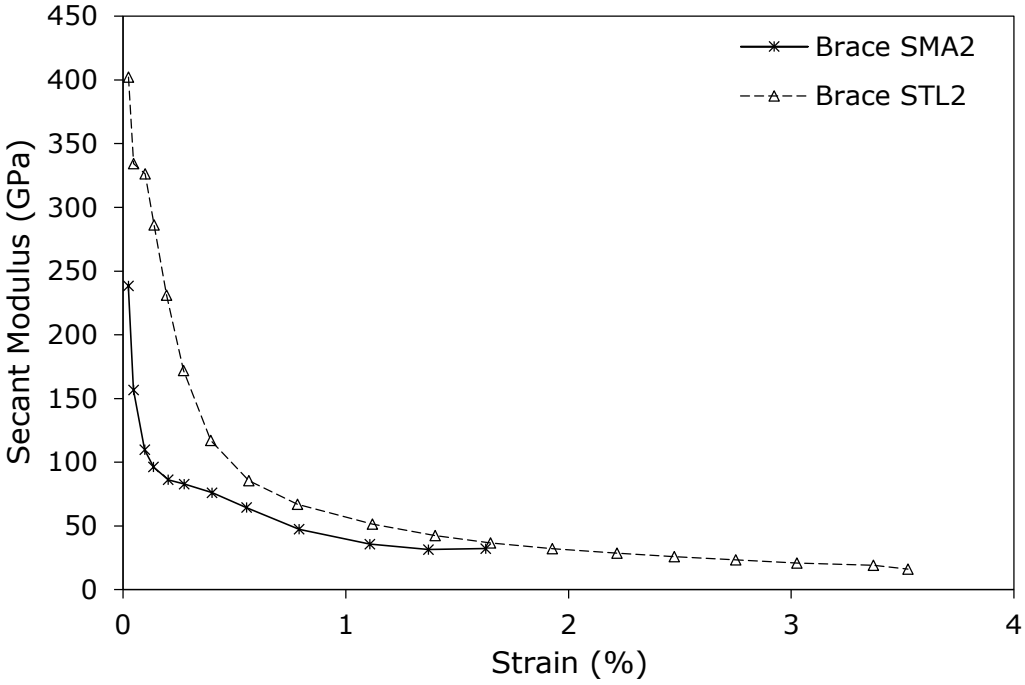


Figure 3-16 Secant stiffness of braces

3.6.3 Energy Dissipation

The cumulative energy dissipation of the braces up to the target elongation of 35 mm is provided in Figure 3-17. The energy dissipation provided by the steel braces to 28 mm elongation was slightly greater than that of the SMA braces. However, at the target elongation, the cumulative energy dissipation of the SMA braces exceeded that of the steel braces. This trend indicates that the rate of increase of energy dissipation was greater for the SMA braces. Brace SMA2 dissipated approximately 10% less energy than Brace SMA1 as a result of the previous cycles imposed on the SMA link. The SMA braces maintained the same level of energy dissipation capacity for each repetition of loading; therefore, both first and second repetitions contributed approximately 50% to the total energy dissipation. Conversely, due to the permanent deformation of the steel braces, resulting from the first repetitions of loading, the

energy dissipated during the second repetition of loading was significant less than the first repetition. The first repetitions dissipated approximately 75% of the total energy, while the second repetitions dissipated approximately 25% of the total.

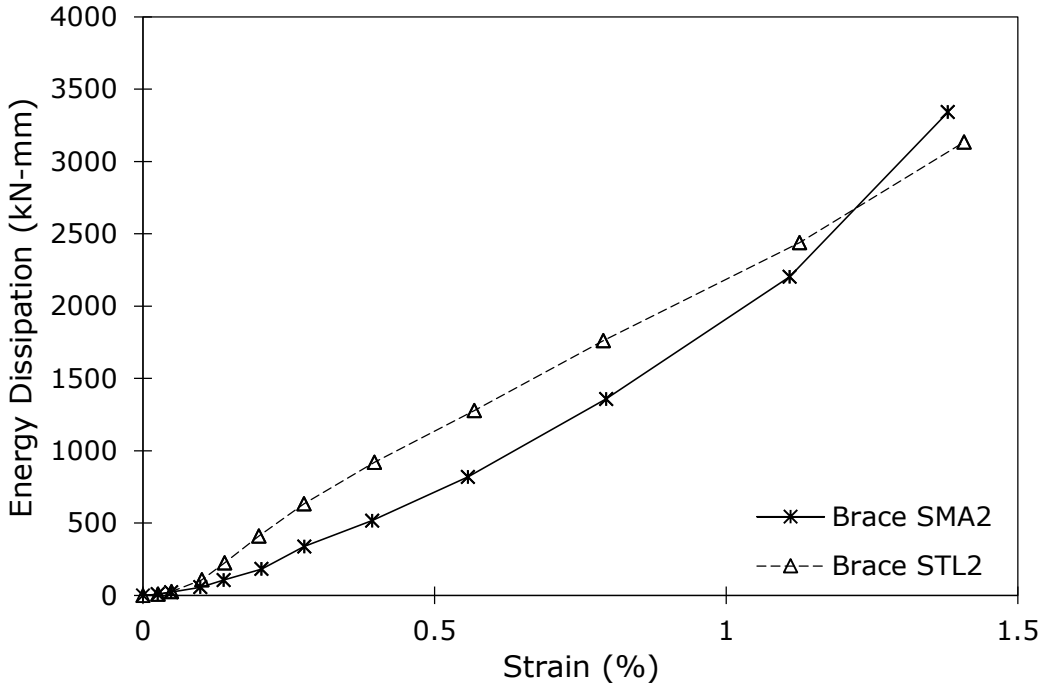


Figure 3-17 Cumulative energy dissipation of braces

3.6.4 Residual Deformations

The SMA braces sustained significantly less residual deformations than the steel braces at each cycle of loading as demonstrated by the force-elongation responses (Figure 3-12 to Figure 3-14). At the target displacement of 35 mm, the SMA braces recovered approximately 95% of the target elongation (33.5 mm), while the steel braces recovered less than 5% of the elongation (1.5 mm). Therefore, reloading of the SMA braces initiated at very small elongations, while reloading of the steel braces initiated at larger permanent deformations corresponding to the residual elongation from the previously unloading. Residual elongations for both steel and SMA braces were not affected by the repetitions to the same elongation.

3.7 Numerical Analysis

The performance of the proposed braces to retrofit squat reinforced concrete walls was assessed using the nonlinear finite element program VecTor2. The numerical analyses focused on the response of the third-scale control Wall SQ1, and companion retrofitted Walls SQ1S (SMA braces) and SQ1R (steel braces). VecTor2 is based on the Modified Compression Field Theory (MCFT) and the Disturbed Stress Field Model (DSFM). The authors previously validated the modelling techniques used herein using Vector2 by successfully simulating the response of repaired and retrofitted squat reinforced concrete shear walls (Cortés-Puentes and Palermo 2011, 2012). These walls had similar characteristic to those presented in this study.

3.7.1 Finite Element Modelling

The control and retrofitted walls were modelled with four reinforced concrete zones: one for the web, one for the foundation block, and two for the embedded loading beam at 1660 mm from the base (Figure 3-18). The web consisted mainly of 100 mm-thick, 90 mm × 90 mm rectangular concrete elements, and the horizontal and vertical internal steel reinforcement were modelled with discrete truss elements. The material properties corresponded to the materials used for the construction of Wall SQ1 in the experimental program. The compressive strength of the concrete elements was 22.5 MPa based on 28th day cylinder compression tests. The properties of the 9.5 mm-diameter reinforcement, obtained from coupon tests, were: yield stress of 495 MPa and corresponding yield strain of 0.3%, and ultimate stress of 735 MPa and corresponding ultimate strain of 16%. The interface between the vertical steel reinforcement and concrete was modelled with bond-link elements, which were assigned with a bond-slip relationship following the Eligehausen formulation (Eligehausen et al. 1983). The SMA and steel braces were modelled with tension-only truss elements with length of 2540 mm to account for the length of the links and the adjoining rigid steel elements (Figure 3-18(b)). These truss elements were connected only at the base and top of the walls. A tri-linear stress-strain relationship with upper and lower strength plateau and residual strain (Abdulridha et al. 2013) defined the

response of the SMA braces, and the Seckin model with Bauschinger effect and non-linear strain hardening defined the response of the steel braces (Wong et al. 2013).

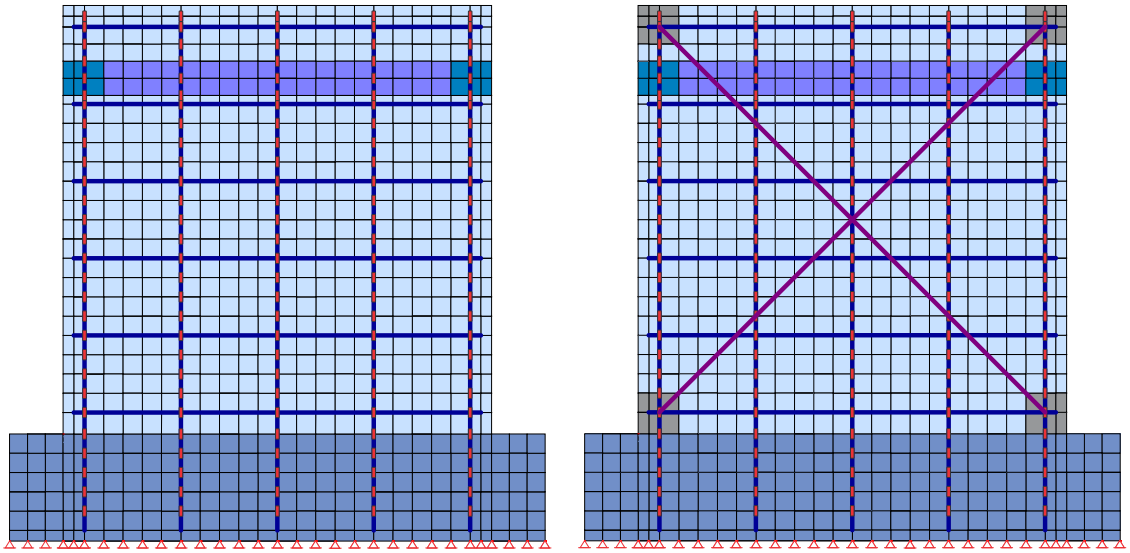


Figure 3-18 Finite element models: (a) control wall; and (b) retrofitted walls

The mechanical properties reported in Table 3-1, based on cyclic testing of the SMA and steel braces (Figure 3-13 and Figure 3-14), defined the truss elements for the SMA and steel braces. The yield stress, f_y, and modulus of elasticity, E, of the braces were determined at the strain corresponding to the pseudo-yield and yield point of the SMA and steel links at 3% and 0.3% strain, respectively. The ultimate stress, f_u, corresponded to the rupture stress of the braces. The model assumed an ultimate strain of 2.2% for the SMA braces based on the test results for the additional brace SMA3. The ultimate strain of the steel brace of 3.4% corresponded to the average rupture strain of the steel braces. The cross-sectional areas included two braces (one on each side of the wall) corresponding to the cross-sectional area of the SMA and steel links. The models were based on the assumption of damage concentrating in the links with negligible elastic deformations in the rigid steel elements. The finite element models also included heavily reinforced zones at the top and bottom corners of the walls to simulate anchoring of the retrofitting system (Figure 3-18(b)). Reverse cyclic lateral loads were applied along the loading beam. Lateral displacements were incremented by a factor of 2 in the pre-yield stage up to 2.4 mm and by a factor of 1.4 in the damage stage, from 3.6 mm to 40 mm. In the post-damage stage, the

displacements were increased in 10 mm increments. The loading protocol consisted of two repetitions for each displacement level. This loading protocol followed the quasi-static testing protocol recommended by FEMA 461 (ATC 2007).

Table 3-1 Properties of braces

Brace	Diameter (mm)	Area (mm^2)	f_y (MPa)	f_u (MPa)	E (MPa)	ε_u (%)
SMA	11.8	220	368	525	76000	2.2
Steel	11.3	200	450	646	286000	3.4

Note: f_y = yield stress; f_u : ultimate stress; E = modulus of elasticity; and ε_u = ultimate strain

3.7.2 Finite Element Analysis Results

Force-Displacement Response

Figure 3-19 to Figure 3-21 illustrate the force-displacement responses of Walls SQ1, SQ1S (SMA braces), and SQ1R (steel braces), and Figure 3-22 provides the envelope responses for the first repetitions of positive loading of the Walls. The analyses predicted strength at first yield of the internal vertical reinforcement (2.3 mm displacement) of 94 kN, 109 kN, and 122 kN for Walls SQ1, SQ1S, and SQ1R, respectively. Wall SQ1 experienced peak strength of 127 kN at 15 mm due to yielding of the longitudinal reinforcing bars. This strength was sustained to 50 mm displacement. The strength of the retrofitted walls linearly increased from first yield to the displacement corresponding to pseudo-yielding of the SMA braces (20 mm) and yielding of the steel braces (10 mm). At pseudo-yielding/yielding of the braces, the strength capacity of Walls SQ1S and SQ1R were 209 kN and 212 kN, respectively; while at ultimate, the strength capacities were 220 kN and 234 kN, respectively, representing increases of 73% and 84% relative to control wall SQ1. Wall SQ1S experienced an ultimate displacement of 40 mm, which was similar to that predicted for Wall SQ1, while Wall SQ1R attained an ultimate displacement of 30 mm.

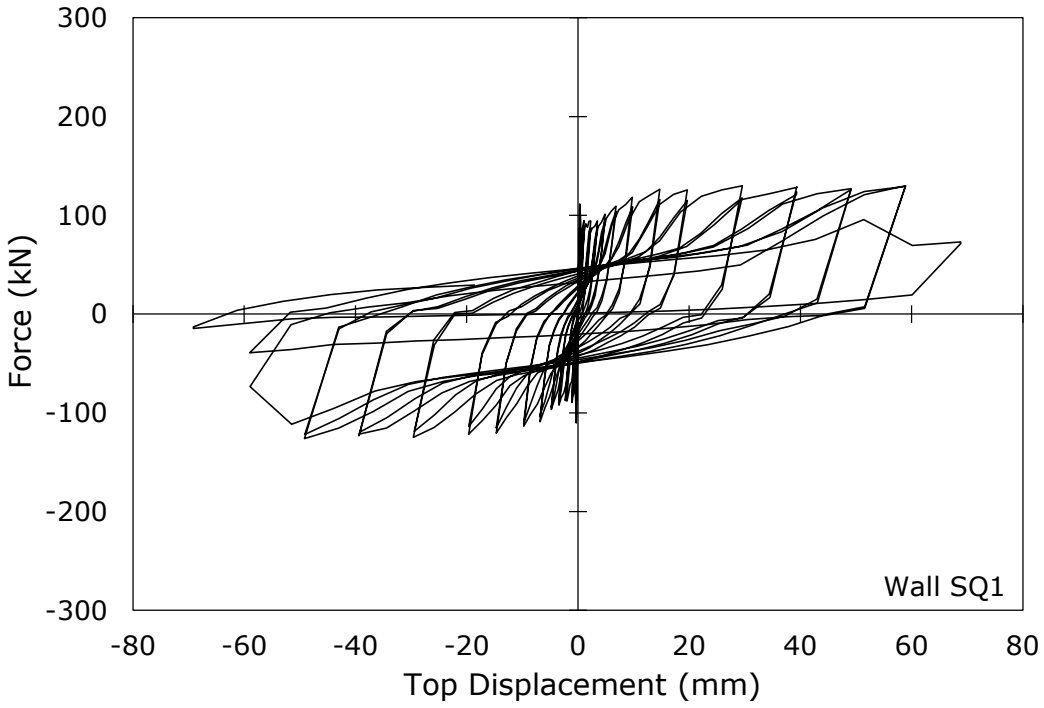


Figure 3-19 Predicted response of Wall SQ1

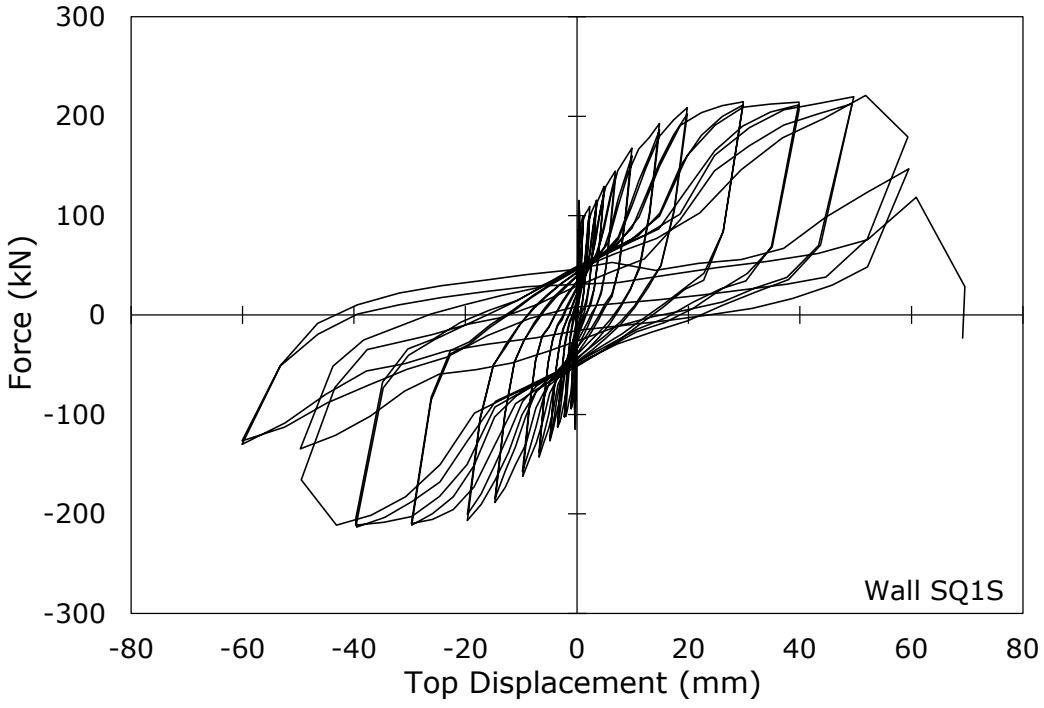


Figure 3-20 Predicted response of Wall SQ1S

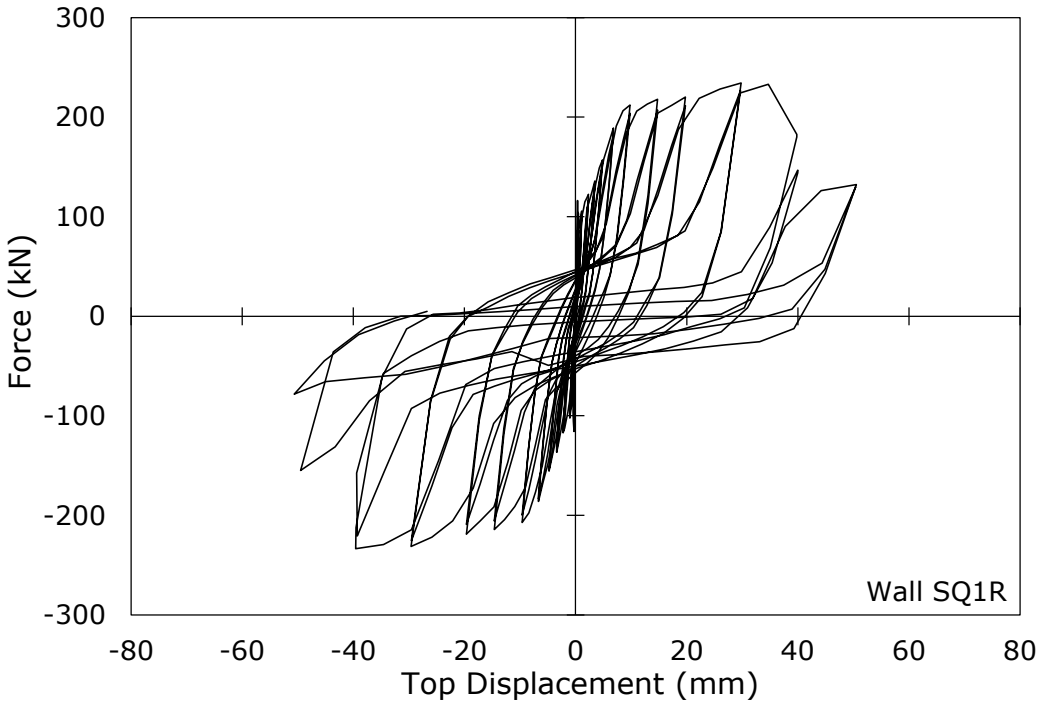


Figure 3-21 Predicted response of Wall SQ1R

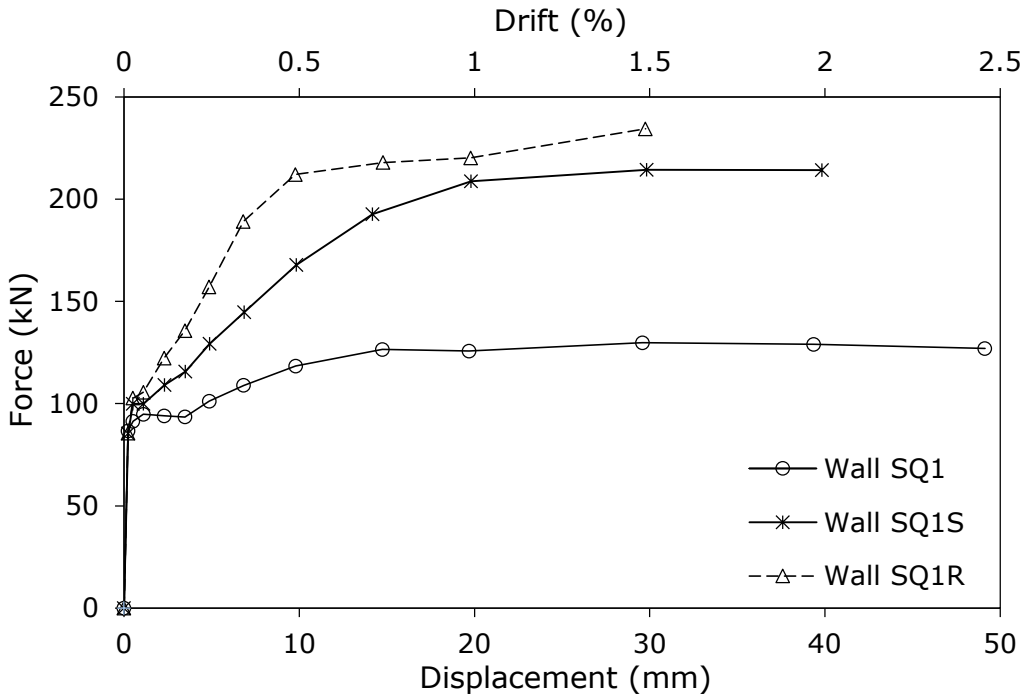


Figure 3-22 Envelope of force-displacement response of walls

Up to ultimate displacement, the constitutive models used to represent the SMA and steel braces satisfactorily captured the stress-strain response as observed during testing of the respective bare braces (Figure 3-23 and Figure 3-24). Note that the SMA constitutive model slightly underestimates the energy dissipation during unloading owing to the linear unloading rules. However, Abdulridha et al. (2013) demonstrated that the model was capable of capturing the response of SMA-reinforced concrete structural components.

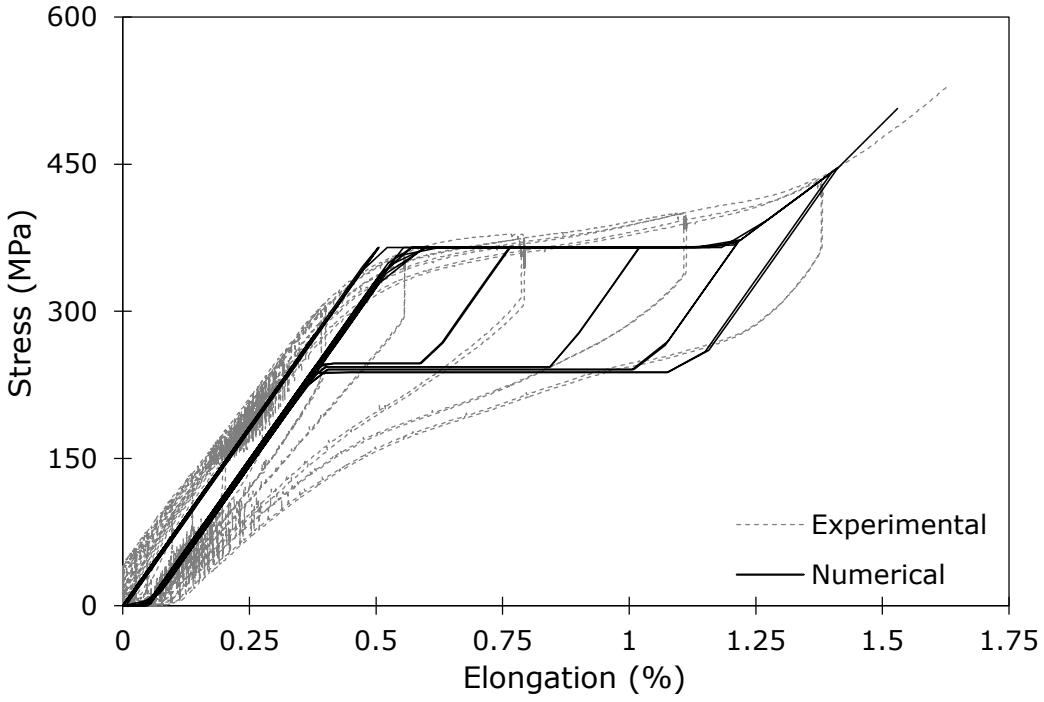


Figure 3-23 Comparison of SMA brace model with experimental response

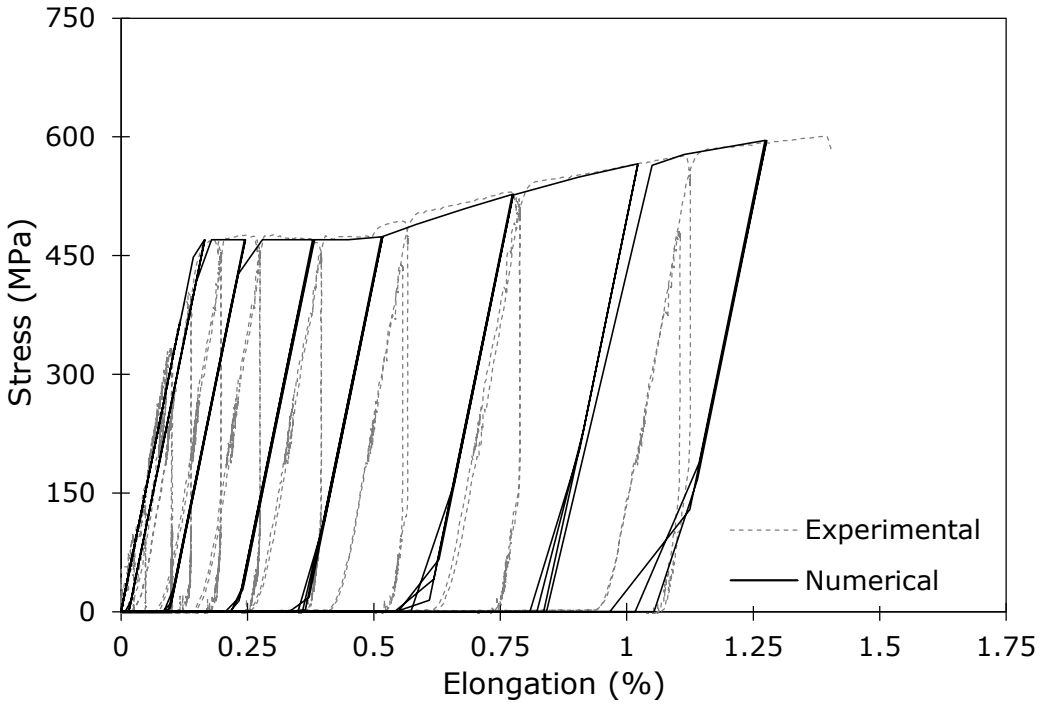


Figure 3-24 Comparison of steel brace model with experimental response

The force-displacement hysteretic response at 30 mm displacement is provided in Figure 3-25. In addition to strength improvements, the retrofitting systems did not alter the residual strength at zero displacement (approximately 50 kN), maintaining the level of pinching of the control wall. However, the SMA and steel braces altered the shape of the hysteretic cycles resulting in different residual displacements, with the SMA braces more effective at reducing the residual displacements than the steel braces. The larger hysteretic cycles of the retrofitted walls resulted in increased energy dissipation. Both retrofitting systems reduced the stiffness and strength degradations that were predicted in the control wall. The re-centering mechanism of the SMA braces resulted in similar first and second repetitions to the same displacement with minimum strength degradation, while yielding and the larger permanent deformations of the steel braces resulted in second repetitions with slightly greater strength and stiffness degradations. The strength degradation due to repetitions in loading was approximately 9% for Wall SQ1, 3% for Wall SQ1S, and 4% for Wall SQ1R.

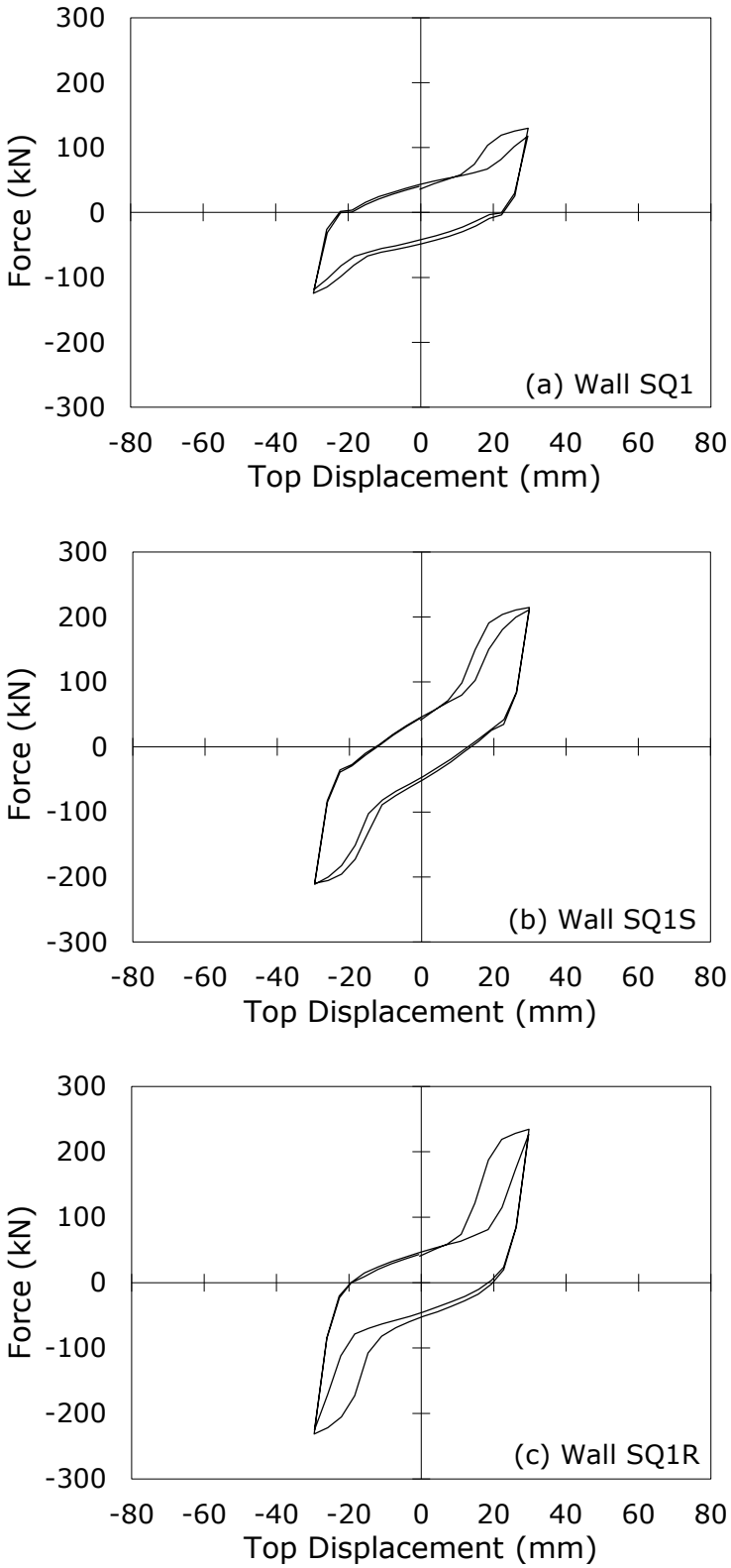


Figure 3-25 Cycle to 30 mm displacement: (a) SQ1; (b) SQ1S; and (c) SQ1R

The analysis predicted a major horizontal crack at the base of Wall SQ1 that promoted rocking throughout the simulation (Figure 3-26). This major crack, along with sliding at the base, resulted in stiffness and strength degradations between consecutive loading cycles and repetitions in loading. Similarly, the simulations predicted rocking in Walls SQ1S and SQ1R as a result of a major horizontal crack that surfaced at 200 mm from the base of the wall, just above the retrofitting system anchor plates (Figure 3-26). The heavily reinforced concrete elements simulating the anchoring plates increased the stiffness of the lower 200 mm of the wall, shifting the location of the horizontal crack away from the base of the wall. Localized cracking and rocking of the walls resulted in rupturing of the internal vertical reinforcing steel at one end of the wall and high compressive stresses at the other end. Rupturing of reinforcing steel was captured during the first repetition to 60 mm, 50 mm, and 40 mm displacement for walls SQ1, SQ1S, and SQ1R, respectively. At 30 mm displacement, the plastic strain of the outermost longitudinal reinforcement in the walls was 6.9%, 8.9%, and 9.4% for SQ1, SQ1S, and SQ1R, respectively.

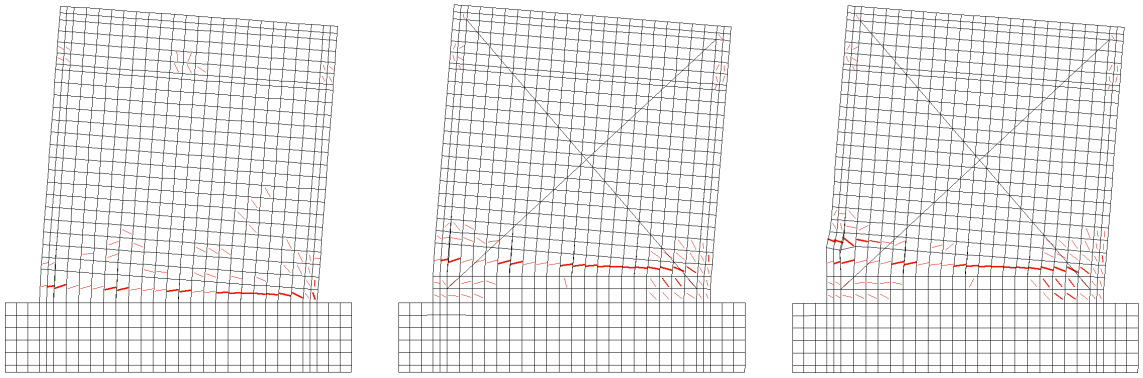


Figure 3-26 Damage of shear walls at 30 mm: (a) Wall SQ1; (b) Wall SQ1S; and (c) Wall SQ1R

Table 3-2 summarizes the response parameters for all three walls. The stiffness, strength, and ductility ($\mu = \Delta_u / \Delta_y$) of the walls were determined based on the equivalent stiffness elastic-plastic (bi-linear) yield model (Park 1989). The ultimate load and the ultimate displacement, Δ_u, corresponded to the cycle prior to failure of the walls (rupture of steel). The energy dissipation at ultimate, E_u, corresponds to the

cumulative energy of all repetitions of loading, and the residual displacement at ultimate, Δ_{ru}, corresponds to the displacement at zero load.

Table 3-2 Predicted response parameters of Walls SQ1, SQ1S, and SQ1R

Wall	Yield	Ultimate				Stiffness (kN/mm)	Ductility (mm/mm)
	Disp. (mm)	Disp. (mm)	Strength (kN)	Cum. Energy (kN-mm)	Residual Disp. (mm)		
SQ1	6.25	50	127	53597	37.2	20.3	8.00
SQ1S	12.50	40	220	48680	17.0	17.6	3.20
SQ1R	8.00	30	234	31147	18.5	29.3	3.75

Note: Disp. = displacement; and Cum. = cumulative

Ductility

As provided in Table 3-2, the control wall (SQ1) experienced ultimate displacement larger than the retrofitted walls. Differences in the ultimate displacements are attributed to redistribution of stresses due to the additional axial forces exerted by the retrofitting systems, which induced earlier rupture of the internal reinforcement. Ductility of Walls SQ1, SQ1S, and SQ1R were based on the bi-linear idealization of the cyclic responses, which does not satisfactorily match the predicted envelope responses of the retrofitted walls. A tri-linear model based on yielding of the internal reinforcement and yielding of the braces provides a better fit. Yielding of the internal reinforcement for Walls SQ1S and SQ1R occurred approximately at the same displacement as Wall SQ1. Assuming that the yield point of the retrofitted walls corresponded to the yield point estimated for the control wall, the ductility of Walls SQ1S and SQ1R would be 6.4 and 4.8, respectively. Note, however, that the reduced ductility of SQ1S and SQ1R are accompanied with significant increases in lateral strength, and it is a combination of strength and displacement capacities to achieve the performance point.

Energy Dissipation

The larger cycles of the retrofitted walls resulted in increases of energy dissipation at each displacement level as demonstrated in Figure 3-27. Wall SQ1 experienced the largest dissipation of energy at ultimate (Table 3-2), as a direct result of the larger displacement at failure. However, prior to failure, the retrofitted walls exhibited

greater energy dissipation compared to the control wall. Walls SQ1S and SQ1R provided similar energy dissipation, approximately 33% greater than Wall SQ1 up to 30 mm displacement (Figure 3-27). At 40 mm displacement, the energy dissipation capacity of Wall SQ1S exceeded that of Wall SQ1R, mainly due to earlier failure of Wall SQ1R. Similar to the bare brace tests, Wall SQ1R dissipated more energy during the first repetitions of loading, while Wall SQ1S dissipated approximately the same energy during the first and second repetitions.

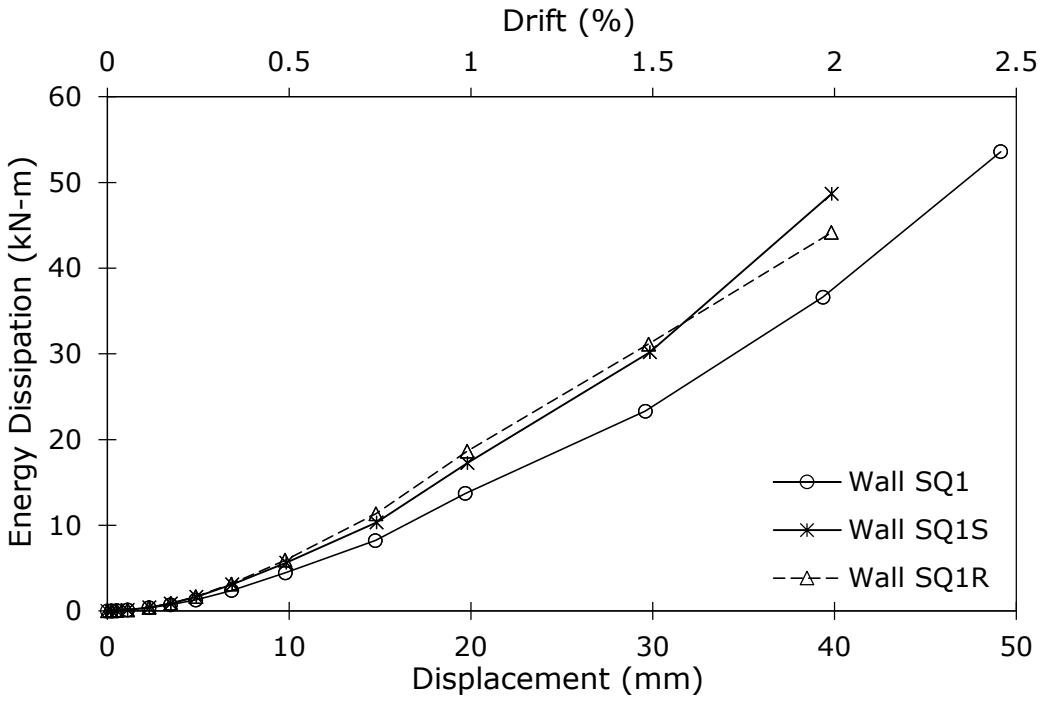


Figure 3-27 Cumulative energy dissipation of walls

Residual Displacement

The residual displacements at each displacement level are provided in Figure 3-28; while the corresponding displacement recovery capacities are illustrated in Figure 3-29. [The displacement recovery capacity is the ratio of the difference between the peak displacement and the residual displacement to the peak displacement.] With increases in lateral displacements up to 30 mm, the recovery capacities continually decreased for Walls SQ1 and SQ1R, while Wall SQ1S maintained a constant recovery capacity beyond 10 mm displacement. At ultimate, Walls SQ1, SQ1S, and SQ1R

experienced residual displacements of 37.2 mm, 17 mm, and 18.5 mm, respectively (Table 3-2). The corresponding displacement recovery capacities were approximately 24%, 55%, and 34%, respectively. In addition, at 30 mm (ultimate displacement of SQ1R), Wall SQ1S experienced residual displacement of 13.6 mm, and Wall SQ1R experienced residual displacement of 19.7 mm. These residual displacements corresponded to 60% and 87% of the residual displacement of Wall SQ1 (22.7 mm), further demonstrating the greater re-centering capability of the SMA braces.

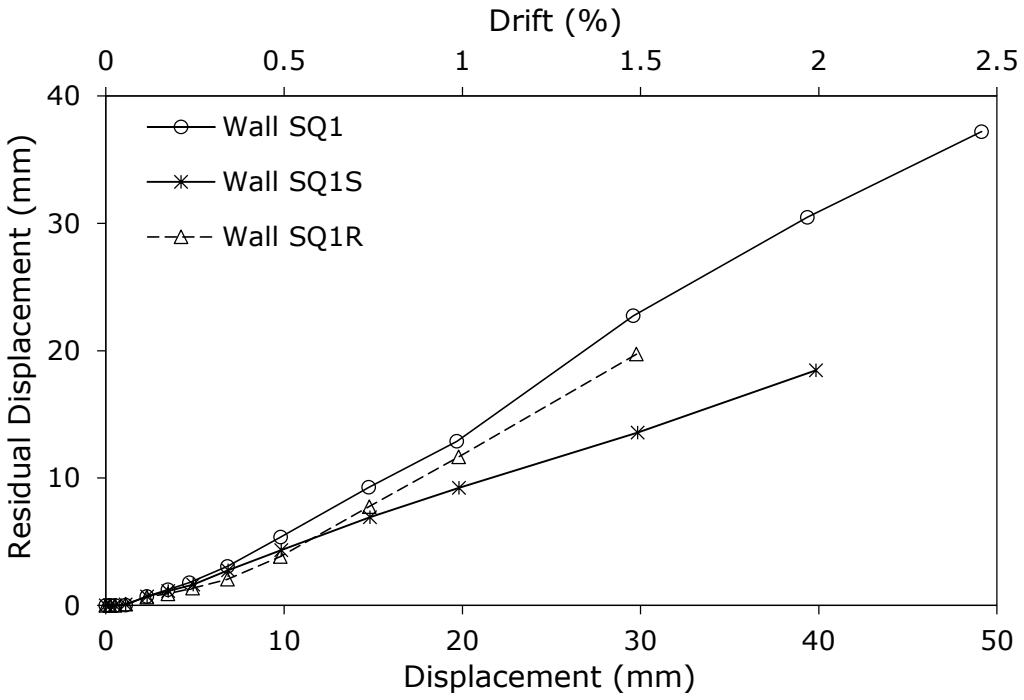


Figure 3-28 Residual displacement of walls

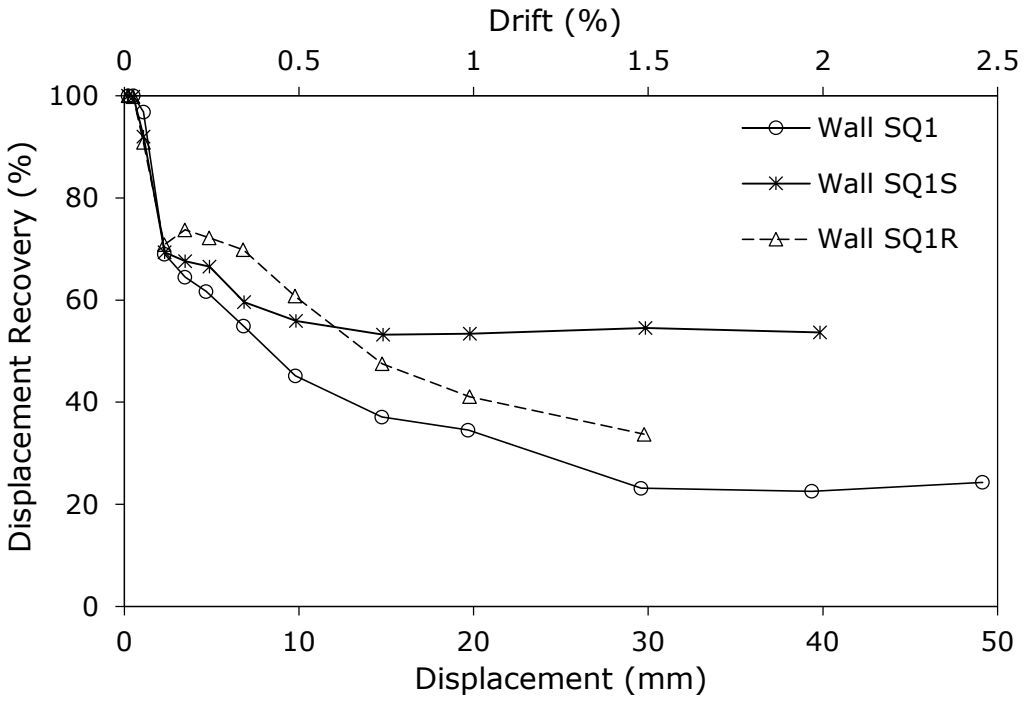


Figure 3-29 Displacement recovery of walls

3.8 Conclusions

An SMA tension brace was developed to retrofit seismic deficient reinforced concrete shear walls. The objective of the retrofitting system was to improve strength and energy dissipation, while reducing permanent deformations. The SMA braces consisted of an SMA link connected to rigid steel members with mechanical couplers. Companion steel braces were also constructed. Based on bare brace tests and numerical modelling of reinforced concrete shear walls retrofitted with either SMA or steel braces, the following conclusions are drawn:

1. The SMA and steel braces sustained comparable strength and displacement capacities exceeding the design target elongation. Testing of an additional SMA brace demonstrated that the elongation of the SMA link was significantly improved by reducing the cross-section between the mechanical couplers.

2. The energy dissipation of the braces was dependent on the stress-strain response of the SMA and steel links. The cumulative energy dissipation of the

steel braces increased linearly, while it increased exponentially for the SMA braces. The steel braces dissipated greater energy up to the cycle prior to the target elongation, while the SMA braces dissipated more energy at the target elongation and beyond.

3. The SMA braces experienced excellent deformation recovery due to re-centering of the SMA link. Conversely, the steel brace experienced significant permanent deformations due to yielding of the steel link.

4. Results from numerical simulations indicated that the SMA and steel braces increased the lateral strength relative to the control wall. The greater increase of strength provided by the steel braces was due to the greater strength of the steel links. Furthermore, the retrofitting systems reduced the stiffness and strength degradations that were predicted in the control wall.

5. Walls SQ1S (SMA braces) and SQ1R (steel braces) sustained smaller drifts than the control wall. Nevertheless, Wall SQ1S exceeded the calculated performance point drift.

6. The analyses predicted greater energy dissipation capacity for the retrofitted walls relative to the control wall. At the target displacement, Wall SQ1S dissipated slightly greater energy than Wall SQ1R.

7. The numerical results demonstrated the superior re-centering capabilities of the SMA braces. At ultimate, Wall SQ1S recovered more than 50% of the lateral displacement.

In summary, this study illustrates that squat reinforced concrete shear walls retrofitted with superelastic, tension-only SMA braces, experienced increases in strength, energy dissipation, and displacement recovery, and reductions in stiffness and strength degradations. Furthermore, these braces can be designed following a performance-based methodology. Although this study was limited to numerical analysis, future testing of the walls retrofitted with the proposed braces will provide data to corroborate the models presented herein.

3.9 Acknowledgments

The authors wish to express their gratitude to Public Works and Government Services Canada (PWGSC) and the Canadian Seismic Research Network [Grant: NETGP/350698-07], a Natural Sciences and Engineering Research Council of Canada strategic network, for providing funding for the development of novel retrofitting techniques to mitigate seismic damage of reinforced concrete structures.

3.10 References

Abdulridha, A., and Palermo, D. (2014). "Response of a hybrid SMA reinforced concrete shear wall." *Tenth U.S. National Conference on Earthquake Engineering*, Network for Earthquake Engineering Simulation, Anchorage, AK, USA.

Abdulridha, A., Palermo, D., Foo, S., and Vecchio, F. J. (2013). "Behavior and modeling of superelastic shape memory alloy reinforced concrete beams." *Eng Struct*, 49, 893–904.

Alam, M. S., Nehdi, M., and Youssef, M. A. (2009). "Seismic performance of concrete frame structures reinforced with superelastic shape memory alloys." *Smart Struct Syst*, 5(5), 565–585.

Alam, M. S., Youssef, M. A., and Nehdi, M. (2007). "Utilizing shape memory alloys to enhance the performance and safety of civil infrastructure: a review." *Canadian J. Civ. Eng.*, 34(9), 1075–1086.

Alam, M. S., Youssef, M. A., and Nehdi, M. (2008). "Analytical prediction of the seismic behaviour of superelastic shape memory alloy reinforced concrete elements." *Engineering Structures*, 30(12), 3399–3411.

ASCE. (2007). *ASCE/SEI 41-06 Seismic rehabilitation of existing buildings*. American Society of Civil Engineers, Reston, VA, USA.

ASTM. (2014). *ASTM F2516-14 Standard test method for tension testing of nickel-titanium superelastic materials*. ASTM International, West Conshohocken, PA, USA.

ASTM. (2016). *ASTM A615/A615M-16, Standard specification for deformed and plain carbon-steel bars for concrete reinforcement*. ASTM International, West Conshohocken, PA, USA.

ATC. (1996). *ATC-40 Seismic evaluation and retrofit of concrete buildings*. Applied Technology Council, Redwood City, CA, USA.

ATC. (2005). *FEMA 440 Improvement of nonlinear static seismic analysis procedures*. Applied Technology Council, Washington D.C., USA.

ATC. (2007). *FEMA 461 Interim testing protocols for determining the seismic performance characteristics of structural and nonstructural components*. Federal Emergency Management Agency, Washington D.C., USA.

Auricchio, F., Fugazza, D., and DesRoches, R. (2006). "Earthquake performance of steel frames with Nitinol braces." *J Earthq Eng*, 10(sup001), 45–66.

Billah, A. H. M. M., and Alam, M. S. (2012). "Seismic performance of concrete columns reinforced with hybrid shape memory alloy (SMA) and fiber reinforced polymer (FRP) bars." *Construction and Building Materials*, 28(1), 730–742.

Christopoulos, C., Filiatrault, A., and Folz, B. (2002). "Seismic response of self-centring hysteretic SDOF systems." *Earthq Eng Struct Dyn*, 31(5), 1131–1150.

Cortés-Puentes, W. L., and Palermo, D. (2011). "Modelling seismically repaired and retrofitted reinforced concrete shear walls." *Comput Concr*, 8(5), 541–561.

Cortés-Puentes, W. L., and Palermo, D. (2012). "Modeling of RC shear walls retrofitted with steel plates or FRP sheets." *J Struct Eng*, 138(5), 602–612.

Cortés-Puentes, W. L., and Palermo, D. (2015). "Performance of retrofitted squat concrete shear walls." *The 11th Canadian Conference on Earthquake Engineering*, Canadian Association for Earthquake Engineering, Victoria, BC, Canada.

DesRoches, R., McCormick, J., and Delemont, M. (2004). "Cyclic properties of superelastic shape memory alloy wires and bars." *J Struct Eng*, 130(1), 38–46.

Dolce, M., Cardone, D., Ponzo, F. C., and Valente, C. (2005). "Shaking table tests on reinforced concrete frames without and with passive control systems." *Earthq Eng Struct Dyn*, 34(14), 1687–1717.

Effendy, E., Liao, W. I., Song, G., Mo, Y. L., and Loh, C. H. (2006). "Seismic behavior of low-rise shear walls with SMA bars." *Earth & Space 2006*, American Society of Civil Engineers, Houston, TX, 1–8.

Eligehausen, R., Popov, E. P., and Bertéro, V. . (1983). *Local bond stress-slip relationship of deformed bars under generalized exitations*. Report, Earthquake Engineering Center, University of California, Berkeley, CA, USA.

Janke, L., Czaderski, C., Motavalli, M., and Ruth, J. (2005). "Applications of shape memory alloys in civil engineering structures - overview, limits and new ideas." *Mater Struct*, 38(279), 578–592.

Nehdi, M., Alam, M. S., and Youssef, M. A. (2010). "Development of corrosion-free concrete beam–column joint with adequate seismic energy dissipation." *Eng Struct*, 32(9), 2518–2528.

Newmark, N. M., and Hall, W. J. (1982). *Earthquake spectra and design*. Engineering monographs on earthquake criteria, structural design, and strong motion records ; v. 3, Earthquake Engineering Research Institute, Berkeley, CA, USA.

NRC. (1965). *National building code of Canada*. Associate committee on the national building code, National Research Council of Canada, Ottawa, ON, Canada.

NRC. (2010). *National building code of Canada*. Associate committee on the national building code, National Research Council of Canada, Ottawa, ON, Canada.

Park, R. (1989). "Evaluation of ductility of structures and structural assemblages from laboratory testing." *Bull N Z Natl Soc Earthq Eng*, 22(3), 155–166.

Saiidi, M. S., O'Brien, M., and Sadrossadat-Zadeh, M. (2009). "Cyclic response of concrete bridge columns using superelastic Nitinol and bendable concrete." *ACI Struct J*, 106(1), 69–77.

Saiidi, M. S., Sadrossadat-Zadeh, M., Ayoub, C., and Itani, A. (2007). "Pilot study of behavior of concrete beams reinforced with shape memory alloys." *J Mater Civ Eng*, 19(6), 454–461.

Saiidi, M. S., and Wang, H. (2006). "Exploratory study of seismic response of concrete columns with shape memory alloys reinforcement." *ACI Struct J*, 103(3), 436–443.

Song, G., Ma, N., and Li, H.-N. (2006). "Applications of shape memory alloys in civil structures." *Eng Struct*, 28(9), 1266–1274.

Tazarv, M., and Saiidi, M. S. (2015). "Reinforcing NiTi superelastic SMA for concrete structures." *Journal of Structural Engineering*, 141(8), 04014197, 1–10.

Wong, P. S., Vecchio, F. J., and Trommels, H. (2013). *VecTor2 and Formworks user's manual: second edition*. Manual, Dept. of Civil Engineering, University of Toronto, Toronto, ON, Canada.

Youssef, M. A., Alam, M. S., and Nehdi, M. (2008). "Experimental investigation on the seismic behavior of beam-column joints reinforced with superelastic shape memory alloys." *J Earthq Eng*, 12(7), 1205–1222.

Youssef, M. A., and Elfeki, M. A. (2012). "Seismic performance of concrete frames reinforced with superelastic shape memory alloys." *Smart Struct Syst*, 9(4), 313–333.

Zafar, A., and Andrawes, B. (2012). "Incremental dynamic analysis of concrete moment resisting frames reinforced with shape memory composite bars." *Smart Mater Struct*, 21(2), 025013, 1–14.

Chapter 4

Seismic Retrofit of Concrete Shear Walls with SMA Tension Braces

Authors: W. Leonardo Cortés-Puentes, Dan Palermo

Abstract

A bracing system consisting of tension-only, superelastic Nickel-Titanium, Shape Memory Alloys (SMA) was developed and implemented as a retrofitting methodology for seismically deficient squat reinforced concrete shear walls. The bracing system incorporates SMA links that serve as resettable fuses with unique re-centering and energy dissipation properties that result in improved hysteretic response. The study focused on one-third scale walls that represented pre-1970s reinforced concrete shear walls susceptible to shear sliding and diagonal tension cracking. Four walls, two control and two retrofitted with the SMA bracing system, were tested under reversed cyclic loading. The SMA braces demonstrated excellent performance as a retrofitting device improving the seismic response of squat reinforced concrete shear walls including lateral strength capacity, ductility, energy dissipation, and displacement recovery. The retrofitting system was central in minimizing damage at the base of the walls. [Supplementary experimental results for the seismic retrofit of the concrete shear walls with SMA tension braces are presented in Appendix B.]

Keywords

Shape memory alloys; tension braces; seismic retrofit; reinforced concrete; squat shear walls.

4.1 Introduction

Advancements in Shape Memory Alloys (SMAs) have translated into the development of smart retrofitting systems that are capable of improving the seismic response of existing seismically deficient reinforced concrete shear walls. These novel retrofitting systems possess re-centering and dynamic properties that can improve strength, ductility, and energy dissipation, while mitigating damage and reducing residual deformations. Comprehensive characterization of superelastic SMAs (Dolce and Cardone 2001a; b; Fang et al. 2015; McCormick et al. 2007; Nemat-Nasser and Guo 2006; Piedboeuf et al. 1998; Tyber et al. 2007) has provided confidence in the use of these materials for the development of reinforcing and retrofitting strategies for seismic applications. The majority of these studies have focused on commercially available superelastic Nickel-Titanium (NiTi) SMAs, which have the capacity to recover up to 98% of the deformations experienced by the material when subjected to strains up to 6% and provide equivalent viscous damping approaching 7% (DesRoches et al. 2004).

Given the capacity to recover significant strain levels, superelastic SMAs have been explored as reinforcing and retrofitting materials for a large range of concrete structures (Alam et al. 2007; Janke et al. 2005; Song et al. 2006). Experimental and numerical studies demonstrated that superelastic SMAs reduce residual deformations and provide excellent energy dissipation in concrete beams (Abdulridha et al. 2013; Kuang and Ou 2008; Malagisi et al. 2014; Saiidi et al. 2007; Zafar and Andrawes 2013), concrete columns (Nakashoji 2014; Saiidi et al. 2009; Saiidi and Wang 2006; Tazarv and Saiidi 2015), concrete beam-column joints (Cruz-Noguez and Saiidi 2012; Nehdi et al. 2010; Youssef et al. 2008), concrete frames (Alam et al. 2009; Meshaly et al. 2014; Youssef and Elfeki 2012; Zafar and Andrawes 2012), and concrete shear walls (Abdulridha and Palermo 2014; Ghassemieh et al. 2012). The benefits of superelastic SMAs as the main components in dampers and restraining systems for concrete bridges (Adachi and Unjoh 1999; DesRoches and Delemont 2002; Ozbulut and Hurlebaus 2010) and steel buildings (Silwal et al. 2015) have also been evaluated.

Bracing systems based on superelastic SMAs are capable of improving the seismic response of structures (Salichs et al. 2001; Soul and Yawny 2015). While various researchers have developed SMA-bracing systems to improve the lateral response of steel structures (Auricchio et al. 2006; Dezfuli et al. 2017; Gao et al. 2016; McCormick et al. 2006; Motahari et al. 2007; Qiu and Zhu 2017; Speicher et al. 2017; Sultana and Youssef 2016; Yang et al. 2010), only a few have focused on reinforced concrete structures (Dolce et al. 2005; Effendy et al. 2006; Liao and Mo 2006; Meshaly et al. 2014). Results from experimental and numerical studies have demonstrated that bracing systems and passive control devices incorporating superelastic SMA wires, rods, and rings are effective in reducing vibrations and improving re-centering, while providing energy dissipation. Although effective in improving the response of structures, SMA braces have some limitations. Braces based on SMA wires employ a significant number of wires to develop sufficient force capacity and require specialized fabrication not feasible in field applications. Braces incorporating SMA rods may experience buckling due to the high compressive stresses associated with large lateral displacement demands imposed on the structure, which alters the expected failure mode of the braces and limits the contributions of the SMA to strength and energy dissipation. In addition, bracing systems based on SMA rings require stiff rigid cables or steel truss members to ensure maximum re-centering. Other SMA-bracing systems combining traditional Buckling Restrained Braces (BRB) with SMA rods (Miller et al. 2012) have demonstrated satisfactory energy dissipation that can potentially reduce displacement demands in structures. The steel core of the BRB, however, limits the recovery capacity of the braces.

Effendy et al. (2006) conducted the only study, known by the authors, on external bracing of squat reinforced concrete shear walls with SMAs. The walls, reinforced with external bi-diagonal superelastic SMA rods in combination with internal reinforcing steel, experienced lateral strength similar to control walls reinforced with equivalent internal reinforcing steel. The low tensile straining and compression buckling of the SMA rods limited the re-centering and energy dissipation benefits of the SMA.

4.2 Research Significance

Previous research highlighted salient features of SMAs that can be exploited to improve seismic response. Conversely, a number of shortcomings have been encountered in the application of SMAs in bracing systems, in addition to limitations of SMA rods including low modulus of elasticity and high cost relative to traditional structural steel. The cost of superelastic SMA rods can be up to 40 times the cost of ASTM A36 hot-rolled steel and 20 times greater than SAE Grade 316 stainless steel rods. Note that the A36 structural steel is the typical material for tie rod braces. To address these challenges, the authors developed an efficient, tension-only SMA bracing system that is practical and suitable for a wide range of concrete structures. Furthermore, the proposed braces are also applicable to steel structures.

The SMA bracing system, presented herein, incorporates optimized SMA links with reduced length that serve as fuses where recoverable deformations are concentrated. The links, in turn, are coupled to rigid steel elements that sustain negligible elastic deformations. The SMA links are resettable elements that can be removed or replaced while the steel elements remain connected to the retrofitted structure. By optimizing the length of the SMA link, the cost of the brace is significantly reduced. The cost of fabrication and installation of the proposed SMA brace is approximately 65% greater than that of equivalent braces incorporating ASTM A36 hot-rolled steel and SAE 316 stainless steel links. Given the re-centering effect of the SMA, and the potential reduction in residual lateral drift and associated residual damage, the criteria used to select the SMA bracing system should not be solely assessed on the initial investment. Savings in post-earthquake repairs would offset the initial cost of the retrofitting system.

This study presents experimental results of seismically deficient squat reinforced concrete shear walls retrofitted with the proposed SMA bracing system. Squat shear walls are the focus of this study given the expected prevailing diagonal deformations, which would impose large elongations in the SMA braces and activate the beneficial recovery properties.

4.3 Experimental Program

Two control walls (Wall SQ1 and Wall SQ2) and two retrofitted walls (Wall SQ1S and Wall SQ2S) with aspect ratio of 1.0 were subjected to incremental reverse cyclic lateral loading. Wall SQ1 (2000 mm in length × 2000 mm in height × 100 mm in thickness) represented a lightly reinforced shear wall prone to shear sliding at the base (Figure 4-1), and Wall SQ2 (2000 mm × 2000 mm × 125 mm) represented a stronger shear wall with boundary zones that is controlled by diagonal tension cracking (Figure 4-2). The shear walls were 1/3rd-scale models of a prototype shear wall designed according to the 1965 edition of the National Building Code of Canada (NRC 1965). Full details of the prototype structures are provided elsewhere (Cortés-Puentes and Palermo 2012).

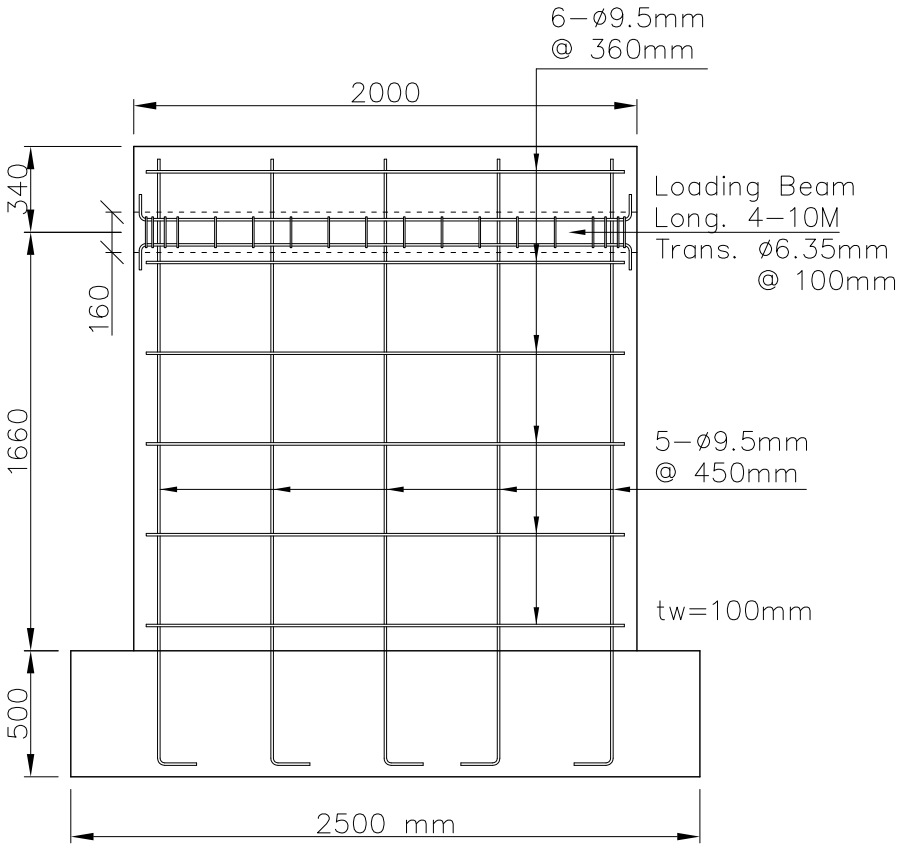


Figure 4-1 Detail of Walls SQ1 and SQ1S

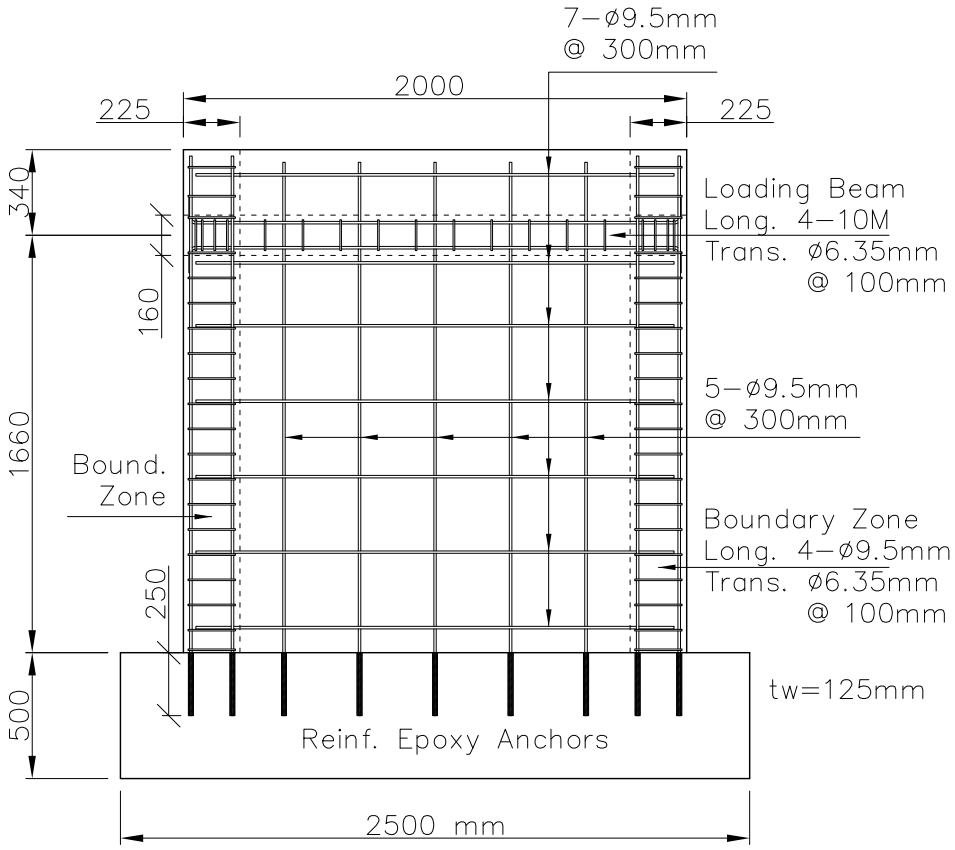


Figure 4-2 Detail of Walls SQ2 and SQ2S

Walls SQ1/SQ1S were reinforced with a single-layer of 5-ϕ9.5 mm vertical reinforcing bars (0.18% reinforcement ratio) and 6-ϕ9.5 mm horizontal reinforcing bars (0.21% reinforcement ratio) as illustrated in Figure 4-1. [Note that ϕ refers to diameter.] The design of Walls SQ2/SQ2S included 225 mm-long boundary zones at the ends of the walls with concentrated vertical reinforcement (Figure 4-2). The web region of Walls SQ2/SQ2S, reinforced with 5-ϕ9.5 mm vertical reinforcement and 7-ϕ9.5 mm horizontal reinforcement, contained the same vertical reinforcement ratio (0.18%) and approximately the same horizontal reinforcement ratio (0.20%) as Wall SQ1/SQ1S. The boundary zones were reinforced with 4-ϕ9.5 mm longitudinal reinforcing bars (1.0% reinforcement ratio) and ϕ-6.35-mm transverse ties spaced at 100 mm (0.51% reinforcement ratio).

Walls SQ1S and SQ2S were further retrofitted with four SMA tension-only diagonal braces, externally attached to the lower and upper corners on each side of the walls as illustrated in Figure 4-3.

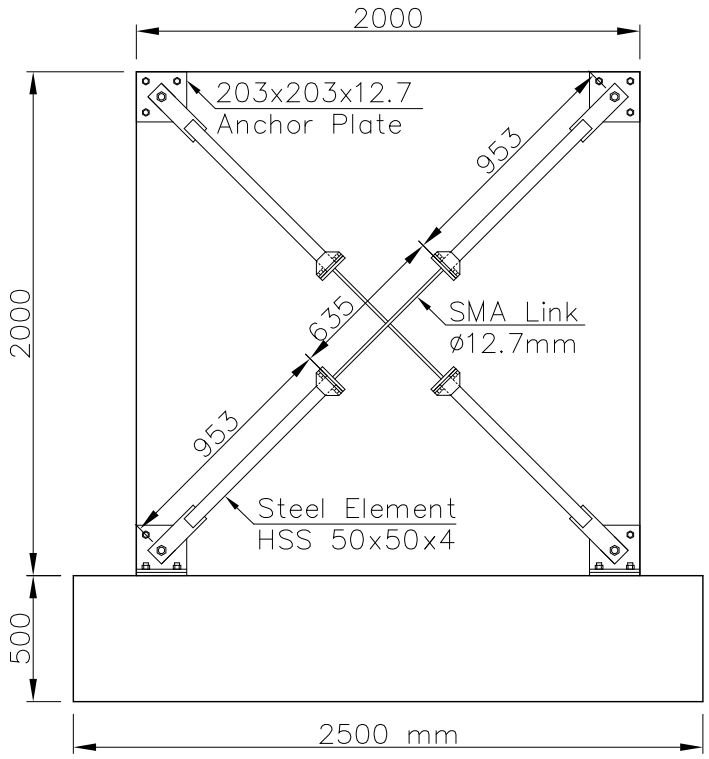


Figure 4-3 External retrofit of Walls SQ1S and SQ2S

The walls were constructed on heavily reinforced foundation blocks (2500 mm in length × 1400 mm in width × 500 mm in height) that simulated rigid foundation conditions. The foundation blocks were anchored to the strong floor of the structures laboratory with high strength anchor bolts. Beams with a depth of 160 mm and reinforced with 4-10M (ϕ11.3 mm) longitudinal reinforcing bars were embedded within the walls at a height of 1660 mm from the base to serve as a strengthened zone through which the lateral loading was imposed (Figure 4-1 and Figure 4-2). The exception was Wall SQ1, which was strengthened with externally bonded fibre reinforced polymer sheets along the location of the loading beam and at the top corners. The vertical reinforcement of Walls SQ1 and SQ1S terminated with standards hooks that were cast within the foundation blocks, while the vertical reinforcement in Walls SQ2 and SQ2S was anchored 250 mm into the existing

foundation blocks with epoxy. [Note that Walls SQ2 and SQ2S were constructed on the foundation blocks that were originally used for SQ1 and SQ1S.] Properties of the concrete and reinforcing bars are listed in Table 4-1 and Table 4-2, respectively.

Table 4-1 Concrete material properties

Wall	f'_c (MPa)	ε'_c (%)
SQ1	22.52	0.269
SQ1S	24.73	0.184
SQ2	20.26	0.187
SQ2S	27.37	0.222

Note: $f'c$ = compressive strength at the day of testing, and
ε'_c = compressive strain corresponding to f'_c

Table 4-2 Reinforcement material properties

ϕ (mm)	f_y (MPa)	ε_y (%)	f_u (MPa)	ε_u (%)
9.5	495	0.30	735	16
11.3	460	0.30	660	16

Note: ϕ = diameter, f_y = yield stress, ε_y = yield strain
f_u = ultimate stress, and ε_u = ultimate strain

The SMA braces consisted of 635 mm-long SMA links (Figure 4-4) connected to 953 mm-long rigid steel elements (Figure 4-5). The total length of the braces was 2540 mm. The SMA links were fabricated with smooth 12.7 mm-diameter Nitinol (nickel-titanium alloy) superelastic SMA rods with reduced diameter of 11.8 mm (cross sectional area of 110 mm^2) over a length of 500 mm, bar-lock couplers secured at the ends of the SMA rods with 18 shear-off bolts, and stiff steel plates placed on the inside of the couplers. The transition zone between the net and reduced cross sections of the SMA link was linear along a length of 7.5 mm to reduce stress concentration. To ensure tension-only forces in the SMA rods, one of the steel plates was welded to an end coupler, while the other plate was free (Figure 4-4). The rigid steel elements were fabricated with 50 mm × 50 mm × 4 mm hollow structural sections (HSS), 76 mm wide × 19 mm thick steel plate at one end, and stiff flanges at the other end to provide a connection to the SMA links. The ends of the SMA links were placed into the HSS and connected to the flanges of the rigid steel elements with high-strength, 15.9 mm-diameter (5/8 in) bolts (Figure 4-6).

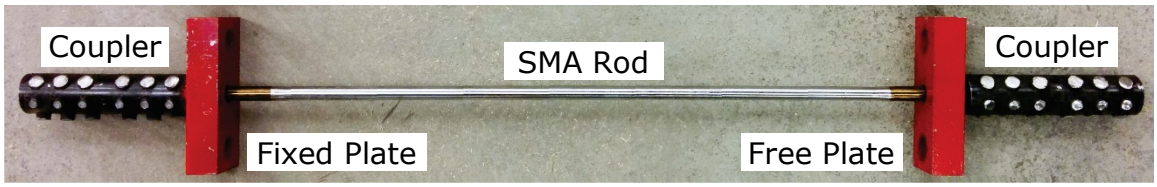


Figure 4-4 SMA link

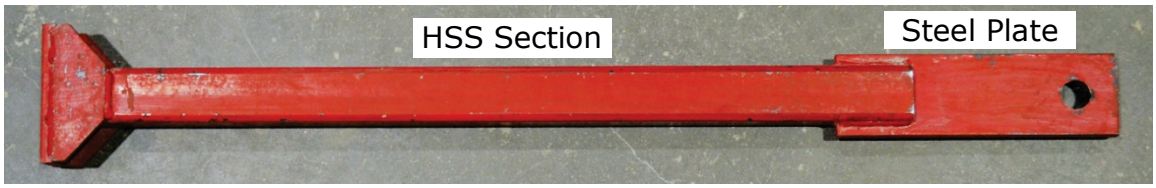


Figure 4-5 Rigid steel element

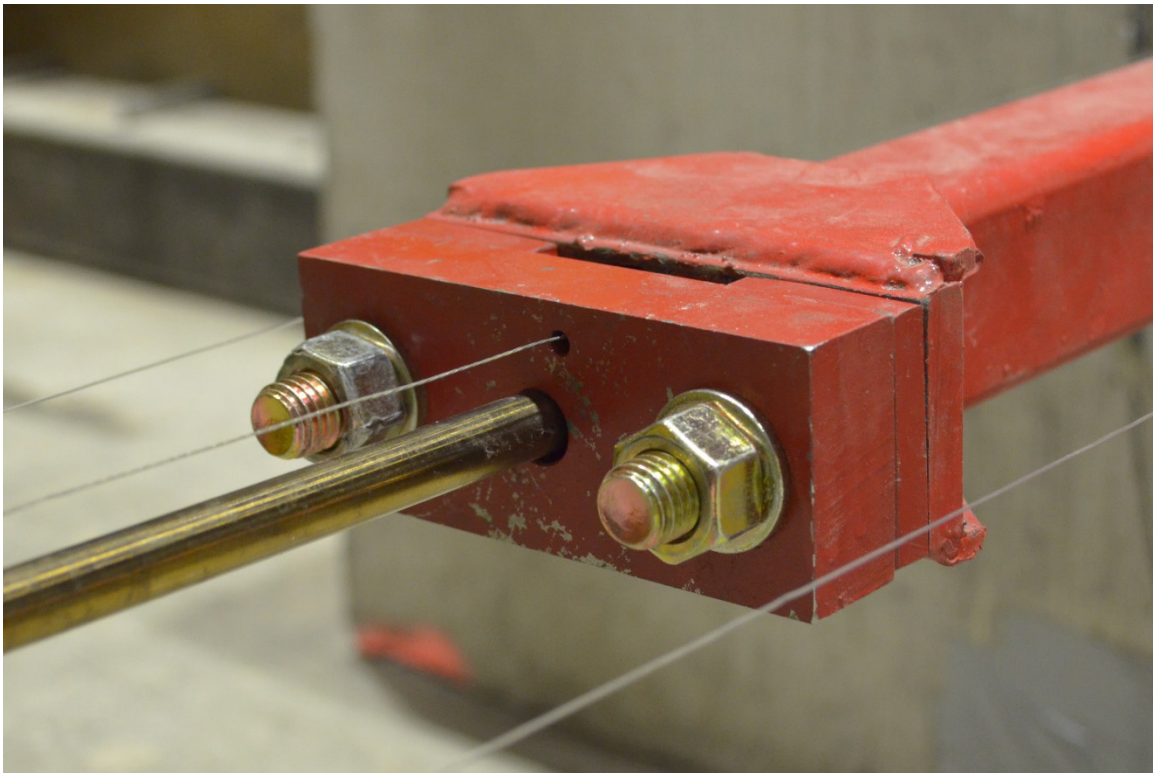


Figure 4-6 Connection of SMA link to rigid steel element

The characterization of the stresses and strains of the SMA was based on a loading protocol with an initial cycle to 6% strain and a second cycle to rupture, following the procedures specified in ASTM F2516-14 (ASTM 2014). The SMA rods had an upper plateau stress (pseudo-yielding) of 407 MPa at 3% strain; a lower plateau stress of 186 MPa at 2.5%; an ultimate stress (rupture) of 1054 MPa at 19.8%;

and a residual strain of 0.6% for the cycle to 6% (Figure 4-7). The second cycle to rupture resulted in an upper plateau stress of 357 MPa. The minimum operating temperature of the SMA to ensure superelastic behaviour, based on the fully annealed temperature, was -10˚C.

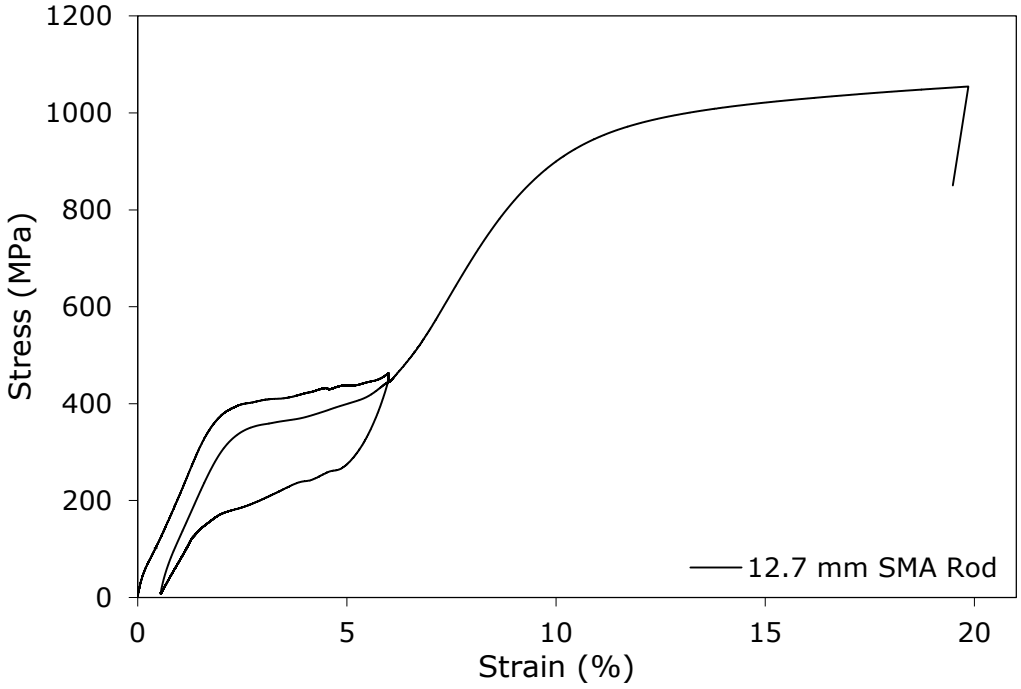


Figure 4-7 Stress-strain of 12.7-mm SMA rod

The SMA braces were initially designed to experience a target elongation of 38 mm, which corresponds to a strain of 6% in the SMA link, matching the strain recovery capacity of the SMA rods. Bare testing of the SMA braces under axial cyclic loading established the mechanical properties of the SMA braces (Cortés-Puentes and Palermo 2017). Testing was first conducted on SMA braces incorporating SMA links with the original diameter of 12.7 mm (Figure 4-8). The braces experienced an average pseudo-yield stress of 353 MPa, an average lower plateau stress of 172 MPa, and an ultimate stress of 525 MPa. Pseudo-yielding of the SMA braces initiated at approximately 0.4% elongation (1.6% elongation in the SMA link), based on an offset of 0.05% (0.2% offset in the link). Deformations corresponding to pseudo-yielding in the braces was concentrated in the SMA links, while the steel components experienced negligible elastic deformations. Although negligible, the elastic deformation of the

steel plates connecting the SMA links to the braces resulted in a sharp decrease of approximately 10 kN in strength at the initiation of unloading. Rupture at the location of the couplers occurred at 41 mm elongation, corresponding to 1.61% elongation of the full brace and 6.45% elongation of the SMA link. Figure 4-8 illustrates a typical force-elongation response of the SMA tension braces tested to failure. Although the target strain was achieved, further testing was conducted on the SMA brace with a reduced diameter of 11.8 mm in the central portion of the SMA link to provide a reserve strain capacity. The additional SMA link was fabricated with a Shape-Memory-Effect (SME) SMA rod. The SME-SMA had the same chemical composition and smoothness as the superelastic Nitinol SMA link, but did not possess the recovery properties after the removal of load. The main objectives of testing the additional link were to assess the increases in ductility of the SMA braces and strain capacity of the SMA links, and evaluate the ability to control the location of failure in the SMA links due to the reduced diameter of the SMA links. Previous tests on SMA-reinforced beams (Abdulridha et al. 2013) demonstrated that a reduced diameter in superelastic SMA rods does not alter the pseudo-elasticity, while ensuring that rupture does not initiate at the location of the couplers. This study demonstrated that the reduced diameter did not affect the stress-strain response of the SMA rods. The reduced diameter resulted in an ultimate elongation of the SMA link of 8.8%, corresponding to an elongation capacity of 56 mm. Full details of the bare brace testing can be found elsewhere (Cortés-Puentes and Palermo 2017).

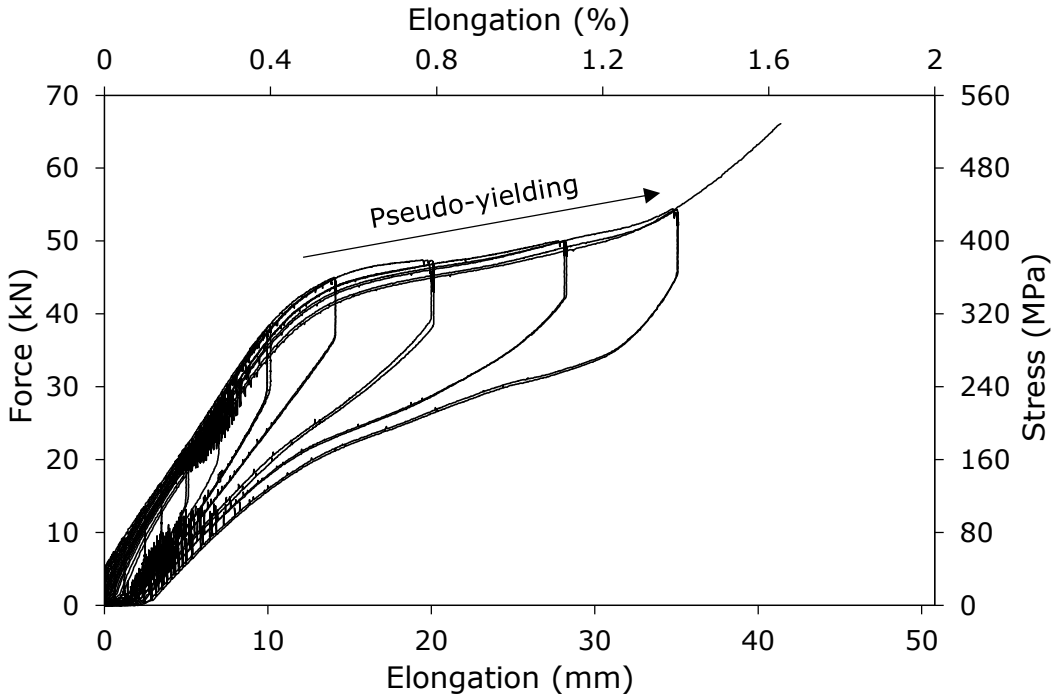


Figure 4-8 Force-elongation response of SMA brace

The pseudo-static loading protocol recommended by FEMA 461 (ATC 2007) was implemented during testing of the walls. Loading initiated with a pre-cracking cycle to 0.3 mm top displacement. The cycles were incremented by a factor of 2 in the pre-yielding stage and by a factor of 1.4 in the post-yield stage (damage stage) until the predetermined target displacement of 40 mm (2% drift) was achieved. The capacity spectrum method specified by ATC-40 (ATC 1996) and FEMA 440 (ATC 2005) was used to establish the performance point (lateral strength and displacement) for retrofitted structures. The performance point corresponds to the intersection of the capacity curve of the retrofitted structure with the reduced elastic demand. Nonlinear finite element analyses were used to calculate the performance point, which corresponded to approximately 37 mm (1.85% drift) of top lateral displacement in Wall SQ1. The SMA links were continually redesigned until the capacity curve of the retrofitted wall intersected the reduced elastic demand curve at the performance point. Full details of this analysis are provided elsewhere (Cortés-Puentes and Palermo 2017). Note that the performance point in this study corresponds to the collapse prevention performance level as defined by ASCE 41-06 (ASCE 2007).

Beyond the target displacement, the loading cycles were incremented by 10 mm. Each cycle consisted of two repetitions. No external axial loads were imposed on the walls. Based on the analysis of the prototype structure, the axial load ratio ($P/A_g f'_c$) on the walls ranged from 1% to 1.7%. At these levels of axial load, the response of the shear walls was not expected to deviate significantly relative to zero axial load. Note, however, that previous experimental testing (Gulec and Whittaker 2009) illustrated that as the axial load increases to higher levels, the shear strength increases, the drift capacity and energy dissipation are maintained, and the residual displacements are reduced. Furthermore, high axial loads increase the compressive stresses in the ends of the wall, contributing to crushing and diagonal compression failure modes. The in-plane lateral loading was applied with an actuator positioned at 1660 mm from the base of the wall (shear span of 0.83) as illustrated in Figure 4-9. One end of the actuator was mounted to an A-frame, while the other end was connected to the walls. A lateral supporting frame was positioned near the top of the walls to control out-of-plane displacements.

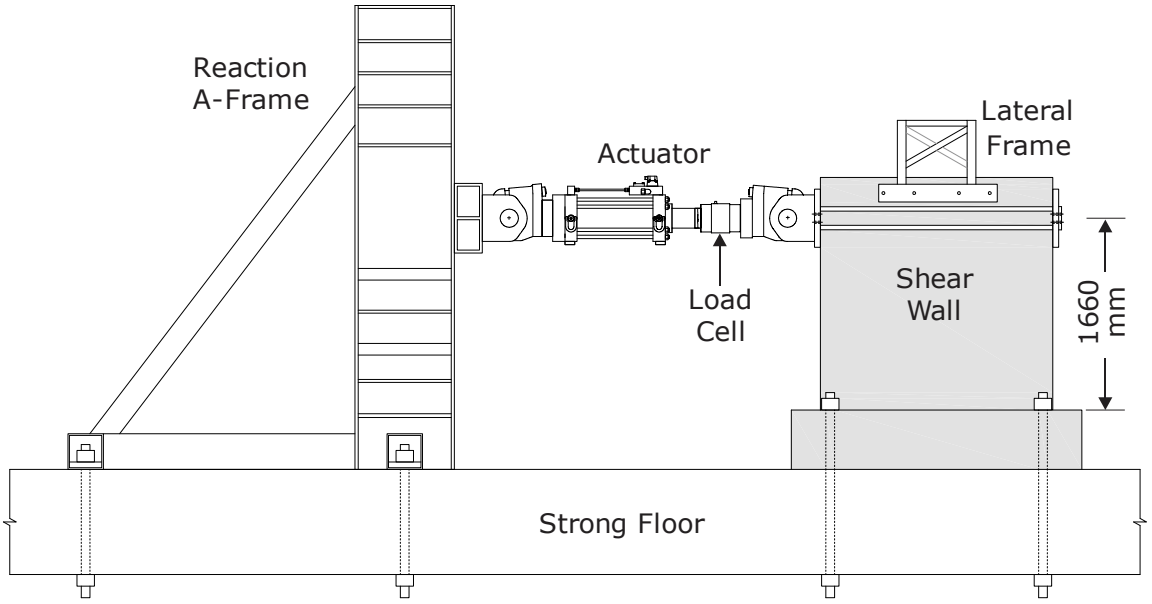


Figure 4-9 Test setup

Displacement Cable Transducers (DCTs) and Linear Variable Differential Transducers (LVDTs) were used to measure lateral and vertical displacements, diagonal deformations, bond slip, and sliding at the base of the walls. Strain gauges

were attached to the internal reinforcing steel to measure local straining where yielding and heavy damage was expected and to the SMA links to monitor the response of the braces.

4.4 Experimental Results

The results presented herein focus on the strength-displacement responses and the observed damage of the walls. The lateral displacements were measured at 2000 mm from the base of the walls. The positive displacements and strengths correspond to pushing the actuator (Figure 4-9). Conversely, negative displacements and strengths correspond to pulling the actuator.

4.4.1 Response of Walls SQ1 and SQ1S

Figure 4-10 and Figure 4-11 illustrate the lateral load-displacement responses of Walls SQ1 and SQ1S. First cracking along the base of the wall occurred during loading to 0.6 mm for SQ1 and SQ1S corresponding to lateral strengths of 61 kN and 90 kN, respectively. With increase in loading, damage was concentrated along the base cracking, resulting in behaviour controlled by rocking. Due to the additional stiffness provided by the retrofitting system, the horizontal crack in the boundary regions of Wall SQ1S shifted approximately 170 mm above the base. This crack formed along at weak plane introduced by the presence of the bolts in the anchor plates of the retrofitting system. First yielding of the bar nearest to the ends of the walls was captured by the strain gauges during the cycle to 1.2 mm at the lateral strength of 84 kN and 102 kN for Walls SQ1 and SQ1S, respectively. Yielding of the three vertical bars near the end of the wall was realized during the cycle to 2.4 mm at lateral strengths of 96 kN and 113 kN for Walls SQ1 and SQ1S, respectively. Global yielding of SQ1 and SQ1S, based on the equivalent elastic-plastic response (Park 1989), was 4.5 mm and 8.6 mm, respectively. At yielding, the maximum width of the crack at the base of the walls was approximately 3.8 mm.

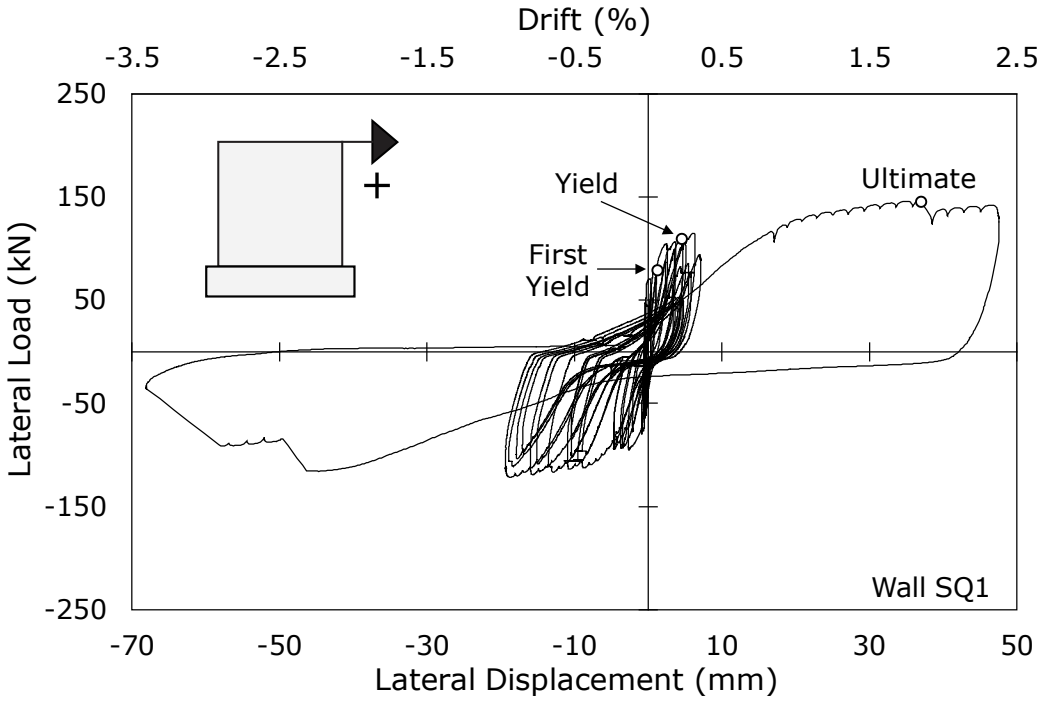


Figure 4-10 Lateral load-displacement response of Wall SQ1

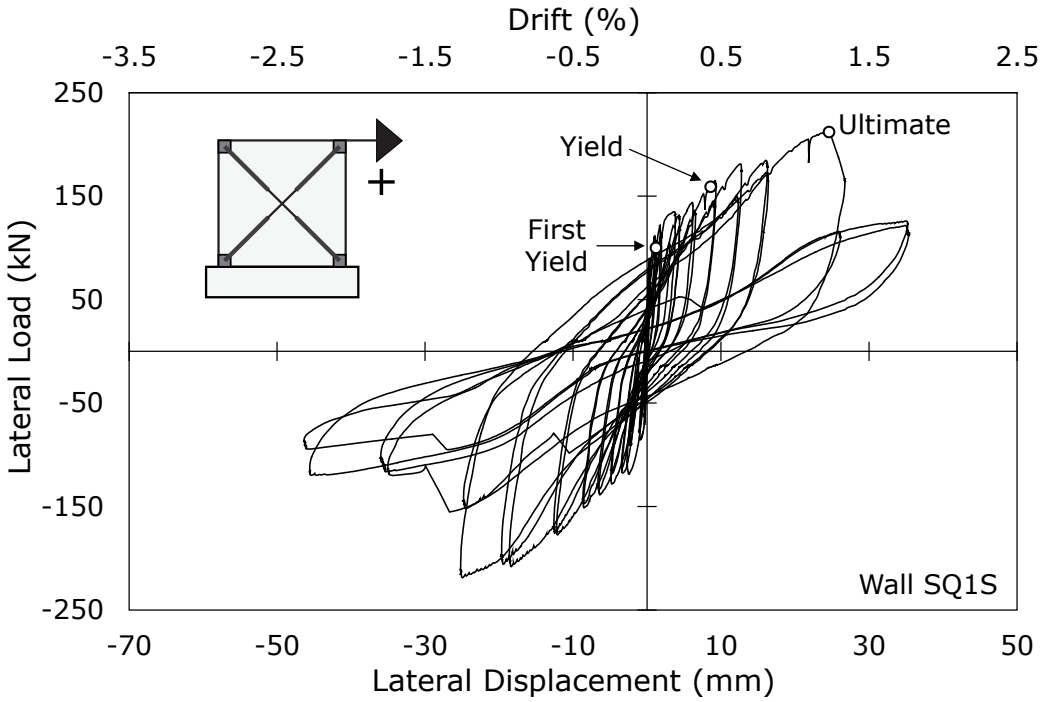


Figure 4-11 Lateral load-displacement response of Wall SQ1S

The lateral strength of Walls SQ1 and SQ1S continued to increase in the post-yield range. Wall SQ1 experienced peak strengths of 145 kN at +37 mm and 123 kN at -19 mm, while Wall SQ1S experienced peak strengths of 213 kN at +24.7 mm and 218 kN at -25 mm.

Note that beyond 5 mm of lateral displacement, Wall SQ1 was loaded asymmetrically due to an instrumentation error. This resulted in recorded displacements that did not necessarily correspond with the intended target displacements. At the intended target displacement to 12 mm (actual recorded displacements of +4.4 mm/-17.8 mm), the wall experienced a strength difference of approximately 54 kN between the negative and positive directions. It was realized that the full capacity of the wall was not achieved as a result of the asymmetrical loading; therefore, an additional cycle to 50 mm was imposed on the wall to capture the post-peak behaviour.

Figure 4-12 and Figure 4-13 illustrate the cracking experienced by Walls SQ1 and SQ1S at ultimate, which corresponded to the cycle prior to a decrease in lateral strength of more than 20%. Failure of Wall SQ1 was the result of rupturing of the longitudinal reinforcing bar nearest to the edge of the wall at +37 mm. Two additional bars ruptured at -46.3 mm and -58 mm, reducing the lateral strength to 36 kN. The LVDTs at the base of Wall SQ1 recorded crack widths of 17 mm and 24 mm at the edges of the main horizontal crack corresponding to lateral displacements of +28 mm and -39 mm in the wall, respectively. Failure of Wall SQ1S occurred at +24.7 mm due to rupturing of the vertical reinforcing bar nearest to the edge of the wall, which was triggered by concentrated damage in the horizontal crack at the base. As a result, the strength of the wall was reduced to 167 kN. Two additional bars ruptured while loading the wall in the negative direction to -35 mm. At ultimate, Wall SQ1S experienced a maximum crack width of 25.8 mm. The residual strength of Wall SQ1S was 121 kN at +35 mm and 95 kN at -35 mm. Walls SQ1 and SQ1S experienced residual displacements of 42.1 mm and 13.5 mm, respectively, following loading to displacements of 50 mm and 25 mm.

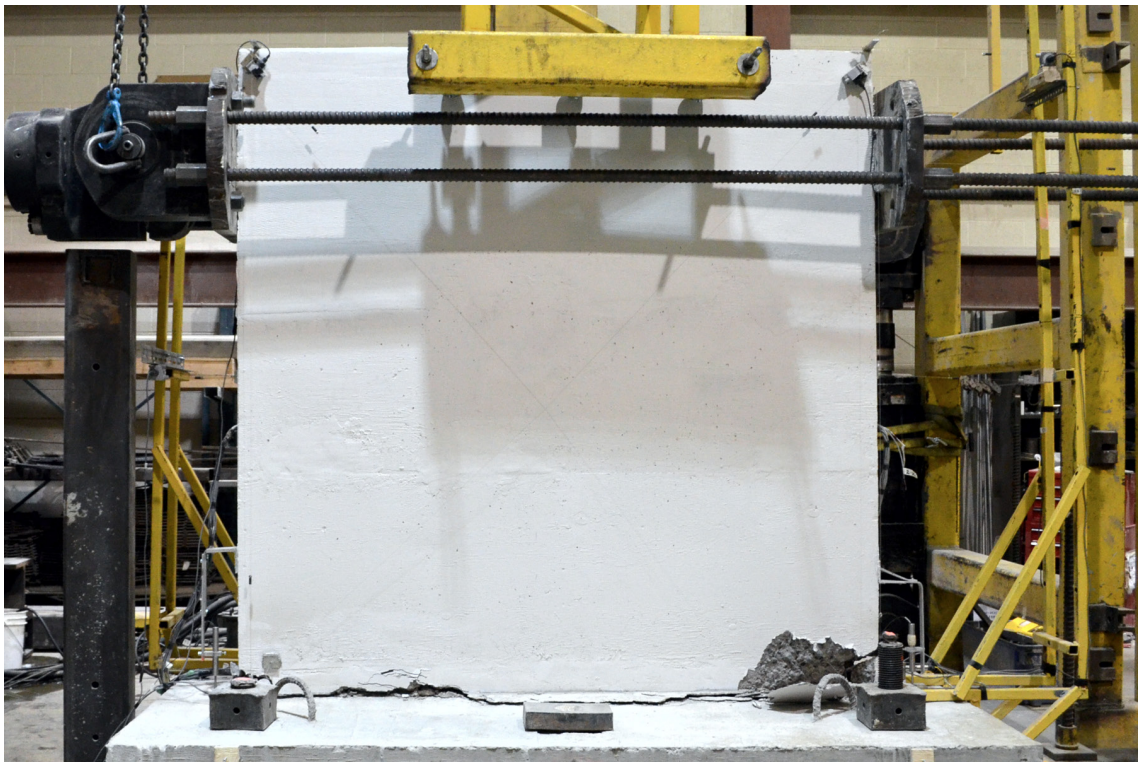


Figure 4-12 Damage of Wall SQ1 at ultimate

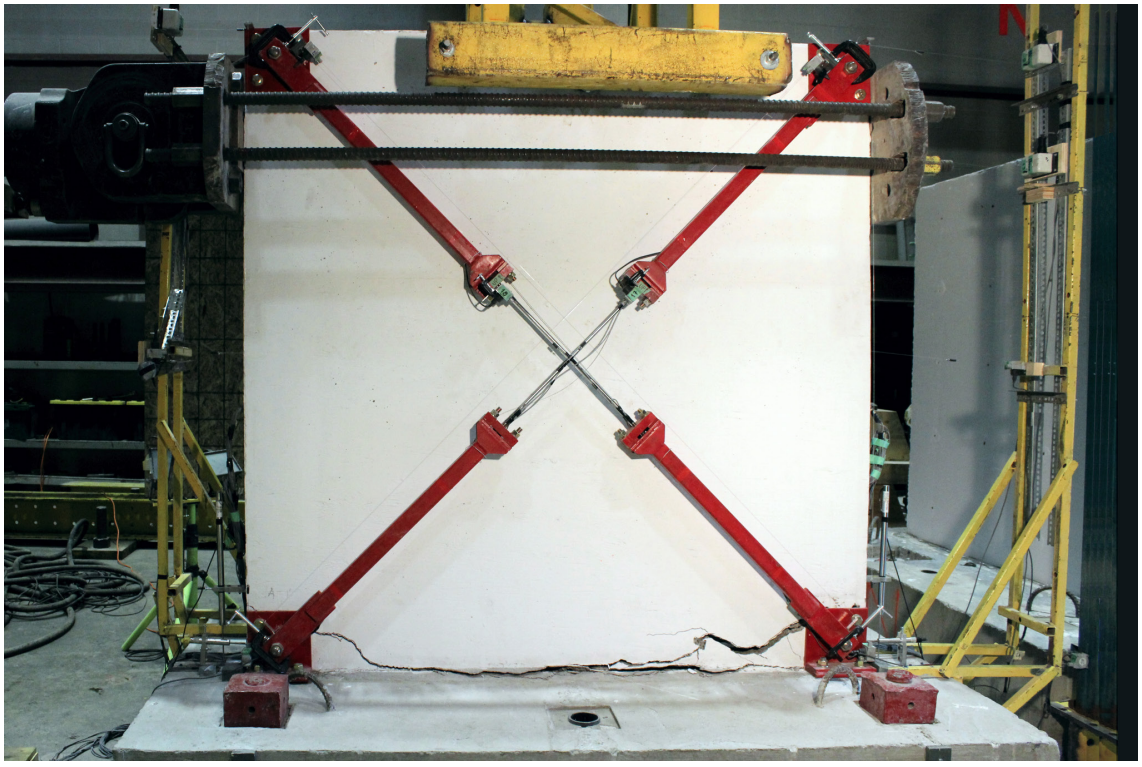


Figure 4-13 Damage of Wall SQ1S at ultimate

LVDTs placed at 250 mm from the base of the walls measured the base slip at the construction joint. At 20 mm of wall lateral displacement, base slips of 18 mm and 18.3 mm were recorded for Walls SQ1 and SQ1S, respectively. At ultimate for Wall SQ1, the large base slip displacement exceeded the stroke capacity of the LVDT. An ultimate slip of 25.8 mm was measured at the left end of Wall SQ1S. Given the localized damage of the walls at the base, the slip corresponded to the width of the horizontal crack. An LVDT placed horizontally at the base of the wall measured maximum sliding displacements of 14.1 mm and 2.8 mm for Walls SQ1 and SQ1S, respectively.

4.4.2 Response of Walls SQ2 and SQ2S

Figure 4-14 and Figure 4-15 illustrate the force-displacement responses of Walls SQ2 and SQ2S. First cracking surfaced at 0.3 mm and 0.6 mm, respectively for Walls SQ2 and SQ2S, at corresponding lateral strengths of 115 kN and 170 kN. The first crack (diagonal) in Wall SQ2 appeared in the lower left quadrant. The first crack in Wall SQ2S appeared along the base at approximately one-third of the length of the wall. First cracking was followed by distributed diagonal cracks that progressed from the base of the wall to the loading beam with increasing lateral loading. The diagonal cracks in both walls initiated as horizontal cracks crossing the boundary zones that propagated diagonally toward the base. First yielding of Walls SQ2 and SQ2S, defined by yielding of the outermost vertical reinforcing bar in the boundary zone, was recorded at lateral displacements of -0.6 mm and -2.8 mm, respectively, corresponding to lateral strengths of 135 kN and 280 kN. Yielding of all the reinforcement in the boundary zones was realized during loading to 5 mm. At this lateral displacement, Wall SQ2 reached its peak strength of 243 kN. Global yielding of SQ2 and SQ2S was determined at 1.7 mm and -6.3 mm at corresponding strengths of 179 kN and 305 kN, respectively.

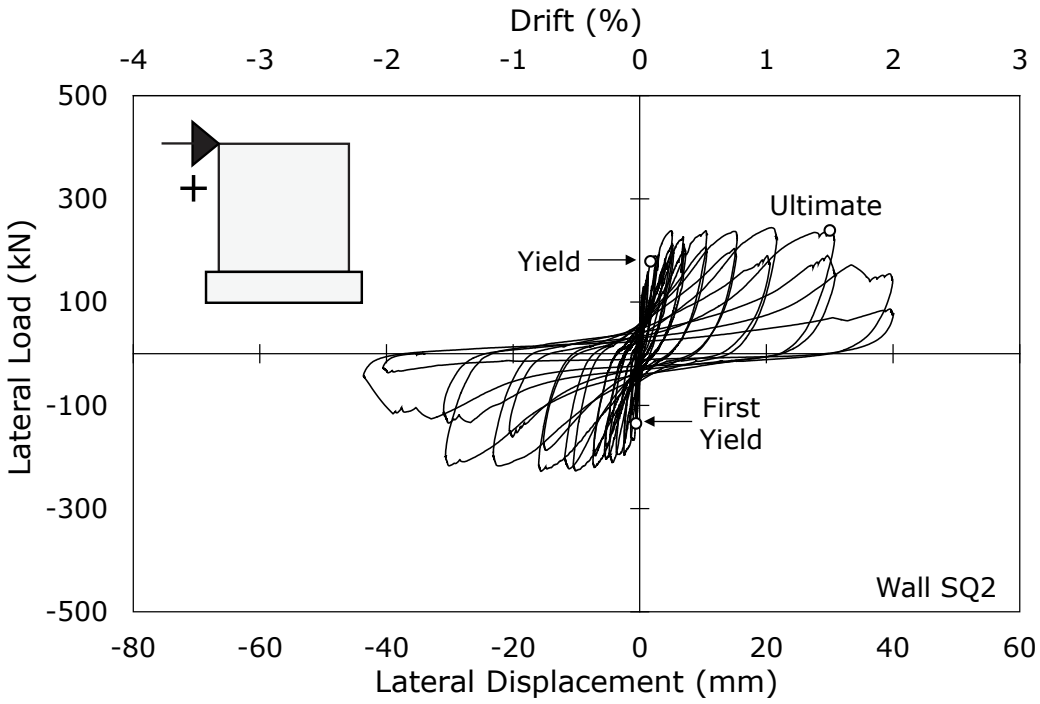


Figure 4-14 Lateral load-displacement response of Wall SQ2

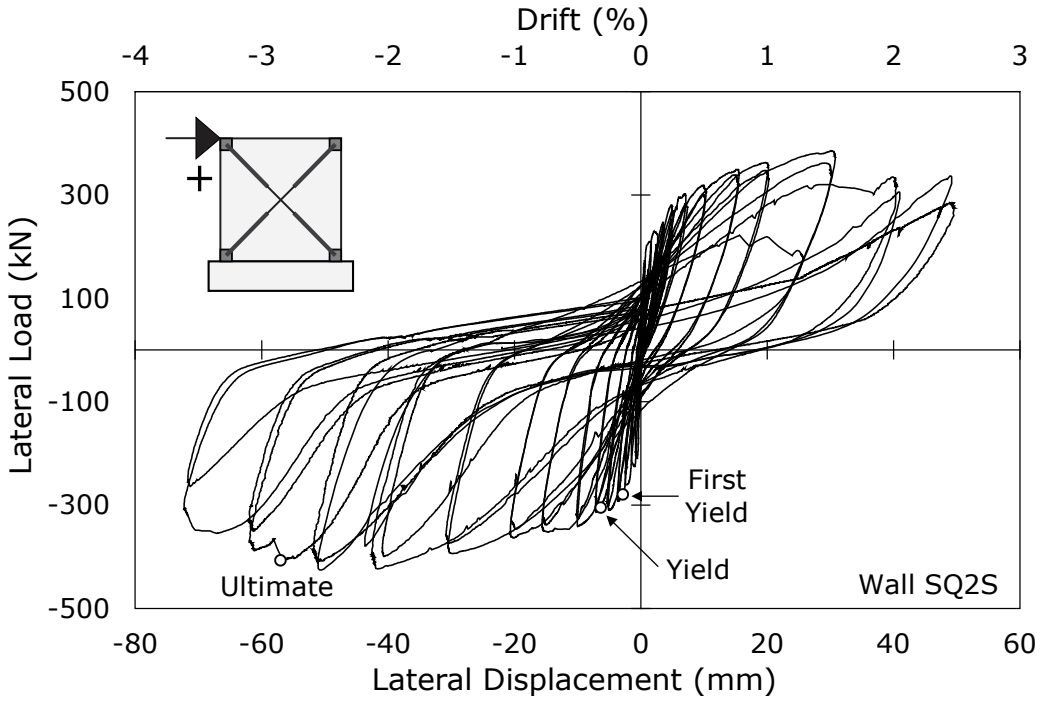


Figure 4-15 Lateral load-displacement response of Wall SQ2S

Additional diagonal and horizontal cracks surfaced in Walls SQ2 and SQ2S after yielding. Notably, a major horizontal crack appeared at the construction joint at the base of the walls. The spacing of the main diagonal cracks ranged between 200 mm and 300 mm. In the boundary zones, the horizontal cracks were spaced between 100 mm and 200 mm, in conformity with the spacing of the transverse reinforcement. Concentrated damage along the horizontal crack at the base of Wall SQ2 led to significant rocking of the wall and localized yielding of the longitudinal reinforcement. This resulted in notable degradation in strength and stiffness during the second repetitions of loading. Above the base, the reinforcement controlled the diagonal cracking of Wall SQ2. As a result, Wall SQ2 sustained its peak strength to ultimate. Diagonal cracking of Wall SQ2S was controlled by the internal reinforcing steel and the SMA braces, resulting in negligible degradation of response during the second repetitions of loading up to 30 mm. In the post-yield range, Wall SQ2S continued gaining strength due to the contribution of the SMA braces and experienced yielding of the vertical reinforcement throughout the wall. This led to uniform widening of the diagonal cracks during the post-yield loading phases, followed by crack closing upon load reversal due to the clamping effect of the SMA braces. The wall experienced peak strengths of 390 kN at +30 mm and 424 kN at -42 mm.

Figure 4-16 and Figure 4-17 illustrate the crack pattern of Walls SQ2 and SQ2S at ultimate. Failure of Wall SQ2 occurred at 27 mm at corresponding strength of 239 kN while loading to the second repetition to 30 mm, due to concentrated damage at the base (maximum crack width of approximately 15 mm) that resulted in large strains and rupturing of one longitudinal bar in the right boundary zone. At failure, the diagonal cracks in Wall SQ2 were, in general, smaller than 2 mm, with the exception of a number of 5 mm- to 7 mm-wide cracks located in the lower portion of the wall near the left boundary zone. Six longitudinal bars ruptured by the end of testing: four in the boundary zones and two in the web. The strength of Wall SQ2 decreased to an average of 53 kN at 40 mm. The post-peak damage of Wall SQ2S differed from that observed in Wall SQ2 despite similarities in the crack pattern. At 30 mm, prior to failure, the horizontal crack at the base in Wall SQ2S widened to approximately 7 mm, while the majority of diagonal cracks had maximum widths between 2.5 mm and 6 mm. At 40 mm, the distributed damage of concrete and

rupturing of one reinforcing bar at the left end of the wall preceded crushing and out-of-plane failure of the right boundary zone, reducing the post-peak strength in the positive direction. Given the heavy damage at the right end of the wall, loading in the positive direction was halted at 50 mm displacement, while loading continued to 70 mm in the negative direction. Rupture of two longitudinal bars in the right boundary zone decreased the strength of the wall during the cycles to -60 mm and -70 mm. The strength of Wall SQ2S at ultimate displacement of -57 mm was 407 kN. The residual strengths of Wall SQ2S at +50 mm and -70 mm was 285 kN and 265 kN, respectively. Wall SQ2 sustained a residual displacement of 23 mm at ultimate cycle to 30 mm, while Wall SQ2S experienced an average residual displacement of 26.7 mm at the cycle to 50 mm.

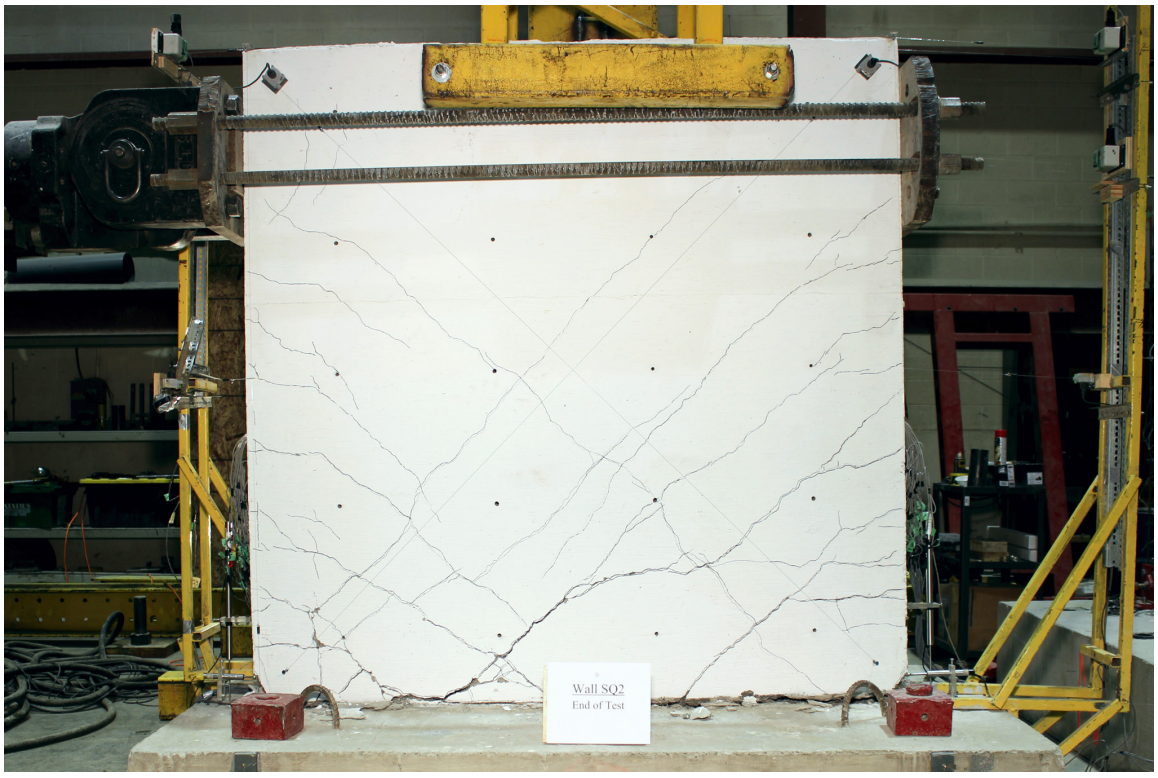


Figure 4-16 Damage of Wall SQ2 at ultimate



Figure 4-17 Damage of Wall SQ2S at ultimate

During loading to 30 mm, the LVDTs at the base of the walls measured base slip of 15.9 mm and 12.4 mm and base horizontal sliding of 16.8 mm and 2.5 mm for Walls SQ2 and SQ2S, respectively. Wall SQ2S experienced a maximum sliding displacement of 15.5 mm at the right end of the wall at ultimate. This large sliding was the result of heavy localized damage in the lower portion of the boundary zone.

4.4.3 Response of SMA Braces

Figure 4-18 and Figure 4-19 show typical responses of the SMA braces and SMA links in Wall SQ1S. The SMA braces experienced tension-only forces and further served to restore the wall to its original position. The onset of pseudo-yielding of the SMA braces at 0.4% occurred at approximately +21 mm and -23 mm of lateral displacement in the wall during the cycle to the ultimate displacements.

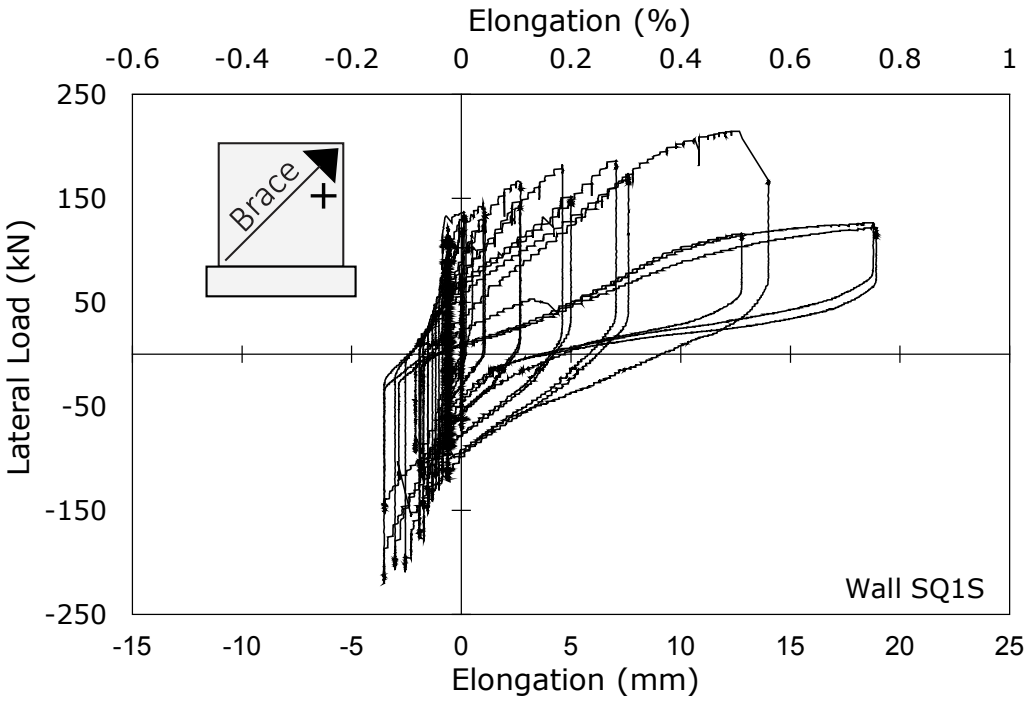


Figure 4-18 Typical wall lateral load-elongation response of SMA braces in Wall SQ1S

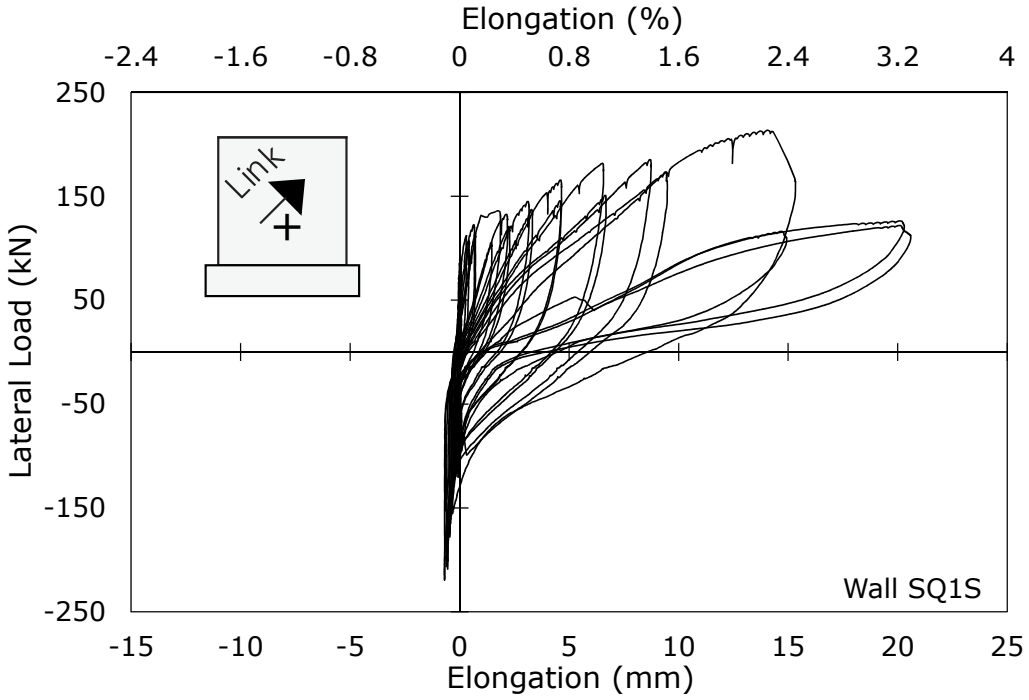


Figure 4-19 Typical wall lateral load-elongation response of SMA links in Wall SQ1S

At ultimate, the braces and links in Wall SQ1S experienced elongations of 12.8 mm (0.5% elongation) and 14.5 mm (2.28% elongation), respectively. Note that the smaller elongations in the braces were due to the compressive straining of the concrete struts of the wall and the noise in the recorded data. Beyond ultimate, the braces were subjected to maximum elongations of 18.9 mm and 23.7 mm during loading of the wall to the positive and the negative directions, respectively. The corresponding maximum percent elongations were 0.74% and 0.93% in the braces and 2.97% and 3.73% in the links. As a result of the rocking response and failure of the wall prior to the design target displacement of 40 mm, the SMA braces sustained elongations that were lower than the design target elongation of 1.5% (38 mm). The elongations in the SMA braces, however, were well within the pseudo-elastic range, thus the recovery capacity of the SMA was utilized.

Rupturing of the internal reinforcing steel bars at ultimate reduced the resistance of the shear wall from recovering, resulting in an increase in the elongation recovery of the SMA braces in the subsequent cycles. Note that the internal reinforcement follows the behaviour of ductile black carbon steel, where the post-yield response is characterized with significant residual straining. While the residual elongation of the SMA braces was approximately 9 mm at 12.8 mm elongation, it was less than 5 mm at 18.9 mm elongation. No rupture of the SMA braces and links was observed while testing Wall SQ1S. Based on the force-elongation response of the bare SMA brace (Figure 4-8) and the strains recorded in the brace (Figure 4-18), the maximum force developed in the SMA braces was 48.1 kN. At the end of testing, the maximum residual elongation of the links was approximately 2 mm, corresponding to approximately 0.3% elongation. The negligible residual elongations of the SMA links in Wall SQ1S, and the elastic response of the steel components, permitted the reuse of the SMA braces for Wall SQ2S.

Figure 4-20 and Figure 4-21 illustrate typical responses of the SMA braces and SMA links in Wall SQ2S. Two SMA braces sustained maximum elongation of 1.1% at +50 mm of lateral displacement of the wall (Figure 4-20), while the other two braces sustained maximum elongation of 1.76% at -60 mm. The corresponding elongations in the SMA links at +50 mm and -60 mm were 5.37% (Figure 4-21) and 6.76%,

respectively. Pseudo-yielding of the SMA braces initiated approximately at 16 mm of lateral displacement. A maximum force of 57.5 kN was calculated for the SMA braces based on the maximum strain in the links and the stress-strain response of the SMA rods (Figure 4-7). [Note that the stress-strain response of the bare brace could not be used to calculate the strength given that the maximum strain of the SMA braces exceeded the rupture strain of 1.61% of the bare braces (Figure 4-8).] Due to out-of-plane damage of the wall beyond 40 mm displacement, the SMA braces and SMA links sustained bending that resulted in negative elongations. The largest negative elongation was approximately 33 mm (Figure 4-20). Post-test inspection revealed that the SMA braces and links in Wall SQ2S did not rupture, the alignment of the retrofitting system remained intact, and the tension-only mechanism did not sustain any damage due to the out-of-plane displacements of the wall. After removal from the wall, the two braces that were active during loading to +50 mm of wall displacement experienced marginal residual elongation. The other two braces that resisted loading, while the wall was subjected to -70 mm of displacement, experienced a permanent elongation of 2 mm (0.08%).

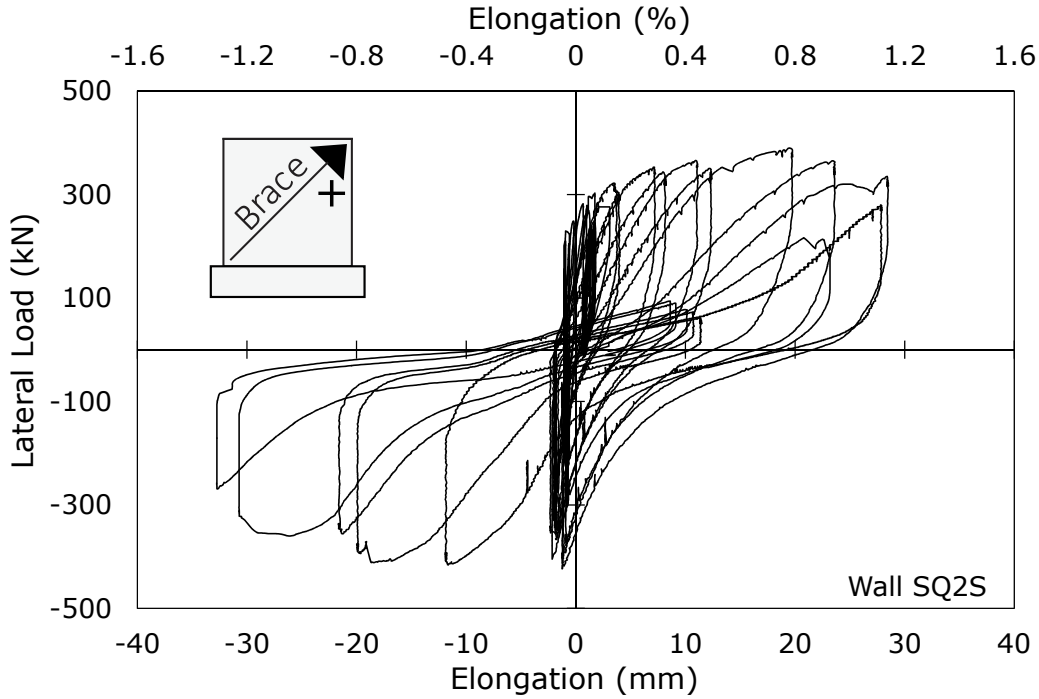


Figure 4-20 Typical wall lateral load-elongation response of SMA braces in Wall SQ2S

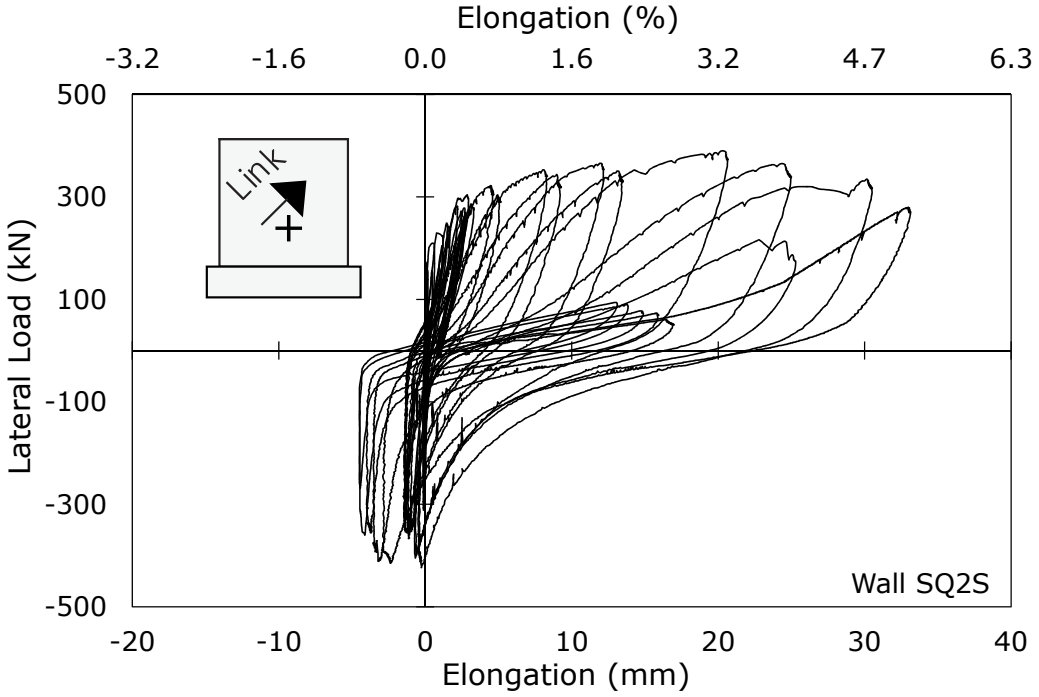


Figure 4-21 Typical wall lateral load-elongation response of SMA links in Wall SQ2S

4.5 Discussion of Results

Table 4-3 summarizes the main behavioral parameters of the walls: shear strength (V), lateral displacement (Δ), drift (%), secant stiffness (K), and failure mechanism. The data correspond to the direction of loading where the walls reached ultimate. Peak lateral capacity corresponded to the maximum force experienced by the walls, while ultimate capacity corresponded to the maximum displacement prior to a drop in strength due to rupturing of the reinforcement.

Table 4-3 Behavioural parameters of walls

Wall	Yield				Peak			Ultimate			
	V_y (kN)	Δ_y (mm)	Drift (%)	K (kN/mm)	V_p (kN)	Δ_p (mm)	Drift (%)	V_u (kN)	Δ_u (mm)	Drift (%)	Failure Mechanism
SQ1	109	4.5	0.23	24.2	145	37	1.85	145	37	1.85	Sliding/ Rupture
SQ1S	159	8.6	0.43	18.5	213	25	1.25	213	25	1.25	Rupture
SQ2	179	1.7	0.09	105.3	243	5	0.25	239	30	1.50	Rupture
SQ2S	-305	-6.3	-0.32	48.4	-424	-42	-2.10	-407	-57	-2.85	Crushing/ Rupture

Note: The - refers to the negative direction of loading

4.5.1 Damage and Failure Mechanism

Cracking at the base of Walls SQ1 and SQ1S was the result of the minimum longitudinal reinforcement not having the capacity to transfer tensile stresses to the surrounding concrete. The observed rocking and sliding in SQ1 resulted in a highly pinched lateral load-displacement response (Figure 4-10). Although similar cracking was observed at the base in SQ1S and rocking was evident, the horizontal component of the forces that developed in the SMA braces, and the additional stiffness provided by the anchor plates, controlled sliding. Sliding in Wall SQ1S was reduced up to approximately 80%, which eliminated kinking of the longitudinal reinforcement at the base and improved the global response (Figure 4-11).

Walls SQ2 and SQ2S experienced widespread diagonal cracking due to the presence of concentrated reinforcement in the boundary zones. In the post-yield range of SQ2, the rocking and sliding at the base caused significant pinching in the lateral load-displacement response (Figure 4-14). The SMA braces in SQ2S controlled shear sliding and improved closure of the diagonal cracks in the post-peak range. As a result, the wall experienced an improved flexural response with reduced pinching (Figure 4-15). The pinching arose due to the re-centering effect of the SMA braces. At 30 mm of lateral displacement, the retrofitting system reduced sliding displacement and width of the horizontal crack at the base by 85% and 53%, respectively. The vertical slip in the lower 250 mm at the ends of the wall were reduced by 22%. The size of the diagonal cracks, however, increased up to 200%.

4.5.2 Strength

The envelopes of the lateral load-displacement responses are illustrated in Figure 4-22, and the typical cycles prior to failure are provided in Figure 4-23 and Figure 4-24. Comparison of the responses demonstrated the improvements in strength of Walls SQ1S and SQ2S.

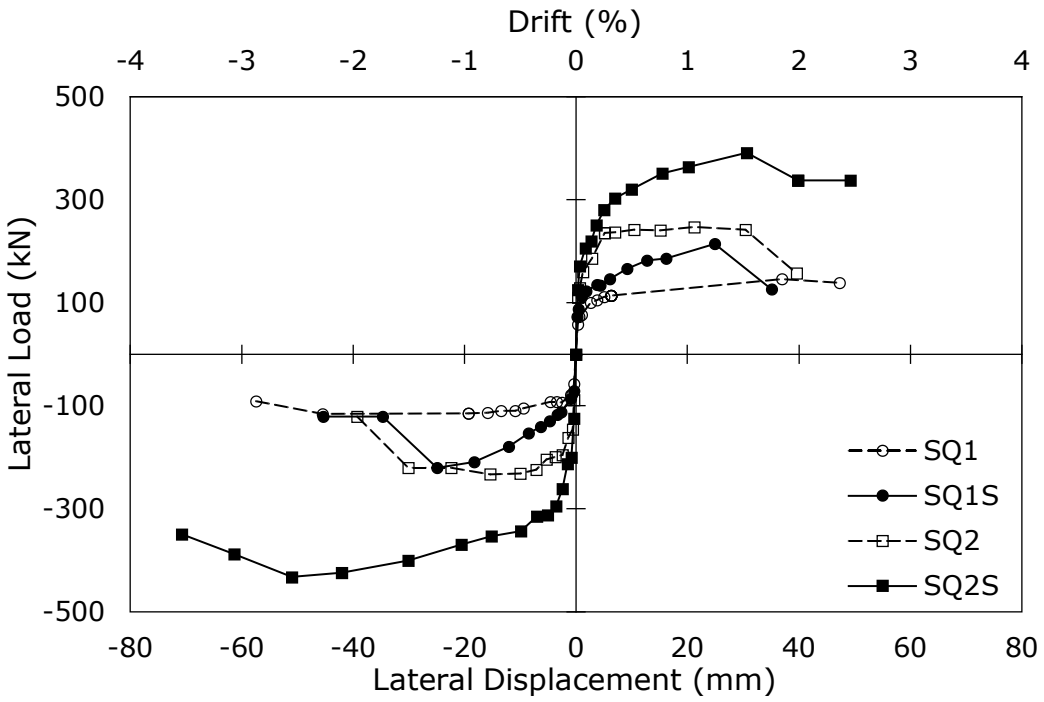


Figure 4-22 Envelope of lateral load-displacement response of shear walls

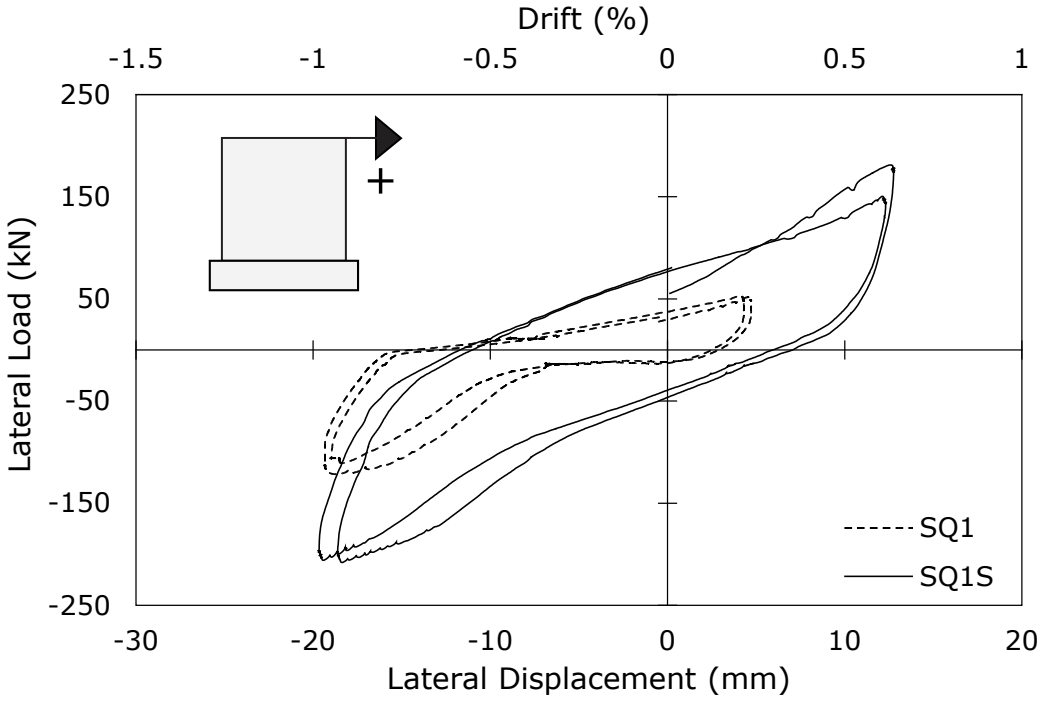


Figure 4-23 Typical cycles prior to failure of Walls SQ1 and SQ1S

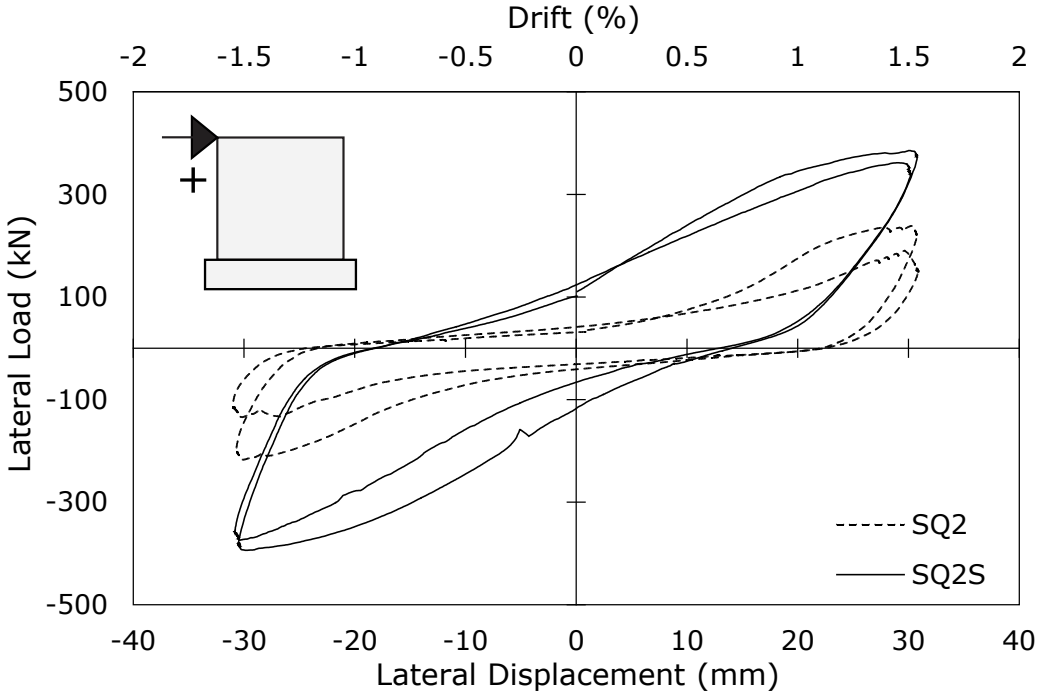


Figure 4-24 Typical cycles prior to failure of Walls SQ2 and SQ2S

The presence of the SMA braces substantially increased the peak shear strength and reduced strength degradation during the second repetitions of loading of Walls SQ1S and SQ2S. The increases in strength of Walls SQ1S and SQ2S with respect to the corresponding control walls were 47% and 74%, respectively. The SMA braces in Wall SQ2S contributed to larger lateral strength due to the higher strains that developed in the braces at larger displacement demands. Walls SQ1S and SQ2S sustained residual strengths very similar to the peak strengths of their corresponding control walls. The residual strength improved stability of the walls at the end of testing.

4.5.3 Stiffness and Drift Capacity

The secant stiffness-lateral displacement responses are illustrated in Figure 4-25. Wall SQ1S experienced slightly greater stiffness than Wall SQ1 up to yielding (15% increase). Beyond 10 mm to failure, the stiffness of Walls SQ1 and SQ1S was comparable. Wall SQ1S experienced lower drift capacity than Wall SQ1 due to the increased straining of the longitudinal reinforcement associated with greater flexural

capacity. Furthermore, Wall SQ1 was subjected to a loading protocol that imposed a single large cycle to ultimate that may have rapidly deteriorated the bond of the longitudinal reinforcing steel to the concrete delaying rupturing of the reinforcement. Given the rigid body behaviour and the single horizontal crack at the base of the wall, the crack width was expected to be approximately 40 mm at the ultimate lateral displacement of 37 mm. At this level of localized crack opening, the reinforcement should have ruptured. Conversely, Wall SQ1S was not affected by debonding and sliding, resulting in a wider crack at the base. The maximum widths of the horizontal crack were 16 mm and 26 mm in SQ1 and SQ1S, respectively, at 25 mm of lateral displacement.

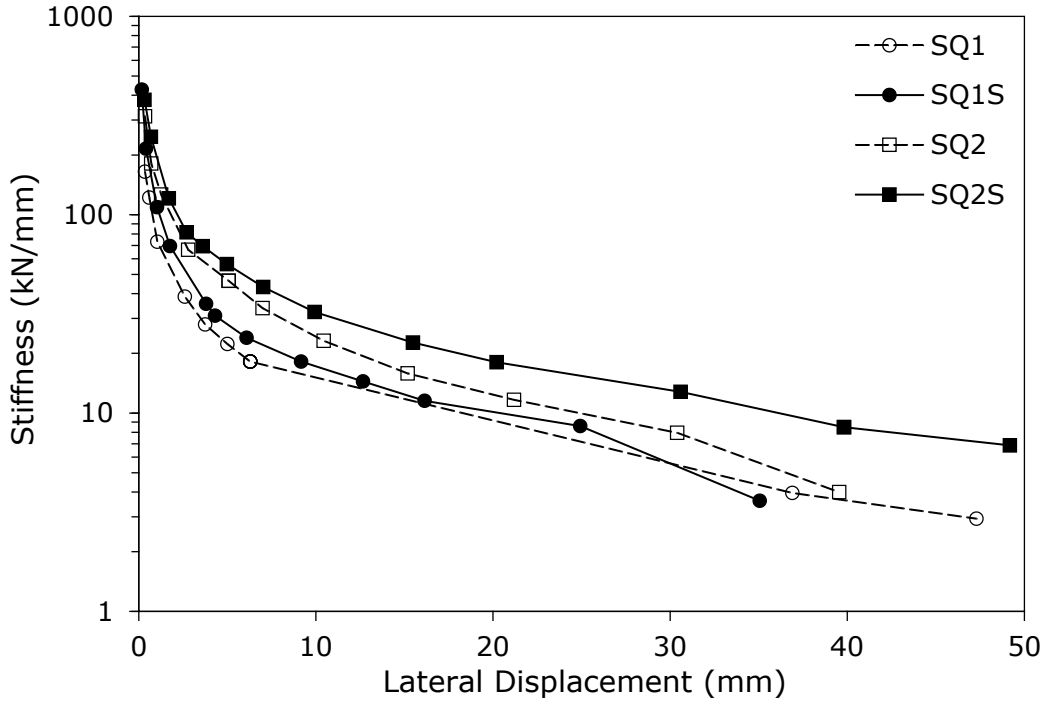


Figure 4-25 Secant stiffness of walls (stiffness in logarithmic scale)

The secant stiffness of Wall SQ2S at yielding and 40 mm of displacement was 29% and 53% greater in comparison to Wall SQ2. Localized damage at the base contributed to degradation of stiffness in Wall SQ2. Conversely, the SMA braces in SQ2S reduced shear sliding, mitigating stiffness degradation. Wall SQ2S provided increased stiffness up to 40 mm of lateral displacement. The out-of-plane damage during loading to 40 mm resulted in significant degradation in stiffness between the

cyclic repetitions in SQ2S (Figure 4-15). Wall SQ2S sustained a maximum drift of 2.85%, and Wall SQ2 sustained a maximum drift of 1.5% in the negative direction of loading. This represents an increase of 90% in drift capacity. In the positive direction, the walls sustained a drift capacity of 1.5%.

4.5.4 Energy Dissipation

Figure 4-26 provides the cumulative energy dissipation of the walls taking into account the two repetitions of loading. The energy dissipation of SQ1 in the positive direction of loading was assumed to be equal to that calculated in the negative direction of loading. [Note that the positive loading did not follow the intended protocol; therefore, a direct measure of energy dissipation was not possible.] To provide a direct comparison with the retrofitted wall, the energy dissipated by SQ1 during a number of cycles to -10 mm and -20 mm that did not correspond to the loading protocol of SQ1S were not included. Increases in strength and drift capacity (specifically for Wall SQ2S), and reductions of strength and stiffness degradation resulted in greater cumulative energy dissipation for the retrofitted walls at the end of the response. Walls SQ1S and SQ2S dissipated 42.9 kN-m and 165.4 kN-m, respectively, corresponding to increases of 90% and 219% with respect to the control walls.

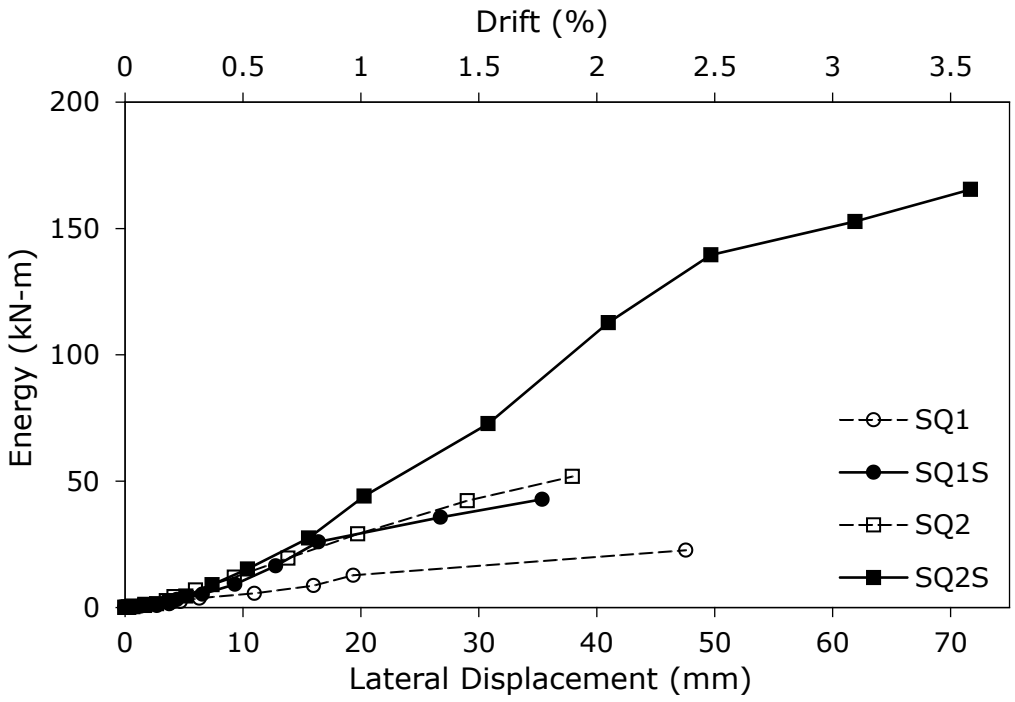


Figure 4-26 Cumulative energy dissipation of walls

4.5.5 Displacement Recovery

Figure 4-27 provides the recovery capacity of the lateral displacements of the walls in the positive direction of loading, calculated as the ratio of the difference between the peak displacement and the residual displacement to the peak displacement. The retrofitted walls experienced greater recovery capacity relative to the control walls at comparable displacements. Re-centering, however, was limited by yielding of the internal longitudinal reinforcing steel. Walls SQ1S and SQ2S recovered 50% and 54% of the lateral displacements at the ultimate positive drifts to 1.25% and 1.5%, respectively. During the last imposed positive displacements, Walls SQ1S and SQ2S recovered 64% and 61%, respectively, while the corresponding control Walls SQ1 and SQ2 recovered 11% and 24%, respectively. Wall SQ1S experienced greater recovery due to localized yielding of the internal reinforcement at the base. The distributed damage and yielding of the internal longitudinal reinforcement in Wall SQ2S slightly reduced the effectiveness of the retrofitting system to recover. Conversely to the control walls, the retrofitted walls experienced a slight increase in recovery capacity

during the last loading stage. This increase was the result of rupturing of the internal longitudinal reinforcing steel, which reduced the resistance to the re-centering action of the SMA braces.

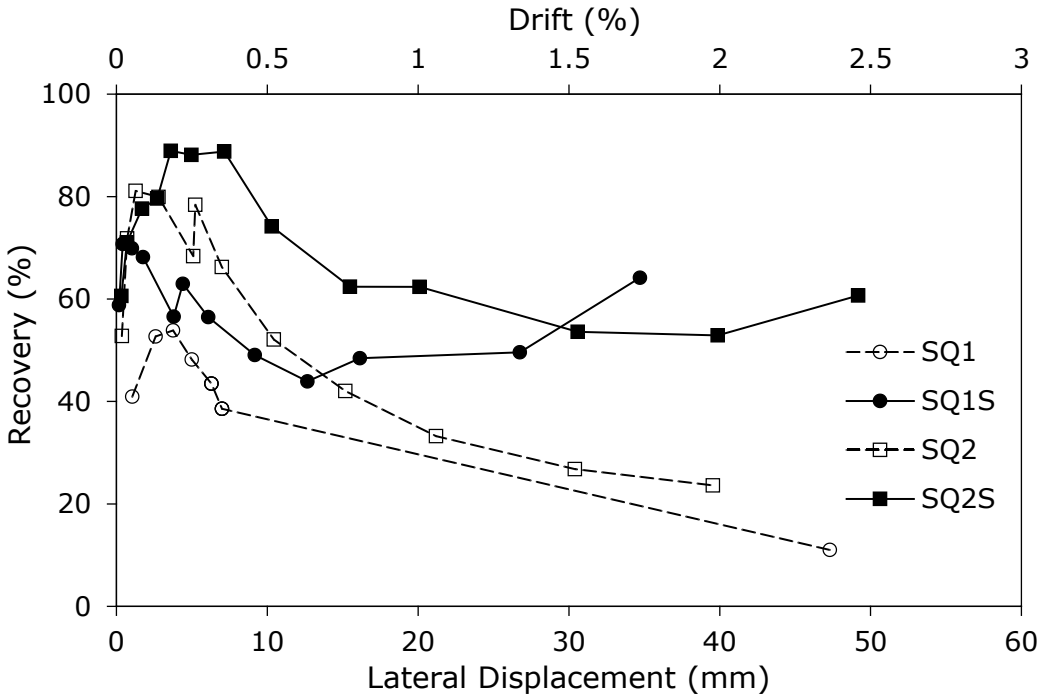


Figure 4-27 Displacement recovery of walls

4.5.6 Shear Distortion

Average shear strains in the walls, γ_{avg}, were calculated from the displacements measured by two diagonal cable transducers that were connected at the bottom and the top of the walls, following the expression suggested by Oesterle et al. (1976):

$$\gamma_{avg} = \frac{\delta_1 d_1 - \delta_2 d_2}{2hl} \tag{4-1}$$

where d_1 and d_2 are the original lengths of the diagonal transducers, δ_1 and δ_2 are the corresponding change of lengths, and h and l are the vertical and horizontal projections, respectively, of the original lengths. For Walls SQ1 and SQ2, the diagonal displacements were measured inside an 1800 mm × 1800 mm square formed by 100 mm offsets from the corners; while for Walls SQ1S and SQ2S, the diagonal

displacements corresponded to the elongation of the SMA braces, between the pin connections at the anchor plates. The original length of the diagonals were 2545.6 mm for Walls SQ1 and SQ2 and 2540 mm for Walls SQ1S and SQ2S. The corresponding vertical and horizontal projections were calculated based on the inclination of the diagonals (45°). Figure 4-28 provides the envelope of the average shear distortions for the positive direction of loading.

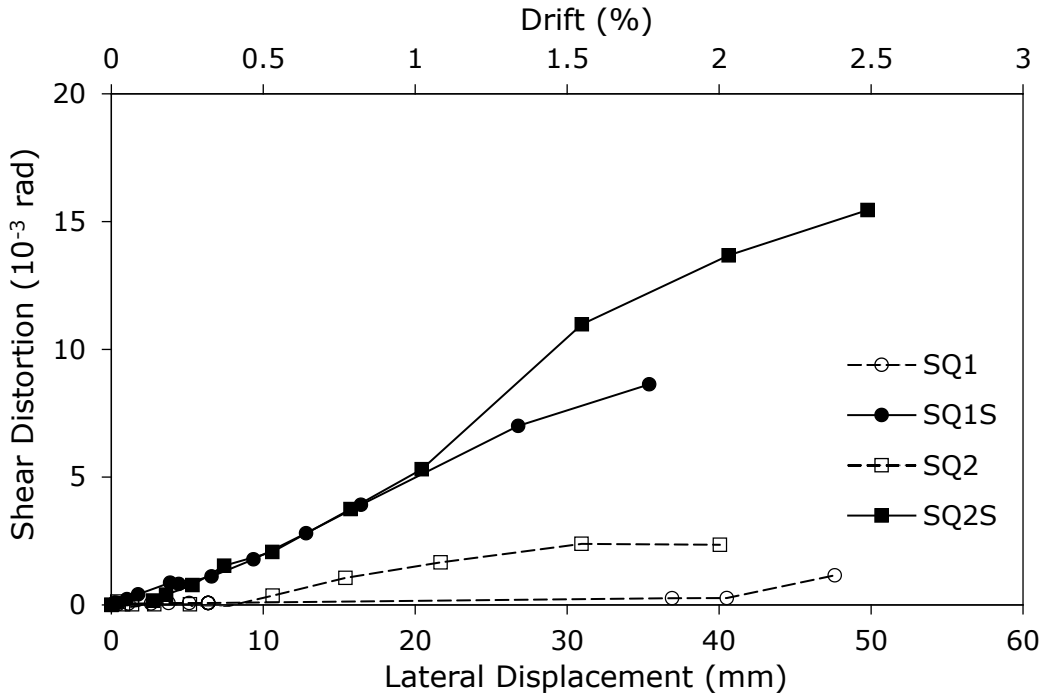


Figure 4-28 Shear distortion of walls

The control walls experienced significantly less shear distortion. The diagonal deformations of Wall SQ1 were negligible due to the rigid body motion of the wall. At 40 mm of lateral displacement (ultimate), the shear distortion was only 0.27×10^{-3} rad, and at 50 mm displacement, the distortion was 1.16×10^{-3} rad. The latter increase of distortion was due to localized damage at the toes of the walls as a result of rupturing of the steel and crushing of concrete. Therefore, the distortion at 50 mm does not represent the global shear distortion of the wall. Wall SQ2 sustained slightly greater shear distortion than Wall SQ1, linearly increasing to 2.39×10^{-3} rad at ultimate lateral displacement of 30 mm. Thereafter, the distortion remained constant. The shear distortion was attributed to the distributed diagonal cracking in the wall.

Walls SQ1S and SQ2S experienced maximum shear distortions of 8.6×10^{-3} rad and 15.5×10^{-3} rad, respectively. The positioning of the displacement transducers along the SMA bracing system also captured base rotations due to slippage of the internal reinforcement (rigid body motion) in addition to the shear distortions within the wall panels. The greater diagonal distortions in SQ2S were the result of distributed damage with wider diagonal cracks. Net shear distortions in the wall panels were calculated from the difference between the average shear distortions (including the base rotations) and the rotations at the top of the wall to provide a comparison with the shear distortions measured in the control walls. [The rotation at the top of the walls was calculated from the vertical displacements measured at the ends of the walls.] The resulting net shear distortion for Wall SQ1S was 1.7×10^{-3} rad at ultimate lateral displacement, which was similar to the control wall SQ1. No damage was evident in Wall SQ1S above the horizontal crack at the base of the wall at the end of testing, confirming the negligible shear distortion in the wall panel. Net shear distortion of 11.2×10^{-3} rad at ultimate was calculated for SQ2S. The greater shear distortion in Wall SQ2S was the result of minimal rigid body rotation at the base and distributed shear cracking in the wall.

The base rotation of Wall SQ1S and the shear distortion of Wall SQ2S introduced significant diagonal elongations that engaged the strengthening and energy dissipation properties of the SMA braces. The diagonal elongations were sufficiently recovered, resulting in residual rotations and shear distortions similar to those experienced by the control walls. Figure 4-29 provides the net shear distortions calculated for Walls SQ2 and SQ2S during loading to 30 mm displacement.

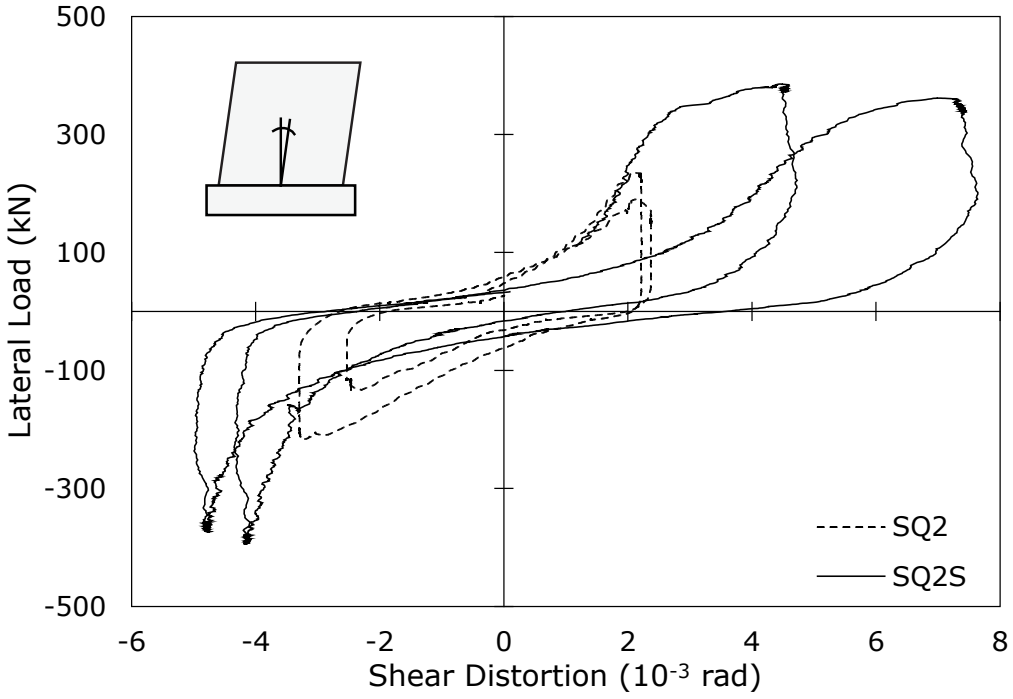


Figure 4-29 Typical net shear distortion response of Walls SQ2 and SQ2S at 30 mm displacement

4.6 Conclusions

An experimental program was conducted to study the performance of tension-only SMA braces to improve the seismic response of squat reinforced concrete shear walls. The walls were susceptible to shear-related damage, and the SMA braces were controlled by the superelastic behaviour of the SMA links. Based on the experimental results, the following conclusions are drawn:

1. The SMA braces slightly shifted the location of the governing crack at the base of Wall SQ1S compared to the control Wall SQ1; however, both walls experienced similar rocking behaviour.

2. The SMA braces in SQ2S limited the base horizontal crack and base rotation that governed the response of the control Wall SQ2. Wall SQ2S experienced pronounced distributed diagonal cracking in the wall panel and distributed yielding of the internal reinforcement. The SMA braces imposed additional compressive stresses in the wall in the post-peak, triggering crushing and out-

of-plane buckling of one of the boundary zones, limiting the stability and the strength capacity of the wall in the positive direction of loading.

3. The tensile forces that developed in the SMA braces increased the lateral strength relative to the control walls. Furthermore, the SMA braces were effective at reducing strength and stiffness degradation and pinching of the hysteretic responses.

4. The SMA braces increased the drift capacity of Wall SQ2S, reduced shear damage at the base, and redistributed damage throughout the wall. The drift capacity of Wall SQ1S was not improved by the SMA braces as a result of behaviour being controlled by base rocking in both the control Wall SQ1 and retrofitted Wall SQ1S. This suggests that walls governed by rocking require additional retrofitting to control localized cracking and base rigid rotations, and to promote distributed damage to improve drift capacity.

5. Energy dissipation was substantially increased by the SMA braces owing to improvements in the lateral load-displacement response. Furthermore, the energy dissipation of Wall SQ1S was similar to the control Wall SQ2, demonstrating the capacity of the SMA braces to improve the seismic performance of lightly reinforced concrete shear walls.

6. Wall SQ1S and SQ2S recovered over 50% of the imposed lateral displacements. The reduced residual displacements in the retrofitted walls improved closure of cracks and reduced damage associated with hysteretic shear degradation. Although the retrofitted shear walls experienced greater diagonal elongations and associated shear distortions, the net residual shear distortions were approximately the same as those experienced by the control walls, demonstrating the re-center capabilities of the SMA braces.

In general, the squat shear walls retrofitted with the SMA braces experienced improved seismic performance including increases in strength, drift capacity, and energy dissipation. Furthermore, the presence of the SMA braces reduced the residual displacements, improved displacement recovery, enhanced crack closure, and reduced damage at the base of the walls.

4.7 Acknowledgments

Financial support provided by the Canadian Seismic Research Network [Grant: NETGP/350698-07], a Natural Sciences and Engineering Research Council of Canada strategic network, is gratefully acknowledged.

4.8 References

Abdulridha, A., and Palermo, D. (2014). "Response of a hybrid SMA reinforced concrete shear wall." *Tenth U.S. National Conference on Earthquake Engineering*, Network for Earthquake Engineering Simulation (distributor), Anchorage, AK, USA.

Abdulridha, A., Palermo, D., Foo, S., and Vecchio, F. J. (2013). "Behavior and modeling of superelastic shape memory alloy reinforced concrete beams." *Engineering Structures*, 49, 893–904.

Adachi, Y., and Unjoh, S. (1999). "Development of shape memory alloy damper for intelligent bridge systems." *SPIE 3671, Smart Structures and Materials 1999: Smart Systems for Bridges, Structures, and Highways*, Newport Beach, CA, USA, 31–42.

Alam, M. S., Nehdi, M., and Youssef, M. A. (2009). "Seismic performance of concrete frame structures reinforced with superelastic shape memory alloys." *Smart Structures & Systems*, 5(5), 565–585.

Alam, M. S., Youssef, M. A., and Nehdi, M. (2007). "Utilizing shape memory alloys to enhance the performance and safety of civil infrastructure: a review." *Canadian Journal of Civil Engineering*, 34(9), 1075–1086.

ASCE. (2007). *ASCE/SEI 41-06 Seismic rehabilitation of existing buildings*. American Society of Civil Engineers, Reston, VA, USA.

ASTM. (2014). *ASTM F2516-14, Standard test method for tension testing of nickel-titanium superelastic materials*. ASTM International, West Conshohocken, PA, USA.

ATC. (1996). *ATC-40 Seismic evaluation and retrofit of concrete buildings*. Report SSC 96-01, Applied Technology Council, Redwood City, CA, USA.

ATC. (2005). *FEMA 440 Improvement of nonlinear static seismic analysis procedures*. Applied Technology Council, Washington D.C., USA.

ATC. (2007). *FEMA 461 Interim testing protocols for determining the seismic performance characteristics of structural and nonstructural components*. Federal Emergency Management Agency, Washington D.C., USA.

Auricchio, F., Fugazza, D., and DesRoches, R. (2006). "Earthquake performance of steel frames with Nitinol braces." *Journal of Earthquake Engineering*, 10(spec01), 45–66.

Cortés-Puentes, W. L., and Palermo, D. (2012). "Modeling of RC Shear Walls Retrofitted with Steel Plates or FRP Sheets." *Journal of Structural Engineering*, 138(5), 602–612.

Cortés-Puentes, W. L., and Palermo, D. (2017). "SMA tension brace for retrofitting concrete shear walls." *Engineering Structures*, 140, 177–188.

Cruz-Noguez, C. A., and Saiidi, M. S. (2012). "Shake-table studies of a four-span bridge model with advanced materials." *Journal of Structural Engineering*, 138(2), 183–192.

DesRoches, R., and Delemont, M. (2002). "Seismic retrofit of simply supported bridges using shape memory alloys." *Engineering Structures*, 24(3), 325–332.

DesRoches, R., McCormick, J., and Delemont, M. (2004). "Cyclic Properties of Superelastic Shape Memory Alloy Wires and Bars." *Journal of Structural Engineering*, 130(1), 38–46.

Dezfuli, M. A., Dolatshahi, K. M., Mofid, M., and Eshkevari, S. S. (2017). "Coreless self-centering braces as retrofitting devices in steel structures." *Journal of Constructional Steel Research*, 133, 485–498.

Dolce, M., and Cardone, D. (2001a). "Mechanical behaviour of shape memory alloys for seismic applications 1. Martensite and austenite NiTi bars subjected to torsion." *International Journal of Mechanical Sciences*, 43(11), 2631–2656.

Dolce, M., and Cardone, D. (2001b). "Mechanical behaviour of shape memory alloys for seismic applications 2. Austenite NiTi wires subjected to tension." *International Journal of Mechanical Sciences*, 43(11), 2657–2677.

Dolce, M., Cardone, D., Ponzo, F. C., and Valente, C. (2005). "Shaking table tests on reinforced concrete frames without and with passive control systems." *Earthquake Engineering & Structural Dynamics*, 34(14), 1687–1717.

Effendy, E., Liao, W. I., Song, G., Mo, Y. L., and Loh, C. H. (2006). "Seismic Behavior of Low-Rise Shear Walls with SMA Bars." *Earth & Space 2006*, American Society of Civil Engineers, Houston, TX, USA, 1–8.

Fang, C., Yam, M. C. H., Ma, H., and Chung, K. F. (2015). "Tests on superelastic Ni–Ti SMA bars under cyclic tension and direct-shear: towards practical recentring connections." *Materials and Structures*, 48(4), 1013–1030.

Gao, N., Jeon, J.-S., Hodgson, D. E., and DesRoches, R. (2016). "An innovative seismic bracing system based on a superelastic shape memory alloy ring." *Smart Materials and Structures*, 25(5), 055030.

Ghassemieh, M., Bahaari, M. R., Ghodratian, S. M., and Nojoumi, S. A. (2012). "Improvement of Concrete Shear Wall Structures by Smart Materials." *Open Journal of Civil Engineering*, 2(3), 87–95.

Gulec, C. K., and Whittaker, A. S. (2009). *Performance-based assessment and design of squat reinforced concrete shear walls*. MCEER, Earthquake Engineering to Extreme Events, Technical Report, MCEER.

Janke, L., Czaderski, C., Motavalli, M., and Ruth, J. (2005). "Applications of shape memory alloys in civil engineering structures - Overview, limits and new ideas." *Materials and Structures*, 38(279), 578–592.

Kuang, Y., and Ou, J. (2008). "Self-repairing performance of concrete beams strengthened using superelastic SMA wires in combination with adhesives released from hollow fibers." *Smart Materials and Structures*, 17(2), 025020.

Liao, W. I., and Mo, Y. L. (2006). "Shake Table Tests of RC Frame with Shape Memory Alloy Bracing Bars." *4th International Conference on Earthquake Engineering*, Taipei, Taiwan, Paper 90.

Malagisi, S., Marfia, S., Sacco, E., and Toti, J. (2014). "Modeling of smart concrete beams with shape memory alloy actuators." *Engineering Structures*, 75, 63–72.

McCormick, J., DesRoches, R., Fugazza, D., and Auricchio, F. (2006). "Seismic vibration control using superelastic shape memory alloys." *Journal of Engineering Materials and Technology*, 128(3), 294–301.

McCormick, J., Tyber, J., DesRoches, R., Gall, K., and Maier, H. J. (2007). "Structural engineering with NiTi. II: mechanical behavior and scaling." *Journal of Engineering Mechanics*, 133(9), 1019–1029.

Meshaly, M. E., Youssef, M. A., Elfath, A., and M, H. (2014). "Use of SMA bars to enhance the seismic performance of SMA braced RC frames." *Earthquakes and Structures*, 6(3), 267–280.

Miller, D. J., Fahnestock, L. A., and Eatherton, M. R. (2012). "Development and experimental validation of a nickel–titanium shape memory alloy self-centering buckling-restrained brace." *Engineering Structures*, 40, 288–298.

Motahari, S. A., Ghassemieh, M., and Abolmaali, S. A. (2007). "Implementation of shape memory alloy dampers for passive control of structures subjected to seismic excitations." *Journal of Constructional Steel Research*, 63(12), 1570–1579.

Nakashoji, B. A. (2014). "Seismic Performance of Square Nickel-Titanium Reinforced ECC Columns with Headed Couplers." Ph.D. Thesis, University of Nevada, Reno, NV, USA.

Nehdi, M., Alam, M. S., and Youssef, M. A. (2010). "Development of corrosion-free concrete beam–column joint with adequate seismic energy dissipation." *Engineering Structures*, 32(9), 2518–2528.

Nemat-Nasser, S., and Guo, W.-G. (2006). "Superelastic and cyclic response of NiTi SMA at various strain rates and temperatures." *Mechanics of Materials*, Shape Memory Alloys, 38(5–6), 463–474.

NRC. (1965). *National building code of Canada*. Associate committee on the national building code, National Research Council of Canada, Ottawa, ON, Canada.

Oesterle, R. G., Fiorato, A. E., Johal, L. S., Carpenter, J. E., Russell, H. G., and Corley, W. G. (1976). *Earthquake Resistant Structural Walls - Tests of Isolated Walls*. Report PCA R/D Ser. 1571, Portland Cement Association, Skokie, IL, USA.

Ozbulut, O. E., and Hurlebaus, S. (2010). "Evaluation of the performance of a sliding-type base isolation system with a NiTi shape memory alloy device considering temperature effects." *Engineering Structures*, 32(1), 238–249.

Park, R. (1989). "Evaluation of ductility of structures and structural assemblages from laboratory testing." *Bulletin of the New Zealand National Society for Earthquake Engineering*, 22(3), 155–166.

Piedboeuf, M. C., Gauvin, R., and Thomas, M. (1998). "Damping behaviour of shape memory alloys: strain amplitude, frequency and temperature effects." *Journal of Sound and Vibration*, 214(5), 885–901.

Qiu, C.-X., and Zhu, S. (2017). "Performance-based seismic design of self-centering steel frames with SMA-based braces." *Engineering Structures*, 130, 67–82.

Saiidi, M. S., O'Brien, M., and Sadrossadat-Zadeh, M. (2009). "Cyclic Response of Concrete Bridge Columns Using Superelastic Nitinol and Bendable Concrete." *ACI Structural Journal*, 106(1), 69–77.

Saiidi, M. S., Sadrossadat-Zadeh, M., Ayoub, C., and Itani, A. (2007). "Pilot Study of Behavior of Concrete Beams Reinforced with Shape Memory Alloys." *Journal of Materials in Civil Engineering*, 19(6), 454–461.

Saiidi, M. S., and Wang, H. (2006). "Exploratory Study of Seismic Response of Concrete Columns with Shape Memory Alloys Reinforcement." *ACI Structural Journal*, 103(3), 436–443.

Salichs, J., Hou, Z., and Noori, M. (2001). "Vibration Suppression of Structures Using Passive Shape Memory Alloy Energy Dissipation Devices." *Journal of Intelligent Material Systems and Structures*, 12(10), 671–680.

Silwal, B., Michael, R. J., and Ozbulut, O. E. (2015). "A superelastic viscous damper for enhanced seismic performance of steel moment frames." *Engineering Structures*, 105, 152–164.

Song, G., Ma, N., and Li, H.-N. (2006). "Applications of shape memory alloys in civil structures." *Engineering Structures*, 28(9), 1266–1274.

Soul, H., and Yawny, A. (2015). "Self-centering and damping capabilities of a tension-compression device equipped with superelastic NiTi wires." *Smart Materials and Structures*, 24(7), 075005.

Speicher, M. S., DesRoches, R., and Leon, R. T. (2017). "Investigation of an articulated quadrilateral bracing system utilizing shape memory alloys." *Journal of Constructional Steel Research*, 130, 65–78.

Sultana, P., and Youssef, M. A. (2016). "Seismic performance of steel moment resisting frames utilizing superelastic shape memory alloys." *Journal of Constructional Steel Research*, 125, 239–251.

Tazarv, M., and Saiidi, S. (2015). "Reinforcing NiTi superelastic SMA for concrete structures." *Journal of Structural Engineering*, 141(8), 04014197, 1–10.

Tyber, J., McCormick, J., Gall, K., DesRoches, R., Maier, H. J., and Maksoud, A. E. A. (2007). "Structural engineering with NiTi. I: basic materials characterization." *Journal of Engineering Mechanics*, 133(9), 1009–1018.

Yang, C.-S. W., DesRoches, R., and Leon, R. T. (2010). "Design and analysis of braced frames with shape memory alloy and energy-absorbing hybrid devices." *Engineering Structures*, 32(2), 498–507.

Youssef, M. A., Alam, M. S., and Nehdi, M. (2008). "Experimental Investigation on the Seismic Behavior of Beam-Column Joints Reinforced with Superelastic Shape Memory Alloys." *Journal of Earthquake Engineering*, 12(7), 1205–1222.

Youssef, M. A., and Elfeki, M. A. (2012). "Seismic performance of concrete frames reinforced with superelastic shape memory alloys." *Smart Structures and Systems*, 9(4), 313–333.

Zafar, A., and Andrawes, B. (2012). "Incremental dynamic analysis of concrete moment resisting frames reinforced with shape memory composite bars." *Smart Materials and Structures*, 21(2), 025013, 1–14.

Zafar, A., and Andrawes, B. (2013). "Experimental flexural behavior of SMA-FRP reinforced concrete beam." *Frontiers of Structural and Civil Engineering*, 7(4), 341–355.

Chapter 5

Modelling of Concrete Shear Walls Retrofitted with SMA Tension Braces

Authors: W. Leonardo Cortés-Puentes, Dan Palermo

Abstract

Recent experimental studies have demonstrated the benefits that the re-centering and energy dissipation capacities of superelastic Shape Memory Alloys (SMA) provide to the hysteretic response of reinforced concrete structures. These studies have provided data for the development and validation of new analysis tools. A recently developed hysteretic constitutive relationship for superelastic SMA materials was successfully implemented in the nonlinear finite element program VecTor2. The model follows a tri-linear envelope with loading and unloading branches that capture the flag-shaped behaviour of superelastic SMAs and the accumulation of plastic straining at large strain demands. Numerical analyses incorporating the SMA constitutive model have provided satisfactory simulations of response of SMA-reinforced concrete beams, beam-column joints, and shear walls. This study implements the SMA model to simulate seismic retrofit of squat reinforced concrete shear walls with tension-only SMA braces. Tension-only truss elements, assigned with the stress-strain parameters obtained from bare brace testing, modelled the response of the SMA braces. The numerical results exhibited satisfactory predictions of lateral strength, drift capacity, cracking, energy dissipation, and displacement recovery. In addition, parametric studies were conducted to assess the effect of axial load and size of the SMA links, the

fuse element of the braces, on the performance of the retrofitted walls. [Additional numerical results of the shear walls are presented in Appendix C.]

Keywords

Numerical analysis; lateral load-displacement response; reinforced concrete; shear walls; retrofitting; SMA; tension braces.

5.1 Introduction

Superelastic Shape Memory Alloys (SMA) possess mechanical properties that can improve re-centering of reinforced concrete structures while increasing energy dissipation and reducing damage. A number of studies have focused on the application of superelastic SMAs as internal reinforcement in concrete structures (Abdulridha et al. 2013; Abdulridha and Palermo 2014; Alam et al. 2009; Nehdi et al. 2010; Saiidi et al. 2007, 2009; Saiidi and Wang 2006; Youssef et al. 2008; Youssef and Elfeki 2012; Zafar and Andrawes 2012). These studies have highlighted the restoring capacity of the SMAs. Fewer studies have investigated external applications of SMAs for seismic retrofitting of concrete structures (Auricchio et al. 2006; Dolce et al. 2005; Effendy et al. 2006; McCormick et al. 2006; Salichs et al. 2001). Effendy et al. (2006) studied external diagonal SMA rods as a strategy to replace internal reinforcing steel in squat reinforced concrete shear walls. The SMA rods increased the lateral strength of the walls but did not improve re-centering. The latter was the result of the low tensile strain demands imposed on the SMA rods and buckling of the rods under compression loading. To overcome these shortcomings, Cortés-Puentes and Palermo (2017a) developed an SMA tension-only brace incorporating SMA links with an optimized length. The length was selected to satisfy a maximum strain limit of 6% in the SMA link to ensure the material was within the full strain recovery limit. Furthermore, the braces were designed such that damage (large strains) would concentrate in the SMA links, while other components of the brace remained elastic. The SMA brace was experimentally verified first through bare brace testing (Cortés-Puentes and Palermo 2017a) followed by retrofitting of squat reinforced concrete shear walls (Cortés-Puentes and Palermo 2017b). Testing of the shear walls demonstrated the effectiveness of the SMA braces to increase lateral strength, drift capacity, energy

dissipation, and displacement recovery, while minimizing increases in the initial stiffness and controlling shear-related damage in the concrete. While research has focused on experimental testing of SMA-reinforced concrete, lacking are complementary studies on modelling of concrete structures reinforced or retrofitted with SMAs.

Numerical analyses of SMA-reinforced or SMA-retrofitted concrete structures require nonlinear tools that employ realistic constitutive relationships. Typical models for superelastic SMAs consist of flag-shaped responses with loading and unloading rules that simulates the pseudo-elasticity response of superelastic SMAs without consideration to residual strains that accumulate during large strain response (Auricchio and Sacco 1997; Graesser and Cozzarelli 1991; Ren et al. 2007). These models have been used to simulate the responses of SMA-reinforced concrete columns (Billah and Alam 2012; Tazarv and Saiidi 2015), beam-column joints (Alam et al. 2008) and frames (Alam et al. 2009; Youssef and Elfeki 2012; Zafar and Andrawes 2012).

Auricchio et al. (2006) and McCormick et al. (2006) utilized the flag-shaped SMA model with full strain recovery to analyze steel frames braced with hybrid SMA elements. The SMA models were incorporated in finite element models that did not capture localized damage in the structure and did not account for potential buckling of the SMA elements under compression. Abdulridha et al. (2013) recently developed a phenomenological tri-linear model for superelastic SMAs. Improvements in this hysteretic constitutive model included explicitly consideration to residual straining and decay of the lower plateau stress. Nonlinear finite element analyses, based on the improved SMA model, successfully predicted the force-displacement response and damage in reinforced concrete structures internally reinforced with SMA rods (Abdulridha et al. 2013; Abdulridha and Palermo 2014). Although effective in predicting the response of SMA-reinforced concrete structures, the improved model requires further validation for other SMA applications such as external retrofit.

5.2 Research Significance

This paper presents nonlinear modelling techniques to simulate the response of squat reinforced concrete shear walls controlled by shear-related failure and retrofitted with an external novel SMA bracing system. The SMA braces are modelled with truss elements and a tension-only constitutive relationship that simulates pseudo-elasticity and accounts for residual straining and decay of the lower stress plateau. Furthermore, a parametric study is conducted to assess the influence of axial loading and size of the SMA links on the response of squat shear walls. In addition, through this study, the constitutive model developed by Abdulridha et al (2013) is further corroborated.

5.3 Shear Walls

5.3.1 General Description

The numerical study was conducted on three squat concrete shear walls retrofitted with SMA tension braces (SQ1S, SQ1aS, and SQ2S) and three companion control shear walls (SQ1, SQ1a, and SQ2). The walls, with the exception of SQ1aS, were previously tested under reverse cyclic loading (Cortés-Puentes and Palermo 2017b). [Experimental results of SQ1a are provided in Appendix B.] Although not tested, the numerical model of SQ1aS served as the companion-retrofitted wall for SQ1a. Figure 5-1 illustrates the geometric and reinforcement details of the walls. Walls SQ1/SQ1S (2000 mm × 2000 mm × 100 mm) were built with normal strength concrete and one layer of minimum longitudinal (steel ratio of 0.18%) and transverse reinforcement in the web (steel ratio of 0.21%). Walls SQ1a/SQ1aS had the same geometric and reinforcement layout as SQ1/SQ1S but were constructed with lower concrete strength. Walls SQ2/SQ2S (2000 mm × 2000 mm × 125 mm) had a thicker cross section to accommodate boundary zones reinforced with two layers of longitudinal steel with reinforcement ratio of 1% and transverse confining hoops. The web of SQ2/SQ2S was reinforced with one layer of reinforcement with minimum steel similar to that provided in SQ1/SQ1S. The walls were built on heavily reinforced foundation blocks (2500 mm × 1400 mm × 500 mm) that simulated rigid foundations. Beams (160 mm

in depth) were embedded in the walls at a height of 1660 mm from the base to serve as a strengthened zone through which the lateral loading was imposed. The longitudinal reinforcement in SQ1/SQ1S was anchored with standard hooks in the foundation blocks, while the longitudinal reinforcement in the other walls was anchored 250 mm into the foundations with epoxy. [Walls SQ1a, SQ2 and SQ2S were constructed on the foundations that were originally used for SQ1 and SQ1S.]

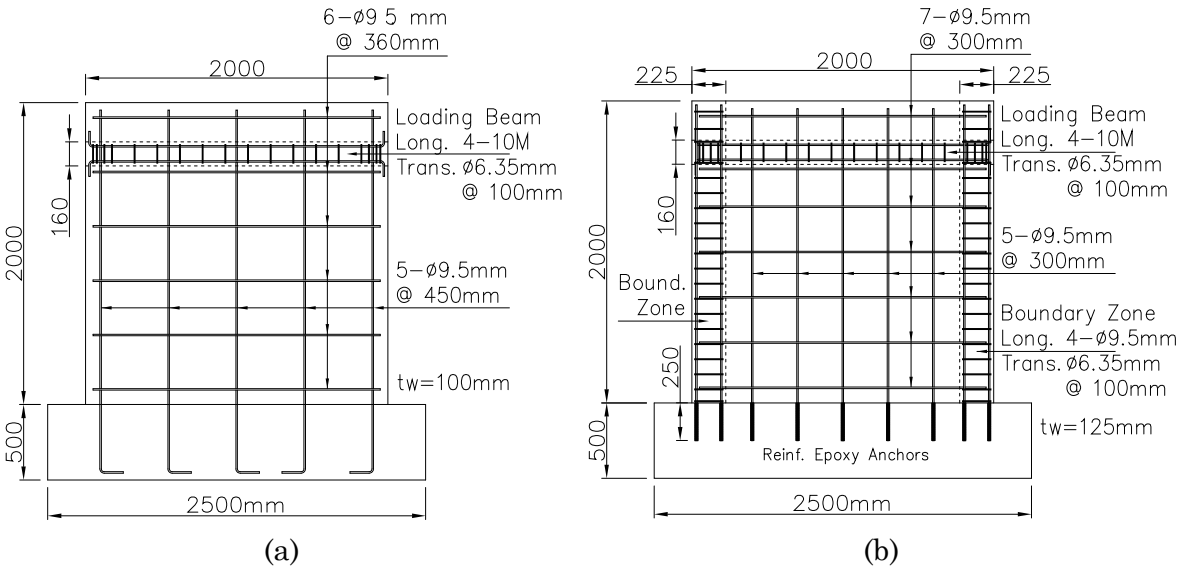


Figure 5-1 Details of shear walls: (a) SQ1/SQ1S and SQ1a/SQ1aS; and (b) SQ2/SQ2S

5.3.2 SMA Tension-Only Braces

Walls SQ1S, SQ1aS, and SQ2S were retrofitted with two 2540 mm-long external diagonal tension-only SMA braces on each side of the wall (Figure 5-2). The SMA braces consisted of 12.7 mm- diameter, 635 mm-long SMA links coupled to 953 mm-long rigid steel elements. The SMA links were fabricated from superelastic Nitinol SMA rods with reduced diameter and cross sectional area of 11.8 mm and 110 mm^2, respectively, along a length of 500 mm. Screw lock couplers and stiff plates connected the SMA links to the rigid steel elements (HSS 50 × 50 × 4 mm). The connections were devised such that one end of the SMA links was free to slide into the rigid steel section to release compressive forces. The braces were connected to the lower and upper corners of the walls through anchor plates (203 mm × 203 mm × 12.7 mm) that were bolted to the wall. Figure 5-3 illustrates the brace.

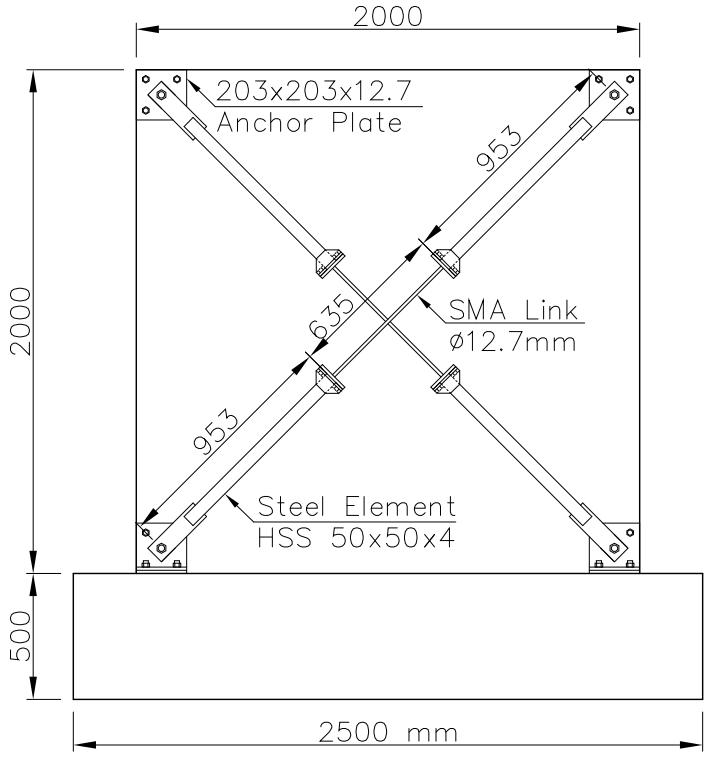


Figure 5-2 External retrofit of Walls SQ1S and SQ2S

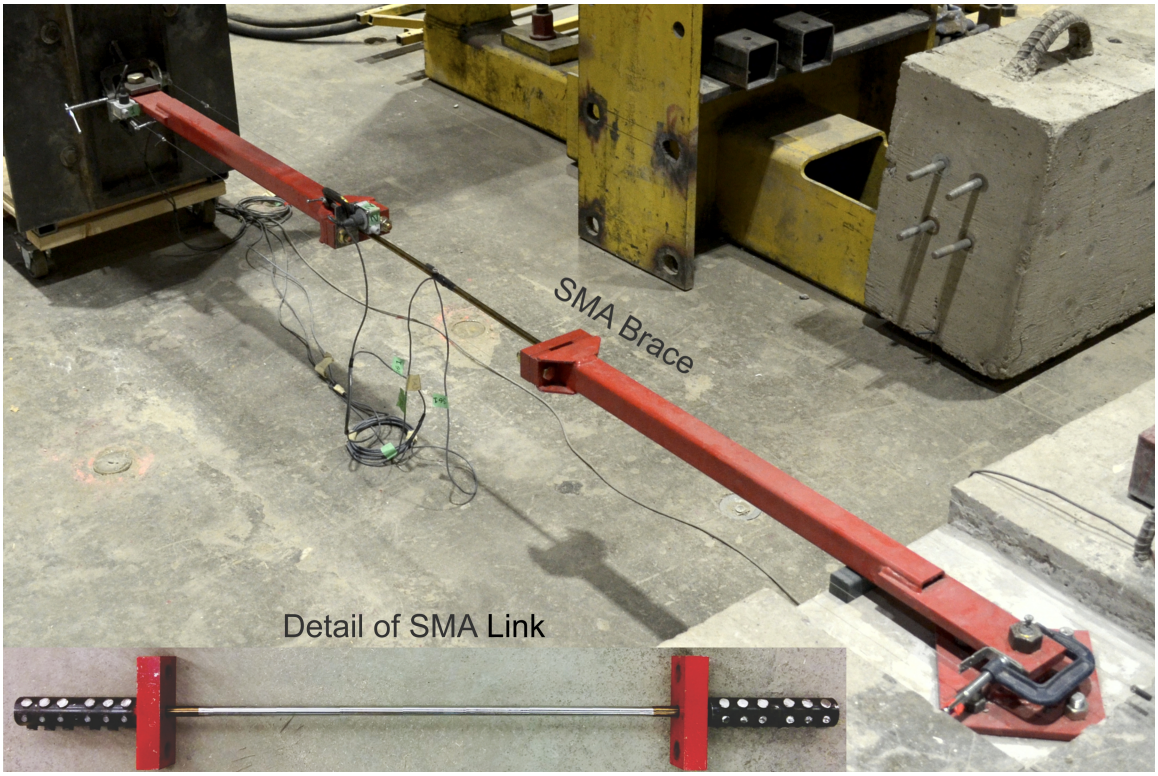


Figure 5-3 SMA Brace

Full details of the SMA braces are provided elsewhere (Cortés-Puentes and Palermo 2017a).

5.3.3 Material Properties

Table 5-1 provides the cylinder compressive strengths and the corresponding peak strains of the concrete used in the construction of the walls. The concrete properties used in the modelling of SQ1aS correspond to those of SQ1a. Table 5-2 provides the peak and ultimate stresses and corresponding strains of the internal deformed reinforcing steel.

Table 5-1 Concrete material properties

Wall	f'_c (MPa)	ε'_c (%)
SQ1	22.52	0.269
SQ1a	9.50	0.255
SQ1S	24.73	0.184
SQ2	20.26	0.187
SQ2S	27.37	0.222

Note: $f'c$ = compressive strength on the day of testing, and
ε'_c = compressive strain corresponding to $f'c$

Table 5-2 Reinforcement material properties

ϕ (mm)	f_y (MPa)	ε_y (%)	f_u (MPa)	ε_u (%)
9.5	495	0.30	735	16
11.3	460	0.30	660	16

Note: ϕ = diameter, f_y = yield stress, ε_y = yield strain
f_u = ultimate stress, and ε_u = ultimate strain

The mechanical properties of the SMA rods were based on tension testing (Figure 5-4) following the loading protocol of ASTM F2516-14 standard (ASTM 2014). The SMA experienced an upper plateau stress of 407 MPa and a lower plateau stress of 186 MPa at corresponding strains of 3% and 2.5%, respectively, during the initial cycle to 6%. The residual strain was 0.6%. During the subsequent cycle, the upper plateau stress reduced to 357 MPa, and rupture occurred at 19.8% at an ultimate stress of 1054 MPa.

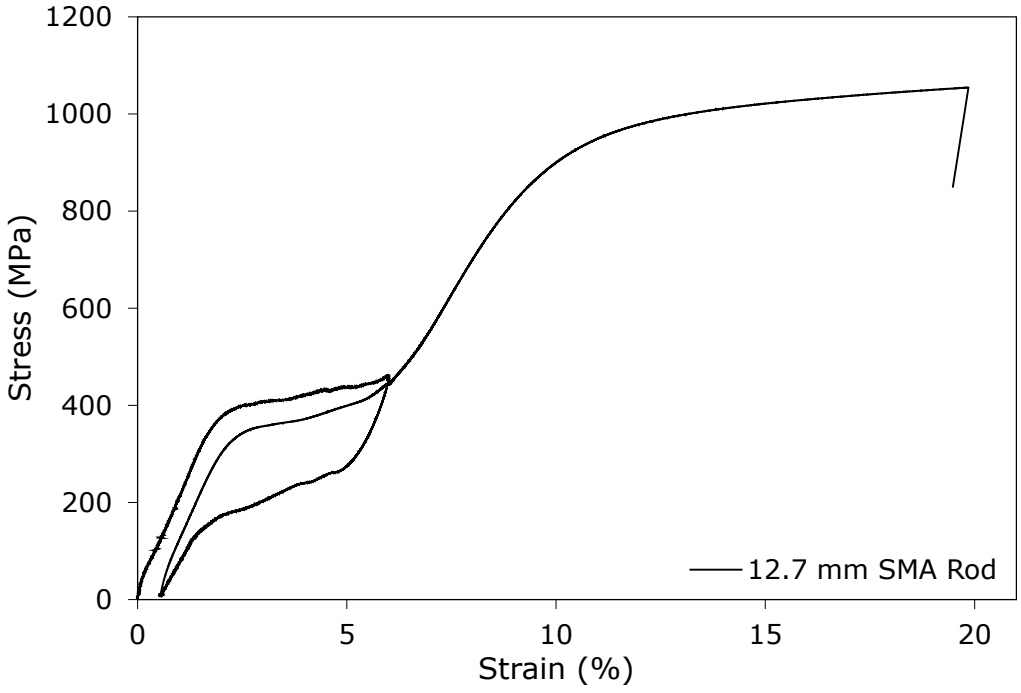


Figure 5-4 Stress-strain response of SMA rod

Figure 5-5 illustrates a typical response of the SMA tension braces tested to failure. The SMA braces experienced pseudo-yield stress of 353 MPa at 0.75% strain (3% in the SMA link), modulus of elasticity of 73 000 MPa, lower plateau stress of 172 MPa at 0.625% strain (2.5% in the SMA link), ultimate stress of 525 MPa, and rupture elongation of 2.2% (8.8% in the SMA link). The pseudo-yield stress corresponds to the sustained stress in the upper plateau, which results from the transformation of the crystalline structure of the material. Details of the cyclic response of the braces are presented elsewhere (Cortés-Puentes and Palermo 2017a).

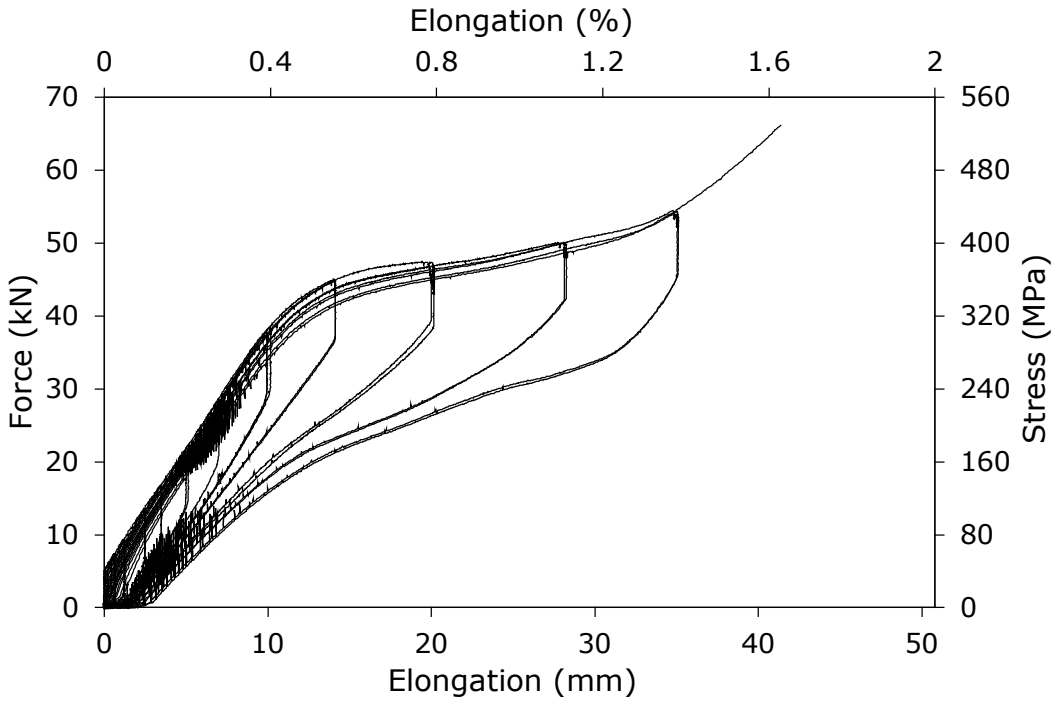


Figure 5-5 Force-elongation response of SMA brace

5.3.4 Loading of Walls

The in-plane lateral loading was applied on the walls at a height of 1660 mm from the base and the corresponding lateral displacements were recorded at the top of the walls, 2000 mm from the base. Loading followed the pseudo-static protocol recommended by FEMA 461 (ATC 2007), initiating with a pre-cracking cycle to 0.3 mm of lateral displacement. The cycles were increased by a factor of 2 in the pre-yielding stage (0.3 mm to 2.4 mm) and by a factor of 1.4 in the damage stage (3.6 mm to 40 mm). Beyond 40 mm, the cycles were increased by 10 mm. Each cycle consisted of two repetitions of the displacement amplitude. An instrumentation error resulted in asymmetric loading of Wall SQ1. From the cycle to 7 mm, the following lateral displacements were imposed on the wall: +6.3 mm/-9.4 mm, +4.5 mm/-10.9 mm, +5.5 mm/-13.5 mm, +7 mm/-15.9 mm, +4.7 mm/-19.3 mm, +3.5 mm/-16.9 mm, +47.6 mm/-68 mm. Furthermore, the displacements imposed on Wall SQ1S were shifted by -5 mm from the cycle to 15 mm. For example, for the intended cycle to +20 mm/-20 mm the recorded displacements were +15 mm/-25 mm.

5.4 Finite Element Modelling

The response of the walls was simulated with the non-linear finite element (FE) program VecTor2 (Wong et al. 2013). VecTor2 is based on the Modified Compression Field Theory (MCFT) and the Disturbed Stress Field Model (DSFM). It employs a smeared, rotating crack approach to model cracked concrete. The program is applicable to membrane concrete structures and incorporates constitutive models for cracked concrete, reinforcing steel, and SMA. Cortes-Puentes and Palermo (2011, 2012) demonstrated the capabilities of VecTor2 to predict the cyclic response of repaired and retrofitted shear walls. Furthermore, Abdulridha et al. (2013) and Abdulridha and Palermo (2014) satisfactorily predicted the response of concrete structures reinforced with SMAs.

5.4.1 Modelling of Concrete

VecTor2 provides default constitutive models that are intended to be used with confidence by the beginner analyst; however, in this study the constitutive models for concrete were selected based on preliminary parametric analyses. The analyses established the models that satisfactorily captured the lateral load-displacement responses of Walls SQ1, SQ1a, and SQ2. The models investigated included: compression base curve and post-peak relationships, compression softening, tension stiffening, tension softening, stress calculation, crack width, hysteretic response, and element slip distortion. For brevity, a brief summary of the models is presented, while full details of the formulations are available elsewhere (Wong et al. 2013).

The Popovics model for the stress-strain response of concrete in compression for normal strength concrete (Popovics 1973) satisfactorily predicted the pre-peak and post-peak responses. The model has been successful in modelling normal concrete strength in repaired and retrofitted reinforced concrete shear walls (Cortés-Puentes and Palermo 2011). The Vecchio 1992-A compression softening formulation (Vecchio and Collins 1993) modelled the reduction in strength and stiffness of the concrete due to co-existing transverse tensile straining. The Collins-Mitchell formulation, a modification of the Vecchio 1982 model (Vecchio and Collins 1986), was selected to

model tension stiffening due to the presence of reinforcing steel, and a descending lineal relationship best captured the tension softening due to the presence of cracks (Vecchio 2000). The advanced Lee-2009 formulation, based on the MCFT and the DSFM, was used to calculate shear stresses that develop on the surface of cracks. The crack width, a parameter that reduces the average compressive stress of concrete when the crack width exceeds a specified limit, was not considered. For the analyses conducted herein, the inclusion of this model predicted concentrated damage along the base of the walls due to substantial degradation of the compressive and shear stresses. As a result, sliding displacements were overestimated, leading to premature failure. The hysteretic response of the concrete was best captured with the nonlinear with cyclic decay model (Palermo and Vecchio 2003). This model accounts for stiffness and strength degradation during reloading, explicitly considers partial loading/reloading, and provides an improved estimate of the plastic offset. The element shear-slip distortion, a phenomenon that improves the prediction of the shear stress-strain response of cracked concrete and the strains in the reinforcing steel, was evaluated with a hybrid model that combines the Walraven model (Walraven and Reinhardt 1981) with the constant rotation lag model (Vecchio and Lai 2004). In this hybrid model, the constant rotation lag is taken as 10° for unreinforced elements, 7.5° for elements with one smeared reinforcement component, and 5° for elements with two or more smeared reinforcement components. For other secondary effects, the default models were selected. The variable Poisson's ratio, based on experimental work conducted by Kupfer et al. (1969), was chosen to capture the lateral expansion of concrete caused by internal micro cracking; the Kupfer/Richart formulation (Vecchio 1992) modelled the concrete strength enhancement due to tri-axial confinement; and the Mohr-Coulomb stress criterion was implemented to determine the tensile strength of concrete at cracking.

5.4.2 Modelling of Reinforcing Steel

The hysteretic stress-strain response of the reinforcing steel was based on the Seckin model (Seckin 1981). The model follows a backbone envelope for ductile steel that is defined by a linear elastic phase, a yield plateau, and a curvilinear strain-hardening phase. The hysteretic model includes the Bauschinger effect, which results in

nonlinear unloading and linear reloading. The Tassios crack-slip relationship (He and Kwan 2001) was used to model dowel action due to slip displacements at cracks that are perpendicular to the reinforcement, and the Asazu model (Asazu et al. 2001) simulated buckling of reinforcement. To capture buckling with this model, the reinforcing steel must be represented by discrete truss elements that, in turn, are connected to the concrete elements with bond-link elements. Bond-slip between the reinforcing steel and concrete was simulated with the Eligehausen formulation (Eligehausen et al. 1983).

5.4.3 Modelling of SMA Braces

Tension-only truss elements simulated the SMA Braces. The response in tension followed the hysteretic constitutive model for superelastic SMA bars developed by Abdulridha et al. (2013) (Figure 5-6). In compression, the reinforcement stress was always zero. The superelastic SMA model includes explicit considerations of permanent strains and the degradation of the lower plateau stress resulting from strain recovery. Loading of the SMA follows an initial linear elastic phase (Austenite phase); a pseudo-yield upper stress, f_y, plateau (forward transformation: Austenite to Martensite phase); and a linear strain hardening phase (Martensite phase) defined by the strain hardening stiffness, E_{sh}. Unloading follows a tri-linear response defined by a linear phase that initiates at the maximum strain, ε_m, and corresponding maximum stress, f_m; a lower stress, f_{unl}, plateau (reverse transformation: Martensite to Austenite phase); and a linear recovery phase from the lower stress plateau to the plastic strain, ε_p. The model assumes that the unloading stiffness, E_1 and E_2, are equal to the initial stiffness E_i, and that the upper stress plateau stiffness, E_f, and lower stress plateau stiffness, E_r, are zero. Reloading stiffness, E_{rl}, is defined by the plastic strain prior to unloading and the pseudo-yield point. The lower stress plateau is defined by the strains ε_{r1} and ε_{r2}. Details of the formulations can be found elsewhere (Abdulridha et al. 2013). The input parameters required in VecTo2 to model the SMA braces are the initial stiffness, E_i, the pseudo-yield upper stress, f_y, the strain corresponding to the onset of strain hardening, ε_{sh}, the ultimate stress, f_u, and the corresponding ultimate strain, ε_u. These parameters are defined by the stress-strain response of the SMA

braces (Cortés-Puentes and Palermo 2017a). Alternatively, the input parameters can be determined from the stress-strain response of the SMA links, obtained from the manufacturer of the SMA rods or from tensile testing. The stresses in the SMA braces are assumed the same as those in the SMA links, while the strains in the braces can be calculated from the strains in the link multiplied by the ratio of the link to brace length.

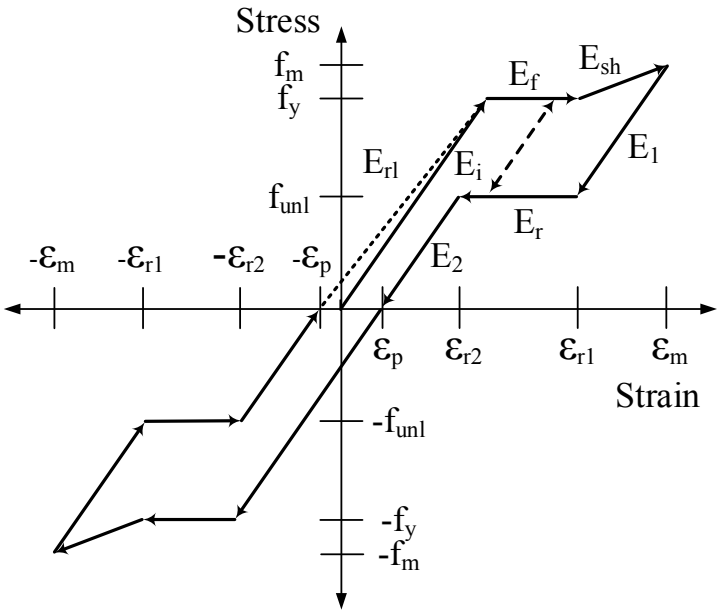


Figure 5-6 Superelastic SMA brace constitutive model (Abdulridha et al. 2013)

Comparison of the numerical and the experimental responses of the SMA braces (Figure 5-7) highlights that the simple trilinear loading-reloading formulation satisfactorily simulates the tension SMA braces. The numerical model captured the elongation recovery but slightly underestimated the hysteretic energy dissipation density (calculated based on the area under the stress-strain hysteretic loops) due to the simplified unloading branch. The numerical and experimental cumulative energy dissipation densities at rupture were 5726 kN-m/m^3 and 6847 kN-m/m^3, respectively, which corresponded to a difference of 16%.

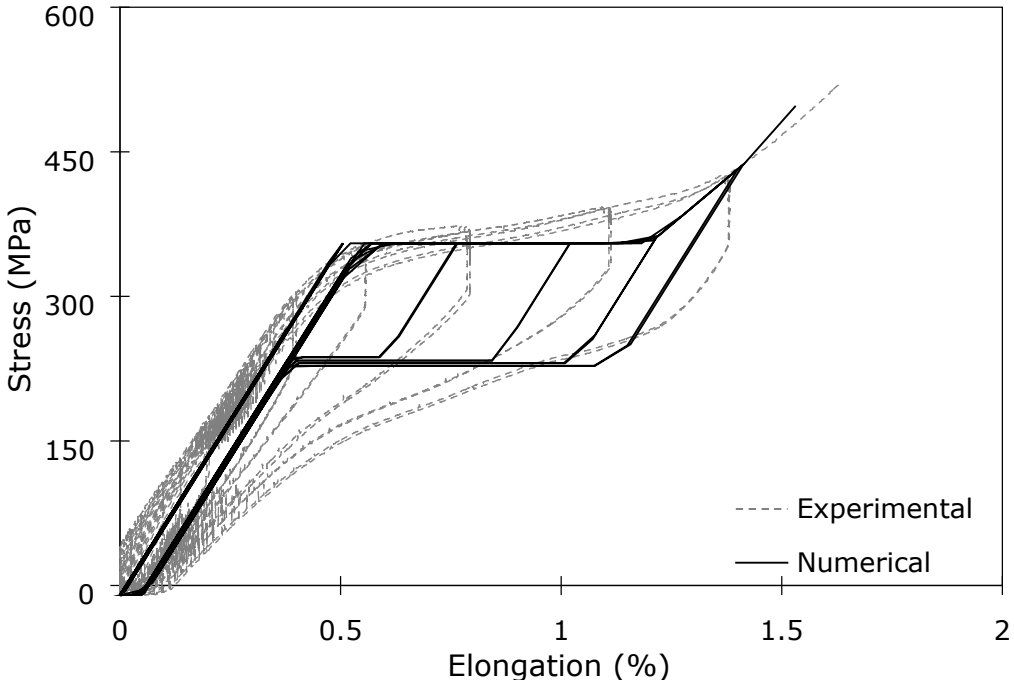


Figure 5-7 Force-elongation response of SMA brace

5.4.4 Finite Element Mesh

The finite element meshes of the walls incorporated four-nodded, two-dimensional, rectangular membrane elements with eight degrees of freedom to model the concrete. The concrete in the web and the boundary zones of the walls were defined by rectangular elements with an aspect ratio of approximately 1. The concrete cover at the ends of the walls were simulated by concrete elements with aspect ratios ranging from 1.5 to 2. The mesh of the foundation blocks and loading beams conformed to the mesh of the web and boundary zones of the walls. The longitudinal and transverse reinforcement within the walls were modelled with discrete two-nodded, one-dimensional, truss elements with the exception of the transverse reinforcement in the boundary zones. The properties of the latter were smeared within the concrete elements. The longitudinal reinforcement was modelled as partially bonded by connecting the steel truss elements to the concrete elements with non-dimensional bond-link elements at common nodes (Figure 5-8). The bond-link element consists of two nodes, each node with two translational degrees of freedoms. One node is

connected to the concrete element, while the other node is connected to the steel truss element. The two orthogonal springs within the link element simulate radial and tangential slips and bond stresses along the steel. The transverse reinforcement was modelled as perfectly bonded by connecting the steel truss elements directly to the nodes of the concrete elements. The cross sectional area of the longitudinal reinforcing steel truss elements near the base of the walls was reduced by 10% to account for the reduced cross-sectional area required to install strain gauges. The confining hoops in the boundary zones, as well as the reinforcement in the foundation blocks and the loading beams, were modelled as smeared reinforcement in the concrete elements. Horizontal and vertical restraining of the nodes at the base of the foundation blocks simulated the fixed support condition of the walls. The numerical analyses conformed to the loading protocols used for testing. Incremental displacements were applied at the ends of the loading beam according to the direction of loading.

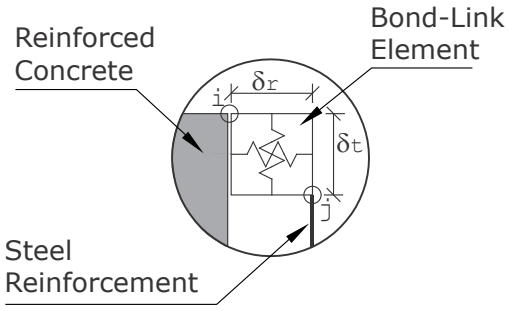


Figure 5-8 Bond-link element (Cortés-Puentes and Palermo 2012)

The finite element mesh for Walls SQ1, SQ1a, SQ1S, and SQ1aS consisted of five concrete zones (Figure 5-9): zone 1 corresponded to the web of the walls, zones 2 and 3 corresponded to the loading beam, zone 4 corresponded to the foundation block, and zone 5 corresponded to a heavily reinforced region that simulated the anchor plates used to connect the SMA braces to the retrofitted wall (SQ1S only). In addition, Wall SQ1S incorporated two truss elements to simulate the SMA braces located on the front and back faces of the wall. Each truss element was assigned a cross-sectional area of 220 mm^2.

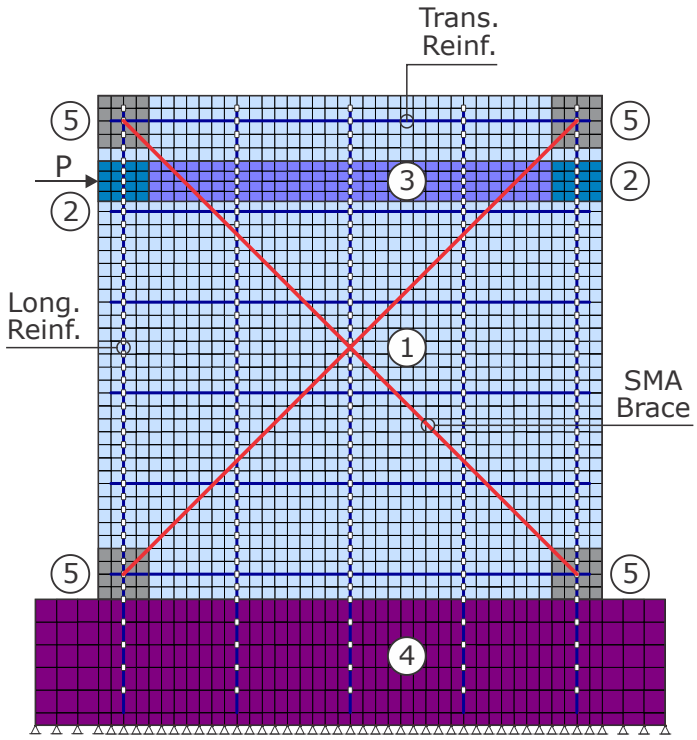


Figure 5-9 Finite element model of Walls SQ1, SQ1a, and SQ1S (SMA braces only in SQ1S)

The finite element model for Walls SQ2 and SQ2S was divided into six zones (Figure 5-10): zone 1 and zone 2 corresponded to the boundary zones and web of the wall, respectively, zone 3 and zone 4 corresponded to the loading beam, zone 5 corresponded to the foundation block, and zone 6 corresponded to the anchor plates for SQ2S. The SMA braces were modelled with two tension-only truss elements with cross sectional area of 220 mm^2, following the same approach used for Wall SQ1S.

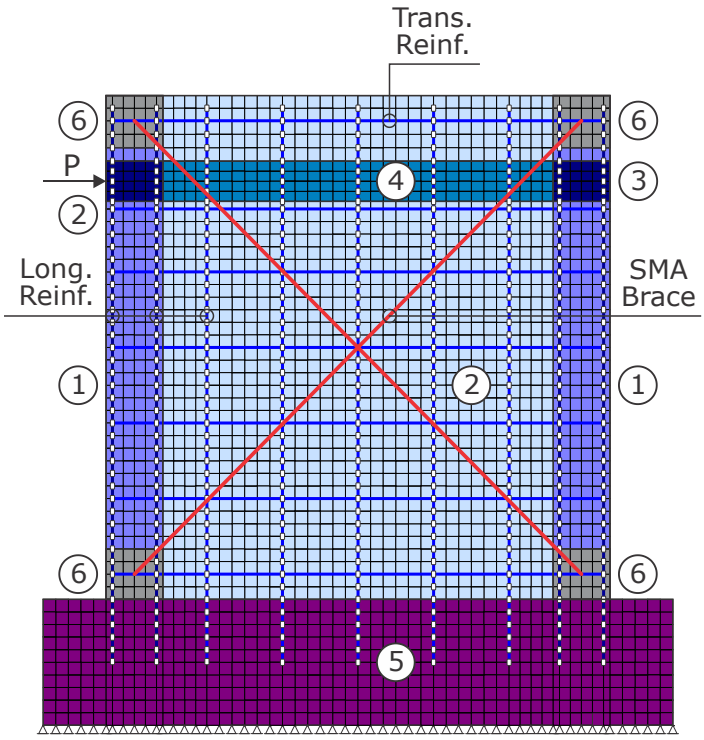


Figure 5-10 Finite element model of Walls SQ2 and SQ2S (SMA braces only in SQ2S)

A sensitivity study was conducted to select the size and number of elements. The objective was to establish a sufficiently fine mesh that could accurately simulate the strain and stress gradients in the walls while capturing the damage. The study investigated three mesh resolutions in the web of the control walls: coarse, medium and fine meshes.

Table 5-3 summarizes the elements used in the walls. The meshing of the walls complied with the minimum of 13 elements and the maximum aspect ratio of 1.5 for shear walls suggested by Palermo and Vecchio (2007). The exception was the elements representing the concrete cover in the boundary zones in Walls SQ2 and SQ2S, which were modelled with a larger aspect ratio to conform to the geometry of the walls.

Table 5-3 Summary of finite element meshes in shear walls

Wall	Mesh	Element size (mm × mm)	Number of concrete elements	Number of steel elements	Number of bond-link elements
SQ1/SQ1a	Fine	50 × 50	1600	448	225
	Medium	90 × 90[a]	576	272	140
	Coarse	150 × 120[b]	304	194	110
SQ2	Fine	50 × 50	1804	735	450
	Medium	100 × 100	552	397	252
	Coarse	150 × 150[b]	272	278	189

Note: characteristic concrete element size in the web and boundary zones.
[a] 90 mm × 100 mm elements along the base of the walls.
[b] 150 mm × 100 mm elements along the base of the walls.

Table 5-4 compares the numerical and experimental response parameters of the control walls with the different meshes. In general, the analyses adequately predicted the lateral strength and the failure mode of the walls. The lateral strength of SQ2, however, was slightly overestimated for all mesh sizes. During loading to the first 10 mm of lateral displacement in SQ2, the models did not completely capture the degradation in strength due to cracking. Rupturing of the longitudinal reinforcing steel in the walls was captured with the three meshes for all the walls. Modelling of the walls with the fine mesh resulted in the most accurate predictions of the response (Figure 5-11 to Figure 5-16).

Table 5-4 Experimental and numerical responses of control shear walls

Wall	Mesh	Peak lateral strength (kN)			Drift (%)		
		Num	Exp	Num/Exp	Num	Exp	Num/Exp
SQ1	Fine	135	145	0.93	1.57	1.85	0.85
	Medium	164	145	1.13	1.60	1.85	0.86
	Coarse	175	145	1.21	1.25	1.85	0.68
SQ1a	Fine	114	117	0.97	2	2	1
	Medium	119	117	1.02	2.5	2	1.25
	Coarse	123	117	1.05	3.9	2	1.95
SQ2	Fine	264	243	1.09	2	1.5	1.33
	Medium	273	243	1.12	2	1.5	1.33
	Coarse	281	243	1.16	2.5	1.5	1.67

Note: Response in the positive direction; Num = Numerical; and Exp = Experimental.

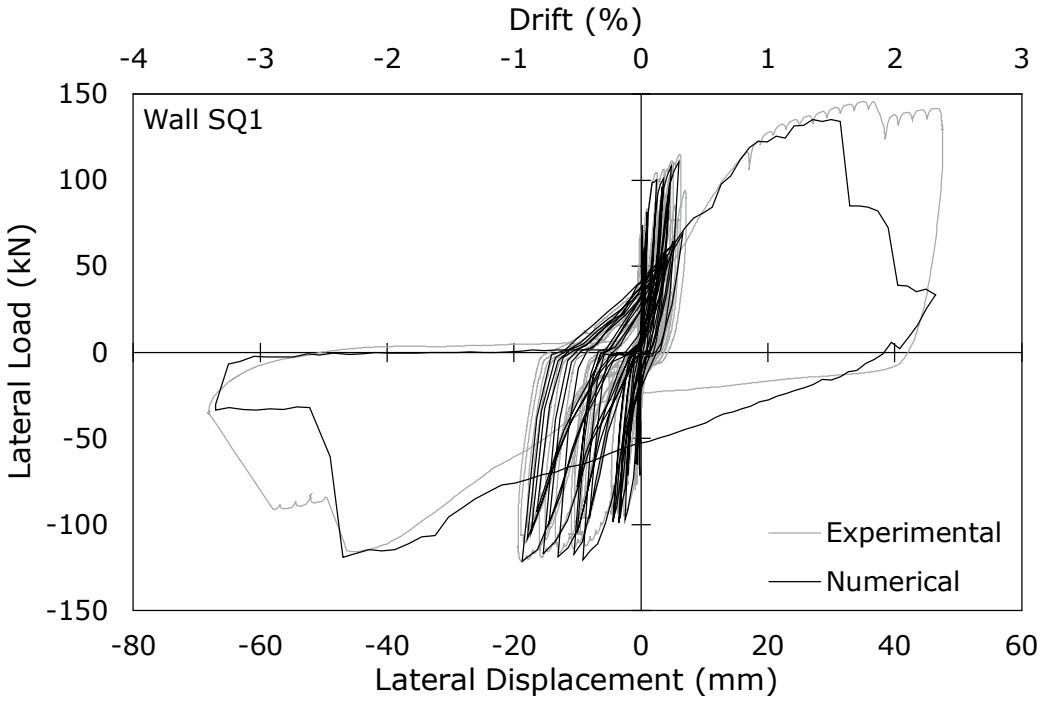


Figure 5-11 Lateral load-displacement response of Wall SQ1

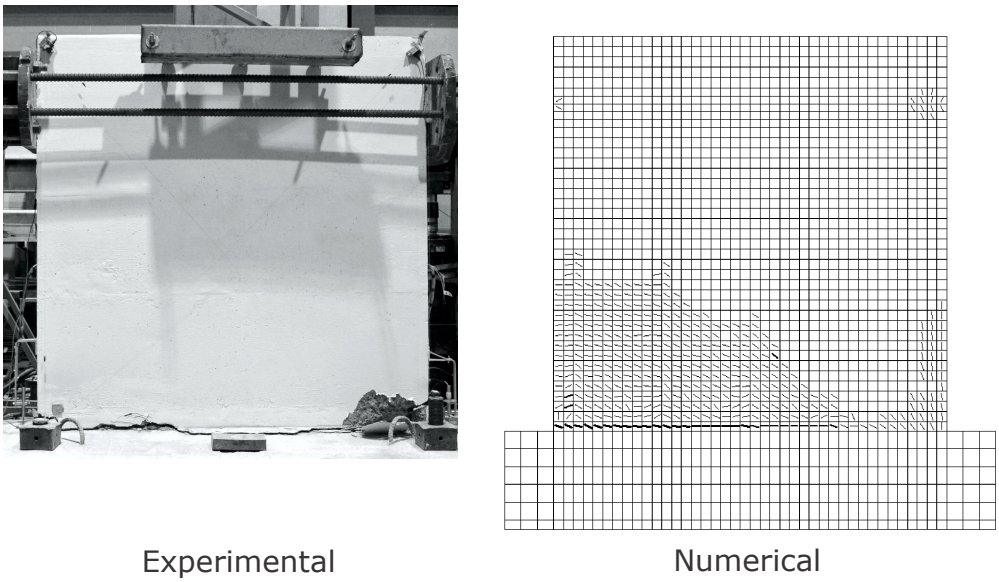


Figure 5-12 Damage of Wall SQ1 at 1.5% drift

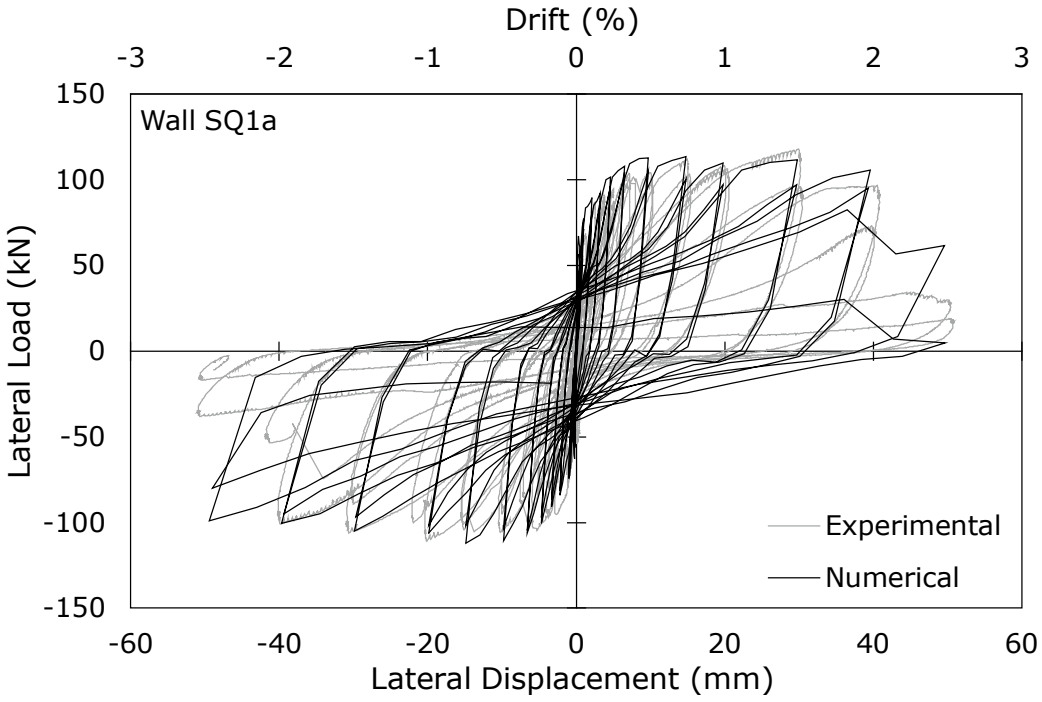


Figure 5-13 Lateral load-displacement response of Wall SQ1a

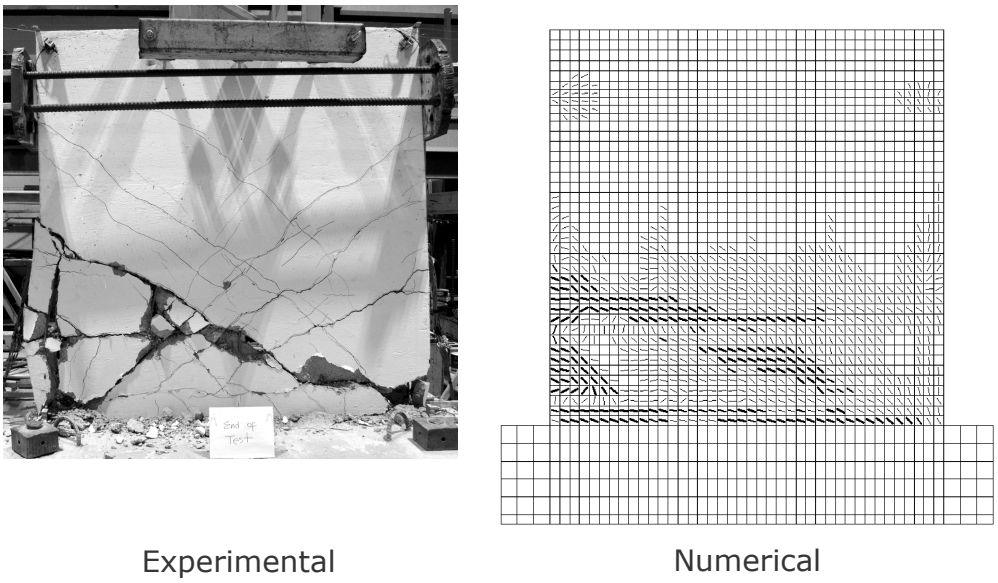


Figure 5-14 Damage of Wall SQ1a at 2% drift

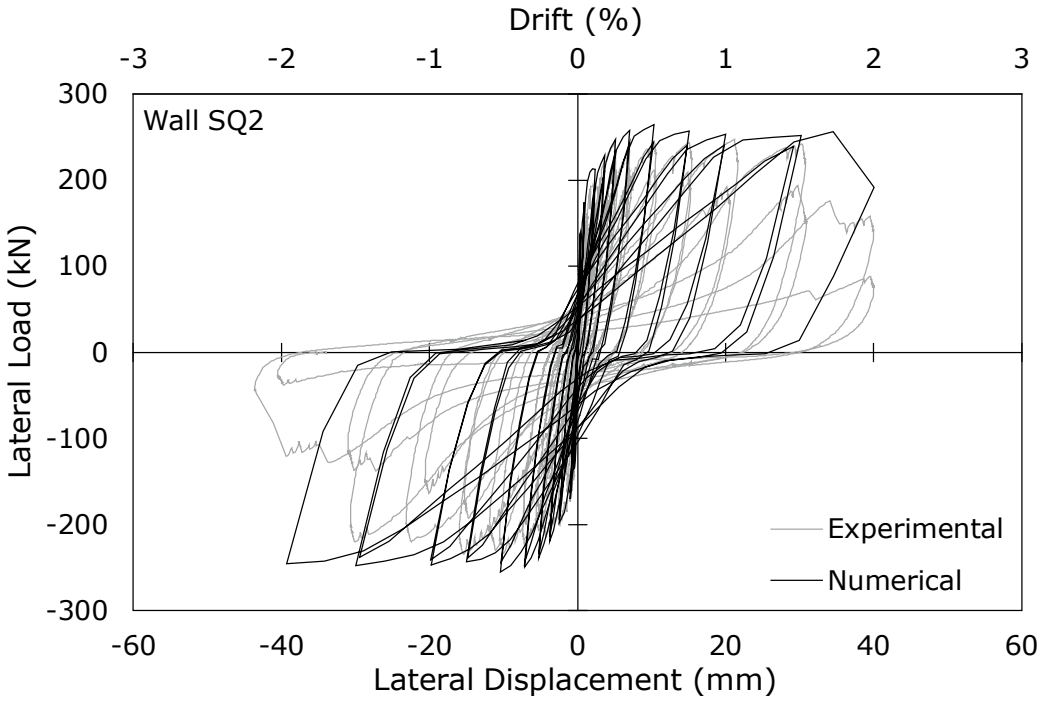


Figure 5-15 Lateral load-displacement response of Wall SQ2

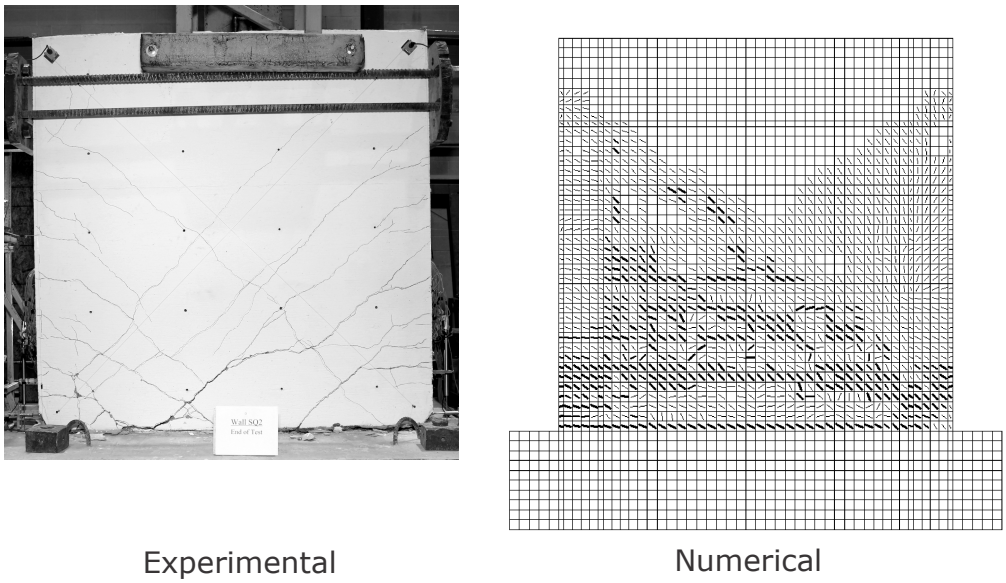


Figure 5-16 Damage of Wall SQ2 at 1.5% drift

The fine mesh captured the discrete cracking of the walls observed during testing, while the medium and coarse meshes predicted distributed damage in the concrete elements. Specifically, the fine mesh captured the dominant horizontal crack at the base of SQ1, which resulted in rocking motion, and the main shear cracks in SQ1a and SQ2. The fine mesh was more successful at capturing the pinching of the hysteretic responses due to shear damage, and the drift capacity of the walls. [Note that the drift capacity at ultimate was determined at rupture of the reinforcing steel or significant drop in lateral strength of more than 20%.] Furthermore, the length of the truss elements representing the fine mesh was the same as the length of the gauge length used in the tensile testing of the reinforcing steel to determine the stress-strain properties. As a result, regularization of the stress-strain response to correspond to the size of the truss elements was not necessary (Pugh et al. 2015). Therefore, the fine mesh was selected to model the walls retrofitted with SMA braces presented herein (Figure 5-9 and Figure 5-10).

5.5 Numerical Analysis of Retrofitted Walls

Table 5-5 compares the numerical with the experimental response parameters of the walls, with the exception of Wall SQ1aS, which was not part of the experimental program. Wall SQ1aS was numerically simulated to assess the contribution of the SMA braces to improve the response of squat shear walls with low concrete strength.

Table 5-5 Experimental and numerical responses of retrofitted walls

Wall	Direction	Peak lateral strength (kN)			Drift (%)		
		Num	Exp	Num/Exp	Num	Exp	Num/Exp
SQ1S	Positive	207	213	0.97	1.15	1.25	0.92
SQ1aS	Positive	192	-	-	2	-	-
SQ2S	Positive	380	391	0.98	-	1.5	-
	Negative	393	424	0.93	3.1	2.85	1.09

Note: Num = Numerical; and Exp = Experimental.

5.5.1 Wall SQ1S

Figure 5-17 compares the experimental and numerical lateral load-displacement responses of Wall SQ1S. The predicted peak lateral strength and drift capacity were

in excellent agreement with the experimental results (Table 5-5). The initial stiffness, however, was slightly overestimated, resulting in a notable difference in lateral strength in the pre-cracking stage. The analysis captured the increase in lateral strength to ultimate and the observed localized damage at the base of the wall (Figure 5-18). The horizontal crack that initiated above the anchor plates and the associated behaviour controlled by rocking was well simulated. Furthermore, the analysis predicted the observed rupturing of the longitudinal reinforcing bars nearest to the edge of the wall while loading to 25 mm of lateral displacement.

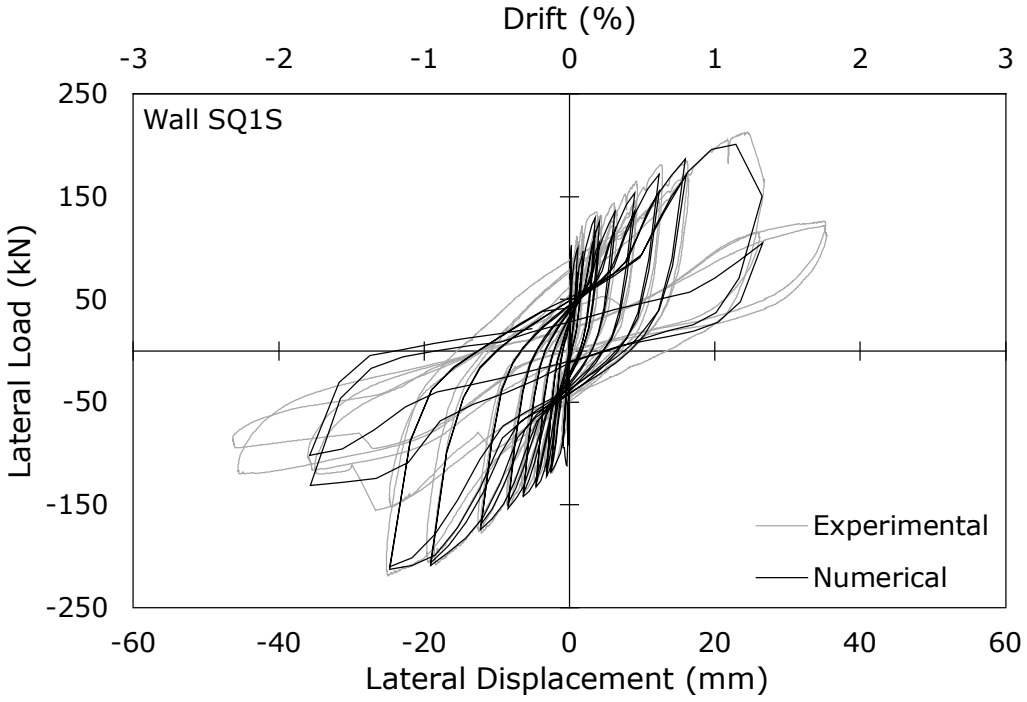


Figure 5-17 Lateral load-displacement response of Wall SQ1S

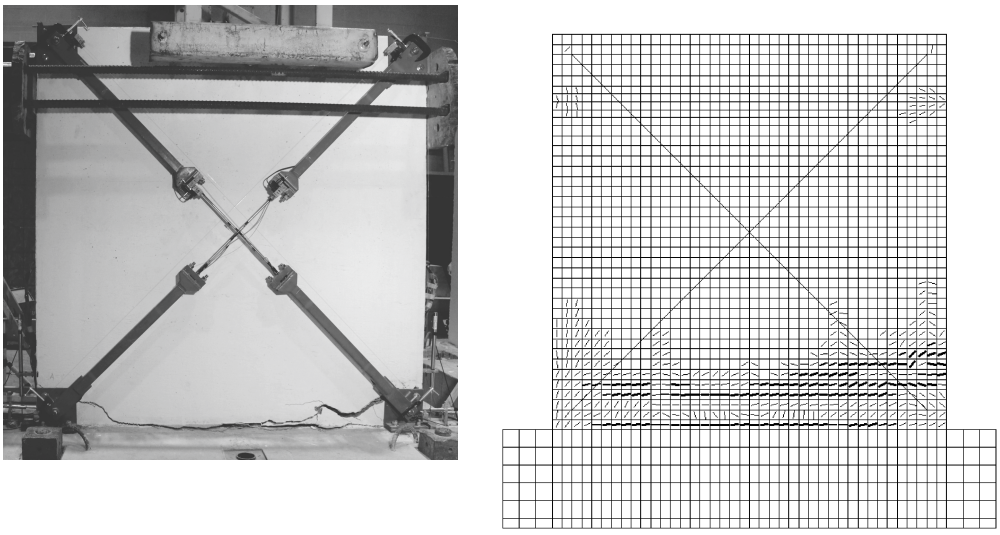


Figure 5-18 Damage of Wall SQ1S at -1.25% drift

In general, the hysteretic cycles and the corresponding pinching established with the model matched the observed response, as demonstrated by the cycle to 20 mm of lateral displacement in (Figure 5-19). The analysis captured the change of stiffness due to closing of the horizontal crack at the base of the wall and the displacement recovery provided by the SMA braces. At 20 mm of lateral displacement, the analysis accurately predicted the observed displacement recovery of 48%. [The displacement recovery is the ratio of the difference between the peak and the residual displacements to the peak displacement.] The reloading stiffness from the negative direction to the positive direction of loading, however, was slightly underestimated. Satisfactory simulation of the hysteretic cycles led to an acceptable prediction of the energy dissipation capacity, which was underestimated by approximately 16%. Prior to failure, at 20 mm of lateral displacement, the numerical and experimental cumulative energy dissipation capacities were 21.9 kN-m and 26 kN-m, respectively. This difference is consistent with the lower energy capacity of the SMA hysteretic model used in this study.

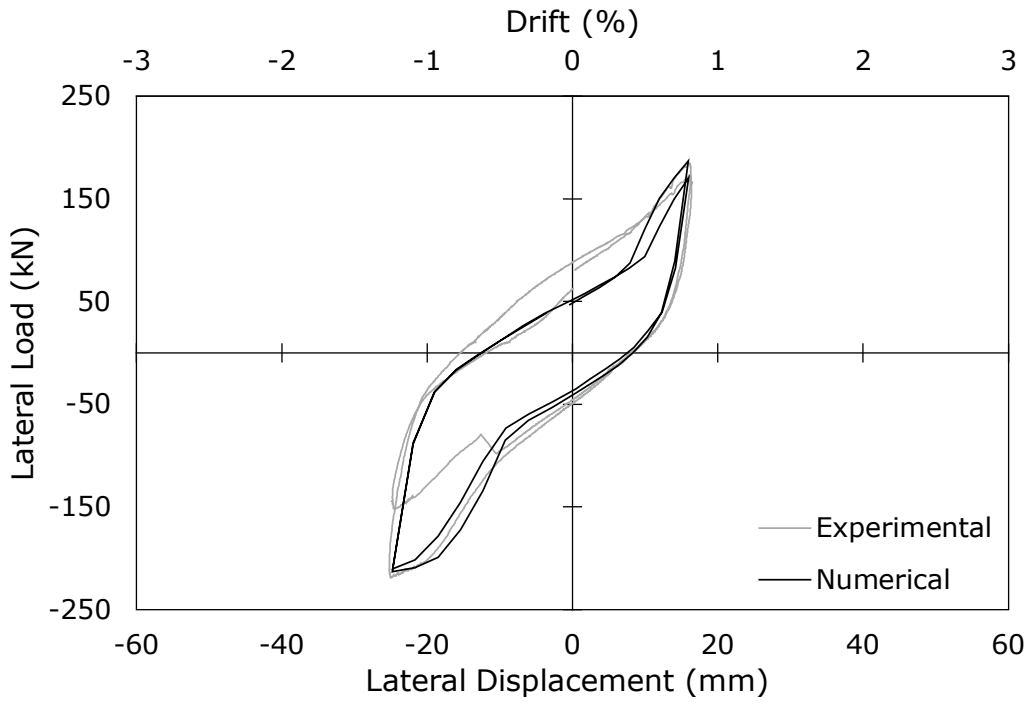


Figure 5-19 Cycle to 20 mm, Wall SQ1S

5.5.2 Wall SQ1aS

Figure 5-20 provides the lateral load-displacement response of Wall SQ1aS based solely on the numerical model. The first part of the response, up to 3.6 mm of lateral displacement, was governed by the linear behaviour of the internal reinforcing steel and the SMA braces. From 3.6 mm to 20 mm of lateral displacement, the response was governed by yielding of the internal reinforcement and increase in lateral strength due to the SMA braces. This phase of the response was similar to SQ1S, but with reduced lateral strength as a result of lower concrete strength. Beyond 20 mm of lateral displacement, the response was governed by pseudo-yielding of the SMA braces, which improved the lateral strength capacity of SQ1aS in comparison to SQ1a. Wall SQ1aS experienced a peak lateral strength of 189 kN at 30 mm (1.5% drift), which was sustained to ultimate at 40 mm (2% drift). The SMA braces were effective at reducing pinching associated with shear degradation and improved recovery of lateral displacements. The drift capacity of SQ1aS, however, was similar to that of SQ1a. The predicted distributed diagonal cracking in the lower half of the wall and

rupturing of longitudinal reinforcing bars in SQ1aS corresponded to the damage observed in SQ1a (Figure 5-21). At 40 mm of lateral displacement, the predicted cumulative energy and displacement recovery of SQ1aS was 41.6 kN-m and 57%, respectively.

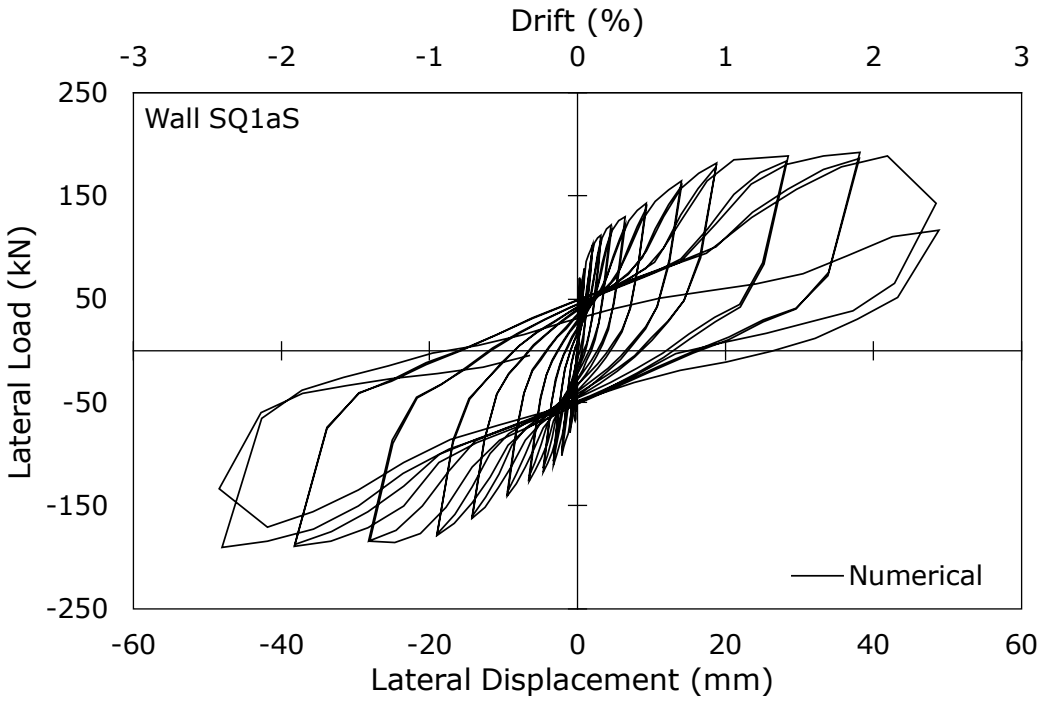


Figure 5-20 Lateral load-displacement response of Wall SQ1aS

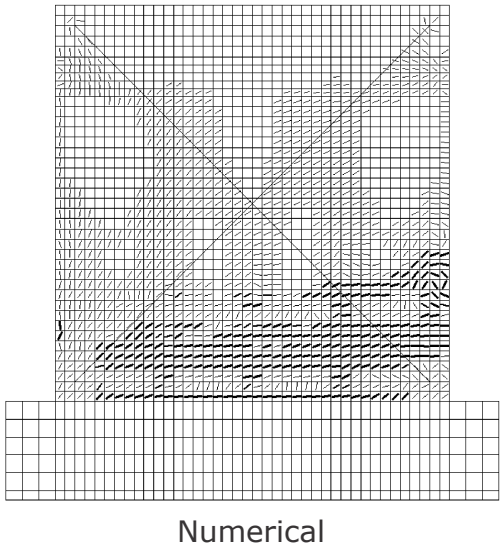


Figure 5-21 Damage of Wall SQ1aS at -2% drift

5.5.3 Wall SQ2S

Figure 5-22 compares the experimental and numerical lateral load-displacement responses of Wall SQ2S. The analysis accurately captured the response of the wall up to 30 mm of lateral displacement (Figure 5-23). Loading and unloading of the hysteretic cycles matched the observed response, capturing the stiffness and the improvement in crack closing due to the recovery capacity of the SMA braces. The average lateral strength of the cycles was slightly underestimated by less than 5%. The analysis predicted a peak lateral strength of 380 kN at +27 mm of lateral displacement. At this displacement, the observed lateral strength was 379 kN. At +30 mm of lateral displacement, the predicted lateral strength slightly decreased to 376 kN, while the observed lateral strength increased to 386 kN. The predicted reduction in lateral strength at +30 mm was the result of high compressive stresses in the concrete, which was evident during testing, specifically during loading to 40 m. Further reduction in strength to 362 kN was predicted at +40 mm. The analysis did not simulate the observed out-of-plane buckling that resulted in heavy concrete damage at +40 mm and +50 mm in one of the boundary zones. [Out-of-plane buckling is a 3-D phenomenon not simulated by the 2-D modelling implemented in this study.] As a result, the lateral strength and the stiffness in the positive direction, specifically for the second repetitions, were overestimated. At +50 mm of lateral displacement, the lateral strength was 13% larger than that observed. Conversely, at -50 mm of lateral displacement, the lateral strength was underestimated by 11%. Given the observed heavy damage in the right boundary zone and the associated instability, testing of the wall was halted in the positive direction and continued only in the negative direction. The simulation of the additional displacements in the negative direction captured the stiffness, the lateral strength, and the drift capacity of the wall. The predicted and observed peak lateral strength capacities in the negative direction were 396 kN and 424 kN, respectively. The analysis captured the observed diagonal cracking while loading in both directions and rupturing of the longitudinal reinforcing steel at ultimate. (Figure 5-24).

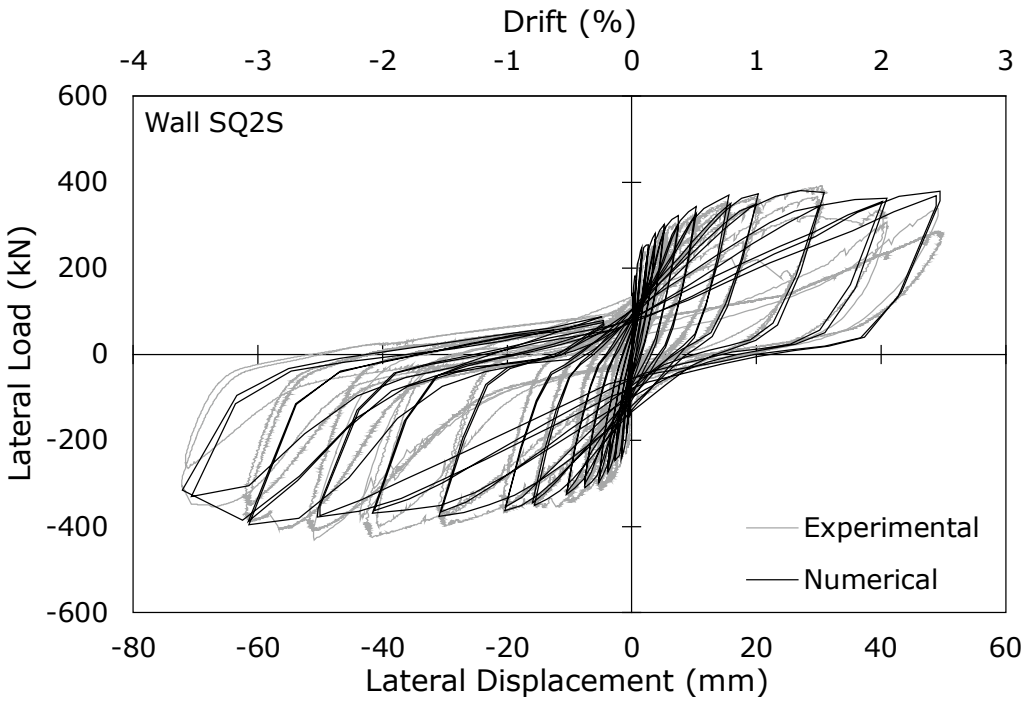


Figure 5-22 Lateral load-displacement response of Wall SQ2S

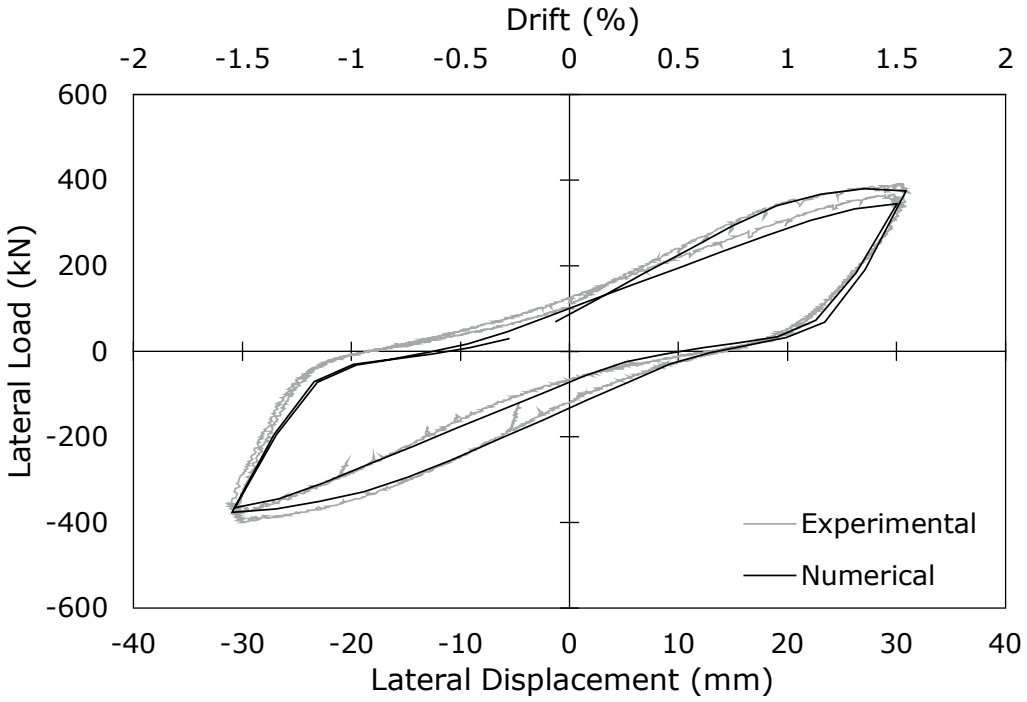


Figure 5-23 Cycle to 30 mm, Wall SQ2S

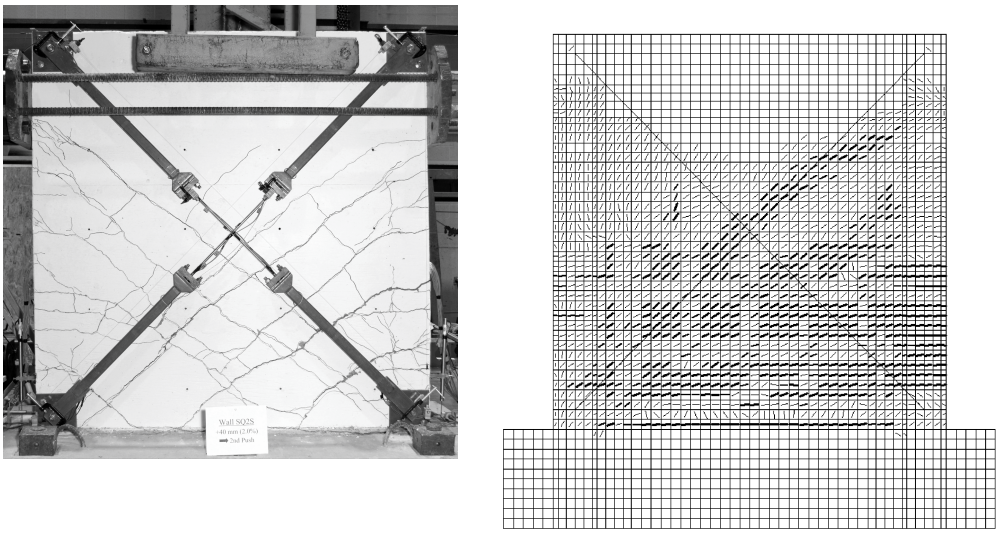


Figure 5-24 Damage of Wall SQ2S at -2% drift

The energy dissipation and displacement recovery were well predicted. The predicted cumulative energy dissipation of 153.3 kN-m at -60 mm of lateral displacement was 8% lower than the observed cumulative energy of 165.9 kN-m. This negligible difference is attributed to the lower energy capacity of the braces predicted by the SMA hysteretic constitutive model and the slightly lower lateral strength capacity in the negative direction of loading beyond -50 mm. The predicted residual displacements were in good agreement with those observed at the ultimate displacements in the positive and negative directions. The numerical model predicted displacement recovery of 56% and 45%, respectively, during loading to +30 mm and -60 mm displacement. The corresponding recorded recovery capacities were 54% and 32%. Minor discrepancies in capturing compressive and out-of-plane damages from 40 mm to 50 mm affected the accuracy of the predicted recovery in the subsequent cycles in the negative direction.

5.6 Parametric Study

Analyses were conducted to investigate four axial load ratios ($P/A_g f'_c$): 0%, 2%, 5%, and 10%, and four sizes of the SMA links, based on nominal diameter of the rods used for the construction of the braces: 10 mm (3/8in), 13 mm (1/2 in), 16 mm (5/8 in), and

19 mm (3/4 in). The axial loads represent a range of possible loading scenarios for squat shear walls. The size of the SMA correspond to readily available superelastic Nitinol SMA rods. For the study, the net cross-sectional area of the SMA rods was reduced to 85% to 88% of the nominal area to replicate the reduction of the diameter in the braces tested in the experimental program. The corresponding areas for the 10-mm, 13-mm, 16-mm, and 19-mm braces were 60 mm^2, 110 mm^2, 175 mm^2, and 250 mm^2, respectively. All other material and geometric properties of the concrete and reinforcing steel, and loading protocol remained constant.

5.6.1 Effect of Axial Loading

Figure 5-25 illustrates the effect of axial loading on the response of the retrofitted walls.

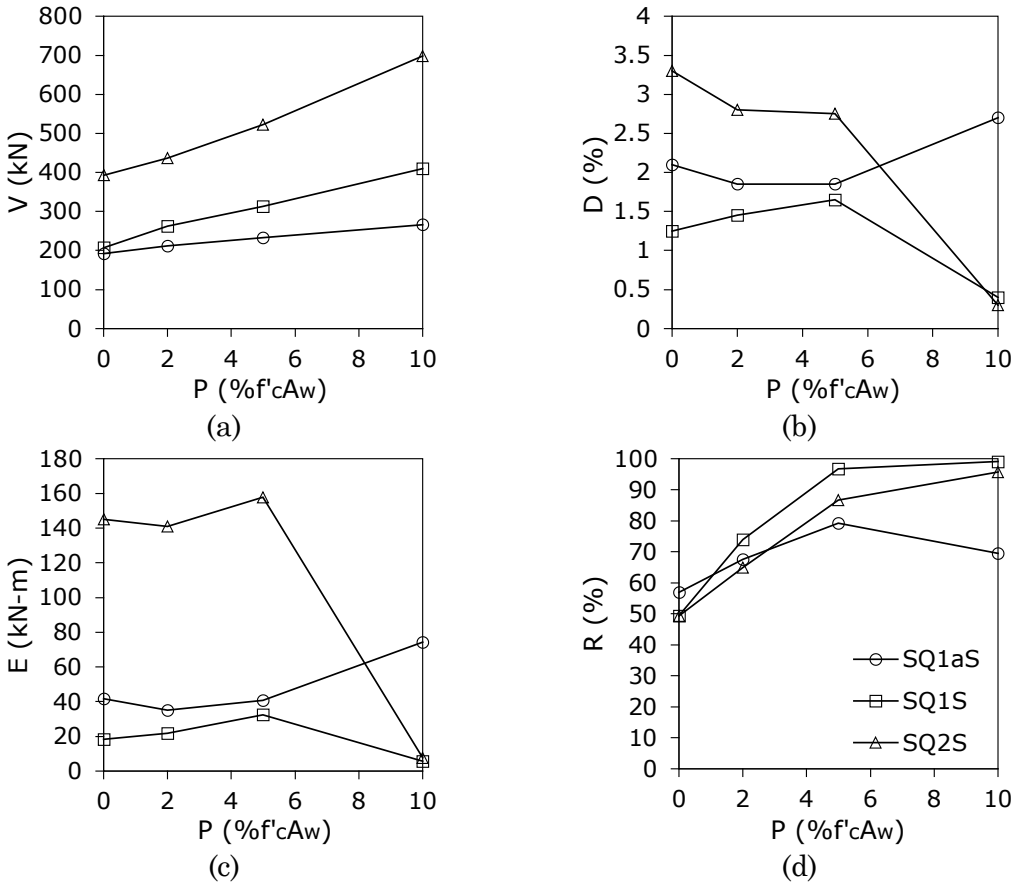


Figure 5-25 Effect of axial loading, *P*: (a) lateral strength, *V*; (b) drift, *D;* (c) cumulative energy dissipation, *E*; and (d) displacement recovery, *R*

With increase in axial loading from 0% to 10%, the lateral strengths of SQ1aS, SQ1S, and SQ2S were increased by 38%, 98%, and 78%, respectively. Note that for the different levels of axial loading, SQ2S experienced approximately double the lateral strength of SQ1aS and SQ1S.

The axial loading affected the damage and drift capacity of the walls. From 0% to 5% axial load, the drift capacity of SQ1S was slightly increased as a result of more distributed damage, which delayed fracture of the internal longitudinal reinforcement. [At lower axial loading, SQ1S experienced localized horizontal cracking at the base.] Conversely, SQ1aS and SQ2S slightly decreased the drift capacity due to greater compressive and shear stresses. Increases in axial loading to 10%, specifically for SQ1S and SQ2S, resulted in compressive stresses in the concrete that exceeded the capacity of the walls (crushing) and reduced the drift capacity to less than 0.5%. As a result of the lower lateral strength capacity, SQ1aS did not experience compressive failure of the concrete and experienced an increase in drift capacity at 10% axial load.

Up to 5% axial load, SQ2S dissipated the largest amount of energy, while SQ1S dissipated the least. Within this range of axial load, the cumulative energy was approximately constant in SQ1aS and increased by approximately 77% and 9% in SQ1S and SQ2S, respectively. The increase in axial load from 5% to 10% reduced the energy dissipation in SQ1S and SQ2S by 82% and 95%, respectively, and increased the energy in SQ1aS by 82%.

In general, the displacement recovery increased with increase in axial load and was dependent on the drift capacity of the walls. Up to 5% axial load, SQ1aS, SQ2S, and SQ1S recovered 79%, 87%, and 97% of the lateral displacements, respectively. The greater recovery in SQ1S is attributed to the lower drift capacity and more localized damage at the base of the wall. The effect on recovery was minimal from 5% to 10% axial load. Specifically for SQ1aS, the recovery was slightly reduced at 10% axial load as a result of a decrease in re-centering of the SMA braces at larger drift capacities. Maximum strain in the braces in SQ1aS was close to the full-recovery strain limit of 6%. Recovery of nearly 100% in SQ1S and SQ2S, for axial load of 10%, was the result of very small drift capacities that limited the strains in the SMA braces.

5.6.2 Effect of Size of SMA Links

Figure 5-26 illustrates the effect of the size of the SMA links on the main behavioral parameters of the retrofitted walls. The walls retrofitted with 19-mm diameter SMA braces experienced an increase in lateral strength of approximately 120 kN with respect to the walls retrofitted with 10-mm-diameter braces. This represents increases in lateral strength of 75%, 65%, and 33% for Walls SQ1aS, SQ1S, and SQ2S, respectively. Therefore, an increase in the size of the links had a greater impact on the strength of shear walls with lower lateral strength capacity.

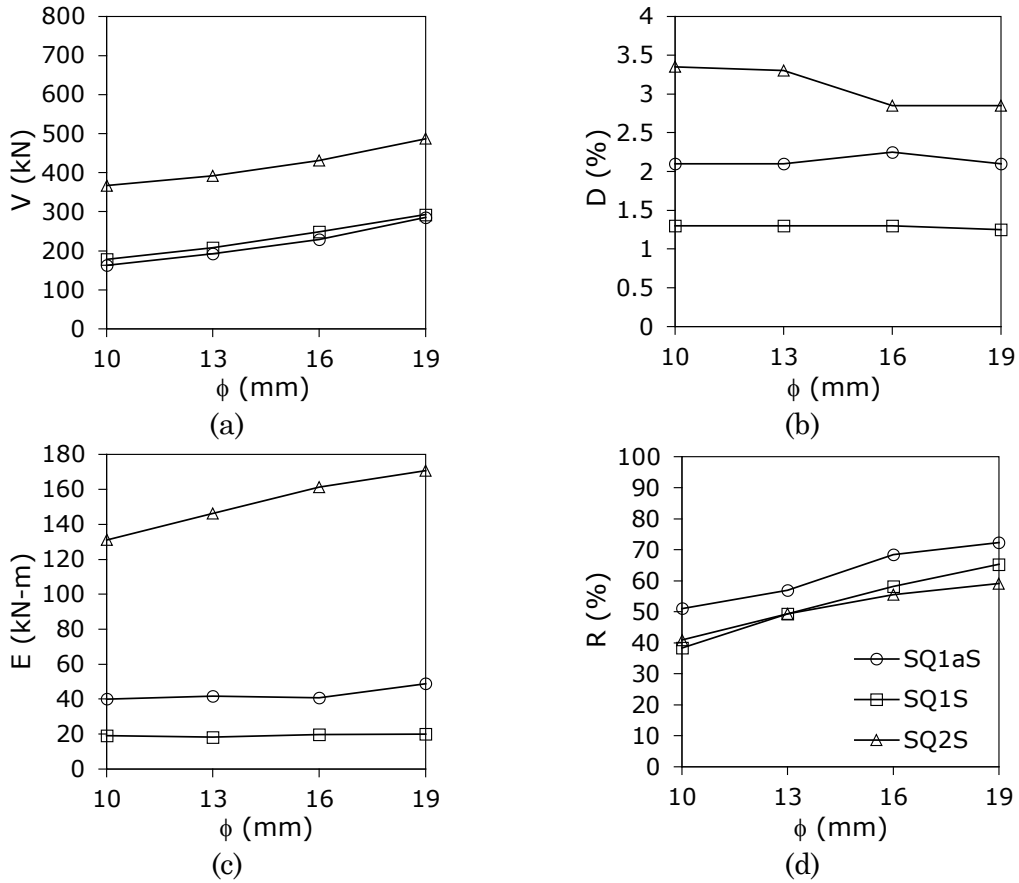


Figure 5-26 Effect of size of SMA links, ϕ: (a) lateral strength, V; (b) drift, D; (c) energy dissipation, E; and (d) displacement recovery, R

The size of the SMA links did not affect the drift capacity of the walls significantly. The drift experienced by SQ1aS and SQ1S remained nearly constant

with increasing size of the links. For SQ2S, however, the increase of the size of the link, specifically from 13-mm to 16-mm, slightly decreased the drift capacity by 14%.

Although the lateral strength increased with increasing size of the links, the cumulative energy of SQ1aS and SQ1S did not vary. The benefits of increased lateral strength were offset by narrower hysteretic loops with limited energy. The energy of SQ1aS and SQ1S was proportional to the drift capacities such that SQ1aS dissipated more energy than SQ1S (approximately double). In addition to greater lateral strength, the larger link diameters in SQ2S resulted in wider hysteretic loops with more energy. The 19-mm diameter SMA brace increased the energy of SQ2S by up to 30%. The increase in energy in SQ2S is attributed to reductions in stiffness and lateral strength degradation due to the ability of the braces to close the diagonal cracks under load reversals.

The restoring forces were increased with an increase in size of the SMA links, improving the displacement recovery of the walls. Walls SQ1S and SQ2S experienced very similar recovery for all the sizes of SMA links. The recovery for the 10-mm, 13-mm, 16-mm, and 19-mm diameter braces was approximately 40%, 50%, 55%, and 60%, respectively. On average, SQ1aS experienced 19% more recovery than the other walls. The recovery in SQ1aS ranged from 51% for the 10-mm braces to 72% for the 19-mm braces. Based on a normalized recovery (ratio of the recovery to the cross-sectional area of the braces), the effectiveness to recover decreased with an increase in the size of the links. The walls experienced maximum normalized recoveries of 85%/mm^2, 52%/mm^2, 39%/mm^2, and 29%/mm^2 for the 10-mm, 13-mm, 16-mm, and 19-mm braces, respectively. These normalized recoveries were predicted for Wall SQ1aS. The size of the SMA did not affect the axial straining and pseudo-yielding of the braces. This is the result of assumed concentrated damage in the SMA with negligible elastic deformation of the steel components of the braces.

5.7 Conclusions

Two-dimensional finite element models were developed to simulate the lateral load-displacement response of squat concrete shear walls retrofitted with SMA tension braces. Modelling of the SMA braces incorporated a tension-only SMA hysteretic

model that captured the superelastic properties of SMAs. The finite element models were corroborated against experimental results and further analyses were used to study the effect of axial load and size of the SMA rods used in the links on the cyclic response of the retrofitted walls. The main conclusions drawn from the numerical analyses are as follows.

1. The response of the walls was dependent on the size of the finite elements defining the web. Refinement of the mesh improved simulation of the lateral load-displacement responses and the failure modes.

2. In general, the numerical models predicted the lateral strength within an acceptable range of discrepancy. Although the drift capacity was slightly overestimated, the lateral strength and the shape of the hysteretic cycles prior to failure were in close agreement with the corresponding recorded response.

3. The energy dissipation of the walls was well predicted. Small differences arose as a result of the slightly lower energy dissipation explicitly considered in the SMA hysteretic constitutive model due to the approximate constant lower stress plateau and linear unloading to the residual strain. A more accurate prediction of the energy dissipation requires an SMA model that better captures the nonlinear unloading of the SMA braces.

4. The displacement recovery capacity of the retrofitted walls was well predicted. The SMA constitutive model captured the re-centering effect of the SMA braces, including closing of cracks under load reversal and reduction in pinching associated with shear degradation.

5. The parametric study highlighted that increases in axial load provided improved lateral load capacity and displacement recovery, and specifically for the walls controlled by sliding shear, shifted the failure mode to diagonal tension cracking. The effect on the drift capacity and energy dissipation was negligible for low axial loads. The higher axial loads, however, increased the compressive axial stresses in the concrete in SQ1S and SQ2S, resulting in premature failure and reduced cumulative energy. The drift capacity and

energy dissipation predicted for SQ1aS did not decline with an increase in axial load.

6. Increases in the size of the SMA resulted in greater lateral strength, energy dissipation, and recovery capacity in the retrofitted walls. However, the efficiency, based on normalized recovery, decreased with an increase in the size of the SMA links. The size of the SMA links had negligible effect on the drift capacity.

In summary, the numerical results demonstrated that the nonlinear finite element method can satisfactorily predict the seismic response of squat reinforced concrete shear walls retrofitted with SMA tension braces providing a sufficiently fine mesh and adequate selection of constitutive models.

5.8 Acknowledgments

The authors gratefully acknowledge the funding provided by the Canadian Seismic Research Network [Grant: NETGP/350698-07], a Natural Sciences and Engineering Research Council of Canada strategic network.

5.9 References

Abdulridha, A., and Palermo, D. (2014). "Response of a hybrid SMA reinforced concrete shear wall." *Tenth U.S. National Conference on Earthquake Engineering*, Network for Earthquake Engineering Simulation (distributor), Anchorage, AK, USA.

Abdulridha, A., Palermo, D., Foo, S., and Vecchio, F. J. (2013). "Behavior and modeling of superelastic shape memory alloy reinforced concrete beams." *Engineering Structures*, 49, 893–904.

Alam, M. S., Nehdi, M., and Youssef, M. A. (2009). "Seismic performance of concrete frame structures reinforced with superelastic shape memory alloys." *Smart Structures & Systems*, 5(5), 565–585.

Alam, M. S., Youssef, M. A., and Nehdi, M. (2008). "Analytical prediction of the seismic behaviour of superelastic shape memory alloy reinforced concrete elements." *Engineering Structures*, 30(12), 3399–3411.

Asazu, N., Unjoh, S., Hoshikuma, J., and Kondoh, M. (2001). "Plastic hinge length of reinforced concrete columns based on the buckling characteristics of longitudinal reinforcement." *Journal of Structure Mechanics and Earthquake Engineering*, 682(I-56), 177–194.

ASTM. (2014). *ASTM F2516-14 Standard test method for tension testing of nickel-titanium superelastic materials*. ASTM International, West Conshohocken, PA, USA.

ATC. (2007). *FEMA 461 Interim testing protocols for determining the seismic performance characteristics of structural and nonstructural components*. Federal Emergency Management Agency, Washington D.C., USA.

Auricchio, F., Fugazza, D., and DesRoches, R. (2006). "Earthquake performance of steel frames with Nitinol braces." *Journal of Earthquake Engineering*, 10(spec01), 45–66.

Auricchio, F., and Sacco, E. (1997). "A superelastic shape-memory-alloy beam model." *Journal of Intelligent Material Systems and Structures*, 8(6), 489–501.

Billah, A. H. M. M., and Alam, M. S. (2012). "Seismic performance of concrete columns reinforced with hybrid shape memory alloy (SMA) and fiber reinforced polymer (FRP) bars." *Construction and Building Materials*, 28(1), 730–742.

Cortés-Puentes, W. L., and Palermo, D. (2011). "Modelling seismically repaired and retrofitted reinforced concrete shear walls." *Computers and Concrete*, 8(5), 541–561.

Cortés-Puentes, W. L., and Palermo, D. (2012). "Modeling of RC shear walls retrofitted with steel plates or FRP sheets." *Journal of Structural Engineering*, 138(5), 602–612.

Cortés-Puentes, W. L., and Palermo, D. (2017a). "SMA tension brace for retrofitting concrete shear walls." *Engineering Structures*, 140, 177–188.

Cortés-Puentes, W. L., and Palermo, D. (2017b). "Seismic Retrofit of Concrete Shear Walls with SMA Tension Braces." *Journal of Structural Engineering*, paper submitted for publication, JRNSTENG-S-17-00077.

Dolce, M., Cardone, D., Ponzo, F. C., and Valente, C. (2005). "Shaking table tests on reinforced concrete frames without and with passive control systems." *Earthquake Engineering & Structural Dynamics*, 34(14), 1687–1717.

Effendy, E., Liao, W. I., Song, G., Mo, Y. L., and Loh, C. H. (2006). "Seismic behavior of low-rise shear walls with SMA bars." *Earth & Space 2006: Engineering, Construction, and Operations in Challenging Environment*, American Society of Civil Engineers, Houston, TX, USA, 1–8.

Eligehausen, R., Popov, E. P., and Bertero, V. V. (1983). *Local bond stress-slip relationship of deformed bars under generalized excitations*. Report No UCB/EERC-83/23, Earthquake Engineering Center, University of California, Berkeley, CA, USA, 162.

Graesser, E. J., and Cozzarelli, F. A. (1991). "Shape-Memory Alloys as New Materials for Aseismic Isolation." *Journal of Engineering Mechanics*, 117(11), 2590–2608.

He, X. G., and Kwan, A. K. H. (2001). "Modeling dowel action of reinforcement bars for finite element analysis of concrete structures." *Computers & Structures*, 79(6), 595–604.

Kupfer, H., Hilsdorf, H. K., and Rusch, H. (1969). "Behavior of concrete under biaxial stresses." *ACI Journal*, 66(8), 656–666.

McCormick, J., DesRoches, R., Fugazza, D., and Auricchio, F. (2006). "Seismic vibration control using superelastic shape memory alloys." *Journal of Engineering Materials and Technology*, 128(3), 294–301.

Nehdi, M., Alam, M. S., and Youssef, M. A. (2010). "Development of corrosion-free concrete beam–column joint with adequate seismic energy dissipation." *Engineering Structures*, 32(9), 2518–2528.

Palermo, D., and Vecchio, F. J. (2003). "Compression field modeling of reinforced concrete subjected to revered loading: Verification." *ACI Structural Journal*, 101(2), 155–164.

Palermo, D., and Vecchio, F. J. (2007). "Simulation of Cyclically Loaded Concrete Structures Based on the Finite-Element Method." *Journal of Structural Engineering*, 133(5), 728–738.

Popovics, S. (1973). "A numerical approach to the complete stress-strain curve of concrete." *Cement and Concrete Research*, 3(5), 583–599.

Pugh, J. S., Lowes, L. N., and Lehman, D. E. (2015). "Nonlinear line-element modeling of flexural reinforced concrete walls." *Engineering Structures*, 104, 174–192.

Ren, W., Li, H., and Song, G. (2007). "A one-dimensional strain-rate-dependent constitutive model for superelastic shape memory alloys." *Smart Materials and Structures*, 16(1), 191–197.

Saiidi, M. S., O'Brien, M., and Sadrossadat-Zadeh, M. (2009). "Cyclic Response of Concrete Bridge Columns Using Superelastic Nitinol and Bendable Concrete." *ACI Structural Journal*, 106(1), 69–77.

Saiidi, M. S., Sadrossadat-Zadeh, M., Ayoub, C., and Itani, A. (2007). "Pilot Study of Behavior of Concrete Beams Reinforced with Shape Memory Alloys." *Journal of Materials in Civil Engineering*, 19(6), 454–461.

Saiidi, M. S., and Wang, H. (2006). "Exploratory Study of Seismic Response of Concrete Columns with Shape Memory Alloys Reinforcement." *ACI Structural Journal*, 103(3), 436–443.

Salichs, J., Hou, Z., and Noori, M. (2001). "Vibration Suppression of Structures Using Passive Shape Memory Alloy Energy Dissipation Devices." *Journal of Intelligent Material Systems and Structures*, 12(10), 671–680.

Seckin, M. (1981). "Hysteretic behavior of cast-in-place exterior beam-column-slab assemblies." Ph.D. Thesis, Department of Civil Engineering, University of Toronto, Toronto, ON, Canada.

Tazarv, M., and Saiidi, M. S. (2015). "Reinforcing NiTi superelastic SMA for concrete structures." *Journal of Structural Engineering*, 141(8), 04014197, 1–10.

Vecchio, F. J. (1992). "Finite Element Modeling of Concrete Expansion and Confinement." *Journal of Structural Engineering*, 118(9), 2390–2406.

Vecchio, F. J. (2000). "Disturbed stress field model for reinforced concrete: formulation." *Journal of Structural Engineering*, 126(9), 1070–1077.

Vecchio, F. J., and Collins, M. P. (1986). "The modified compression-field theory for reinforced concrete elements subjected to shear." *ACI Journal*, 83(2), 219–231.

Vecchio, F. J., and Collins, M. P. (1993). "Compression response of cracked reinforced concrete." *Journal of Structural Engineering*, 119(12), 3590–3610.

Vecchio, F. J., and Lai, D. (2004). "Crack shear-slip in reinforced concrete elements." *Journal of Advanced Concrete Technology*, 2(3), 289–300.

Walraven, J. C., and Reinhardt, H. W. (1981). "Theory and Experiments on the Mechanical Behaviour of Cracks in Plain and Reinforced Concrete Subjected to Shear Loading." *Heron*, 26(1A), 5–68.

Wong, P. S., Vecchio, F. J., and Trommels, H. (2013). *VecTor2 and Formworks user's manual: second edition*. Manual, Department of Civil Engineering, University of Toronto, Toronto, ON, Canada.

Youssef, M. A., Alam, M. S., and Nehdi, M. (2008). "Experimental Investigation on the Seismic Behavior of Beam-Column Joints Reinforced with Superelastic Shape Memory Alloys." *Journal of Earthquake Engineering*, 12(7), 1205–1222.

Youssef, M. A., and Elfeki, M. A. (2012). "Seismic performance of concrete frames reinforced with superelastic shape memory alloys." *Smart Structures and Systems*, 9(4), 313–333.

Zafar, A., and Andrawes, B. (2012). "Incremental dynamic analysis of concrete moment resisting frames reinforced with shape memory composite bars." *Smart Materials and Structures*, 21(2), 025013, 1–14.

Chapter 6

General Conclusions

6.1 Overview

A tension-only, Nickel-Titanium SMA bracing system was developed to retrofit squat reinforced concrete shear walls controlled by shear-related damage. The SMA braces addressed deficiencies of existing retrofitting techniques that lack re-centering capabilities, including external bracing with long SMA rods. The braces possess significant re-centering and energy dissipation properties that improve the seismic response of squat shear walls. Due to the simple design, the optimization of the SMA, and the replaceable SMA components, the braces are feasible retrofitting solutions to improve earthquake resiliency of different concrete structures. The following is a summary of the research and the main conclusions derived from the development of the SMA tension brace, the experimental program, and the numerical analyses.

6.2 SMA Tension Brace for Retrofitting Concrete Shear Walls

The SMA bracing system consisted of SMA links coupled to rigid steel elements. The SMA links were designed to sustain all the damage, while the steel elements were designed to remain elastic. The design of the bracing system was based on the assessment of a seismically deficient squat reinforced concrete shear wall, following the performance-based approach. Testing of SMA and companion steel braces, and preliminary numerical simulations of walls retrofitted with the braces demonstrated the ability of the SMA bracing system to recover deformation and dissipate energy.

The main conclusions from the development of the SMA bracing systems are as follows:

1. The SMA braces experienced hysteretic responses with strength and elongation capacities similar to that of companion steel braces. The elongation capacity of the SMA braces exceeded the design target elongation. A reduction in the cross-sectional area of the SMA links used in the braces improved the elongation capacity.
2. The SMA braces dissipated satisfactory energy. Furthermore, energy dissipation capacity of the SMA braces was not affected by repetition of the loading.
3. Testing of the SMA braces demonstrated the potential use of re-centering systems to improve the response of existing reinforced concrete squat shear walls. The SMA braces provided exceptional elongation recovery.
4. Testing and retesting of the SMA braces demonstrated reusability of the retrofitting system, specifically reusability of the SMA links. The SMA links, therefore, act as fuses that sustain damage during earthquakes, and then are reset and reused to protect the retrofitted concrete structure from future seismic events.
5. The preliminary numerical analysis of an SMA-retrofitted shear wall predicted significant increases in strength and energy dissipation capacities. The retrofitted wall experienced reduced drift capacity as a result of an increase in strength. The drift capacity of the wall, however, exceeded the design target drift.
6. The SMA bracing system improved the strength and stiffness of the retrofitted shear wall. For the second repetitions of loading, the retrofitting system reduced degradation due to concrete damage.
7. In general, the wall retrofitted with the SMA braces exhibited higher energy dissipation and displacement recovery than a companion wall retrofitted with steel braces, demonstrating the excellent re-centering and energy dissipation capabilities of the SMA braces.

6.3 Seismic Retrofit of Concrete Shear Walls with SMA Tension Braces

One-third scale, squat shear walls were retrofitted with the tension-only SMA braces and then tested under incremental reverse cyclic loading. The walls represented seismically deficient shear walls designed in accordance to pre-1970s seismic standards. Two type of walls were tested: lightly reinforced walls controlled by shear sliding, and walls with boundary zones controlled by diagonal cracking. The experimental study focused on the effect of the SMA bracing system on the strength, drift capacity, energy dissipation, re-centering, and damage of the retrofitted shear walls. The main conclusions based on the experimental findings are as follows:

1. The SMA braces substantially increased the strength and reduced the stiffness and strength degradation of the shear walls. As a result, pinching of the strength-displacement response of the retrofitted walls was reduced.
2. The SMA bracing system did not affect the damage and failure mechanism of the lightly reinforced shear wall. Both the control and retrofitted walls were governed by a horizontal crack along the base that resulted in rocking of the walls and rupture of the internal reinforcing steel.
3. Localized damage along the base of the wall with boundary zones was controlled by the SMA retrofitting system, resulting in more distributed diagonal cracking and yielding of the longitudinal reinforcement. Furthermore, the SMA braces transferred additional compressive forces that resulted in crushing and out-of-plane failure of one of the boundary ends of the wall.
4. The SMA braces did not improve the drift capacity of the lightly reinforced wall due to the rocking response. Conversely, the braces improved the drift capacity of the wall with boundary zones as a result of the reduced localized damage along the base and the redistribution of yielding throughout the wall.
5. The retrofitted walls experienced higher energy dissipation than the corresponding control walls mainly due to the energy contributed by the SMA braces.

6. Re-centering of the SMA braces significantly improved recovery of lateral displacements of the retrofitted walls, improved closure of cracks upon load reversal and reduced shear degradation. As a result, the SMA braces improved the shear capacity.
7. Similarities in the net residual shear distortions of the retrofitted walls and control walls further demonstrated the re-centering effect of the SMA braces.

6.4 Modelling of Concrete Shear Walls Retrofitted with SMA Tension Braces

The shear walls tested in the experimental program were modelled with the nonlinear finite element program VecTor2 to demonstrate the applicability of numerical tools to predict the response of SMA-retrofitted squat reinforced concrete shear walls. This phase of the research illustrated the selection of finite elements and constitutive material models, specifically, a recently developed constitutive model for superelastic SMAs, which accounts for residual straining and decay of the lower stress plateau. Furthermore, a parametric study was conducted to assess the effect of axial loading and size of the SMA links on the response of the retrofitted walls. The numerical investigation included an additional control shear wall that was constructed and tested by the author in the structures lab of the University of Ottawa. This was a lightly reinforced and low-strength concrete squat shear wall controlled by diagonal cracking. The main conclusions based on the numerical results are as follows:

1. The numerical results demonstrated that the nonlinear finite element method is a reliable tool to predict the response of squat reinforced concrete shear walls retrofitted with the proposed tension-only SMA bracing system.
2. Accuracy of the predictions increased with a reduction in size of the concrete elements. The fine mesh predicted strength-displacement responses and crack patterns of the shear walls that were in close agreement with the experimental results.
3. In general, the predicted hysteretic cycles and the envelope of lateral load-displacement response closely matched the recorded response of the shear

walls. The strength and the drift capacities of the shear walls were well predicted.

4. Inherent approximations in the SMA constitutive model resulted in the prediction of slightly lower energy dissipation capacity for the retrofitted walls. The differences were within an acceptable range and did not affect the prediction of other behavioural parameters.
5. The analyses captured the displacement recovery of the retrofitted walls and the corresponding improvement in crack closure and reduction in shear degradation.
6. The parametric studies indicated that, in general, higher axial loads increased the lateral strength and recovery capacities, and reduced the drift capacity and energy dissipation of the retrofitted walls. The increase in axial load promoted a more distributed diagonal cracking in the walls governed by sliding shear. Damage of the walls controlled by diagonal cracking was not altered by the increase in axial load.
7. The lateral strength, energy dissipation, and displacement recovery of the retrofitted walls were proportional to the size of the SMA links. The simulations predicted smaller increases in these parameters as the size of the SMA links increased. The drift capacity of the retrofitted walls was negligibly affected by the variation in size of the links.

6.5 Final Remarks

In general, this research presented a novel SMA bracing system for retrofitting squat reinforced concrete shear walls. Experimental and numerical analyses demonstrated the beneficial effects of the SMA braces on the hysteretic response of retrofitted walls. The braces improved lateral strength, drift capacity, energy dissipation, and displacement recovery of walls controlled by shear deformations.

Chapter 7

Future Work

Based on limitations noted during the experimental program, the following are recommendations for future work:

1. The SMA braces were designed and tested to retrofit one-third scale shear walls. Laws of proportionality for the scaled reinforcing steel were not strictly respected given limitations in the material available in the market. To improve scaling of the prototype structure, tests on larger scale shear walls are necessary.
2. Testing of the shear walls did not consider axial loading. Although it is recognized that axial loads affect the behaviour of shear walls, the axial loads of typical squat shear walls are very low. Specifically for the prototype building assessed in the study, the axial loads corresponded to less than 2% of the ratio of the compressive strength ($P/A_g f'_c$). As illustrated by the parametric study, this low level of axial loading does not significantly affect the strength, drift capacity, and energy dissipation of the retrofitted walls; however, re-centering is increased. To corroborate the numerical predictions, additional experimental data including axial loading are required.
3. Concentrated laterals loads were applied to the shear walls rather than distributed loads typically transferred by slabs. Differences in the application of lateral loads may affect the failure mechanism of squat shear walls. Therefore, further experimental tests and numerical simulations are required to study the effect of distributed lateral loads on the performance of squat SMA-retrofitted walls.

The following are additional areas that should be addressed with future work:

1. Improve the drift capacity of the shear walls. Specifically for the walls controlled by sliding shear, additional retrofitting techniques such as confinement of the ends of the walls may increase the drift capacity and reduce shear-related damage. Retrofitting of the boundary zones may also benefit the walls controlled by diagonal cracking, mitigating crushing and out-of-plane failure.
2. Reduce the cost of the SMA components. Less expensive alloys, based on other metals such as aluminum and copper, can potentially improve the re-centering and energy dissipation of reinforced concrete structures. The length of the SMA links can be reduced by incorporating smaller couplers at the ends of the links. The length of the SMA links can be also reduced by designing a bracing configuration that amplifies the strains in the SMA.
3. Investigate the effect of the SMA braces on squat shear walls with different cross-sections and other reinforced concrete structural elements such as columns, beams, and frames. Although this research demonstrated that the SMA braces improved the response of walls controlled by shear, additional testing is required to corroborate the findings and extend the application to other type of structures.
4. Develop a re-centering external retrofitting system based on superelastic SMAs to control diagonal cracking and promote flexural response. This can be achieved by connecting diagonal SMA and steel elements to the wall at different locations. The use of SMA can be minimized by incorporating the material only at critical zones. Another retrofitting strategy is the use of bi-diagonal hybrid SMA-steel or SMA-FRP plates or sheets that are continuously connected to the wall with epoxy or bolts.
5. Improve the constitutive model for superelastic SMAs to capture the stiffness of the upper and lower plateau and the non-linearity of the loading and unloading branches. This requires additional testing and characterization of SMAs.

6. Conduct dynamic analyses to assess the reduction in displacement amplitudes due to the flag-shaped hysteretic response of the SMA braces. This effect is not directly observed when the structure is subjected to reverse cyclic loading given that the displacements are input parameters. Therefore, to realize a more comprehensive understanding of the seismic response of squat reinforced concrete shear walls retrofitted with SMAs, nonlinear dynamic analyses for different simulated earthquakes are required.
7. Assess existing performance-based design methods against nonlinear dynamic analysis and, if required, formulate an improved method to design SMA-retrofitted concrete shear walls.

Appendix A

Development of an SMA Retrofitting System: Supplementary Material

A.1 Seismic Requirements

A.1.1 Design of the Original Wall

An assumed two-storey prototype office building located in Vancouver, British Columbia, was selected to investigate an SMA seismic retrofit of shear walls subjected to significant seismic demand. The analysis and design of the building followed the 1965 version of the NBCC (NRC 1965) in which no seismic detailing was prescribed for shear walls. The lateral force resisting system consisted of 300 mm thick reinforced concrete shear walls in both orthogonal directions, while the vertical force resisting system consisted of 400 mm × 400 mm reinforced concrete columns. The floor system consisted of 200 mm thick flat slabs. Dimensions of the structural elements are illustrated in Figure 3-3. The prototype building is similar to the Type C2 FEMA concrete shear wall building that forms the basis for seismic assessment in FEMA 440 (ATC 2005).

The seismic analysis of the building was performed using the equivalent static force procedure with the assumption of rigid diaphragms without bending deformations to be consistent with the methods of analysis commonly used in the 1960s. Wall 6 (6000 mm × 6000 mm × 300 mm) was selected for the numerical assessment of the retrofitting strategy with SMA. Design of Wall 6 for seismic actions in the North-South direction followed the ultimate limit state method as specified by

the NBCC-1965, which was an alternative to the commonly used working stress method. In general, the use of the ultimate limit state method in the 1960s yielded less flexural reinforcement that resulted in lightly reinforced concrete walls with significant seismic deficiencies. Seismic loads, according to the NBCC-1965, were based on the minimum shear force at the base of the building, V (Equation A-1). The base shear force was a function of the total weight of the structural and non-structural elements, W; the hazard factor, R; the type of construction, C; the importance factor, I; the foundation soil factor, F; and the height of the structure, S. The factor S is an inverse function of the number of storeys, N, of the building above ground.

$$V = RCIFSW\ ; \qquad S = 0.25/(9+N) \tag{A-1}$$

For the analysis of the prototype building, factor R was taken as 4 for the City of Vancouver, factor C was taken as 1.25 for building types other than portal frames or ductile shear walls, factor I was taken as 1 for buildings with normal importance, and factor F was taken as 1.0 for an assumed rock sub-soil condition. The factor S was calculated as 0.023 for the two-storey prototype building. A seismic force of 556 kN, including 5% accidental torsion, and an axial force of 685 kN were calculated for Wall 6. The seismic force was linearly distributed to the floor levels. This distribution resulted in a shear span of 0.81. Material properties were assumed to reflect construction practices of the 1960s: cylinder compression strength of concrete, f'_c, was taken as 21 MPa (3000 psi), and yield stress of reinforcing steel, f_y, was 280 MPa (40 ksi). The design resulted in a horizontal reinforcement ratio, ρ_h, of 0.21% and a vertical reinforcement ratio, ρ_v, of 0.18%. The wall was not designed with any special detailing for ductility or anti-buckling since this was not required by the NBCC-1965.

A.1.2 Seismic Assessment of the Original Wall

The seismic response of the original, non-retrofitted wall, was initially assessed with the NBCC-2010 (NRC 2010) to satisfy the increase in base shear requirements relative to the NBCC-1965, specifically in terms of seismic force and ductility. The ductility capacity of the retrofitted shear wall is predetermined as nominal (minimum ductility capacity) with seismic reduction factor R_d of 1.5. This ductility is intended to

prevent collapse of the retrofitted shear wall when subjected to the design seismic demand. It is expected that the retrofitting system with SMAs improves the seismic response of the original wall and exceeds the requirements specified by the NBCC-2010 and the CSA A23.3-14 (CSA 2014) for concrete shear walls with nominal ductility capacity. No over strength reduction factor, R_o, was considered in the calculation of the required strength since expected material values of f'_c = 25 MPa (1.20f'_c) and f_y = 350 MPa (1.25f_y) were used in the nonlinear analysis of the non-retrofitted and retrofitted walls as recommended by the ATC-40 (ATC 1996) and FEMA-440 (ATC 2005). Based on the expected concrete strength, the axial load ratio ($P/A_g f'_c$) on the wall was 1.5%. The design seismic force (design base shear V) was calculated as follows:

$$V = \frac{S(T_a) M_V I_E W}{R_d} \leq \frac{(2/3) S(0.2) I_E W}{R_d} \tag{A-2}$$

where $S(T_a)$ is the 5% damped spectral response acceleration of the structure at the fundamental period, T_a; M_v is a factor to account for higher modes effect (M_v=1.0 for structures with short fundamental periods); I_E is a factor to reflect the importance of the structure; S(0.2) is the 5% damped spectral response acceleration at T_a=0.2 seconds; and W is the seismic weight of the structure. The fundamental period, T_a, is a function of the height of the building, h_n, and is calculated for shear wall structures as follows:

$$T_a = 0.05 h_n^{3/4} \tag{A-3}$$

Using Equations A-2 and A-3, NBCC-2010 yields a design base shear of 1972 kN for Wall 6 including accidental torsion. The resulting design base shear is 3.55 times larger than that calculated with the NBCC-1965. This suggests that Wall 6 is in need of retrofit for enhancing strength to meet the NBCC-2010 required seismic demand levels. A comprehensive assessment of the seismic response of Wall 6 is performed using the capacity spectrum method as well as the nonlinear finite element program VecTor2. Based on this assessment, the proposed SMA retrofit to improve seismic response is designed.

A.2 Design of the SMA Retrofit

A.2.1 Seismic Assessment of the Retrofitted Wall

The performance of the retrofitted wall was assessed following the capacity spectrum method (ATC 40 and FEMA 440), which has been widely used for other retrofitting strategies. The approach requires a capacity diagram (lateral load vs. spectral displacement), which is evaluated against a reduced elastic (equivalent inelastic) demand diagram (base shear vs. spectral displacement). To develop the capacity diagram, a pushover response (lateral load vs. displacement) was determined from the trace of the predicted hysteretic behaviour. Program VecTor2 was used to predict hysteretic responses from which the pushover curves were developed for the original wall and the SMA retrofitted wall. The numerical analysis of the original wall predicted strength of 1124 kN at a corresponding lateral top displacement of 54 mm. The wall retrofitted with SMA cross bracing was predicted to achieve an ultimate strength of 1760 kN at 54 mm, which represented an increase of strength of approximately 57% with respect to the original wall. [Note that the predictions were based on expected material properties, concrete strength of 25 MPa and steel yield stress of 350 MPa.] The pushover response was converted to a capacity diagram by relating the roof displacements, Δ_{roof}, to spectral displacements, S_d. The roof displacements were divided by the product of the first modal participation factor, PF_1, and the first modal roof displacement, $\phi_{1,roof}$ as follows:

$$S_d = \Delta_{roof} / PF_1 \phi_{1.roof} \tag{A-4}$$

Based on a fundamental triangular modal distribution, which is a good approximation for buildings with short fundamental periods, and the mass distribution of the prototype building, a value of 1.23 was calculated for $PF_1\phi_{1,roof}$ for the prototype wall.

The development of the demand diagram requires the Uniform Hazard Spectrum (UHS) for the location of the structure. For the assessment of the retrofitted prototype building, the UHS for the City of Vancouver was developed based on the NBCC-2010 (NRC 2010). The spectral acceleration ordinates, S_a, were converted to

base shear, V, and the structural period ordinates were converted to spectral displacements, S_d, by using the following equations:

$$V = S_a \alpha_1 W; \qquad S_d = \left(T^2/4\pi^2\right) S_a g \tag{A-5}$$

where α_1 is the first modal mass coefficient, W is the weight of the structure, T is the fundamental period of the structure, and g is the gravitational acceleration.

The elastic demand diagram was then reduced to account for energy dissipation of the retrofitted shear wall by applying the reduction factors SR_A and SR_V, which were calculated based on the effective damping, β_{eff}, of the structure, following the formulations below:

$$SR_A = \left[3.21 - 0.68\ln\left(100\beta_{eff}\right)\right]/2.12; \qquad SR_V = \left[2.31 - 0.41\ln\left(100\beta_{eff}\right)\right]/1.65 \tag{A-6}$$

SR_A was applied to the constant acceleration portion of the linear elastic design spectrum (plateau), while SR_V was applied to the constant velocity portion of the linear elastic design spectrum (descending branch). The effective damping, β_{eff}, which is a combination of the inherent elastic viscous damping of the structure, β_o, and the equivalent viscous damping of the hysteretic loops, β_{eq}, is calculated as follows:

$$\beta_{eff} = \beta_o + k\beta_{eq}; \quad \beta_{eq} = \left(1/4\pi\right)\left(E_D/E_{So}\right) \tag{A-7}$$

where E_D corresponds to the energy dissipated by hysteretic damping (area under the hysteretic loop at the target displacement) and E_{So} corresponds to the maximum strain energy (area of the triangle defined by the target spectral displacement and corresponding strength) as shown in Figure A-1. In the formulation presented in ATC-40 and FEMA 440, a reduction factor k is included to account for the difference between the actual hysteretic loop and an ideal elastic-plastic loop. The k factor was not used in the assessment of the retrofitted walls since the equivalent damping values were established from the predicted numerical hysteretic loop at the selected target displacement. The elastic viscous damping, β_o, was calculated using a model proposed by Farrar and Baker (1995) for squat shear walls. For the required

strength of 1972 kN and corresponding shear stress of 1.10 MPa (calculated with the NBCC-2010), Farrar and Baker's formulation yielded a value of 1.38% for β_0.

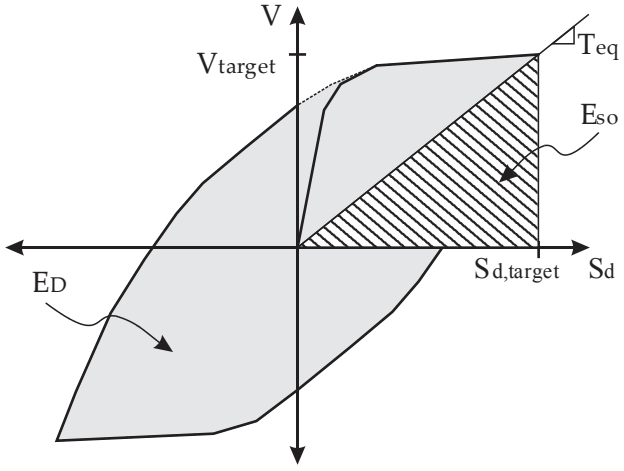


Figure A-1 Graphical representation of hysteretic damping

Following the capacity spectrum method, the retrofitting reinforcement for the prototype wall was continually redesigned until the capacity diagram crossed the reduced elastic demand diagram at the target displacement as shown in Figure 3-4. The target displacement corresponded to the collapse prevention performance level (ultimate capacity) as defined by ASCE 41-06: "*The building remains standing, but only barely; any other damage or loss is acceptable.*" The collapse performance level was determined as the ultimate capacity of the prototype wall as determined using Program VecTor2. The retrofitted system is thus designed to satisfy the strength and ductility requirements of the reduced elastic demand diagram based on the properties of the SMA bracing. The resulting bi-diagonal SMA bracing for the retrofitted prototype wall included external rigid steel elements coupled with 38-mm diameter nickel-titanium SMA rods (1140 mm^2 cross sectional area) on each face of the wall. The length of the SMA rods was optimized to sustain maximum deformation recovery. Yield stress of the retrofitting SMA was taken as 420 MPa. The SMA retrofitting strategy was aimed to improve strength, ductility and energy dissipation capacities. The SMA retrofitting strategy was focused to reduce permanent residual deformation of the shear wall. Satisfactory energy dissipation capacity of the retrofitted wall is reflected in the calculated equivalent damping ratio of 16.4%.

A.3 SMA Braces

Figure A-2 illustrates the SMA braces and the base anchor plates. Note that the top anchor plates, placed on the top corners of the walls, have the same geometry as the base anchor plates but are fabricated with 203 mm × 203 mm plates.

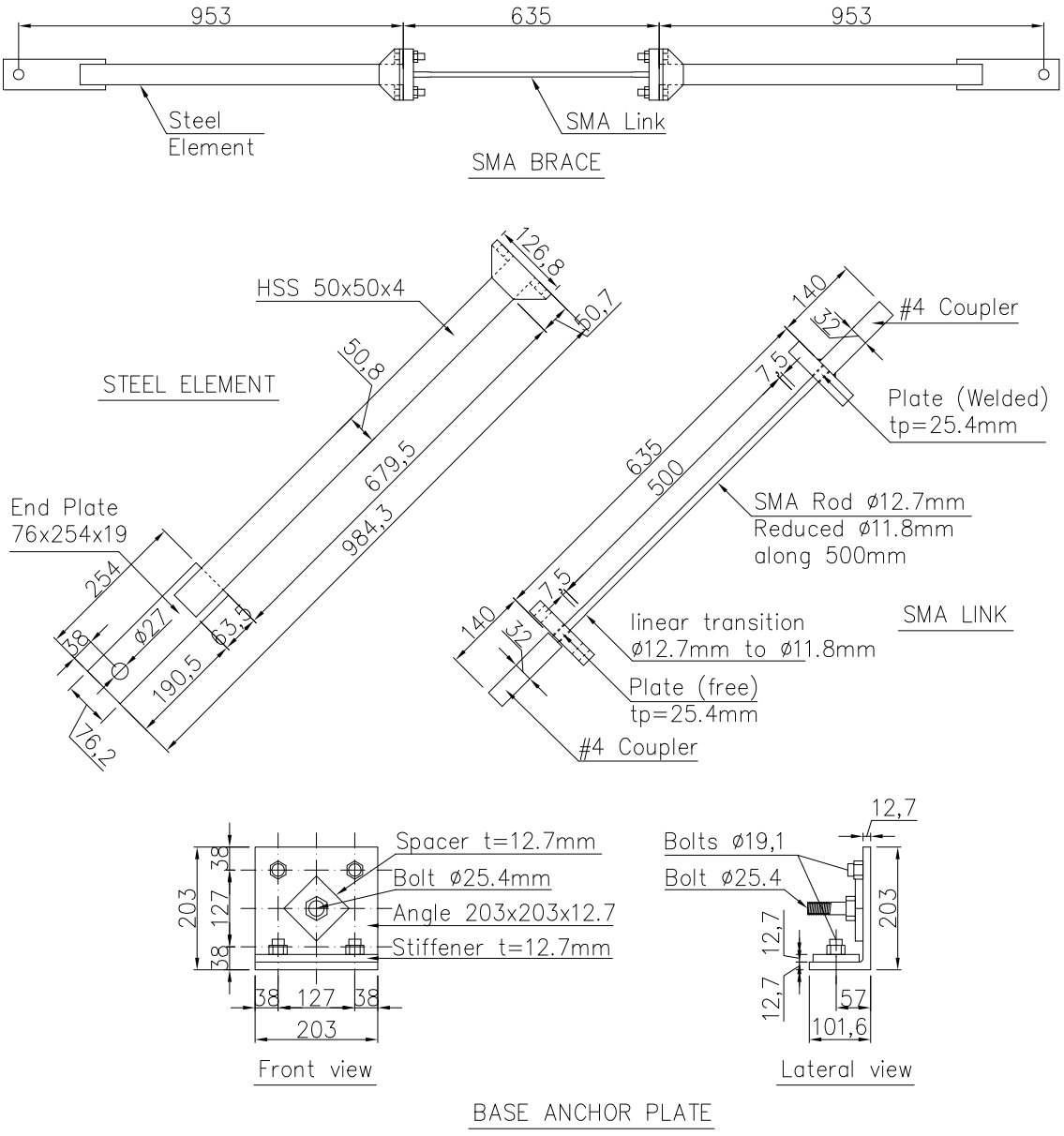


Figure A-2 SMA Brace and base anchor plate (all dimensions in mm)

A.4 References

ATC. (1996). *ATC-40 Seismic evaluation and retrofit of concrete buildings*. Applied Technology Council, Redwood City, CA, USA.

ATC. (2005). *FEMA 440 Improvement of nonlinear static seismic analysis procedures*. Applied Technology Council, Washington D.C., USA.

CSA. (2014). *Design of concrete structures, CAN/CSA-A23.3–14*. Canadian Standards Association, Mississauga, ON, Canada.

Farrar, C. R., and Baker, W. E. (1995). "Damping in low-aspect-ratio, reinforced concrete shear walls." *Earthquake Engineering & Structural Dynamics*, 24(3), 439–455.

NRC. (1965). *National building code of Canada*. Associate committee on the national building code, National Research Council of Canada, Ottawa, ON, Canada.

NRC. (2010). *National building code of Canada*. Associate committee on the national building code, National Research Council of Canada, Ottawa, ON, Canada.

Appendix B

Experimental Program: Supplementary Material

B.1 Construction of Shear Walls

The shear walls were constructed in the structures laboratory of the University of Ottawa. All the walls were constructed in the vertical position and cast in two stages: (1) the foundation blocks; and (2) the wall panels. As a result, a construction joint formed along the base of the walls, which simulated the construction practices of pre-1970s buildings.

B.1.1 Foundation Blocks

Two 2500 mm × 1400 mm × 500 mm foundation blocks were constructed for the shear walls. Foundation block 1 (Figure A-1) was constructed for original Walls SQ1, SQ1a, and SQ2, and foundation block 2 (Figure B-2) was constructed for retrofitted Walls SQ1S and SQ2S. Figure B-3 and Figure B-4 illustrate the construction of the foundation blocks.

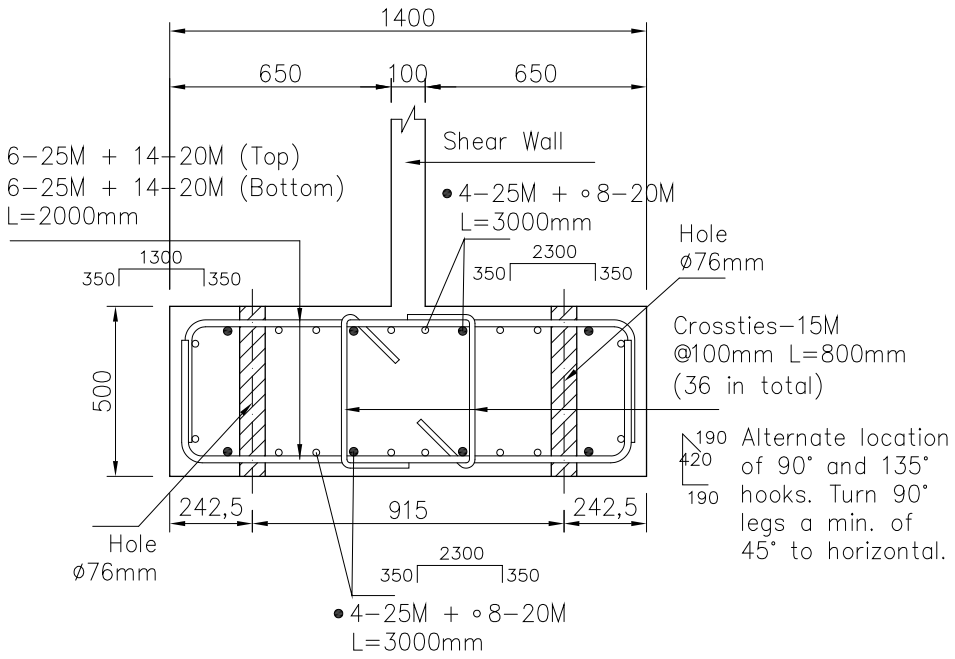


Figure B-1 Cross section with reinforcement layout of foundation block 1

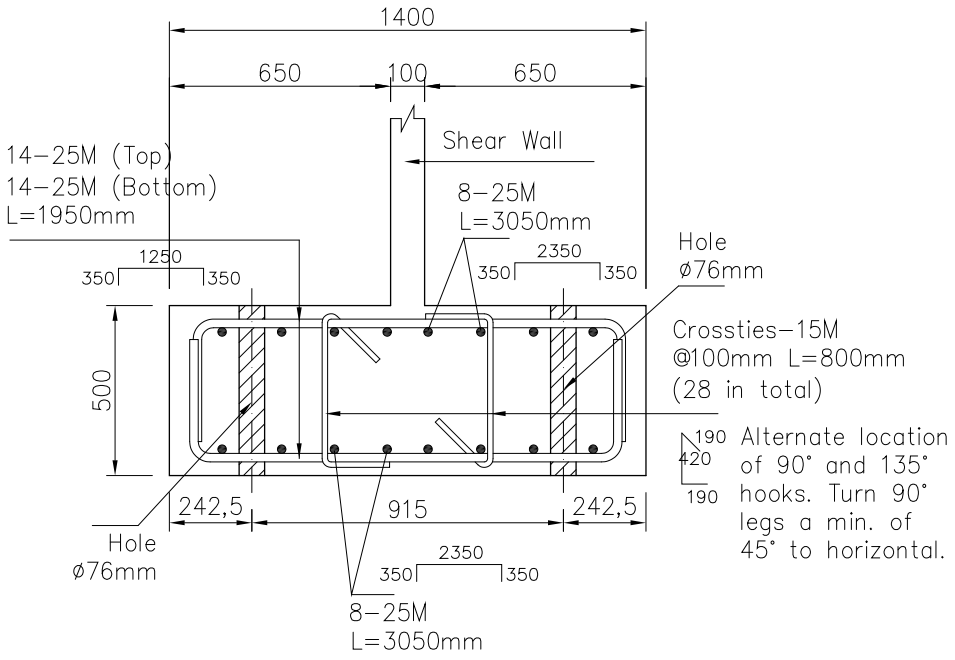


Figure B-2 Cross section with reinforcement layout of foundation block 2



Figure B-3 Steel cage of foundation block 1



Figure B-4 Casting of foundation block 1

B.1.2 Shear Walls

Construction of the walls required fabrication of steel cages with vertical, horizontal, and embedded beam reinforcement (Figure B-5), and wood formwork using 19 mm-thick plywood sheets and 38 mm × 89 mm lumber (Figure B-6). Ready-mix concrete with maximum aggregate size of 10 mm and slump of 180 mm, provided by a local concrete plant, was poured in four layers into the formwork and vibrated with an electrical concrete vibrator (Figure B-6). The formwork was removed after three days, and the concrete was cured by spraying water on the surfaces over seven days at a room temperature ranging from 20°C to 25°C. A number of 100 mm × 200 mm standard concrete cylinders were prepared during casting of the foundation blocks and shear walls.



Figure B-5 Steel cage for Walls SQ2 and SQ2S



Figure B-6 Typical wood formwork and casting of walls

B.1.3 SMA Bracing System

The installation of the retrofitting system was completed after curing of concrete at 28 days. Prior to the installation of the SMA bracing, two single layers of 300 mm wide × 900 mm long carbon FRP sheets in the vertical and horizontal directions were externally bonded around the top corners of the walls to protect them from potential concrete damage (Figure B-7). The anchor plates of the retrofitting system were connected to the lower and upper corners of the wall with 19 mm high-strength through-bolts (Figure B-8). Then, the end of the braces were placed and secured to the anchor plates. Finally, the system was tightened to avoid any gaps that could affect the transfer of loads.

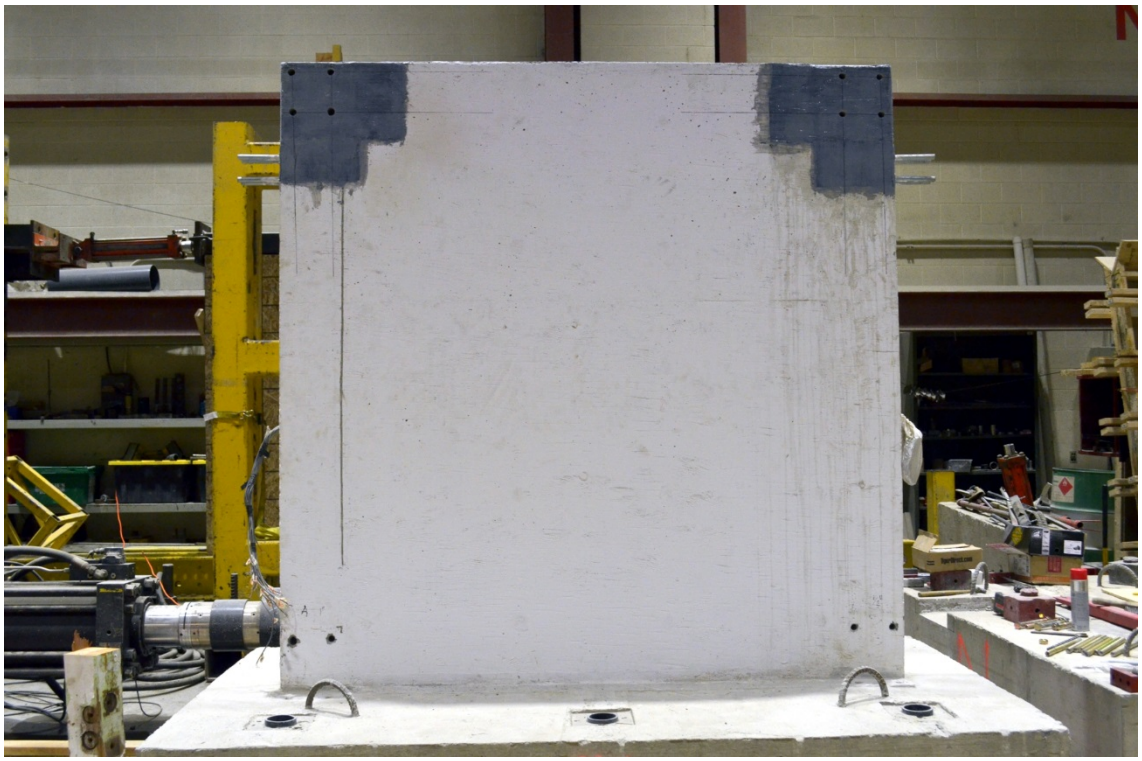


Figure B-7 FRP sheets on walls



Figure B-8 Detail of SMA brace connected to the walls

B.2 Material Properties

B.2.1 Concrete

Standard concrete cylinders (100 mm × 200 mm) were tested in compression at a stress rate of 0.25 MPa/s in accordance with the ASTM C39M-16b standard (ASTM 2016a) to obtain the stress-strain response of the concrete used in the walls (Figure B-9). A number of standard cylinders were used to determine the tensile strength of the concrete, following the split testing procedure in accordance with the ASTM C496M-11 standard (ASTM 2011). A summary of the compressive and tensile properties of the concrete is provided in Table B-1.

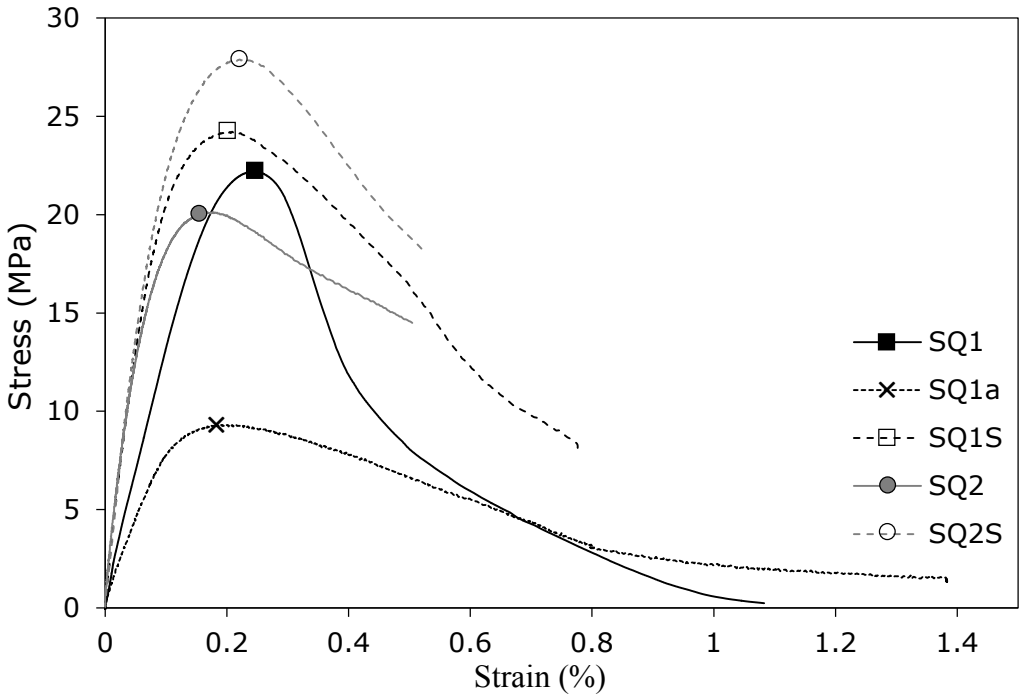


Figure B-9 Typical stress-strain response of concrete used in walls

Table B-1 Properties of concrete

Wall	Compressive Strength, f'_c (MPa)	Compressive Strain at Peak Strength, ε'_c (%)	Splitting Tensile Strength, f_{tsp} (MPa)
SQ1	22.52	0.269	2.42
SQ1a	9.50	0.255	0.54
SQ1S	24.73	0.184	2.56
SQ2	20.26	0.187	1.87
SQ2S	27.37	0.222	3.47

B.2.2 Reinforcing Steel

The stress-strain response of the 9.5-mm and 10M reinforcing steel was established following the ASTM A615M-16 standard (ASTM 2016b) (Figure B-10). In addition, 9.5 mm-diameter bars were anchored with epoxy in one of the foundation blocks and tested to determine the tensile pullout response of the vertical bars used in Walls SQ1a, SQ2, and SQ2S (Figure B-11). The response of the anchored bars (Figure B-12) was comparable to the response obtained from the coupons, indicating full stress development along the embedded length.

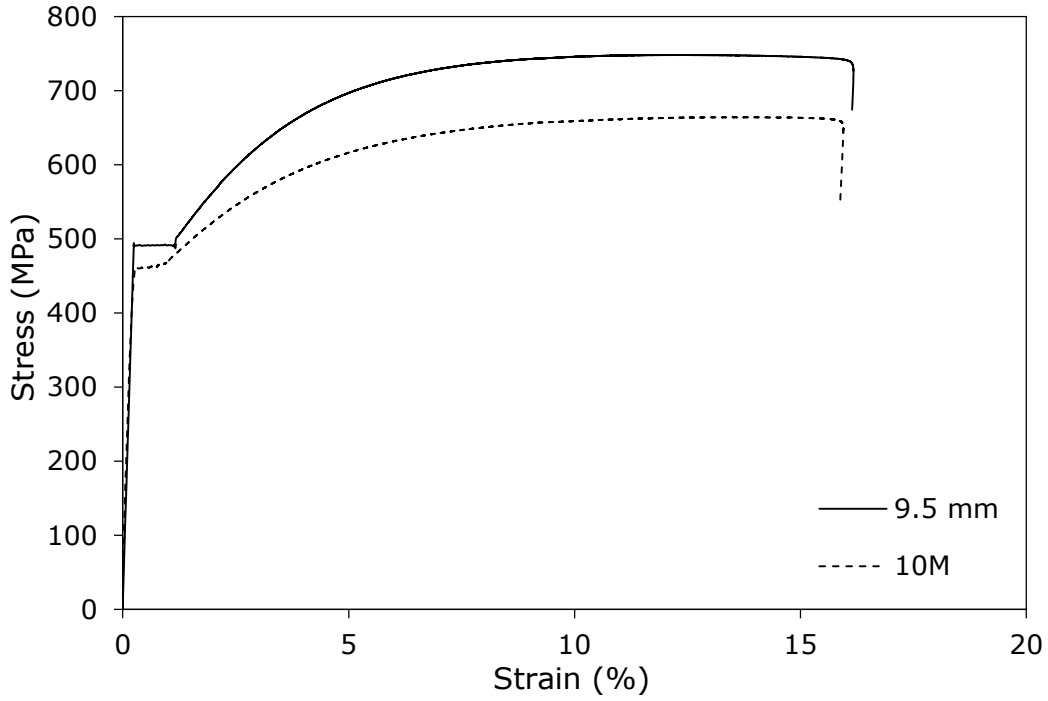


Figure B-10 Typical stress-strain response of reinforcing steel



Figure B-11 Pullout test of 9.5-mm anchored reinforcing bars

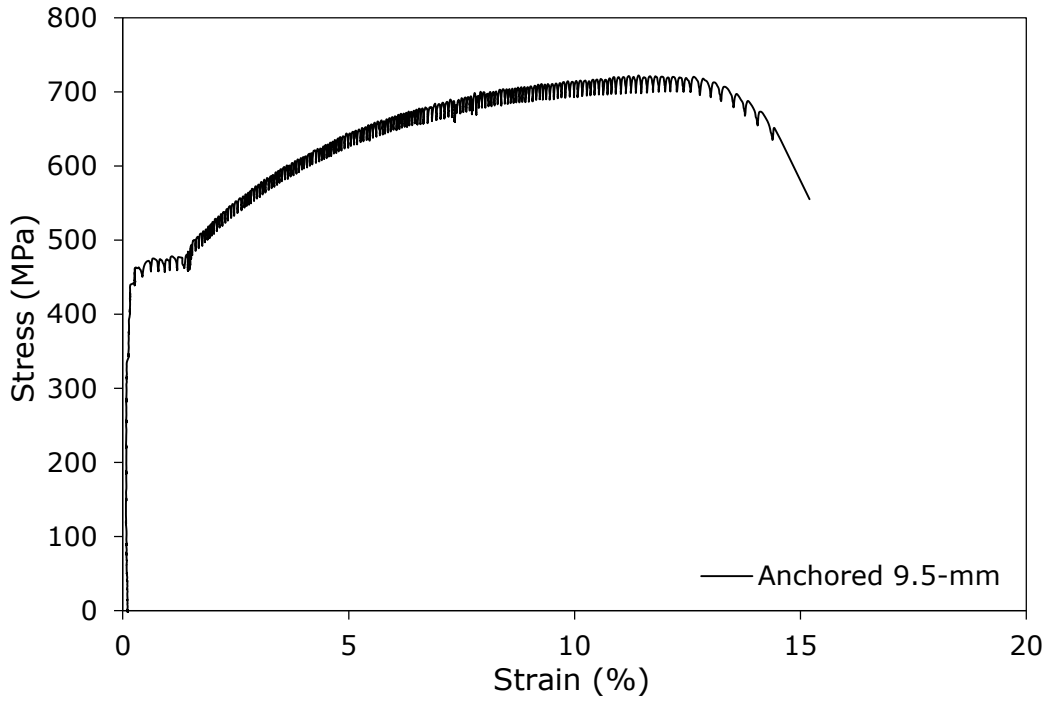


Figure B-12 Typical stress-strain response of 9.5-mm anchored reinforcing bars

B.2.3 Nickel-Titanium SMA

The 12.7-mm superelastic nickel-titanium SMA rods used in the SMA braces had the physical and chemical properties listed in Table B-2. The specified Austenite start temperature, *Af*, was -30˚C, and the specified Austenite finish temperature (fully annealed temperature), *Af*, was -10˚C. Tensile coupon tests were conducted on 300 mm-long SMA coupons following the ASTM F2516-14 standard (ASTM 2014). The cross sectional area of the 100 mm central portion of the coupons was reduced to 11.3 mm to ensure that the plastic elongations and failure did not occur at the grips of the testing machine. Testing was conducted with a 600 kN Universal Testing Machine at an ambient temperature ranging from 20˚C to 25˚C. The stress-strain response of the SMA is illustrated in Chapters 3, 4, and 5.

Table B-2 Properties of Superelastic Nickel-Titanium SMA as provided by the manufacturer, SAES Smart Materials (2012)

Physical Properties	Density	6.5 g/cm3
	Melting Point	1310 ^{0}C
	Modulus of Elasticity	41-75 × 10^3 MPa
	Electrical Resistivity	32 µohm-cm
	Coefficient of Thermal Expansion	11 × 10^{-6}/^{0}C
	Transformation Temperatures, $A_s - A_f$	-30 ^{0}C – (-10) ^{0}C
Chemical Properties	Nickel	55.8 wt.%
	Titanium	Balance
	Iron	0.05 wt.% (max.)
	Carbon	0.02 wt.% (max.)

B.3 Instrumentation

The shear walls were instrumented with displacement measuring sensors, strain gauges, and a load cell. Cable transducers and Linear Variable Differential Transducers (LVDTs) were mounted on the walls to measure displacements at a number of locations. Strain gauges were attached to the internal reinforcing steel to measure local straining. The load cell was part of the actuator (model MTS 273.70) that applied horizontal loading to the walls. The displacement sensors were calibrated

prior to testing each shear wall to guarantee accuracy and precision of the measurements.

B.3.1 Displacement Measurements

Instrumentation of the control walls consisted of fourteen Celesco SP2-12 cable transducers with maximum stroke of 315 mm, two Honeywell JEC-AG LVDTs with stroke range of +/- 75 mm, and two Solartron S Series with stroke range of +/- 25 mm. The exception was the instrumentation for Wall SQ1, which consisted of eleven cable transducers and three LVDTs. Figure B-13 illustrates the location and numbering of the displacement sensors installed on the control walls. Note that Wall SQ1 was not instrumented with transducers C1, C12, and C14 and LVDT L3.

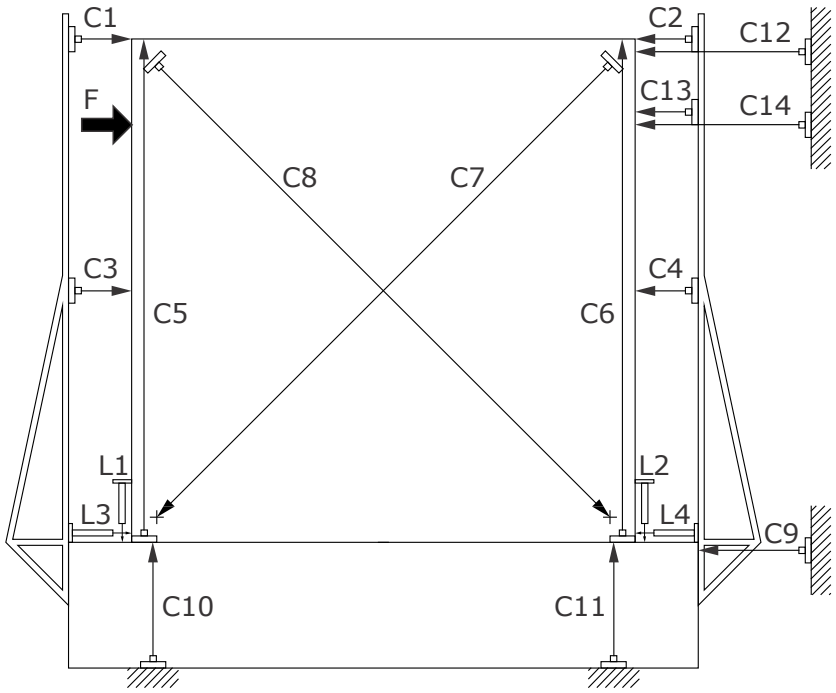


Figure B-13 Displacement sensors on control walls (letter *C* denotes cable transducer, and letter *L* denotes LVDT)

Fourteen displacement transducers and four LVDTs were used to measure the displacements of the retrofitted walls. The layout of the sensors is the same as the layout used for the original walls with the addition of four cable transducers that measured the elongations of the SMA bracing system (Figure B-14).

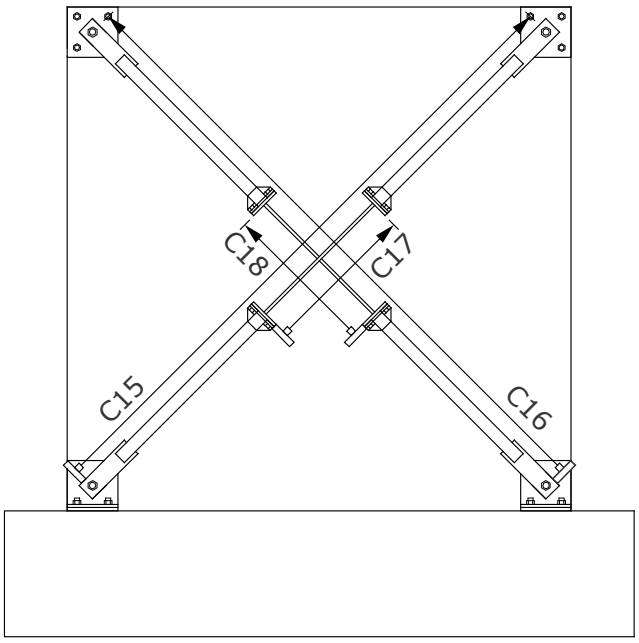


Figure B-14 Additional displacement sensors on retrofitted walls (letter *C* denotes cable transducer)

Five transducers were used to determine the load-lateral displacement responses of the walls at different heights. Transducers C1, C2, and C12 measured horizontal displacements at the top of the walls, transducers C13 and C14 measured horizontal displacement at the height of application of lateral load (at the centre of the loading beam), and transducers C3 and C4 recorded horizontal displacements at mid-height. Transducers C1 to C4 were installed in a light frame anchored at the base of the wall to measure displacements relative to the foundation, and transducers C12 to C14 were installed in an external frame that was fixed to the strong floor of the laboratory. Four sensors were installed to measure vertical deformations and determine shear distortion of the walls. Transducers C5 and C6 measured vertical displacements from base to top at the end of the walls, and transducers C7 and C8 recorded diagonal deformations within an 1800 mm × 1800 mm grid. Three sensors monitored the foundation blocks: transducer C9 recorded horizontal displacements, and transducers C10 and C11 measured uplift displacements. Four transducers measured the elongations of the SMA braces. Transducers C15 and C16 measured the elongations of the braces from end to end, and transducers C17 and C18 measured the

elongations of the SMA links. Transducers C15 to C18 followed the same layout used for the axial testing of the SMA braces. The instrumentation layout for the retrofitted walls did not include transducers C7, C8, C12, and C14. Transducers C7 and C8 were replaced by transducers C15 and C16, and transducers C12 and C14 were removed from the setup. Transducers C12 and C14 were backup sensors to transducers C2 and C13, respectively.

LVDTs L1 and L2 were located at the ends of the walls at a height of 200 mm from the base to monitor cracking at the toes and bond slip at the construction joint (L1 and L2 were located at 250 mm from the base of the retrofitted walls). LVDTs L3 and L4 were placed on the foundation block at a height of 50 mm to measure sliding of the walls. The stroke of LVDTs L1 and L2 was +/- 75 mm, while the stroke of LVDTs L3 and L4 was +/- 25 mm.

B.3.2 Strain Measurements

A number of strain gauges were installed on the reinforcing steel and retrofitting SMA braces to measure longitudinal strain. A maximum of 40 general purpose 10-mm strain gauges (TML FLA-10-11) were placed on the horizontal and vertical reinforcing steel, and twelve post-yield (TML YFLA-10) 10-mm strain gauges were placed on the SMA rods that were part of the SMA braces. Figure B-15 illustrates the location of the strain gauges on the internal reinforcing steel of Walls SQ1, SQ1a, and SQ1S. In the figure, the letter *b* denotes backup strain gauges placed 25 mm above the corresponding main strain gauges. Note that strain gauges 1, 2, and 3 were not installed in Walls SQ1a and SQ1S given that the vertical reinforcement was anchored with epoxy. Figure B-16 shows the location of the strain gauges on the internal reinforcing steel of Walls SQ2 and SQ2S. Backup gauges (denoted with the letter *b*) were located on the second layer of vertical reinforcement in the boundary zones.

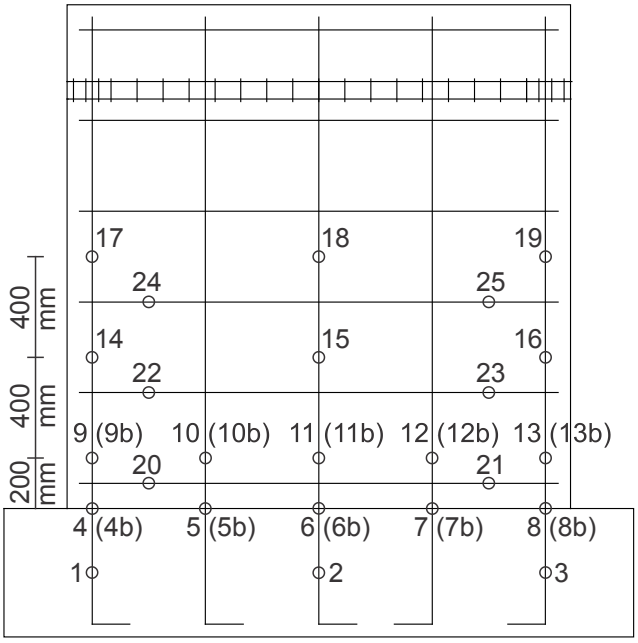


Figure B-15 Strain gauges on reinforcing steel of Walls SQ1, SQ1a, and SQ1S

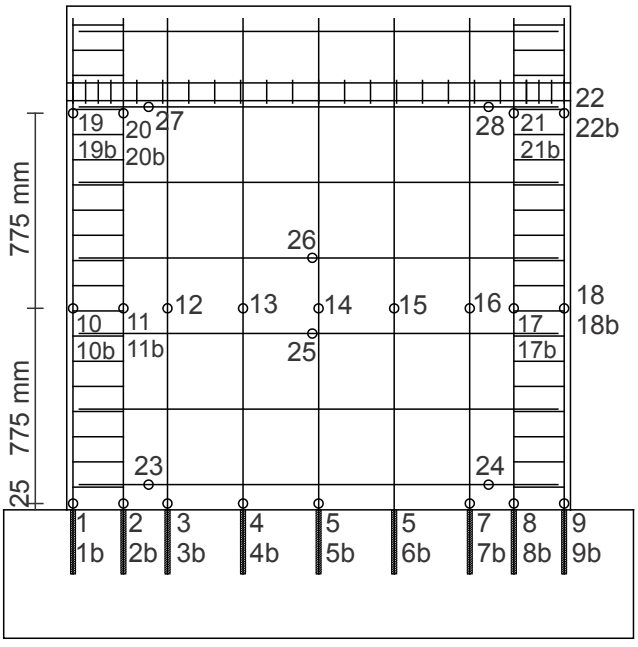


Figure B-16 Strain gauges on reinforcing steel of Walls SQ2 and SQ2S

Figure B-17 illustrates the location of the strain gauges placed on the SMA braces used for retrofitting Walls SQ1S and SQ2S. Three strain gauges were installed on each SMA link, one at the centre at the reduced cross section, and two at the ends

near the couplers (at 20 mm from the connecting plates). The letter *s* in the numbering of the strain gauges refers to SMA. Note that the location of the braces is indicated in parentheses.

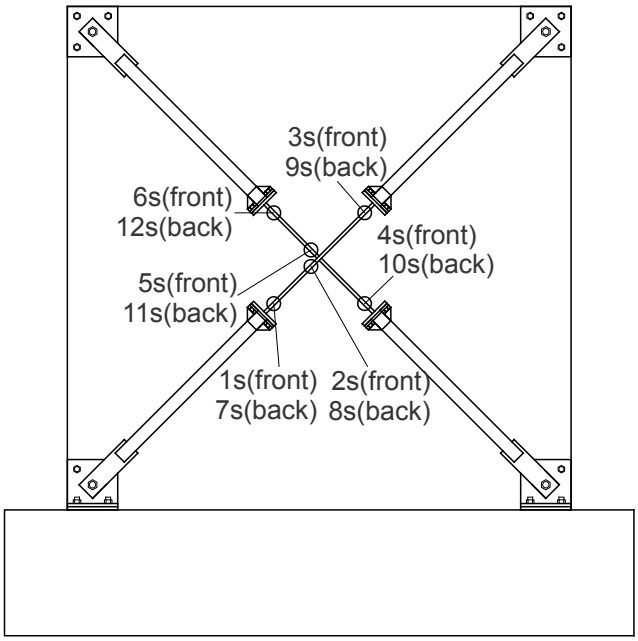


Figure B-17 Strain gauges on SMA braces (letter *s* denotes SMA)

B.3.3 Force Measurements

Applied lateral loads were measured with an MTS 661.31-E01 force transducer that was integral with the hydraulic actuator. The maximum static load capacity of the force transducer was 1000 kN.

B.4 Data Acquisition System

The data acquisition system included a Material Testing System (MTS) used to control the actuator; and a Vishay data acquisition system used to read data from the actuator load cell, displacement sensors, and strain gauges. The MTS consisted of a micro-console and a controller installed in a computer. [Note that testing of the shear walls ran on the MTS displacement-control mode.] The Vishay data acquisition system integrated a series of scanners with a 60-channel control unit and a data acquisition

program, StrainSmart, installed in two computers. The analog signals from the sensors were first read by the control unit, then conditioned by the channel control unit, then converted to digital signals, and finally acquired and controlled by the data acquisition program. During testing, the signals from each channel were periodically scanned at a rate of five scans per second and recorded by the data acquisition program. The MTS controller permitted real-time plots of the load-displacement response acquired from the actuator, and the Vishay data acquisition program permitted real-time digital display of selected instrumentation readings. Figure B-18 illustrates the schematic setup of the data acquisition system.

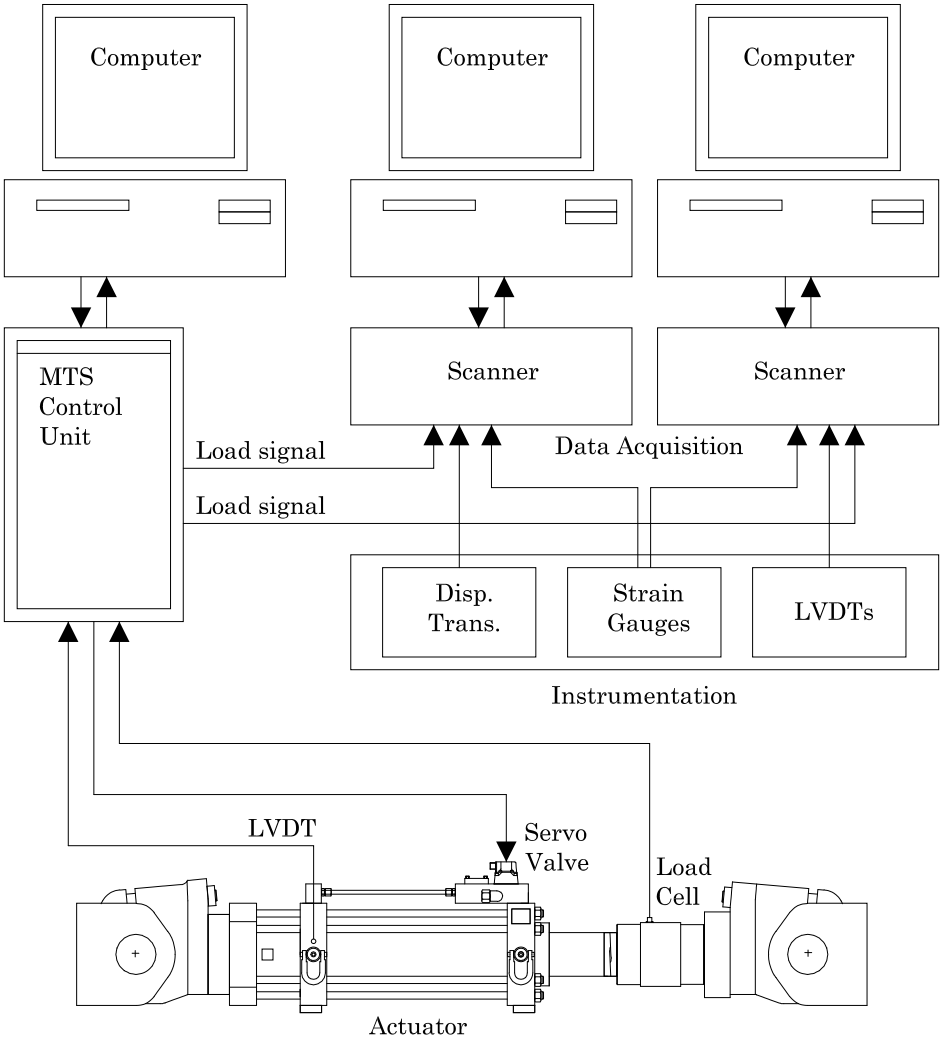


Figure B-18 Flowchart of data acquisition system

B.5 Loading Protocol

In general, lateral loading consisted of a reverse cyclic protocol with two repetitions at each displacement level (Figure B-19), following recommendations from FEMA 461 (ATC 2007). Due to technical problems during testing, the loading protocol for Wall SQ1, from 5 mm displacement, differed from the intended protocol (Figure B-20). No axial loading was imposed on the walls.

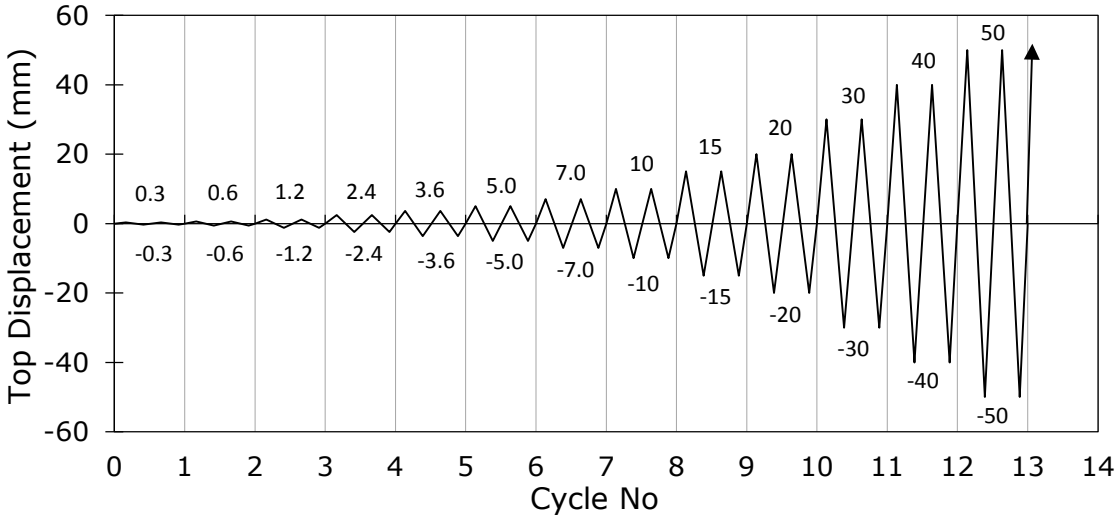


Figure B-19 Loading protocol for the wall tests

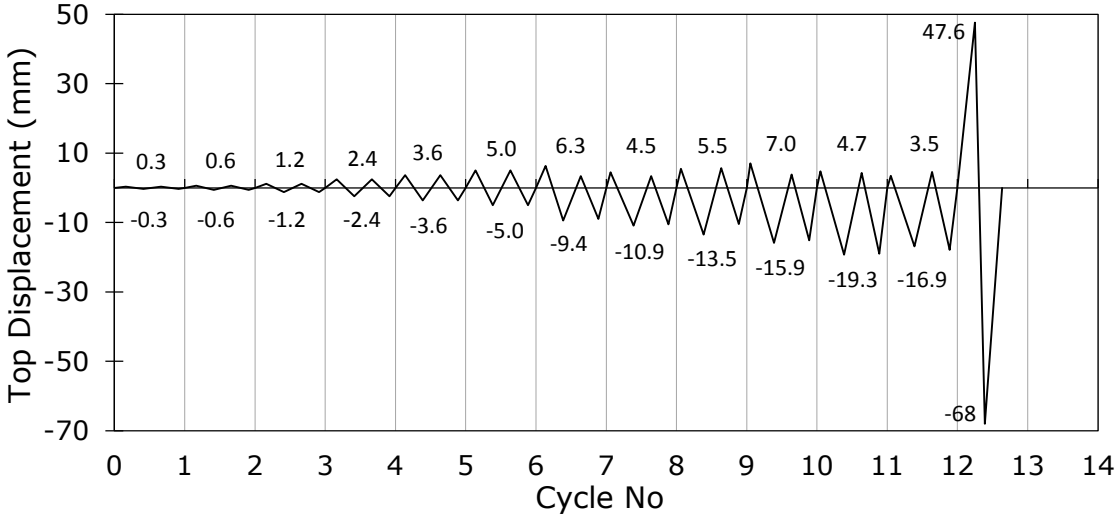


Figure B-20 Actual loading protocol for Wall SQ1 test

B.6 Test Results

B.6.1 Cracking

The cracking pattern of the shear walls at different lateral displacements is illustrated in Figure B-21 to Figure B-51.

B.6.1.1 Wall SQ1

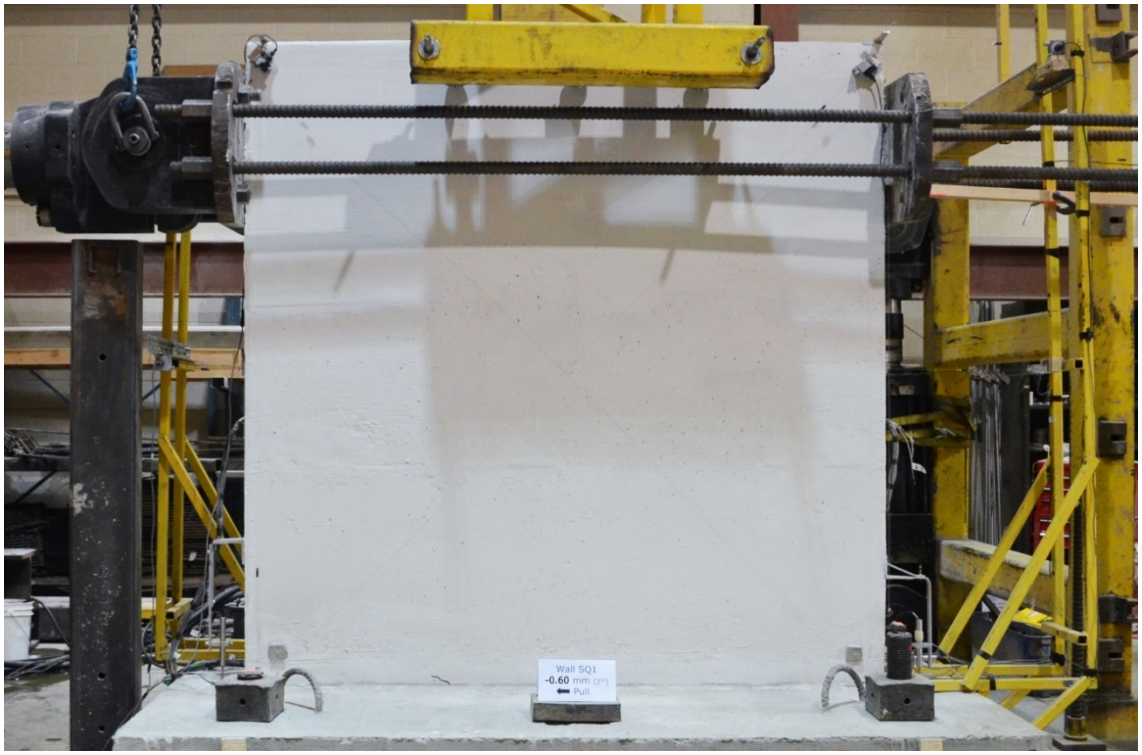


Figure B-21 First cracking of Wall SQ1 at 0.6 mm displacement

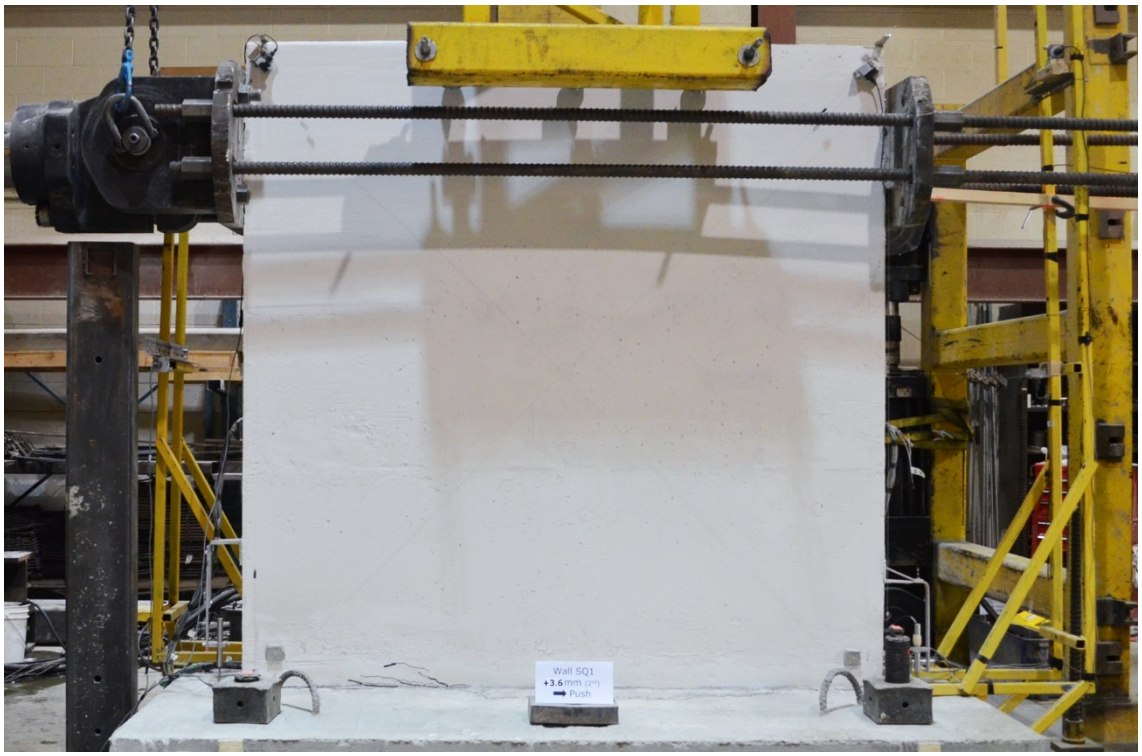


Figure B-22 Cracking pattern of Wall SQ1 at 3.6 mm displacement

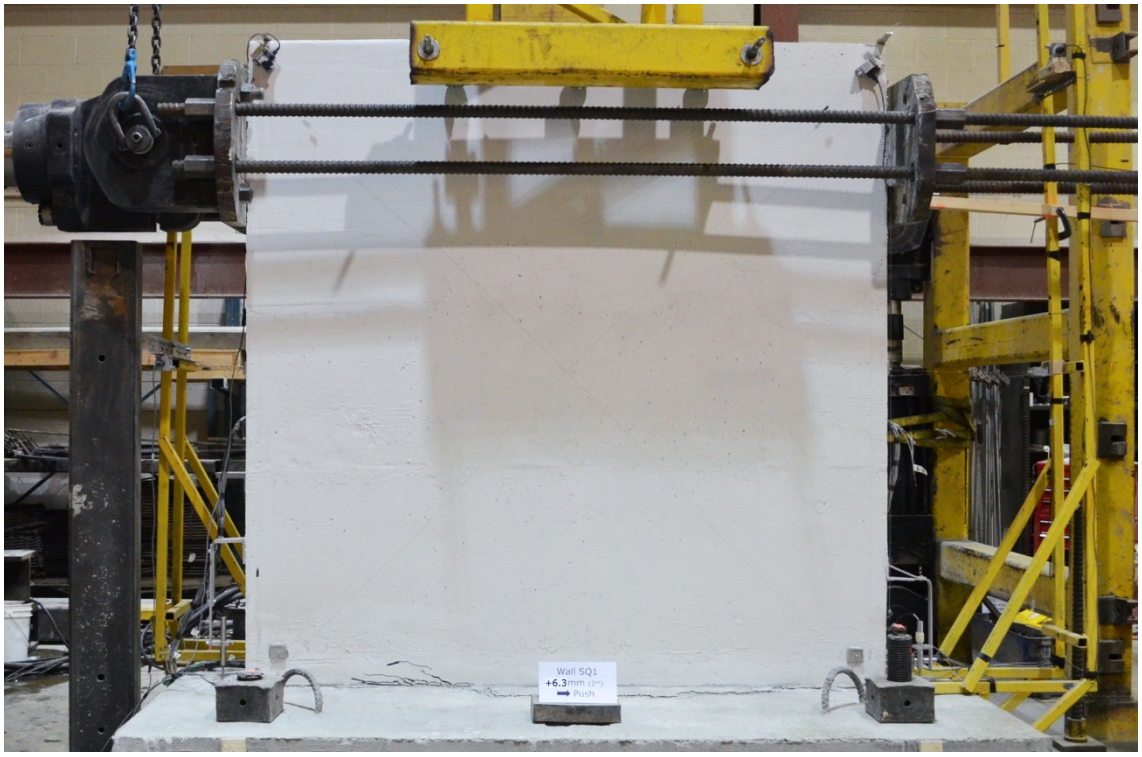


Figure B-23 Cracking pattern of Wall SQ1 at 6.3 mm displacement

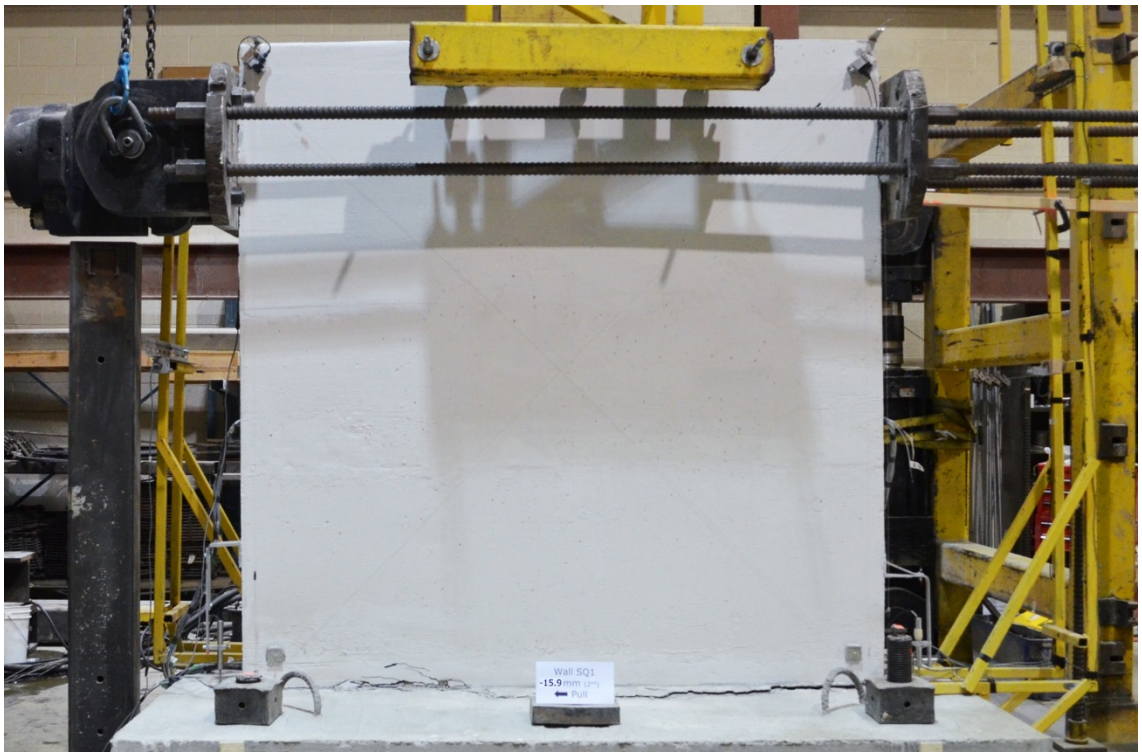


Figure B-24 Cracking pattern of Wall SQ1 at -15.9 mm displacement

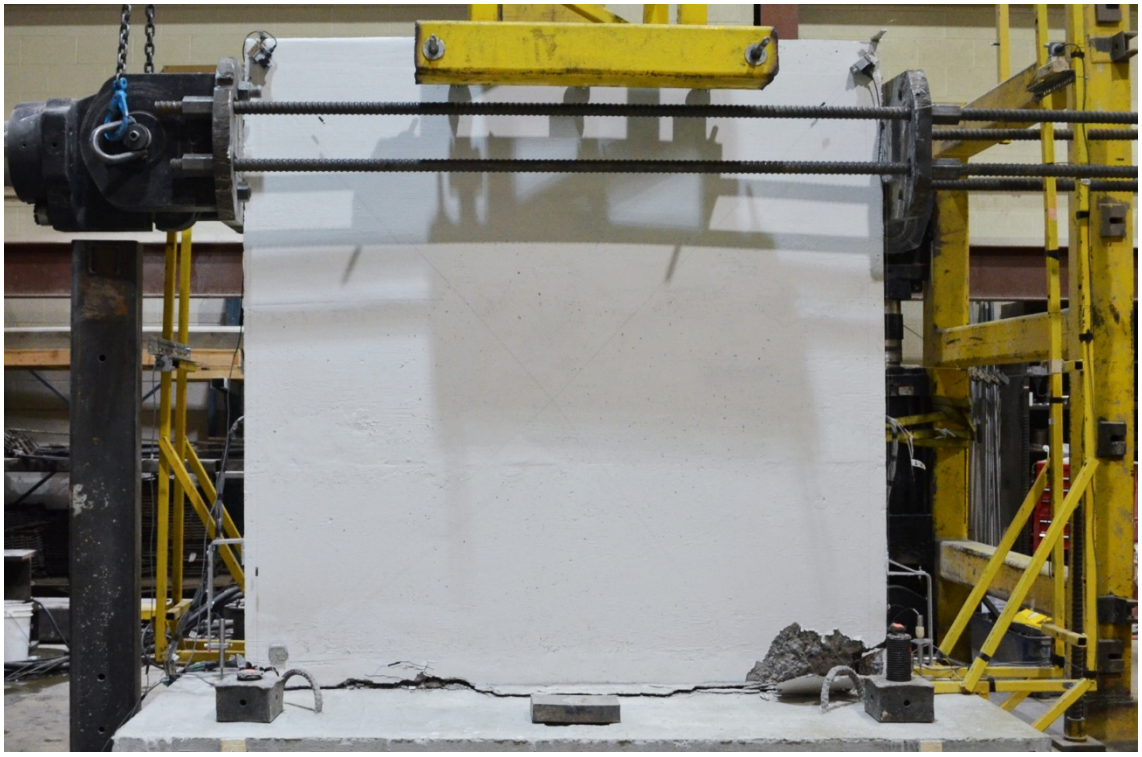


Figure B-25 Cracking pattern of Wall SQ1 at 47.6 mm displacement

B.6.1.2 Wall SQ1a

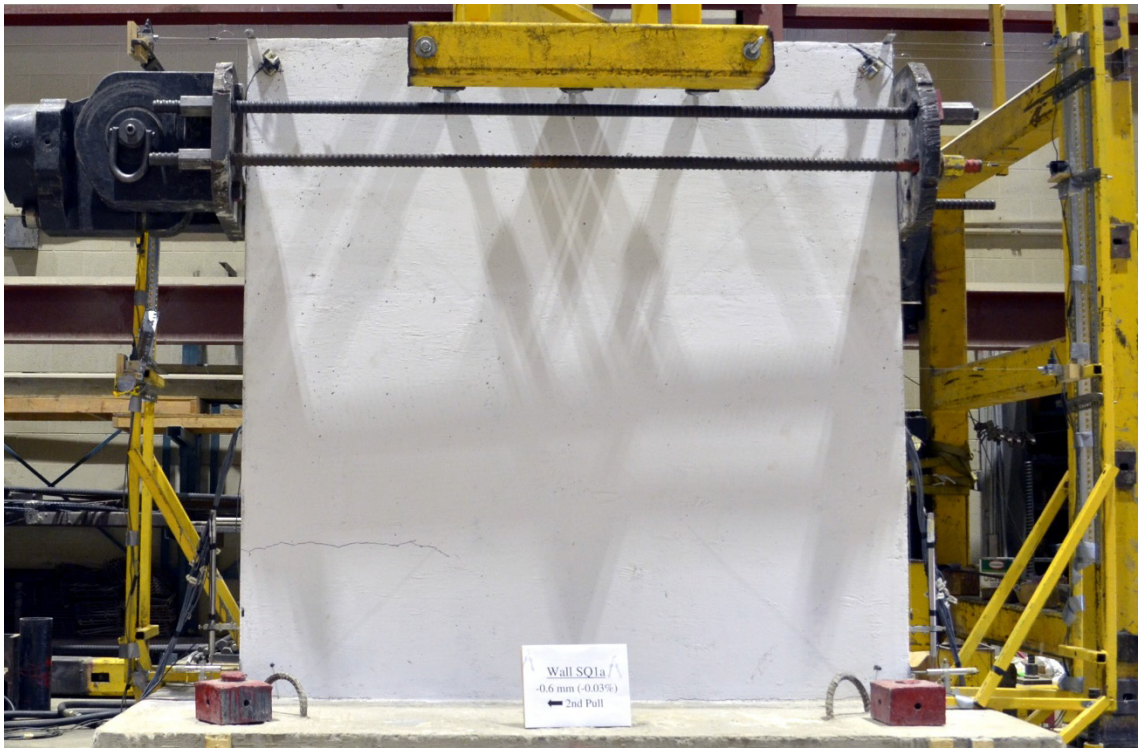


Figure B-26 First cracking of Wall SQ1a at 0.6 mm displacement

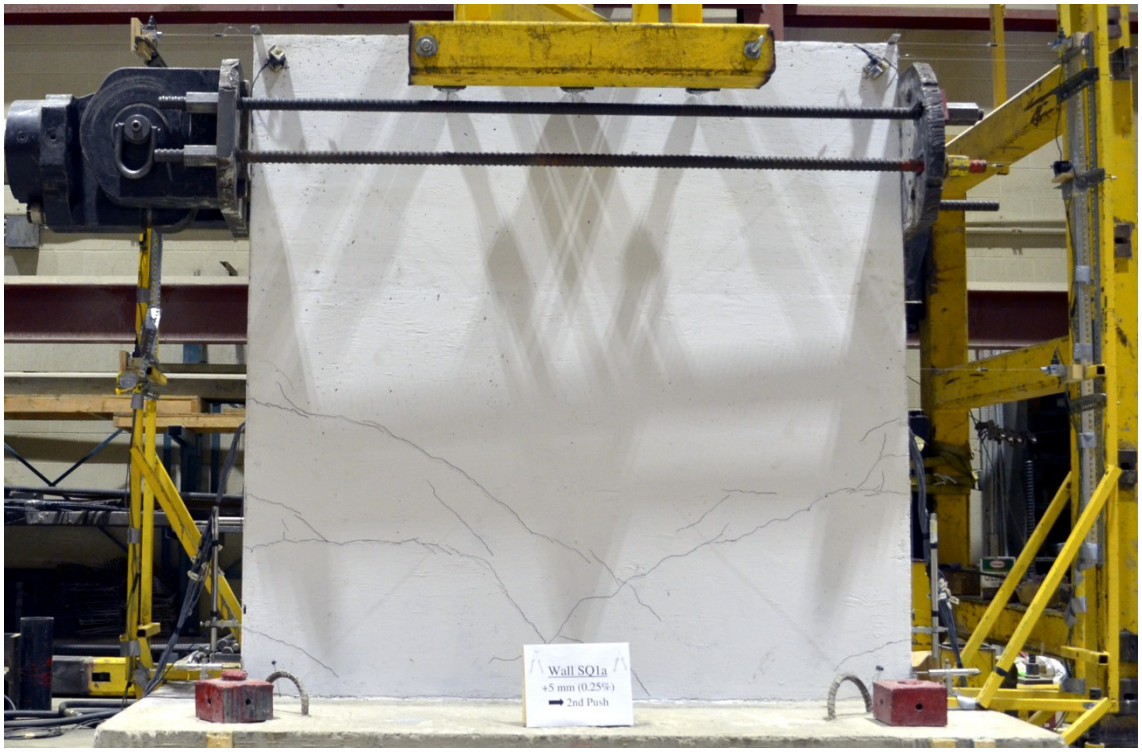


Figure B-27 Cracking pattern of Wall SQ1a at 5.0 displacement

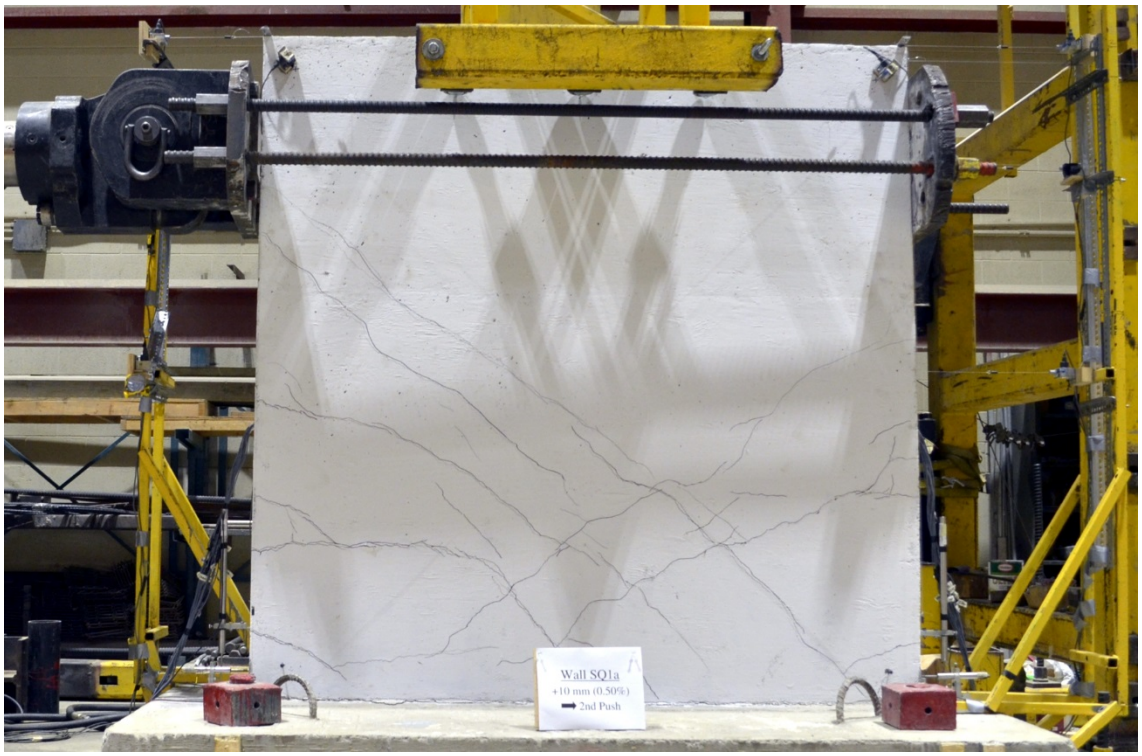


Figure B-28 Cracking pattern of Wall SQ1a at 10 mm displacement

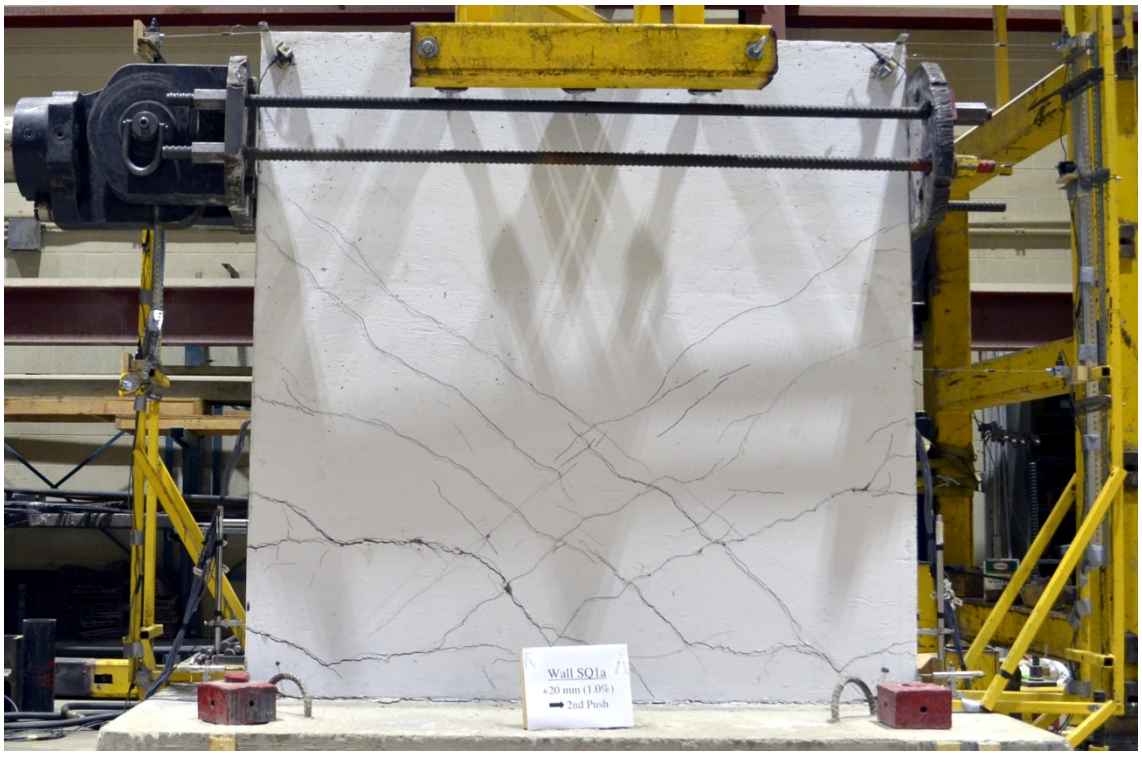


Figure B-29 Cracking pattern of Wall SQ1a at 20 mm displacement

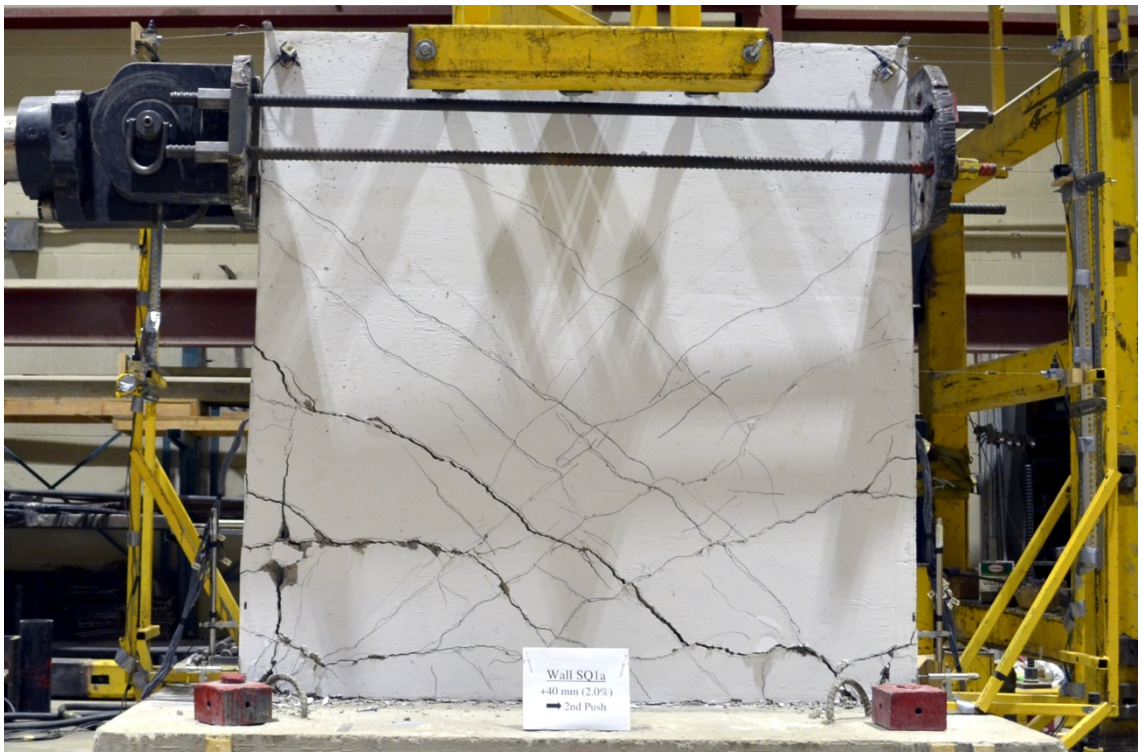


Figure B-30 Cracking pattern of Wall SQ1a at 40 mm displacement

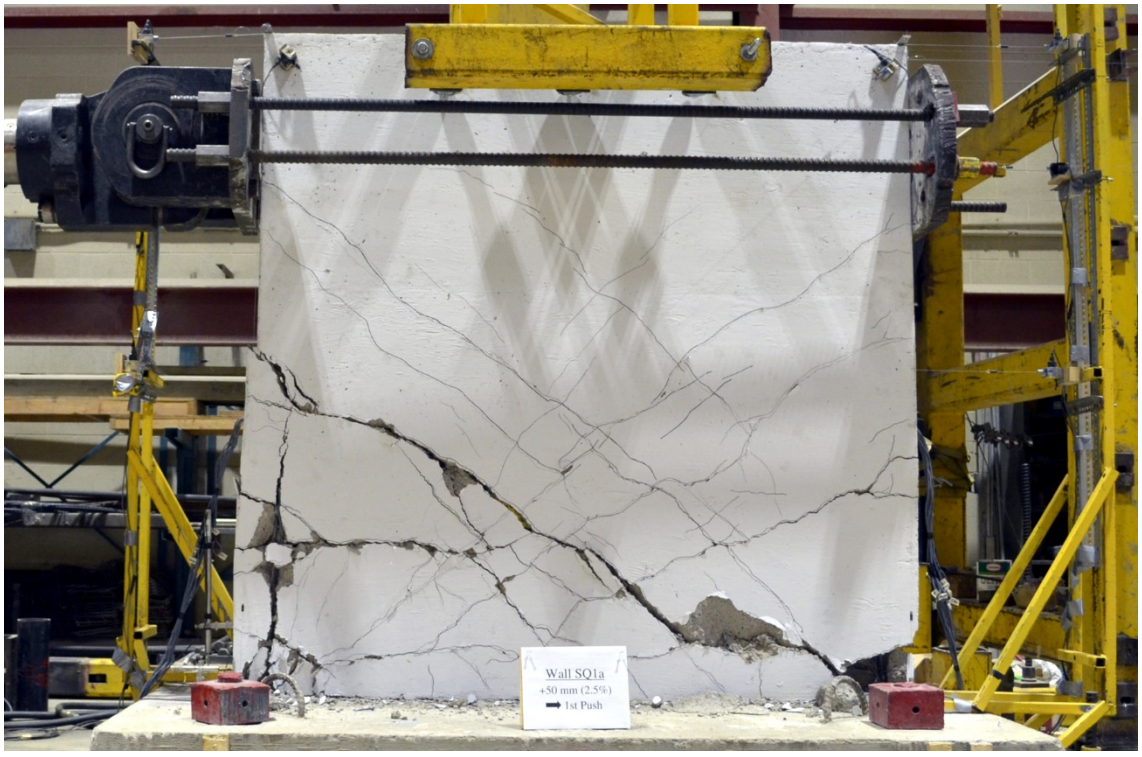


Figure B-31 Cracking pattern of Wall SQ1a at 50 mm displacement

B.6.1.3 Wall SQ1S

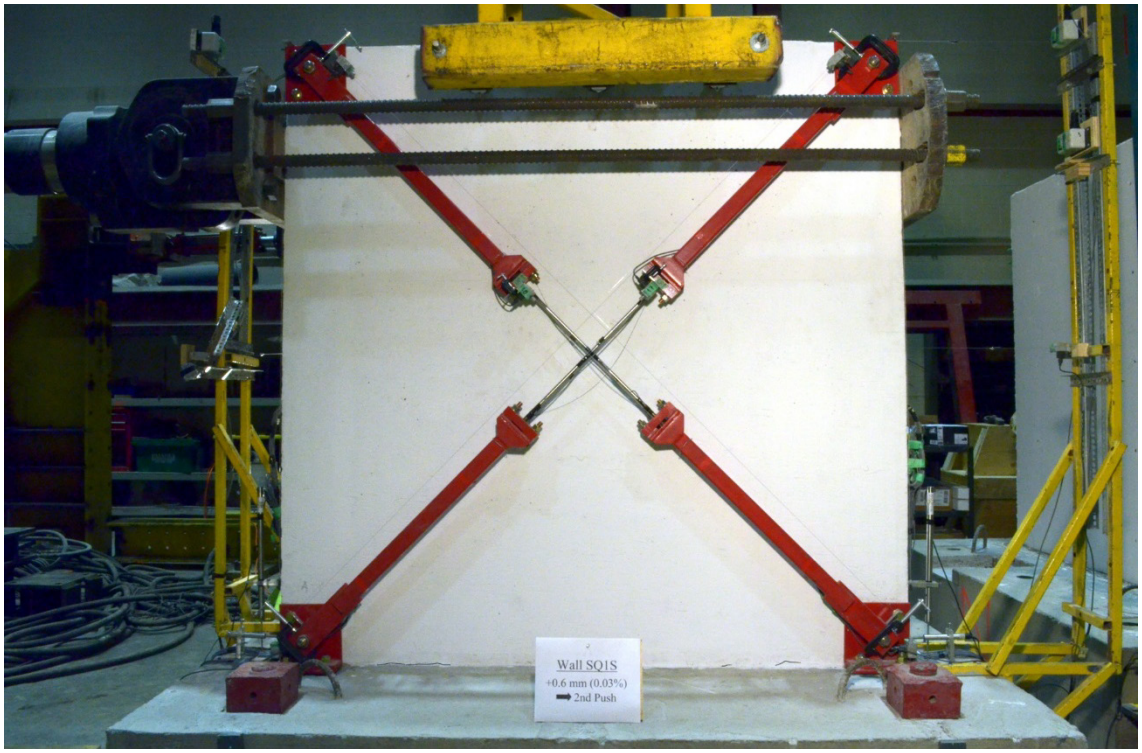


Figure B-32 First cracking of Wall SQ1S at 0.6 mm displacement

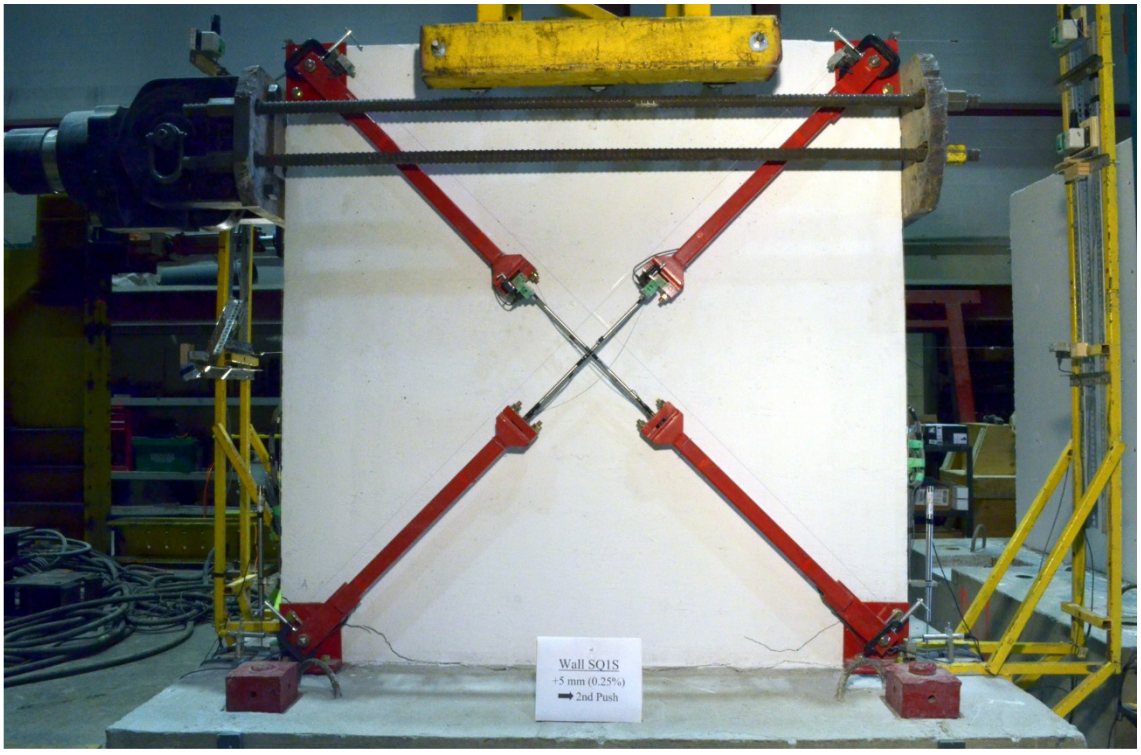


Figure B-33 Cracking pattern of Wall SQ1S at 5.0 displacement

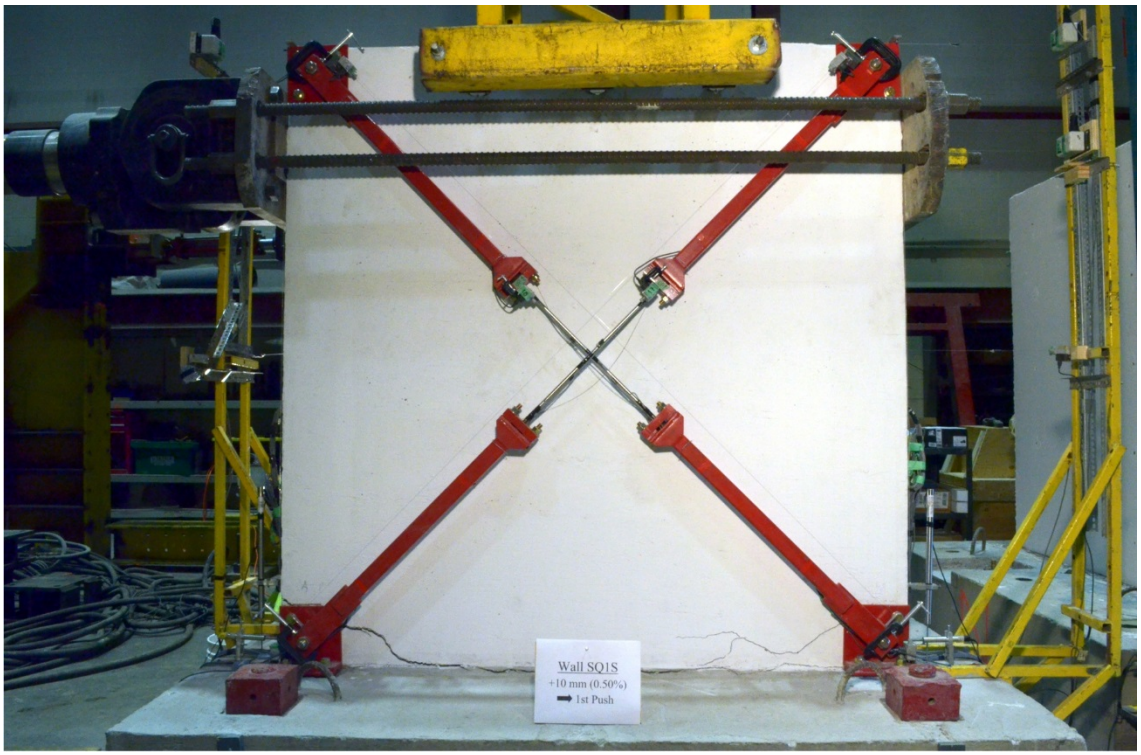


Figure B-34 Cracking pattern of Wall SQ1S at 10 mm displacement

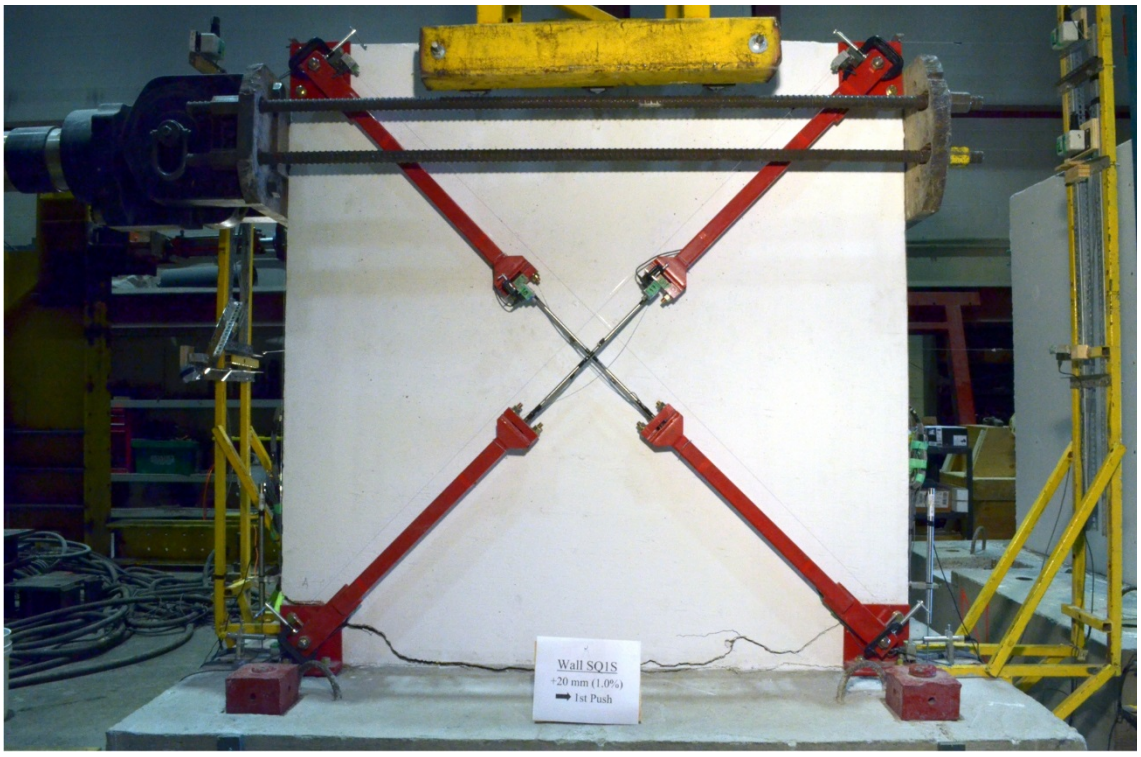


Figure B-35 Cracking pattern of Wall SQ1S at 20 mm displacement

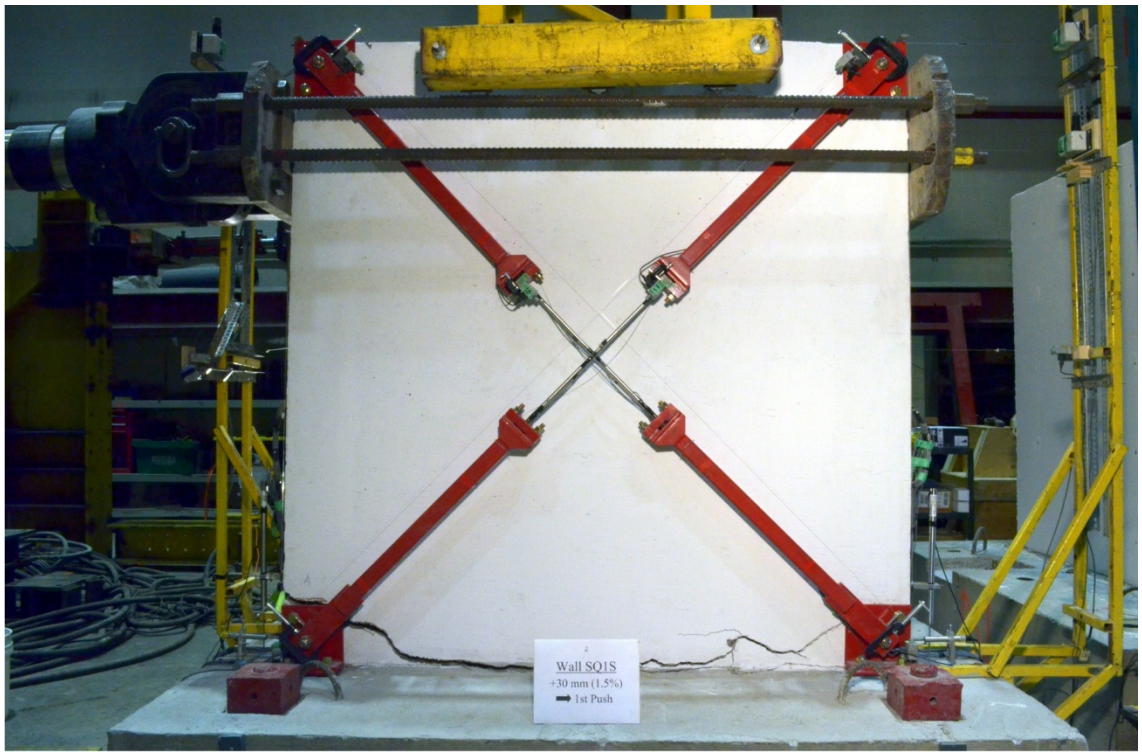


Figure B-36 Cracking pattern of Wall SQ1S at 30 mm displacement

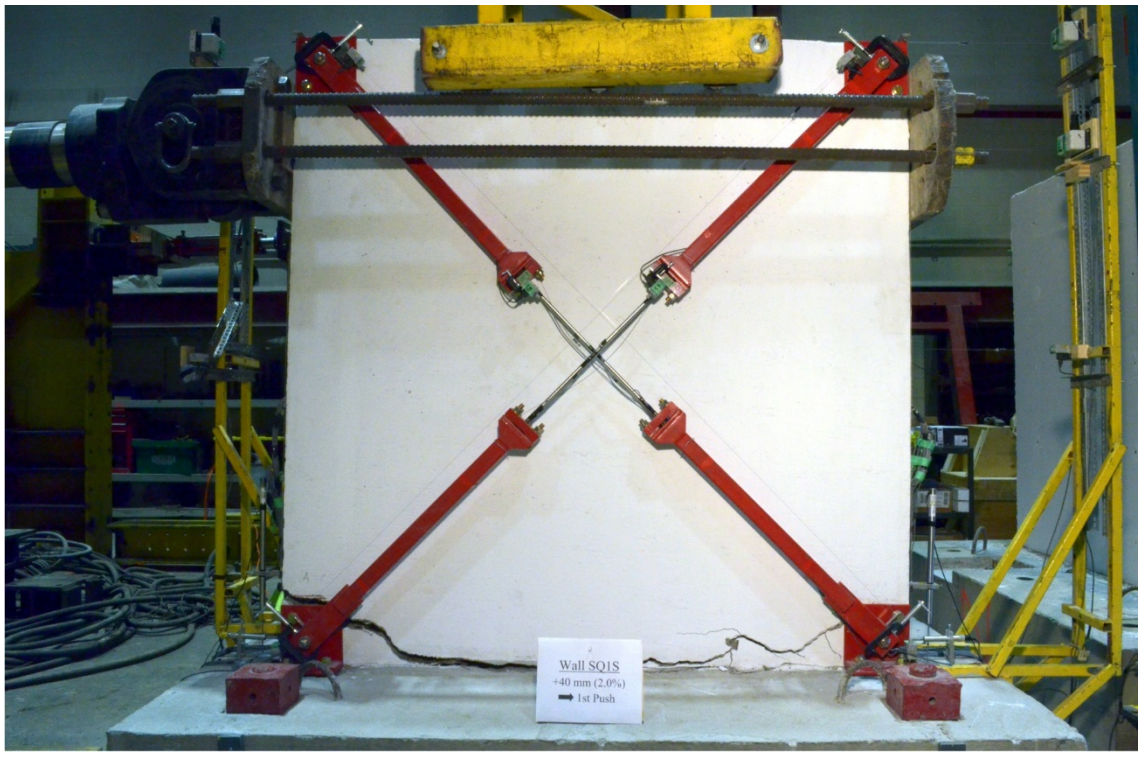


Figure B-37 Cracking pattern of Wall SQ1S at 40 mm displacement

B.6.1.4 Wall SQ2

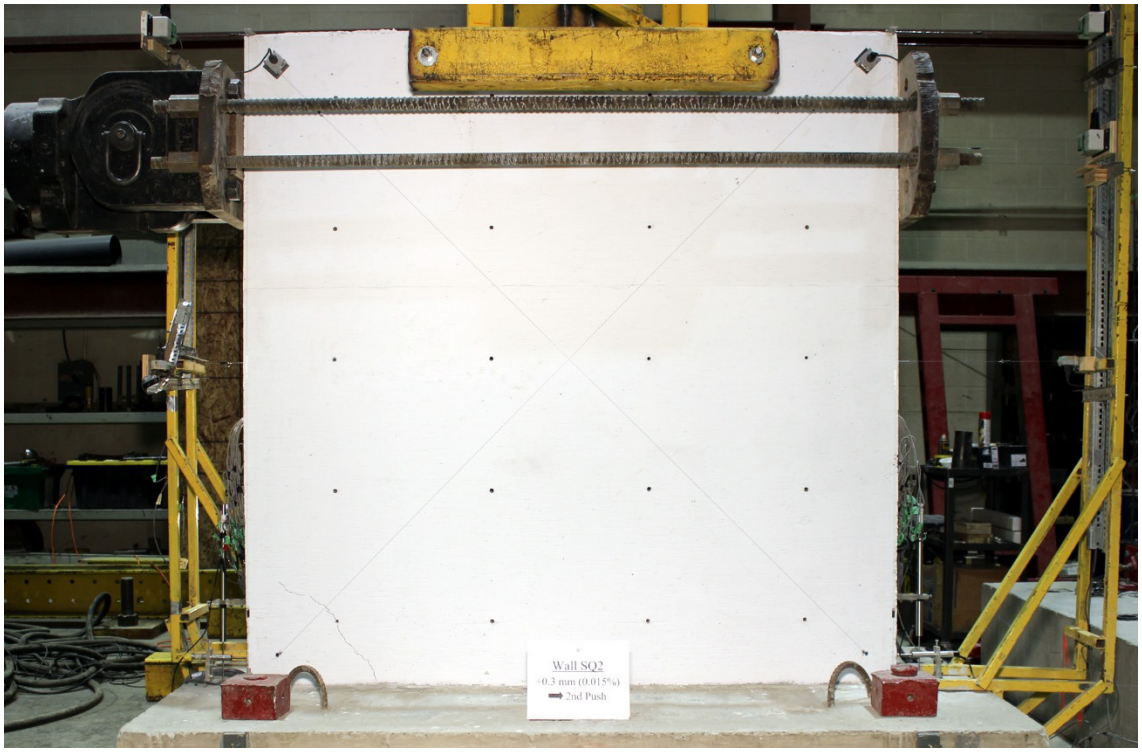


Figure B-38 First cracking of Wall SQ2 at 0.3 mm displacement

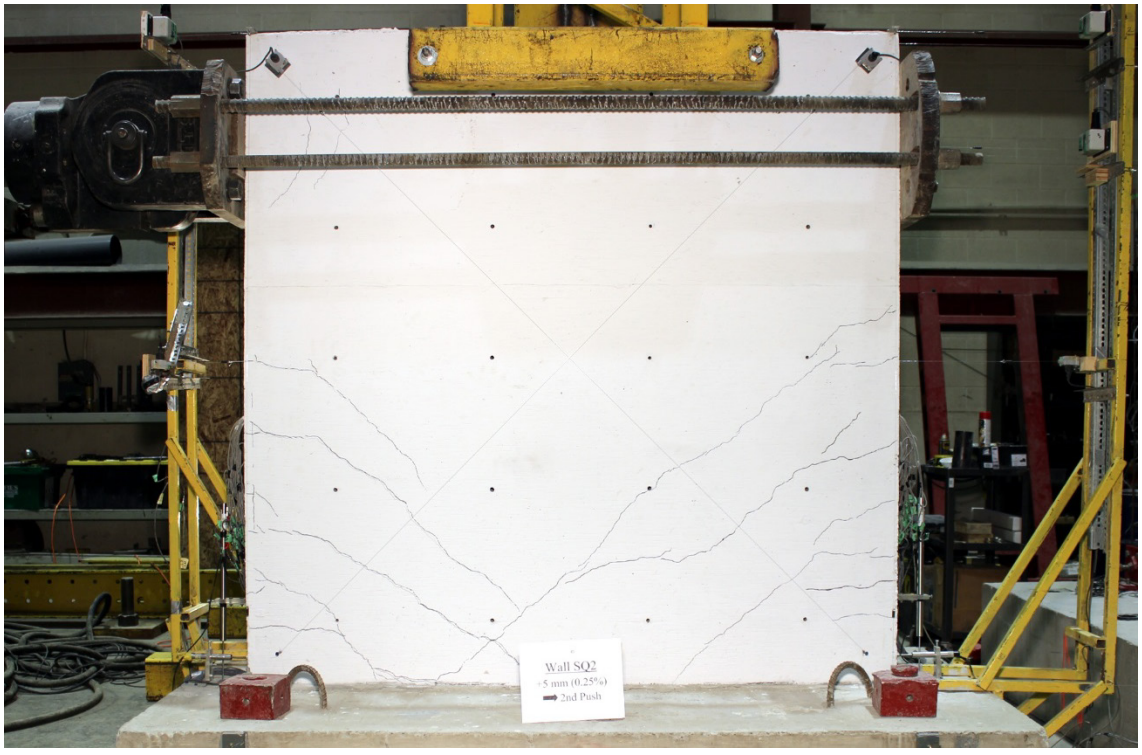


Figure B-39 Cracking pattern of Wall SQ2 at 5.0 displacement

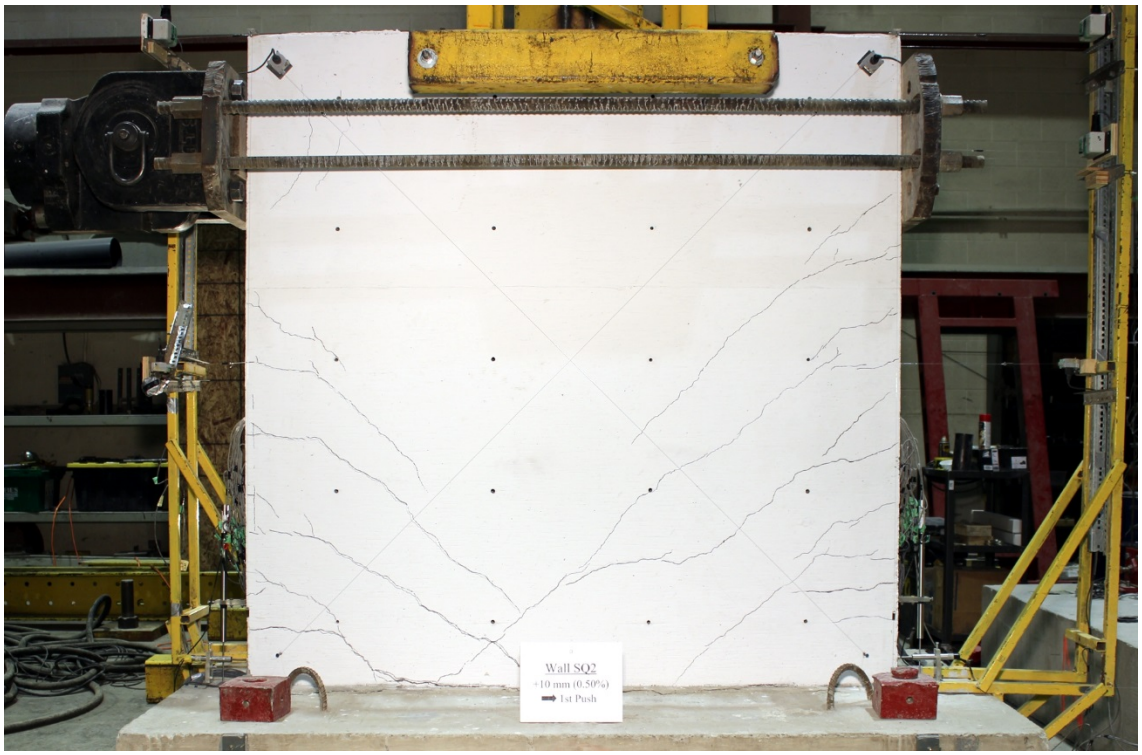


Figure B-40 Cracking pattern of Wall SQ2 at 10 mm displacement

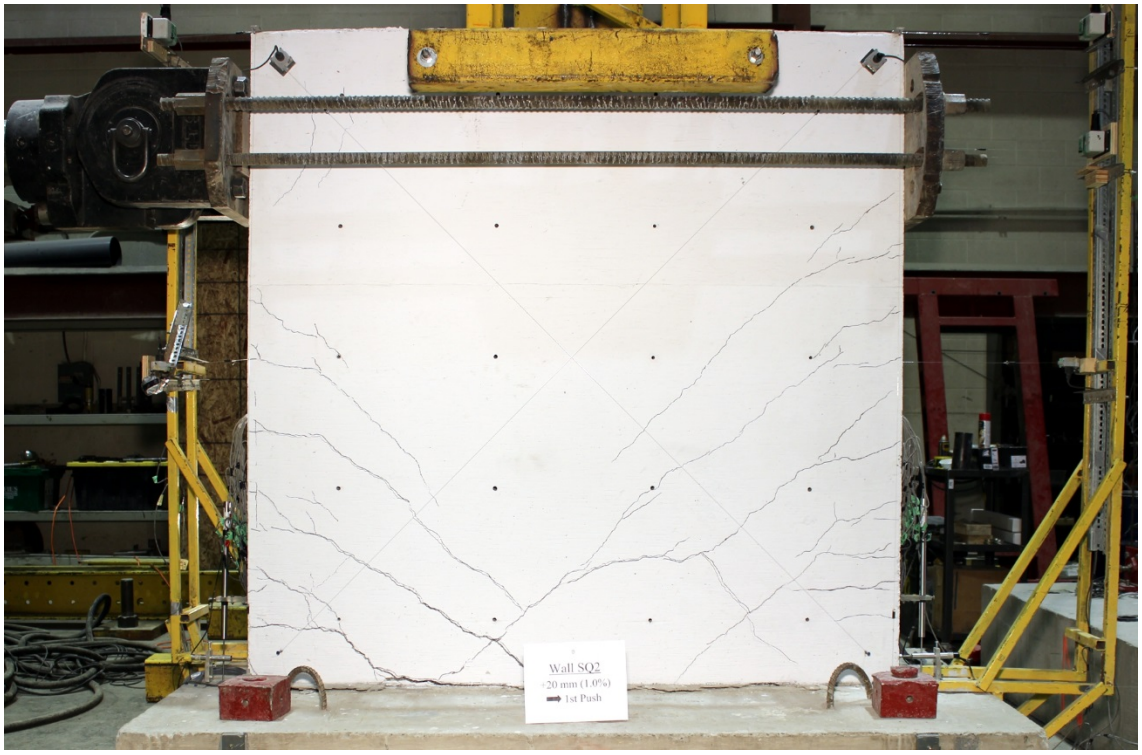


Figure B-41 Cracking pattern of Wall SQ2 at 20 mm displacement

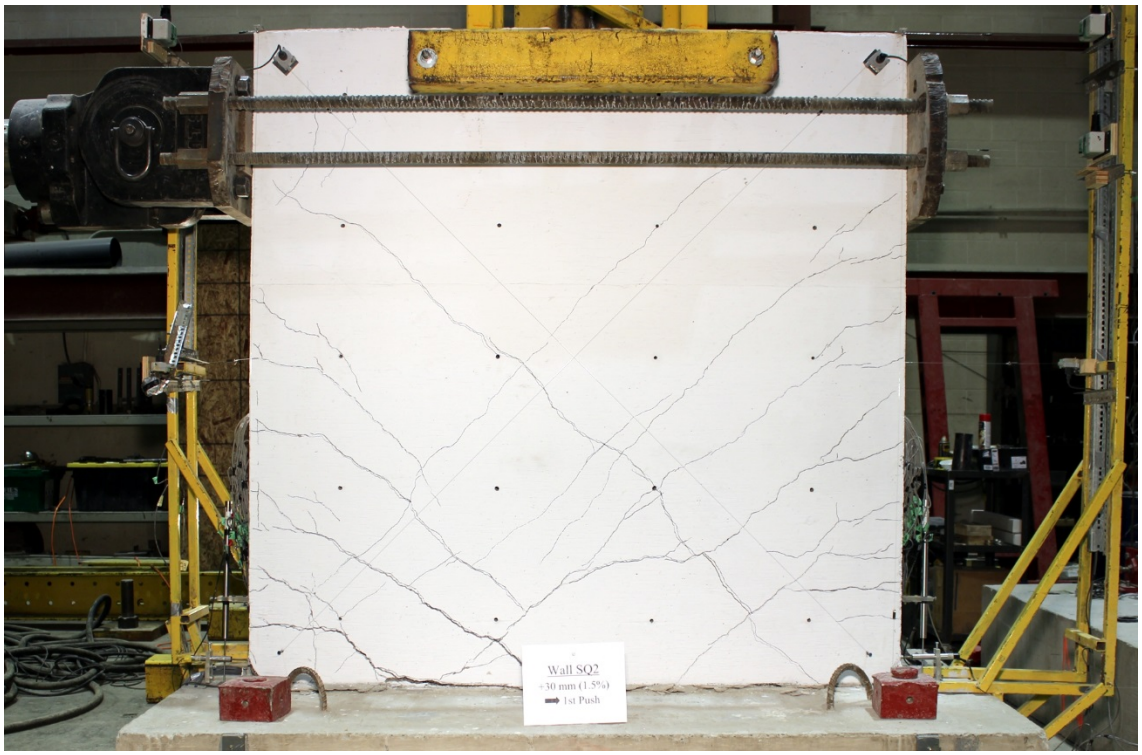


Figure B-42 Cracking pattern of Wall SQ2 at 30 mm displacement

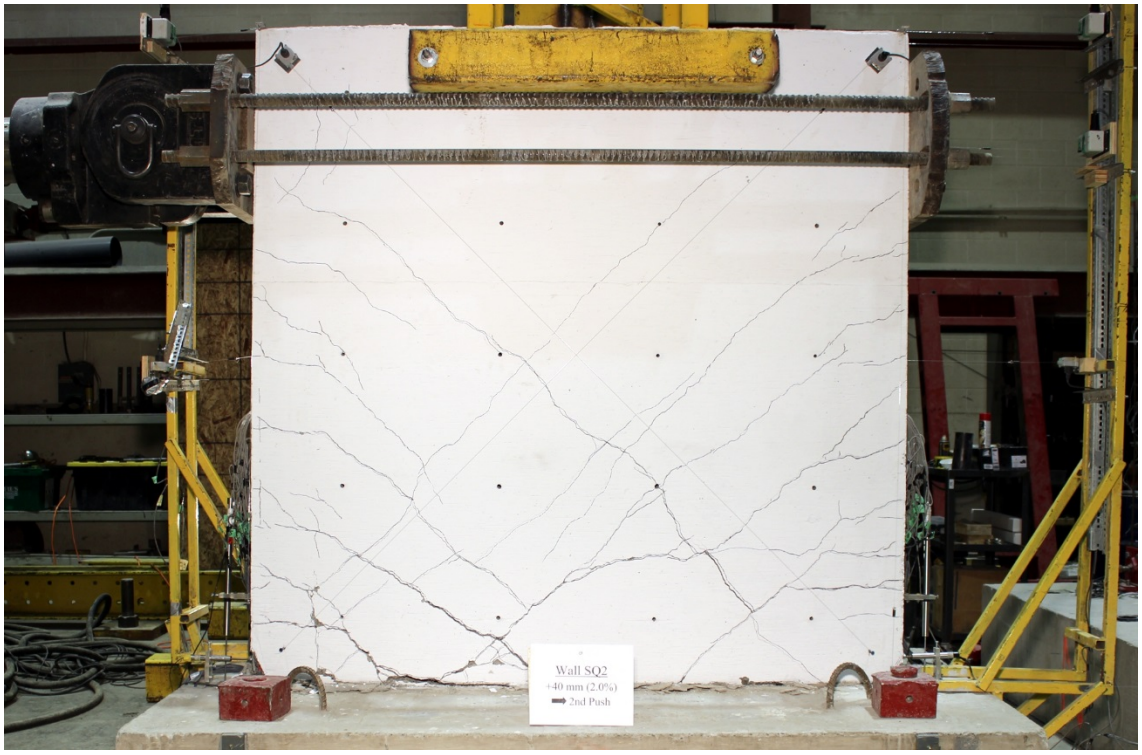


Figure B-43 Cracking pattern of Wall SQ2 at 40 mm displacement

B.6.1.5 Wall SQ2S

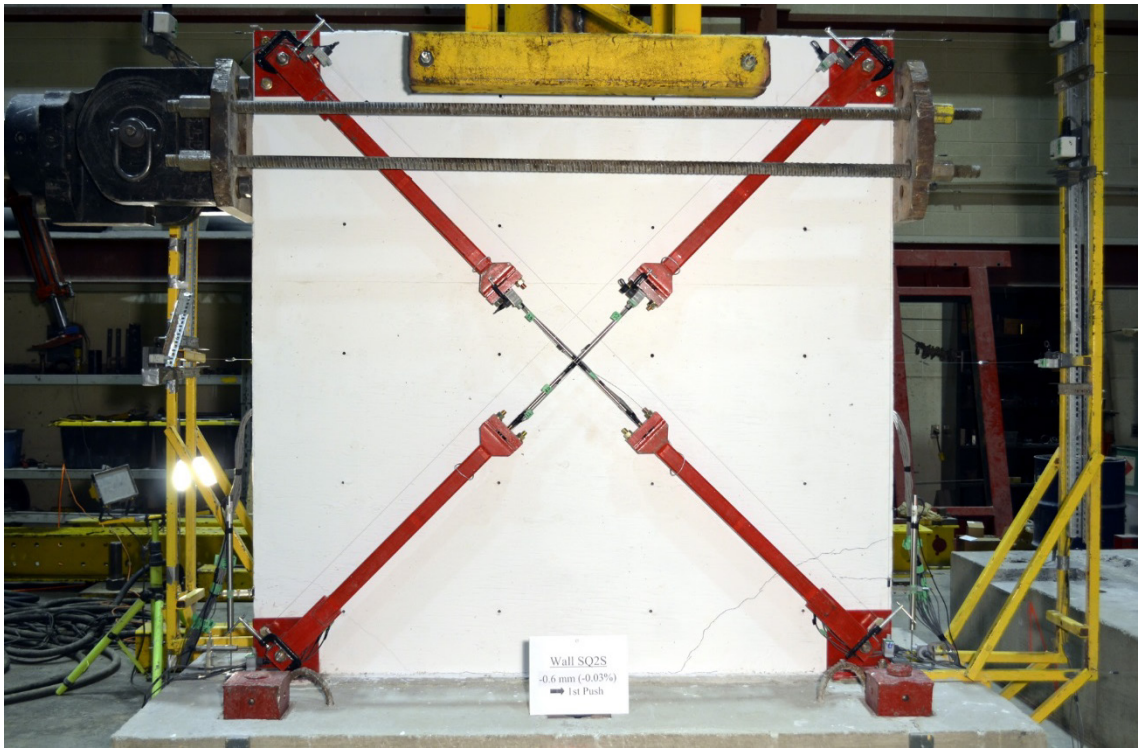


Figure B-44 First cracking of Wall SQ2S at 0.3 mm displacement

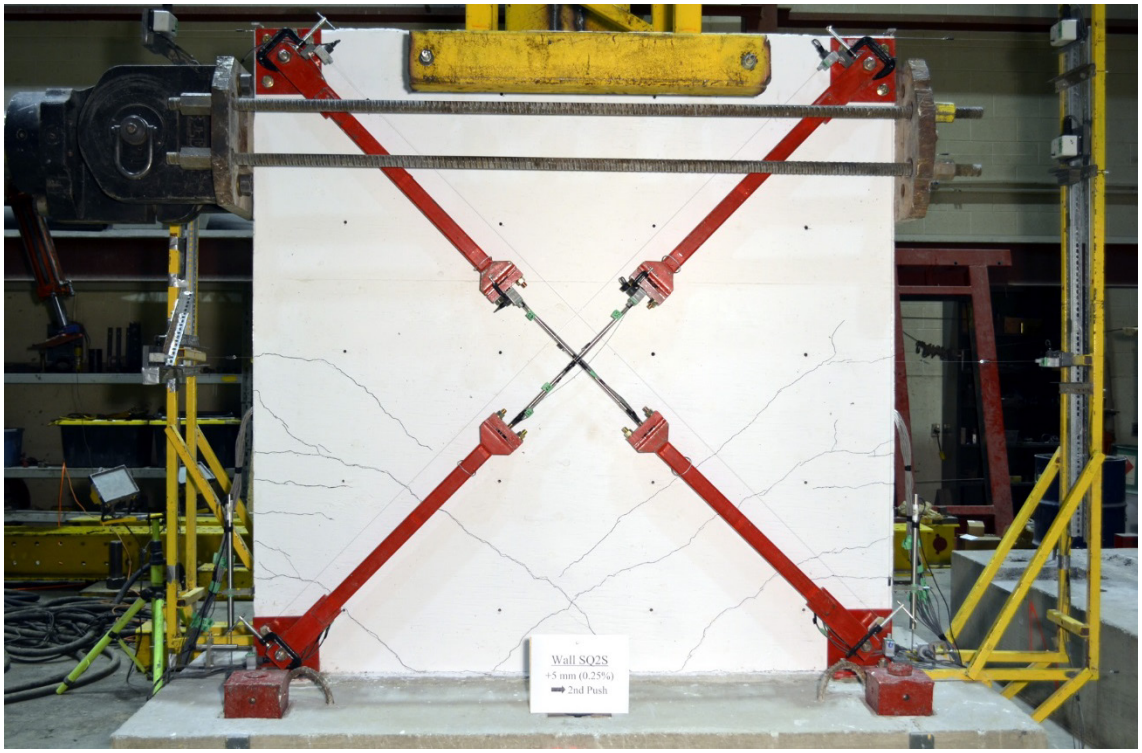


Figure B-45 Cracking pattern of Wall SQ2S at 5.0 displacement

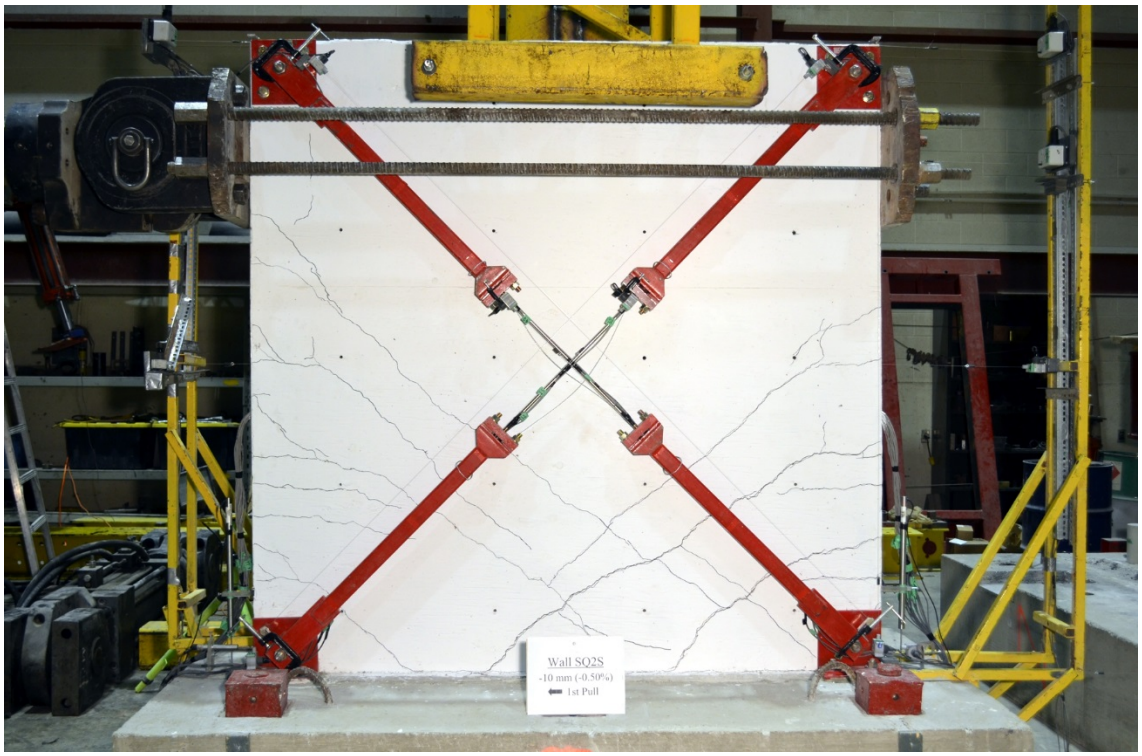


Figure B-46 Cracking pattern of Wall SQ2S at 10 mm displacement

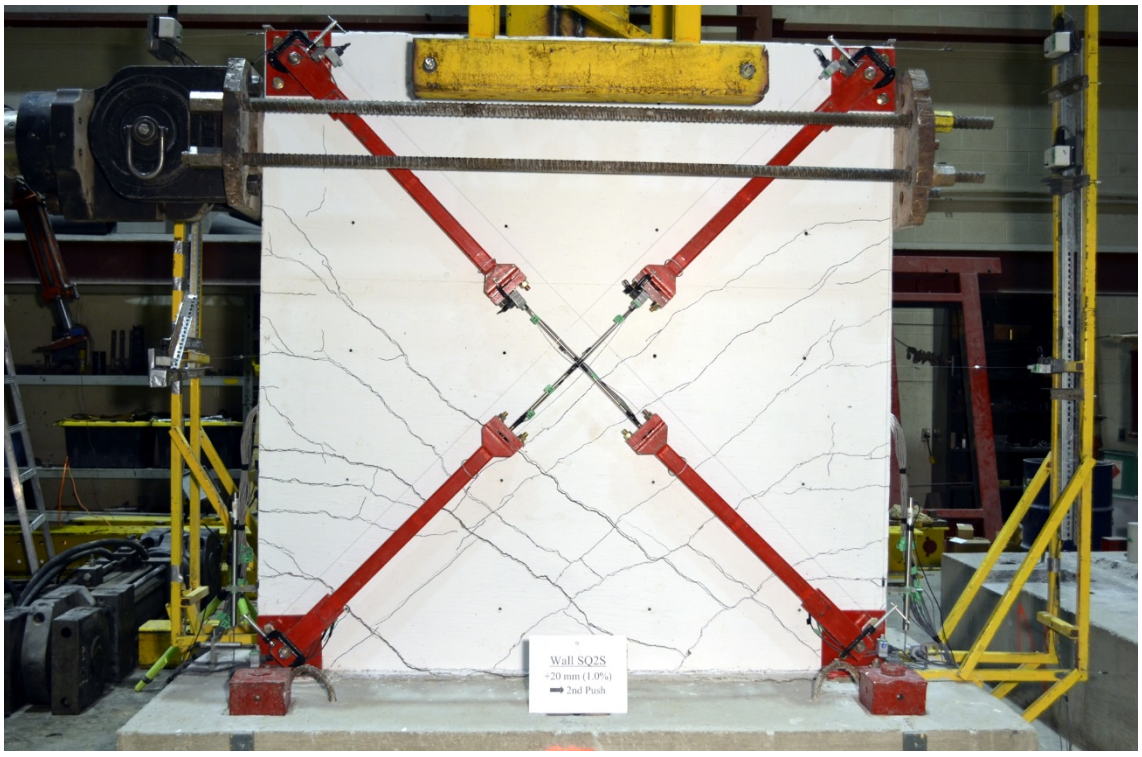


Figure B-47 Cracking pattern of Wall SQ2S at 20 mm displacement



Figure B-48 Cracking pattern of Wall SQ2S at 30 mm displacement



Figure B-49 Cracking pattern of Wall SQ2S at 40 mm displacement

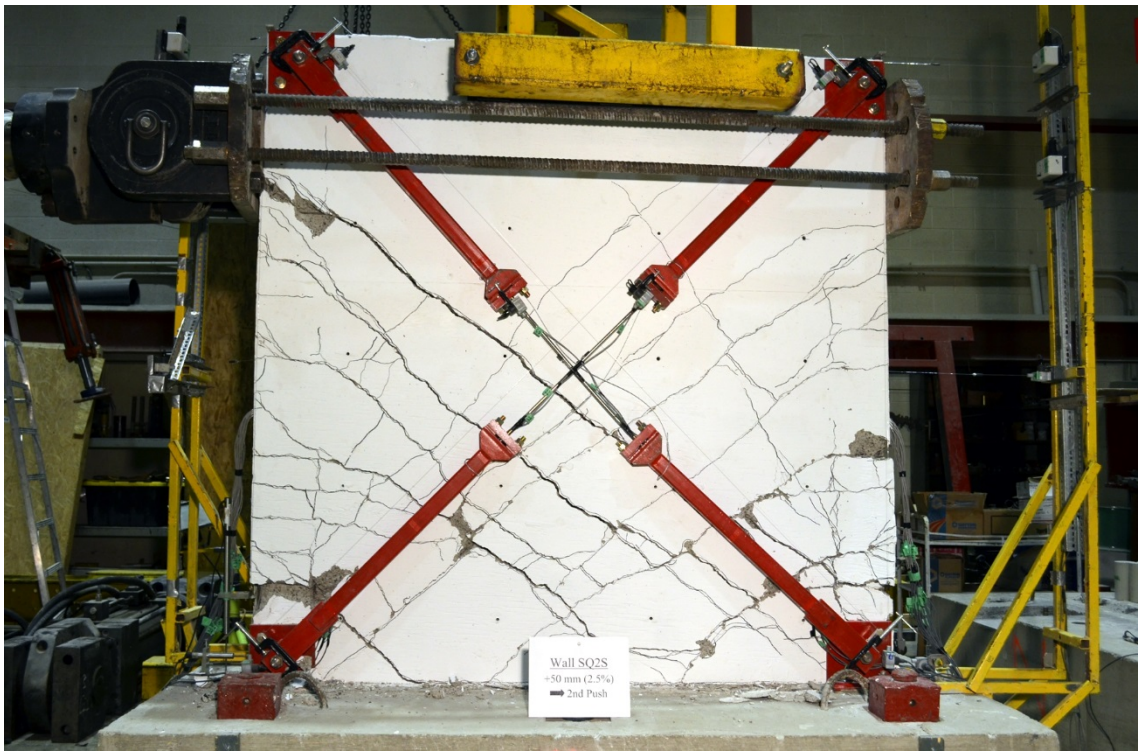


Figure B-50 Cracking pattern of Wall SQ2S at 50 mm displacement

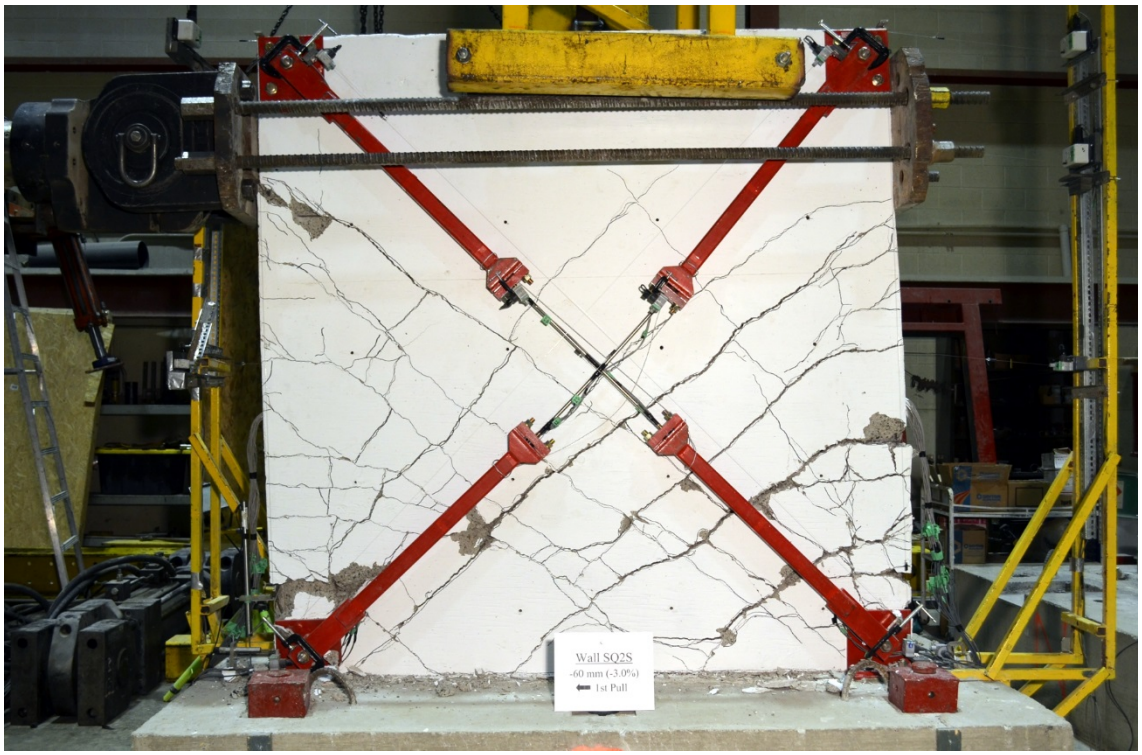


Figure B-51 Cracking pattern of Wall SQ2S at -60 mm displacement

B.6.2 Displacement Response

Additional displacement responses, not presented in Chapter 4, are provided in Figure B-52 to Figure B-69.

B.6.2.1 Wall SQ1

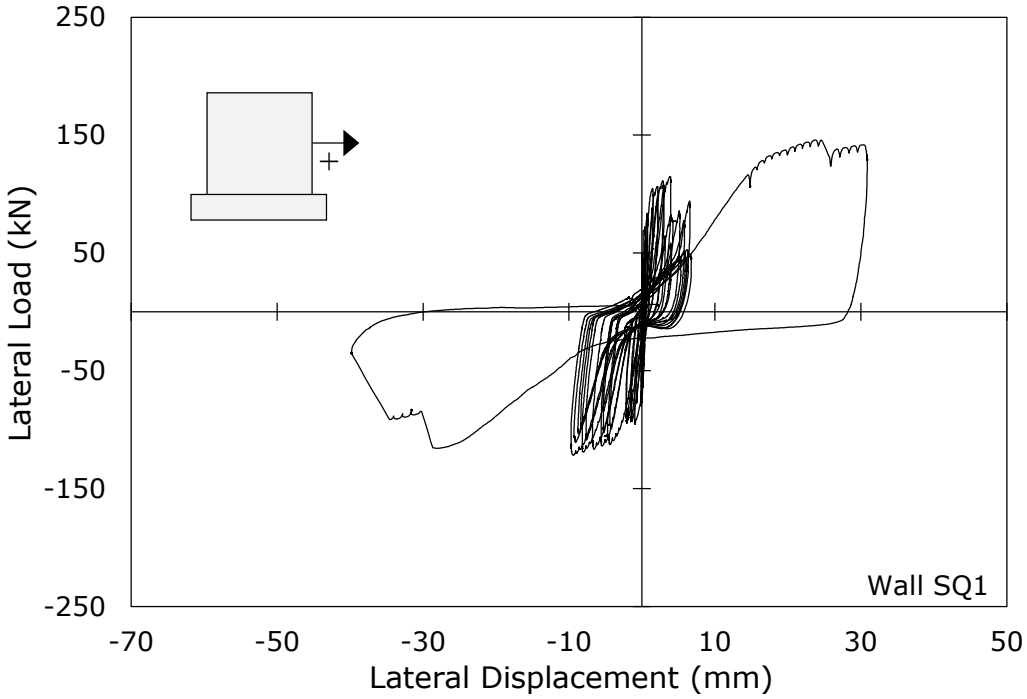


Figure B-52 Lateral load-lateral displacement, sensor C4 in SQ1

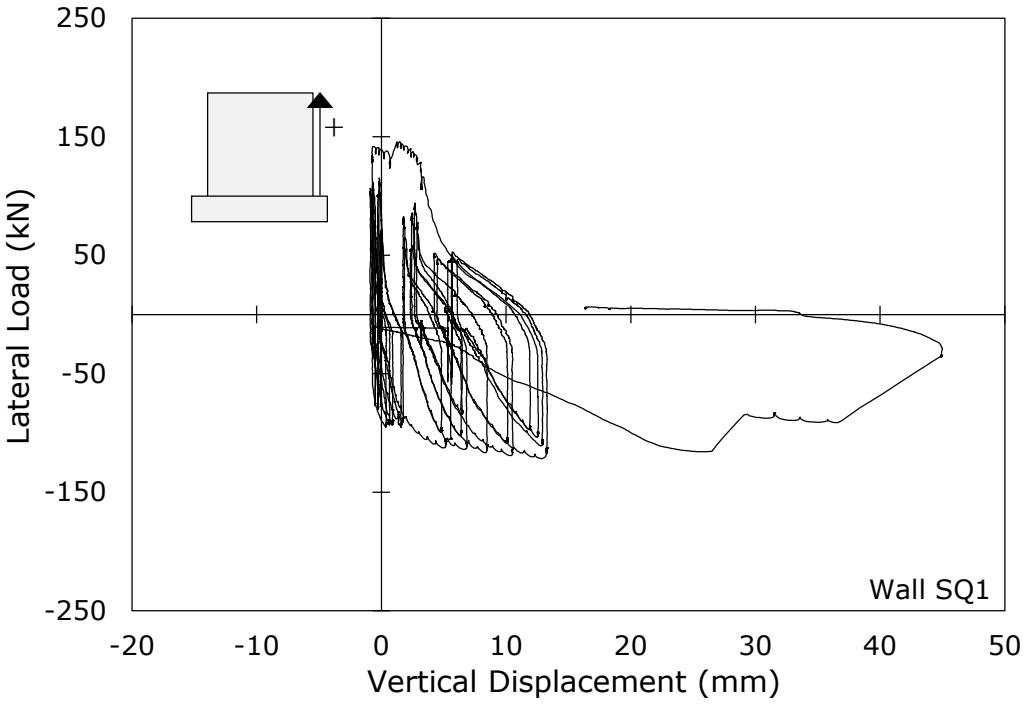


Figure B-53 Lateral load-vertical displacement, sensor C6 in Wall SQ1

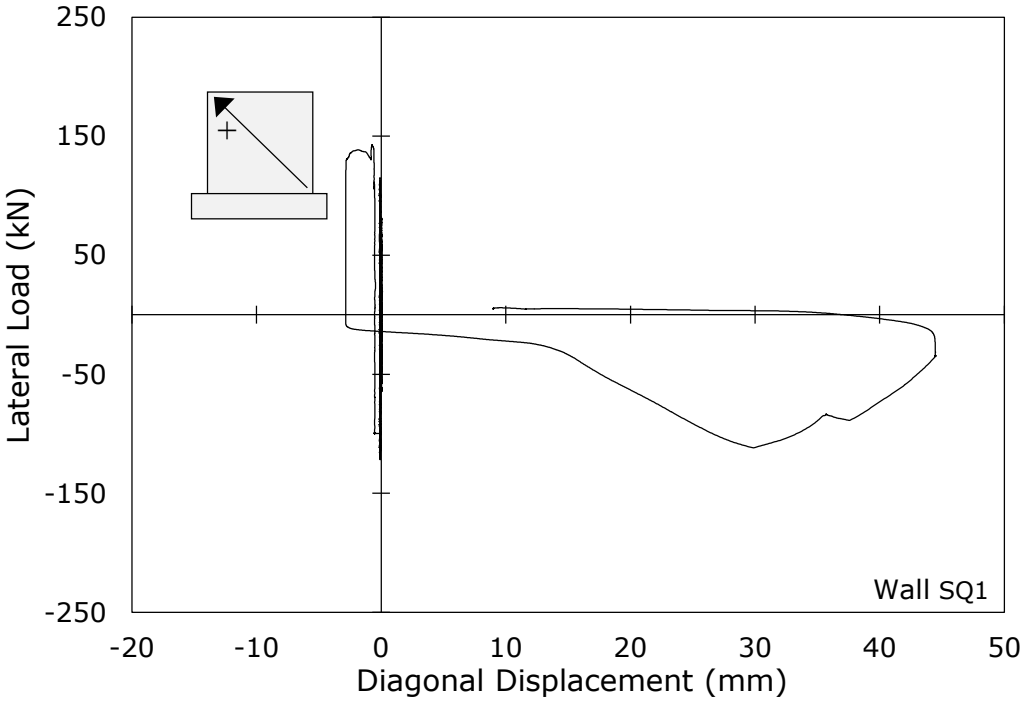


Figure B-54 Lateral load-diagonal displacement, sensor C8 in SQ1

B.6.2.2 Wall SQ1a

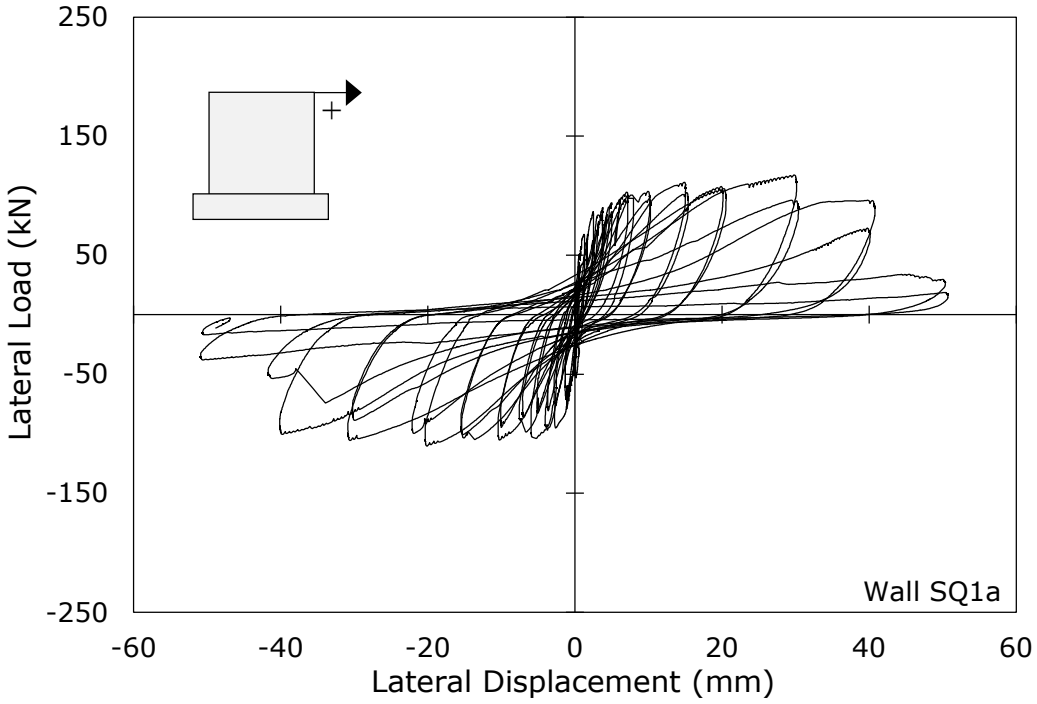


Figure B-55 Lateral load-lateral displacement response, sensor C2 in SQ1a

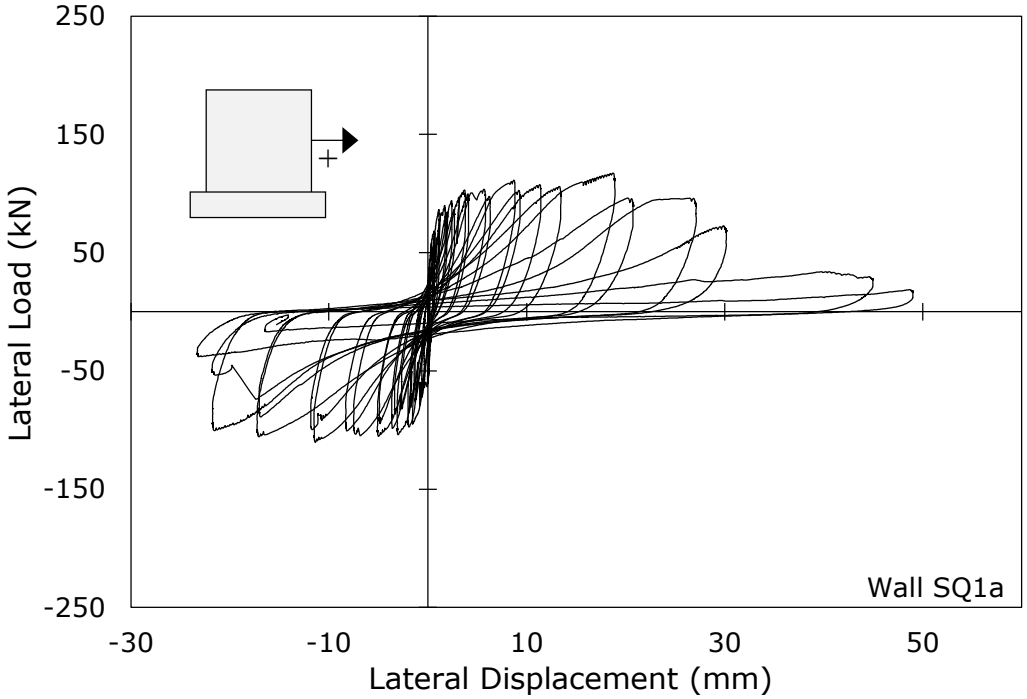


Figure B-56 Lateral load-lateral displacement response, sensor C4 in SQ1a

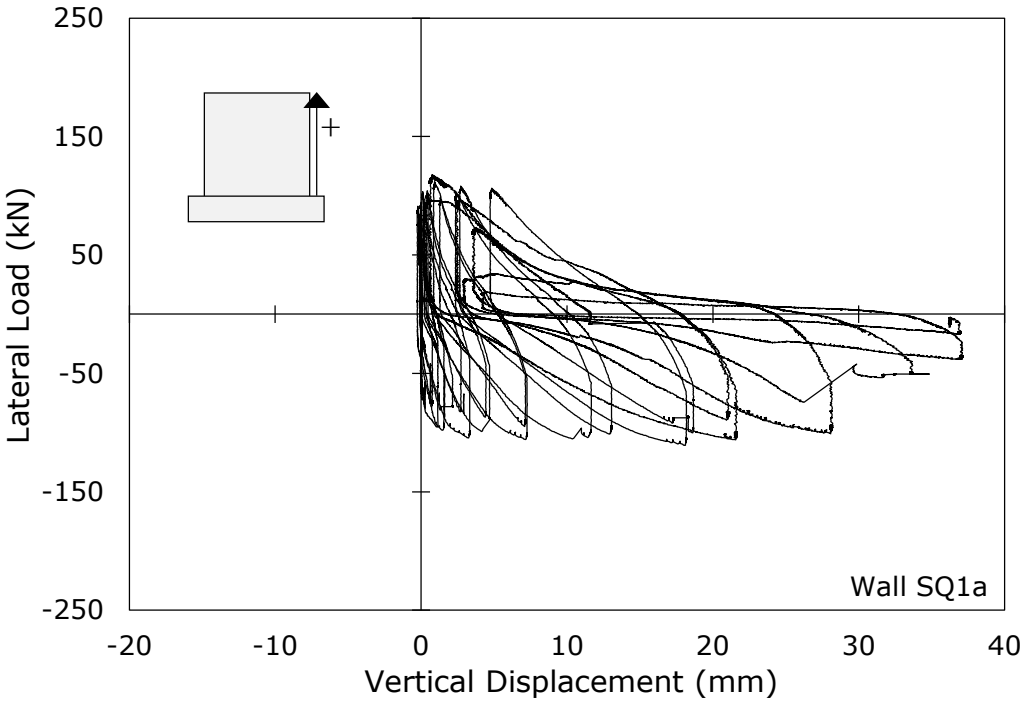


Figure B-57 Lateral load-vertical displacement response, sensor C6 in SQ1a

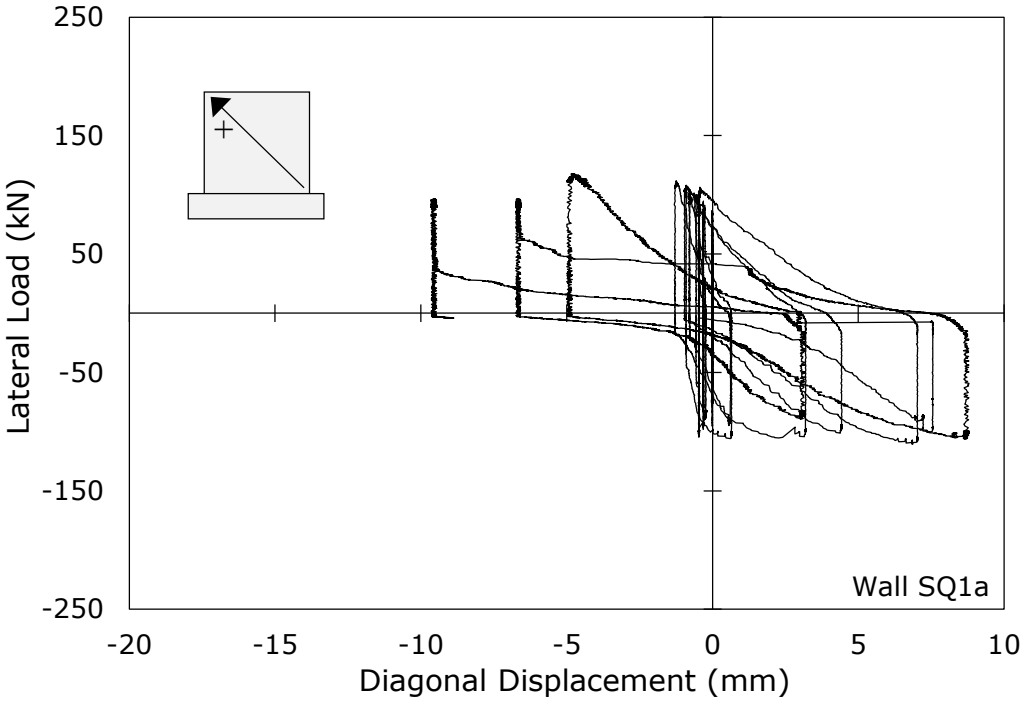


Figure B-58 Lateral load-diagonal displacement response, sensor C8 in SQ1a

B.6.2.3 Wall SQ1S

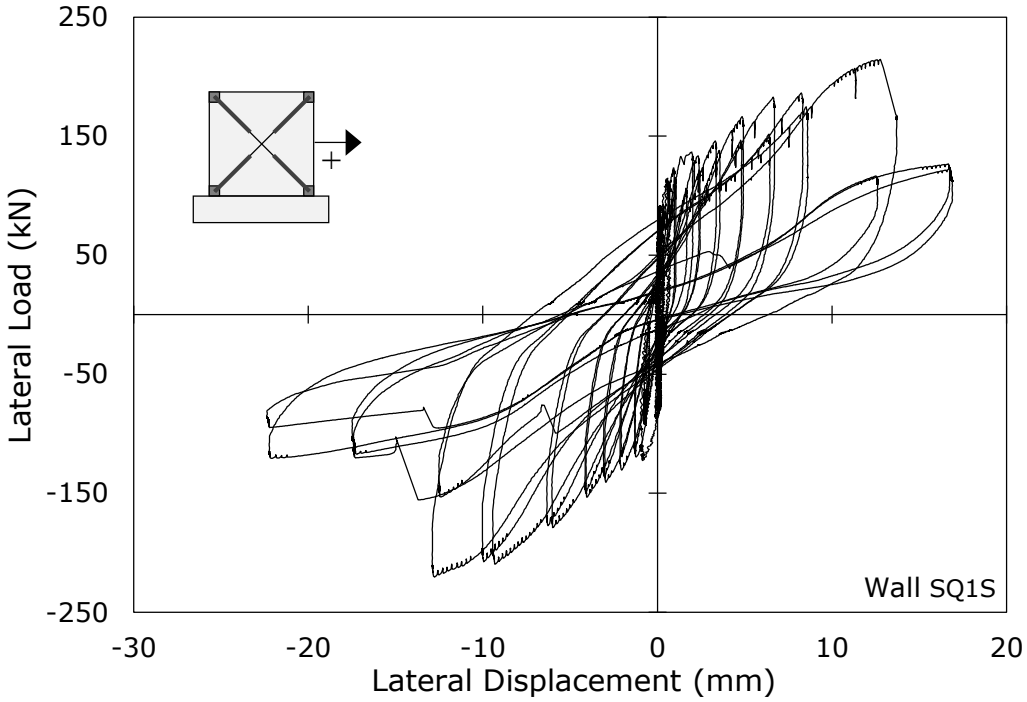


Figure B-59 Lateral load-lateral displacement response, sensor C4 in SQ1S

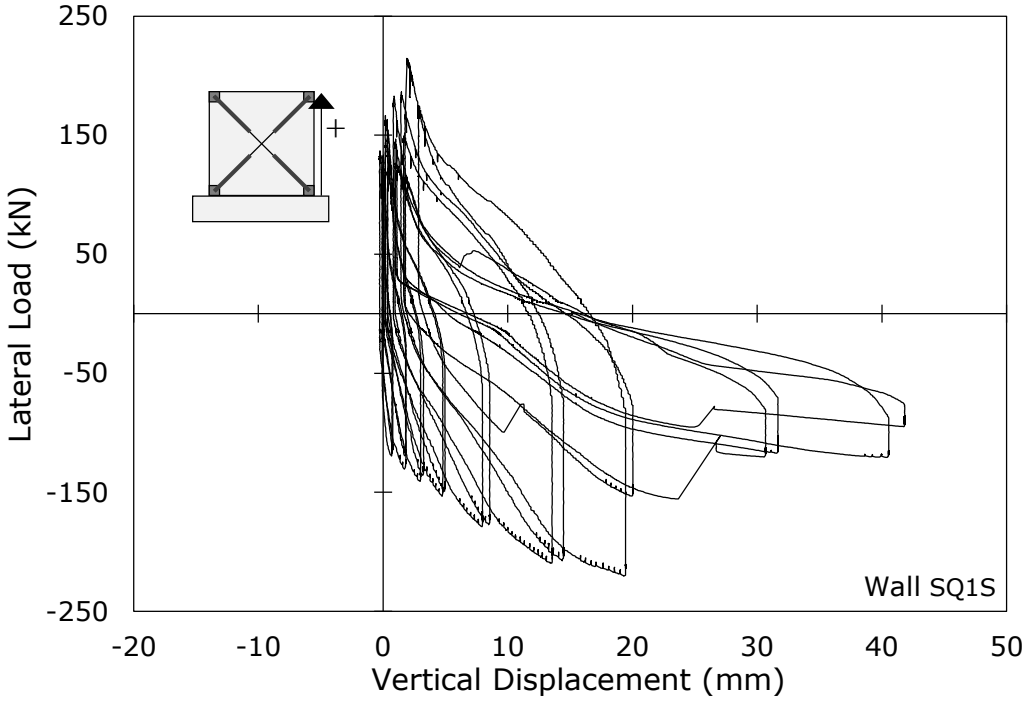


Figure B-60 Lateral load-vertical displacement response, sensor C6 in SQ1S

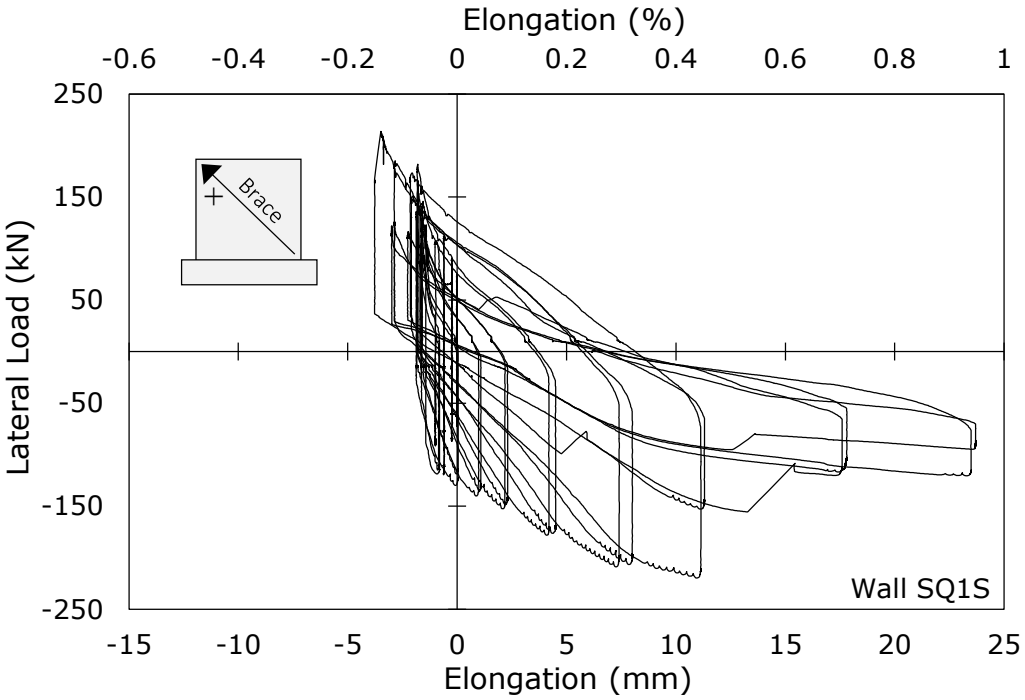


Figure B-61 Lateral load-brace elongation response, sensor C16 in SQ1S

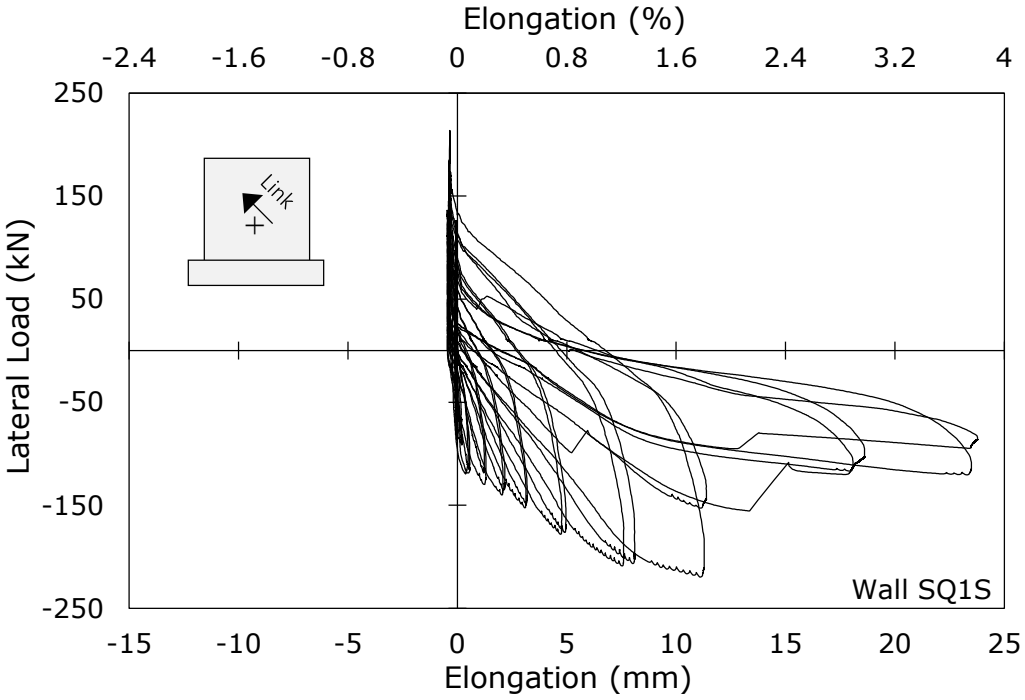


Figure B-62 Lateral load-link elongation response, sensor C18 in SQ1S

B.6.2.4 Wall SQ2

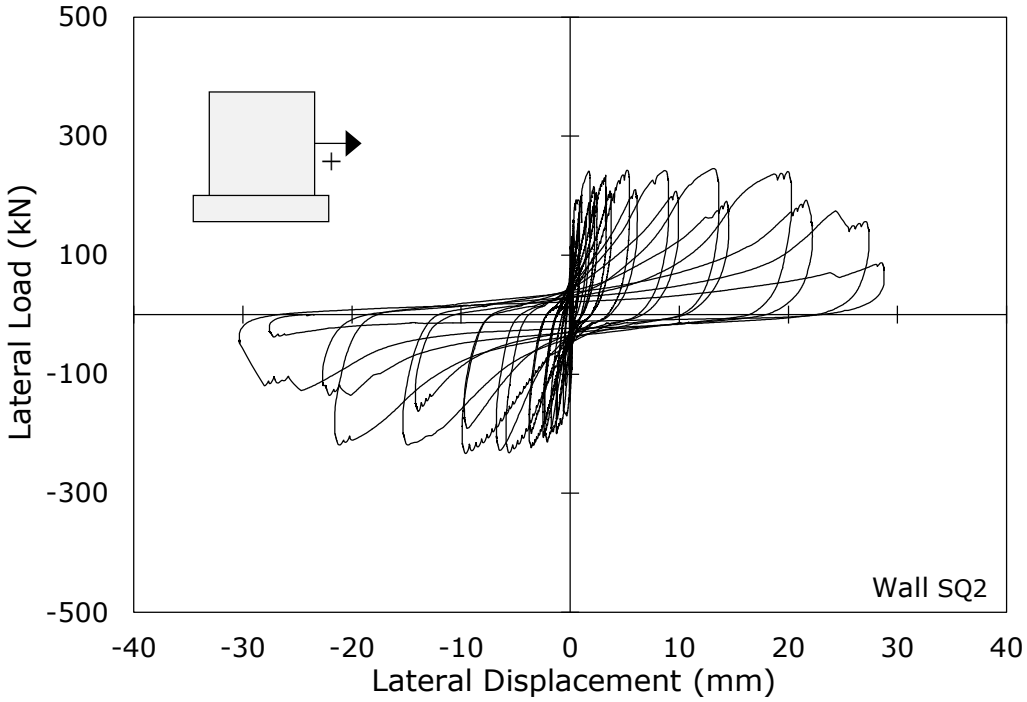


Figure B-63 Lateral load-lateral displacement response, sensor C4 in SQ2

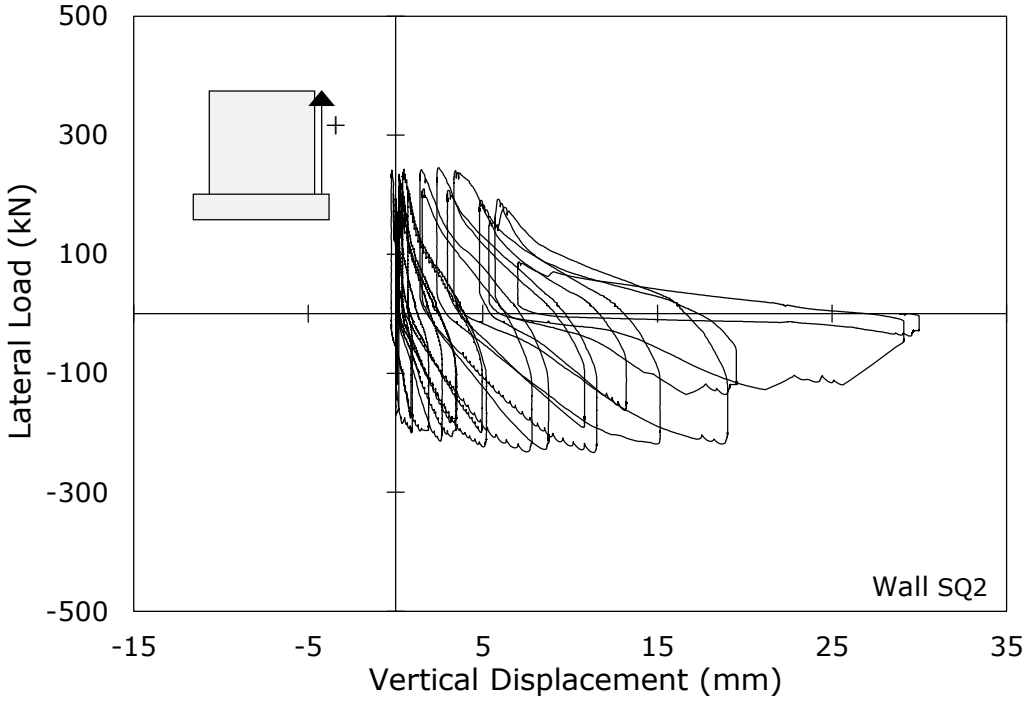


Figure B-64 Lateral load-vertical displacement response, sensor C6 in SQ2

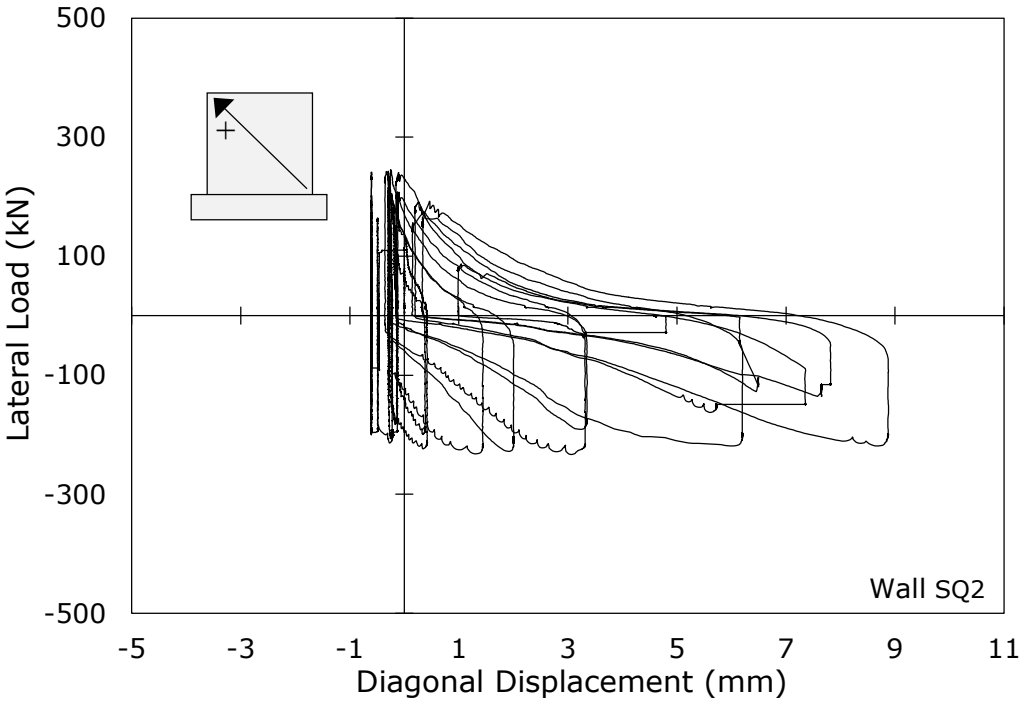


Figure B-65 Lateral load-diagonal displacement response, sensor C8 in SQ2

B.6.2.5 Wall SQ2S

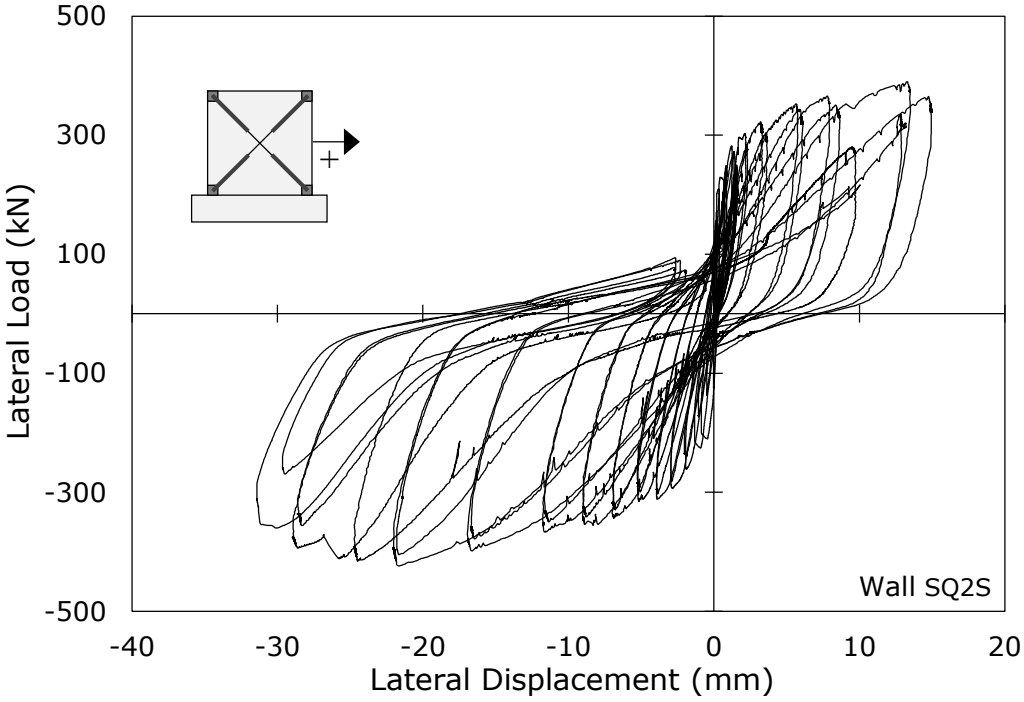


Figure B-66 Lateral load-lateral displacement response, sensor C4 in SQ2S

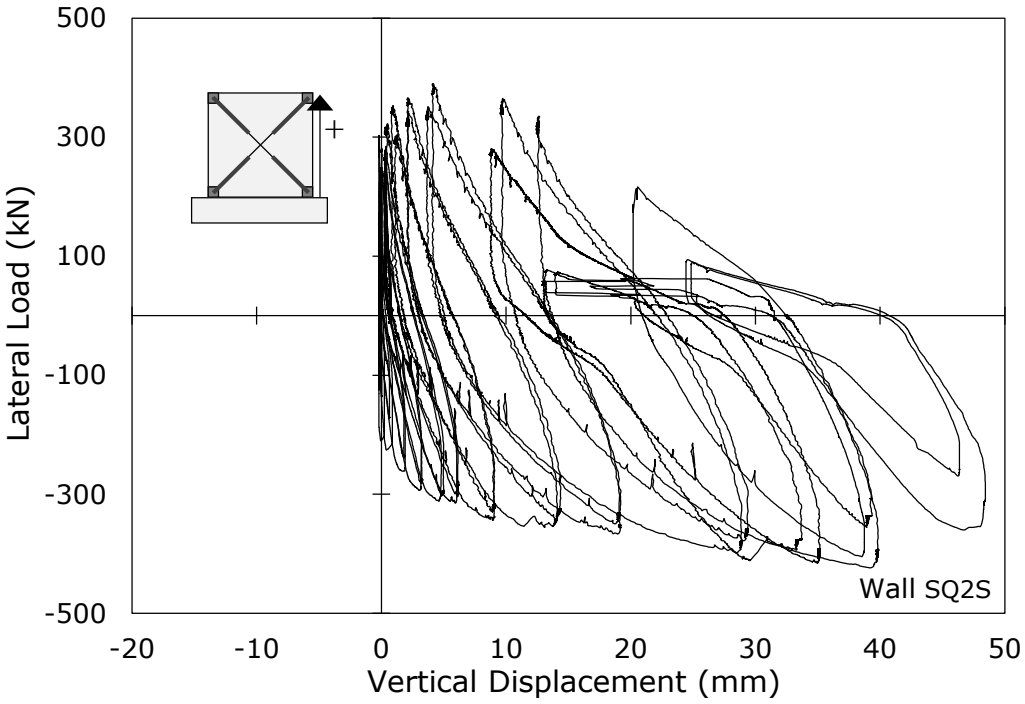


Figure B-67 Lateral load-vertical displacement response, sensor C6 in SQ2S

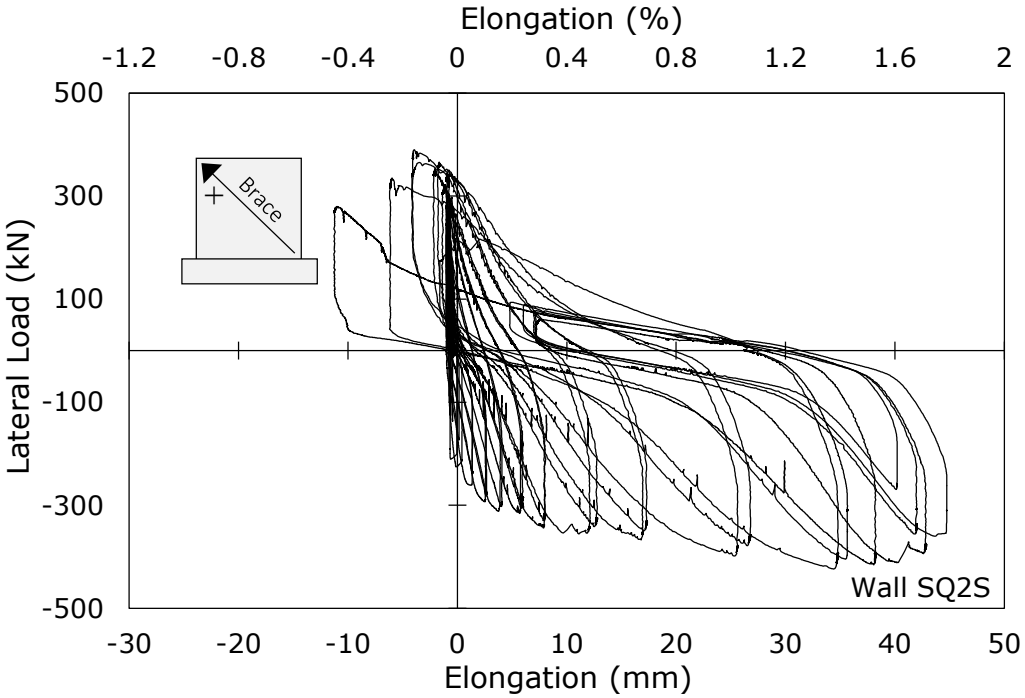


Figure B-68 Lateral load-brace elongation response, sensor C16 in SQ2S

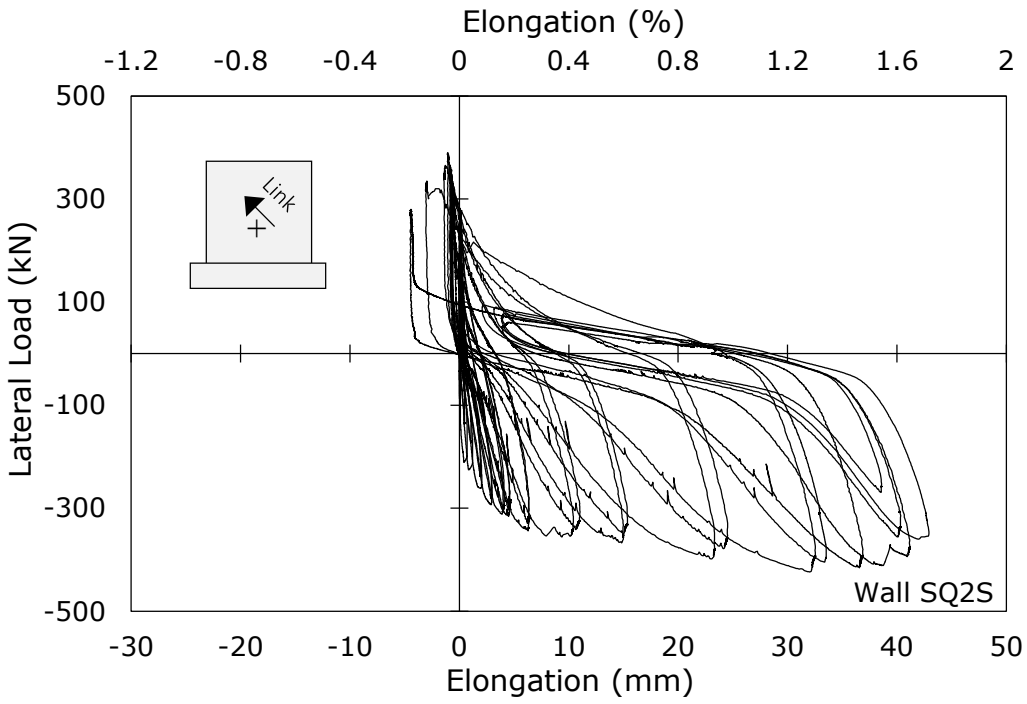


Figure B-69 Lateral load-link elongation response, sensor C18 in SQ2S

B.6.3 Internal Reinforcement Strains

The main strain responses of the internal reinforcement in the walls are illustrated in Figure B-70 to Figure B-103. The response of strain gauges that did not capture yielding are not reported herein.

B.6.3.1 Wall SQ1

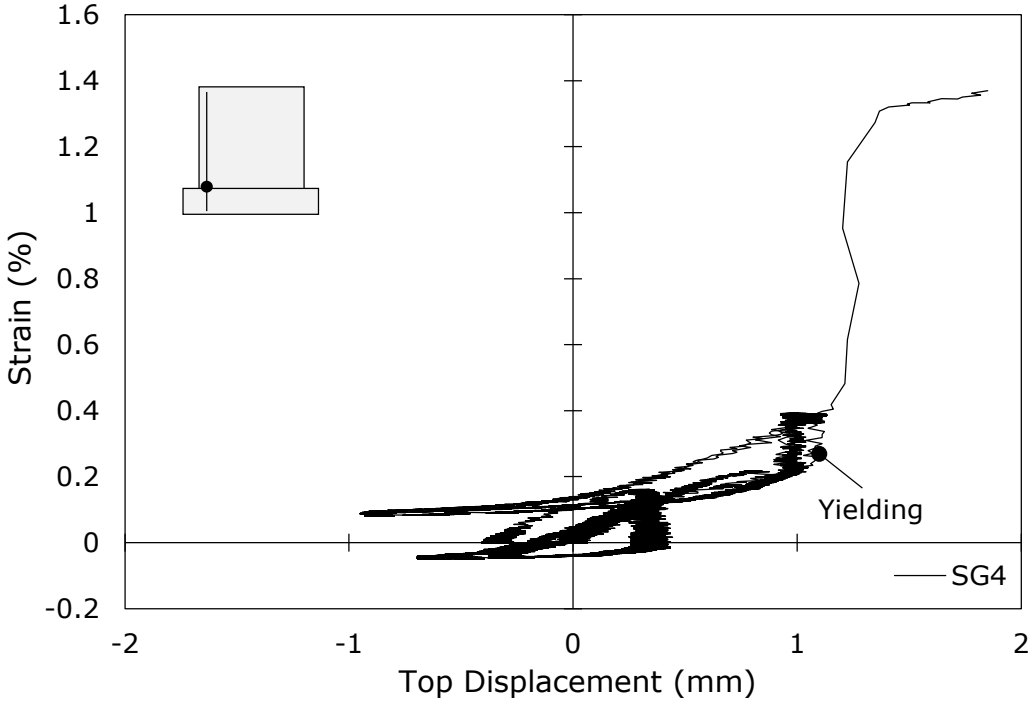


Figure B-70 Strain response of longitudinal reinforcement, strain gauge 4 in SQ1

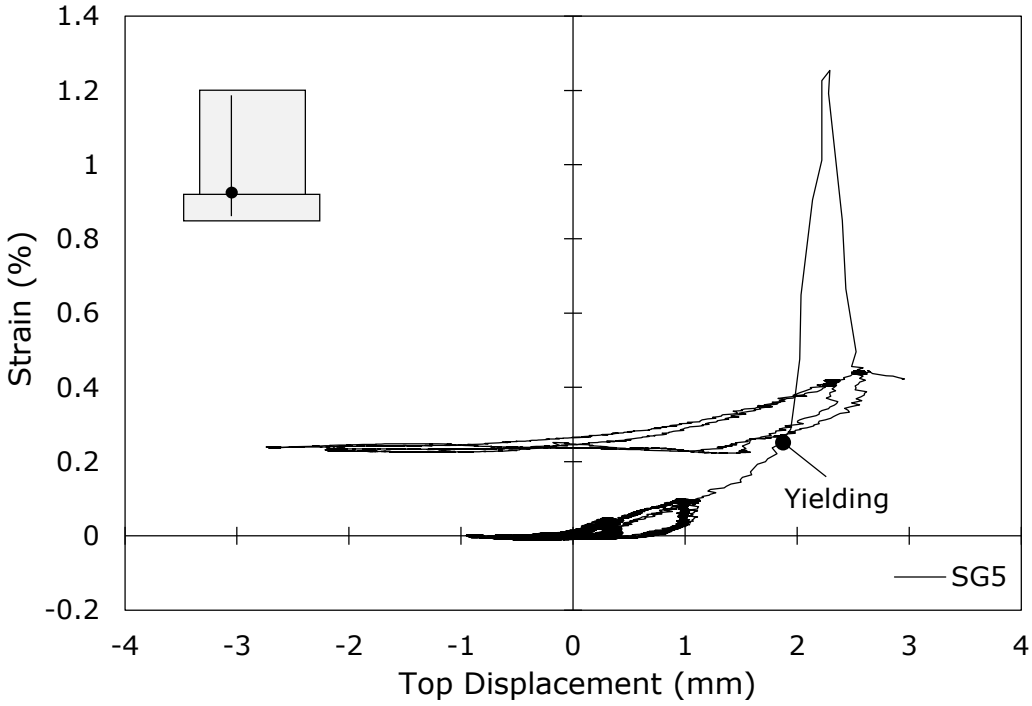


Figure B-71 Strain response of longitudinal reinforcement, strain gauge 5 in SQ1

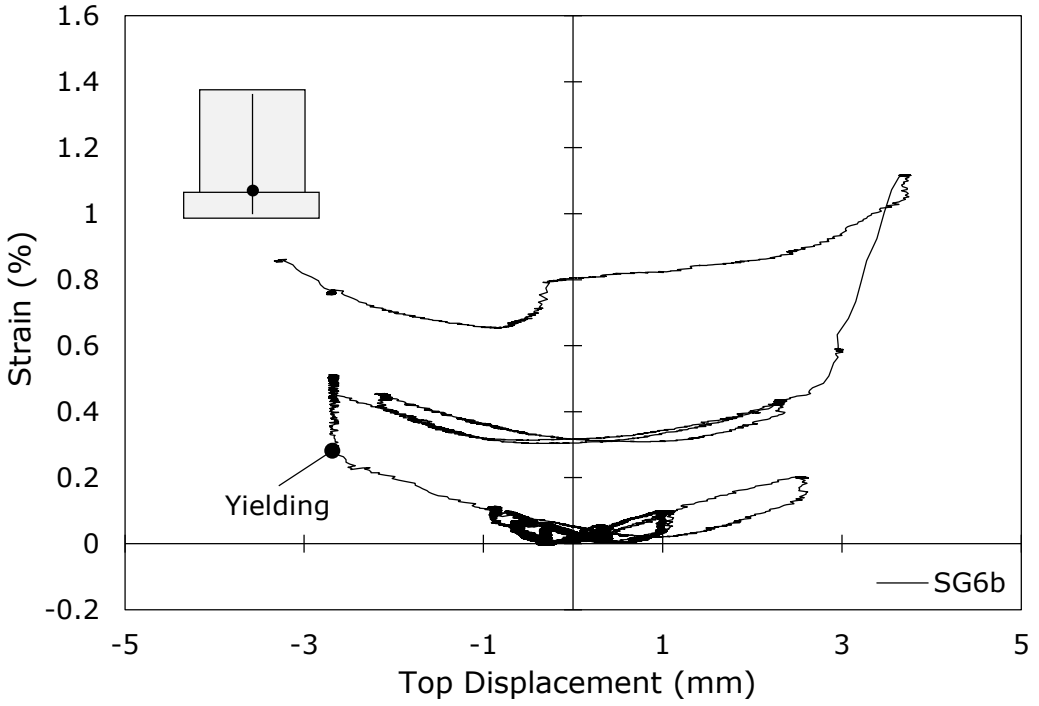


Figure B-72 Strain response of longitudinal reinforcement, strain gauge 6b in SQ1

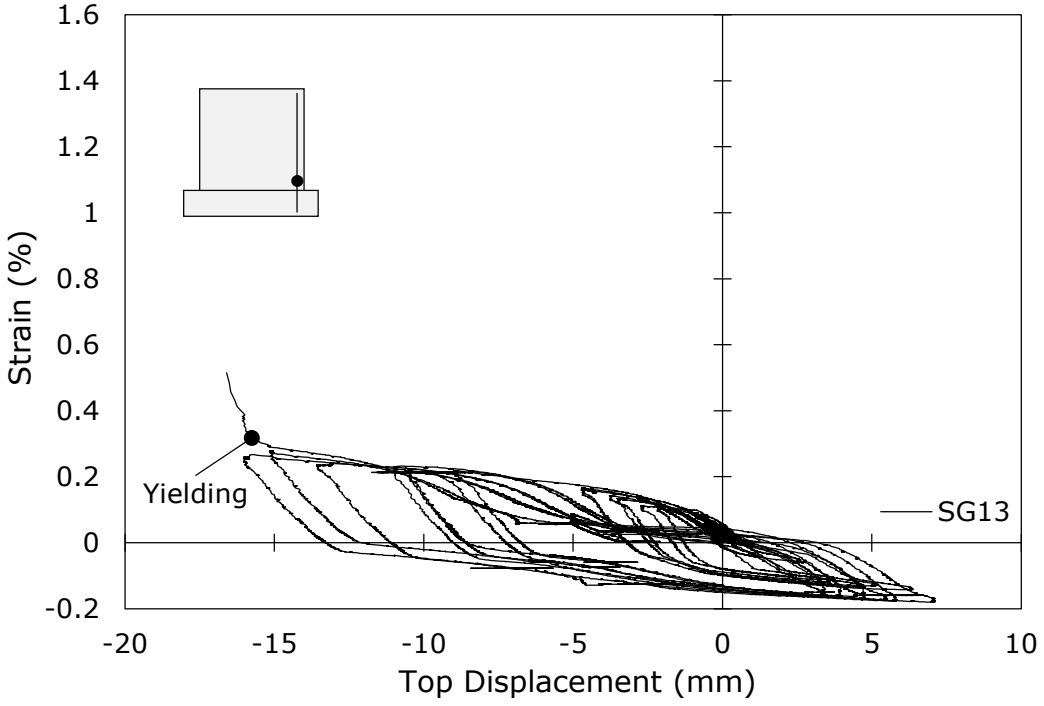


Figure B-73 Strain response of longitudinal reinforcement, strain gauge 13 in SQ1

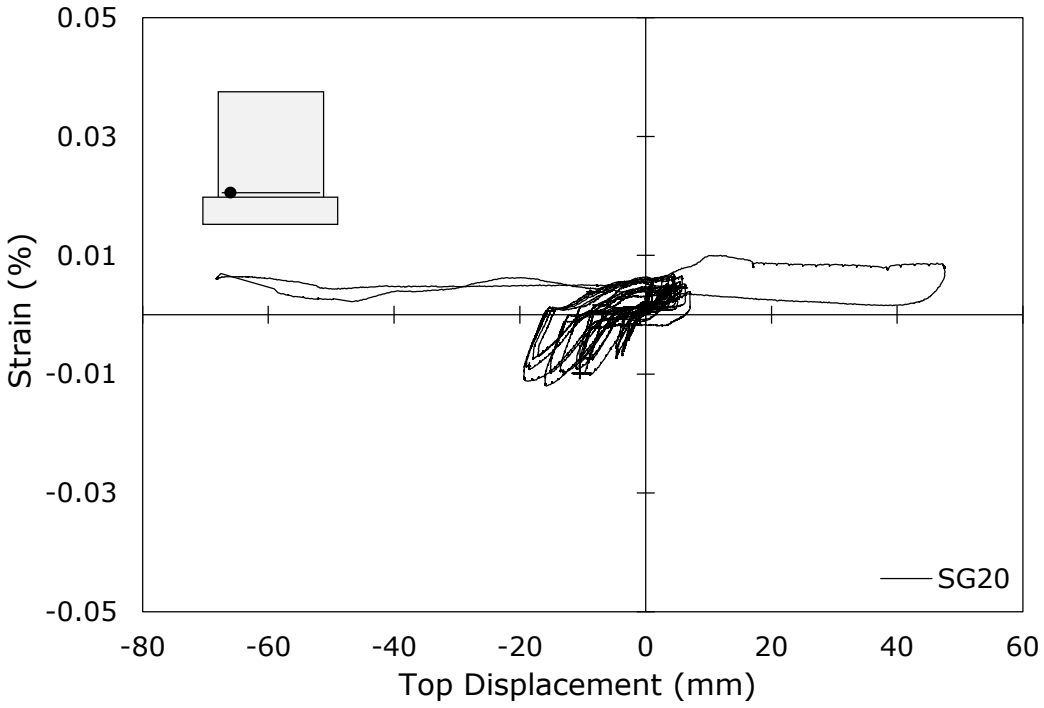


Figure B-74 Strain response of transverse reinforcement, strain gauge 20 in SQ1

B.6.3.2 Wall SQ1a

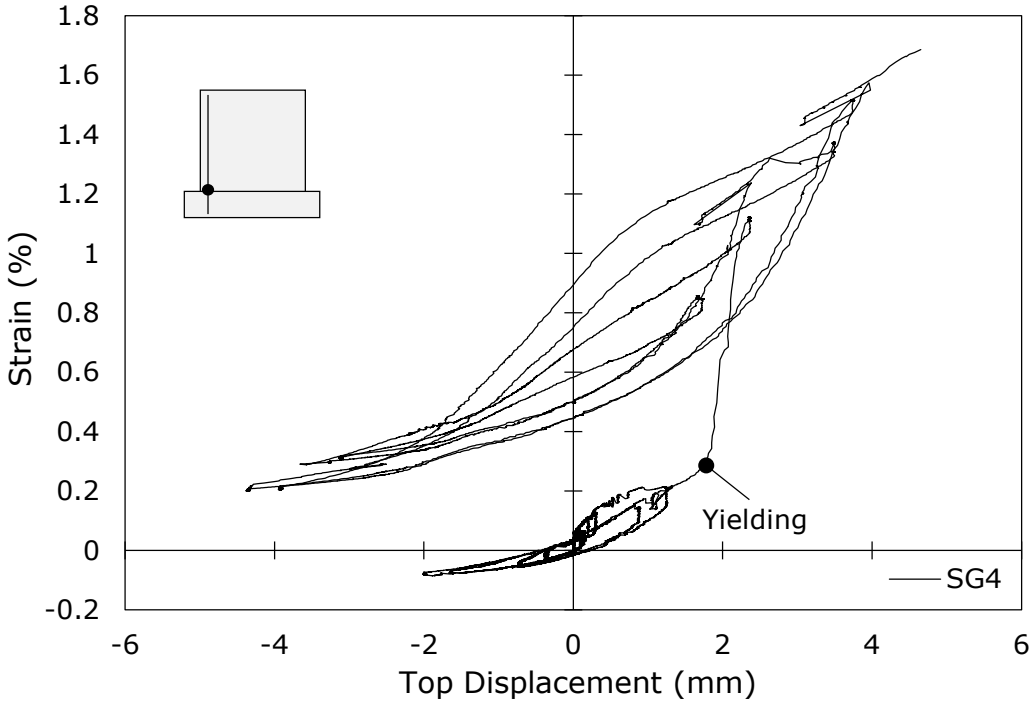


Figure B-75 Strain response of longitudinal reinforcement, strain gauge 4 in SQ1a

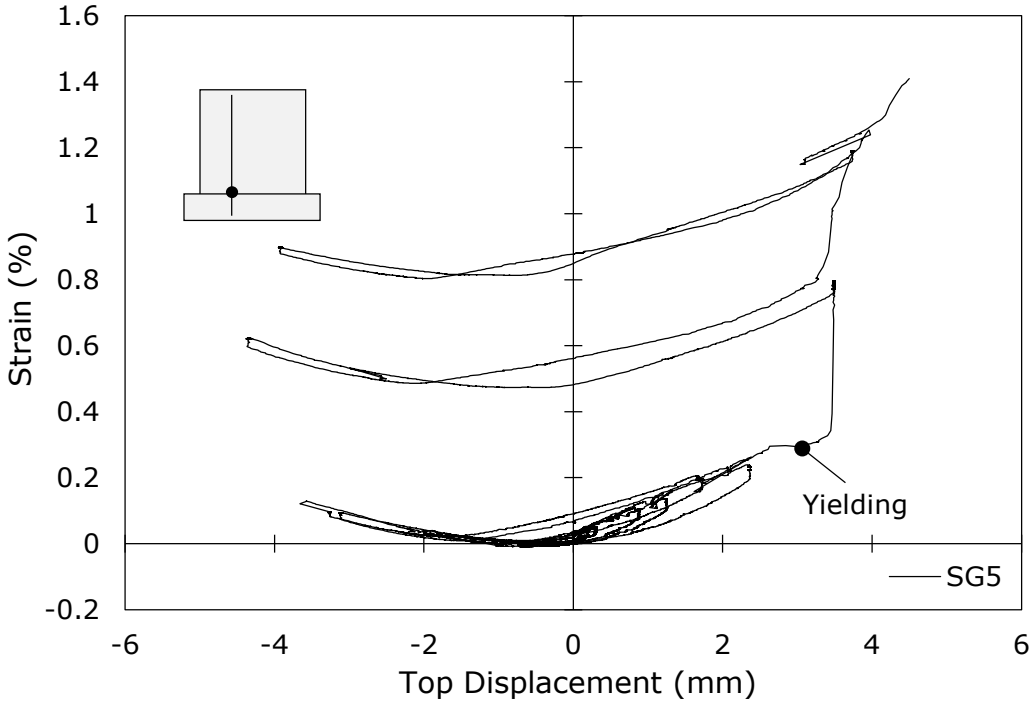


Figure B-76 Strain response of longitudinal reinforcement, strain gauge 5 in SQ1a

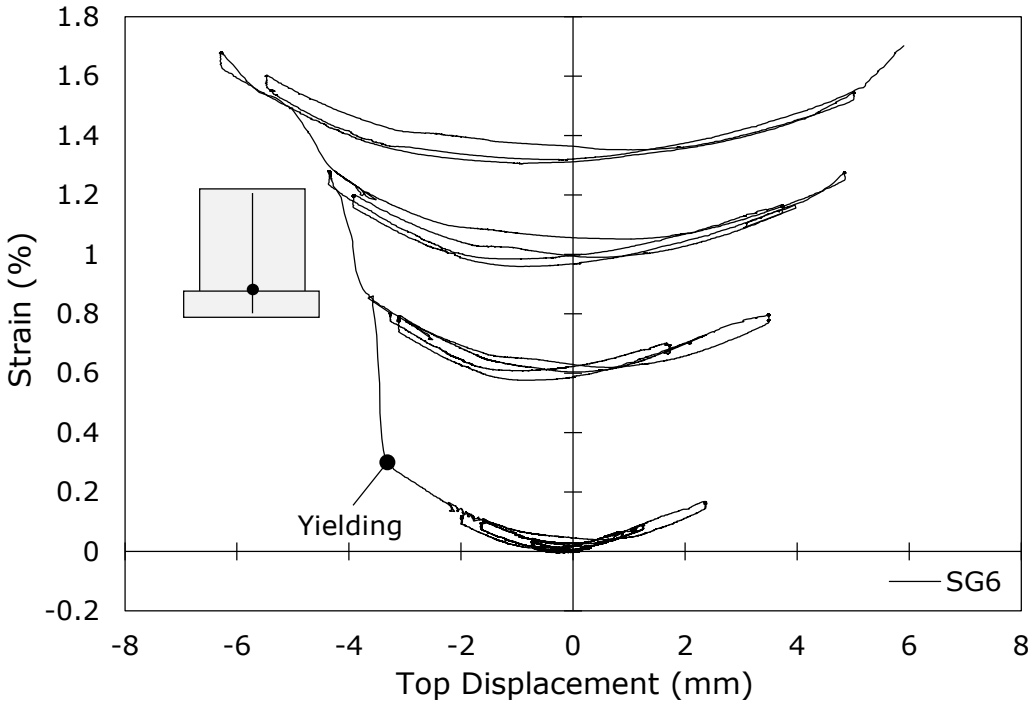


Figure B-77 Strain response of longitudinal reinforcement, strain gauge 6 in SQ1a

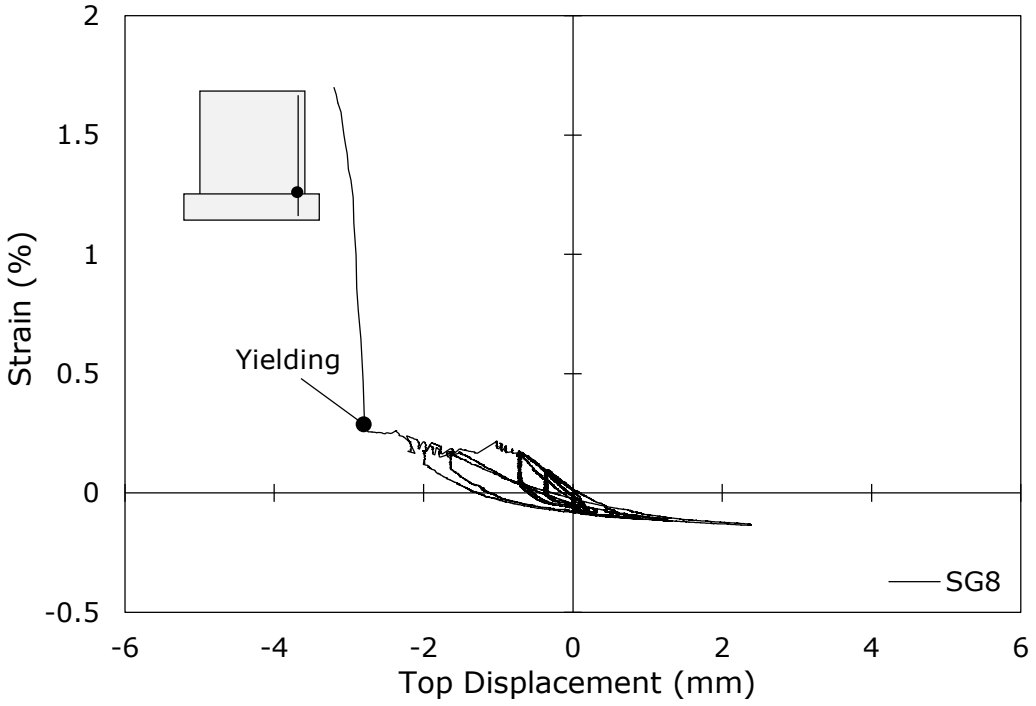


Figure B-78 Strain response of longitudinal reinforcement, strain gauge 8 in SQ1a

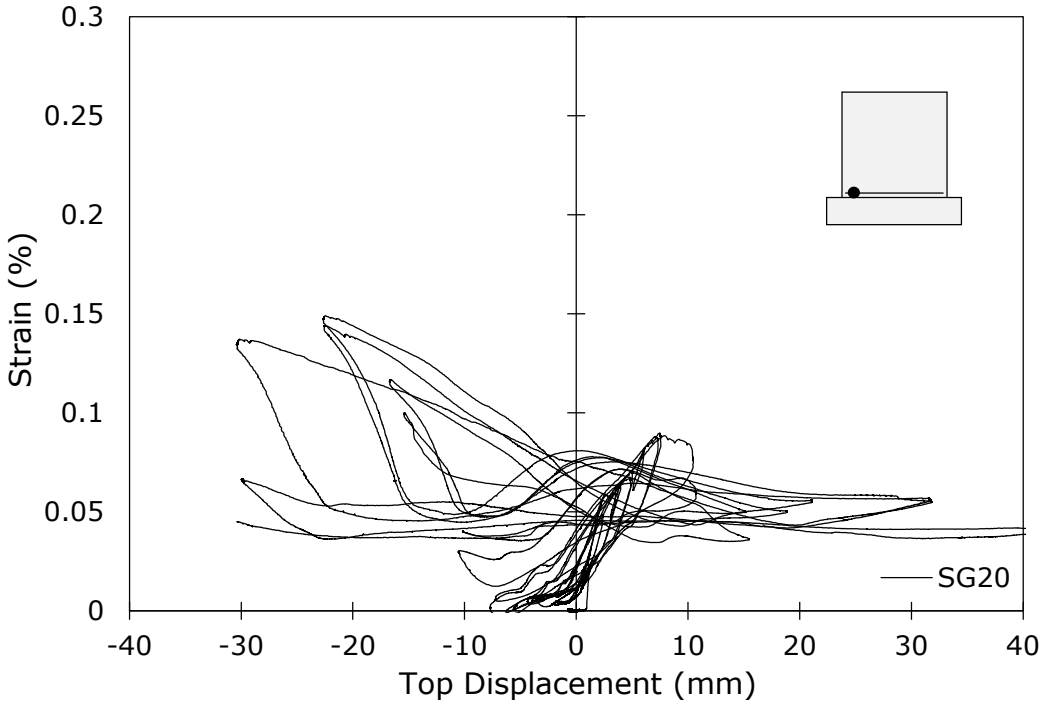


Figure B-79 Strain response of transverse reinforcement, strain gauge 20 in SQ1a

B.6.3.3 Wall SQ1S

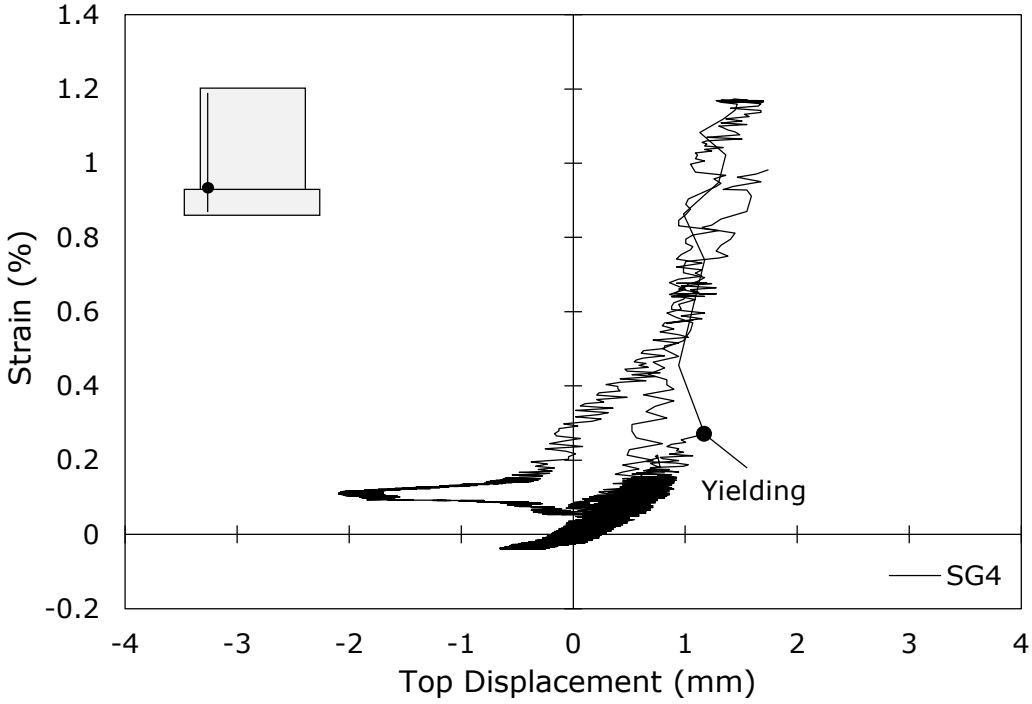


Figure B-80 Strain response of longitudinal reinforcement, strain gauge 4 in SQ1S

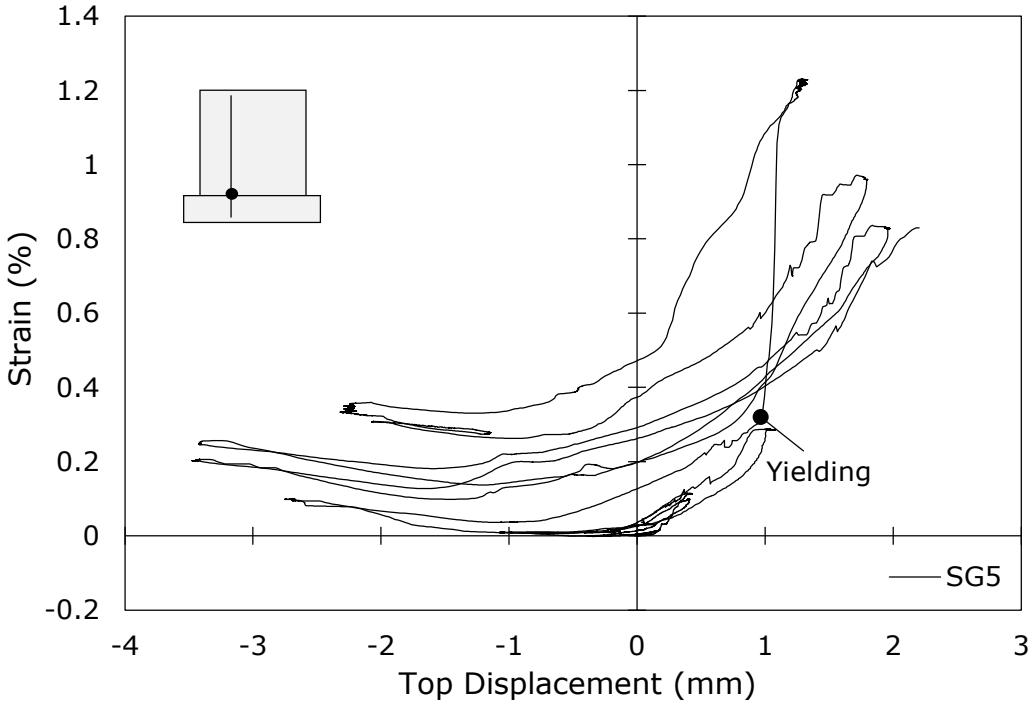


Figure B-81 Strain response of longitudinal reinforcement, strain gauge 5 in SQ1S

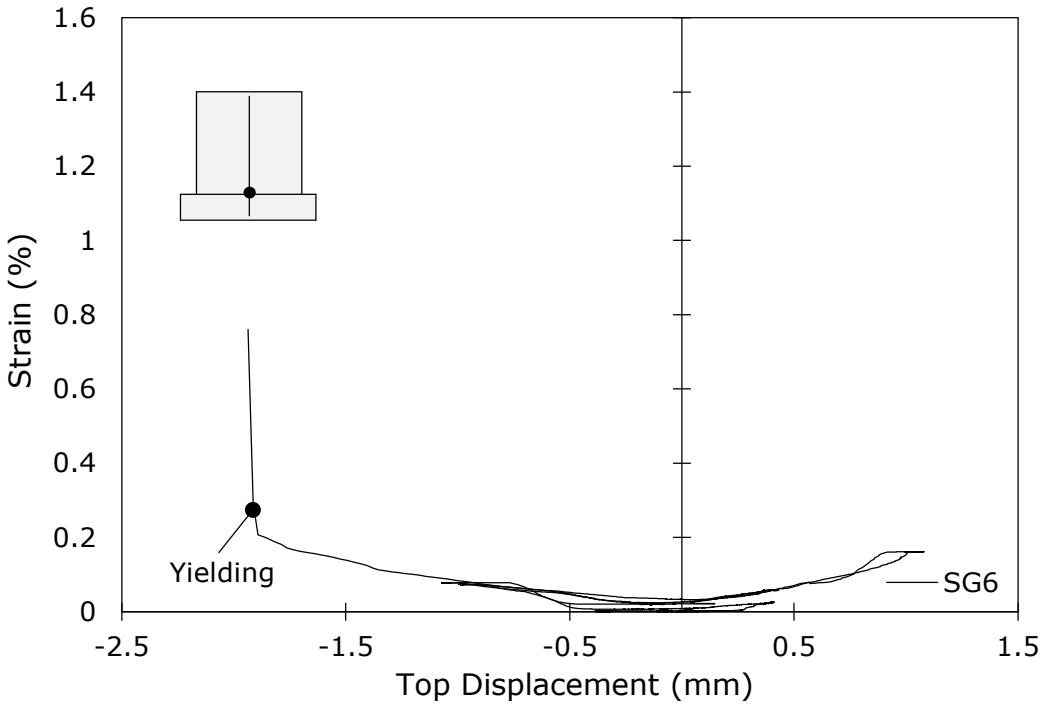


Figure B-82 Strain response of longitudinal reinforcement, strain gauge 6 in SQ1S

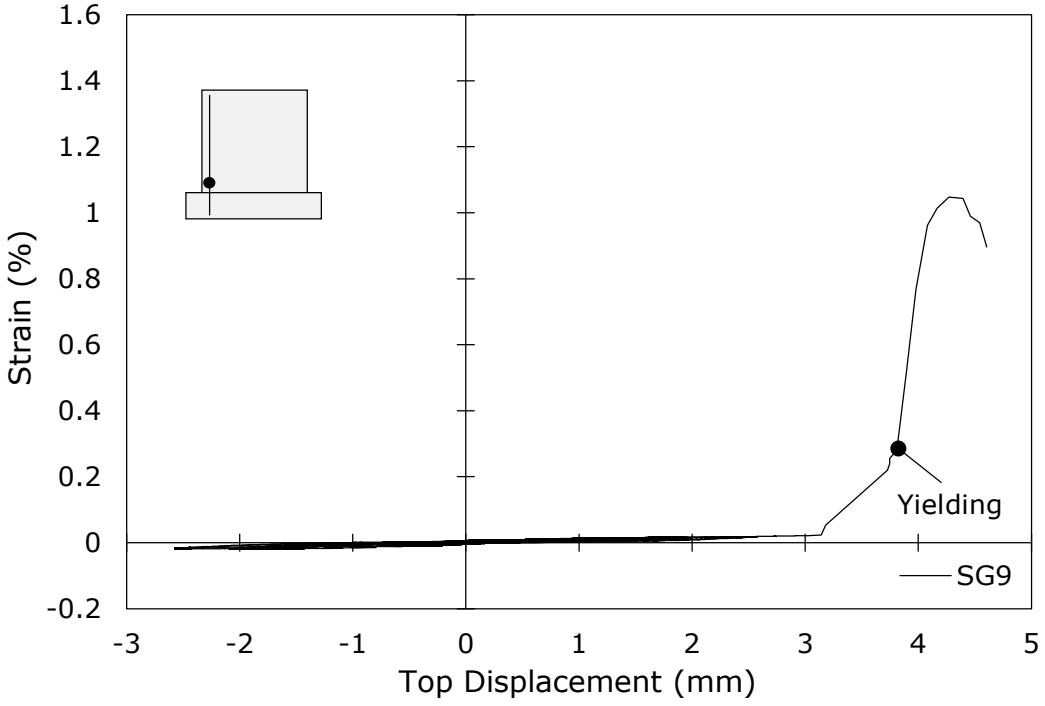


Figure B-83 Strain response of longitudinal reinforcement, strain gauge 9 in SQ1S

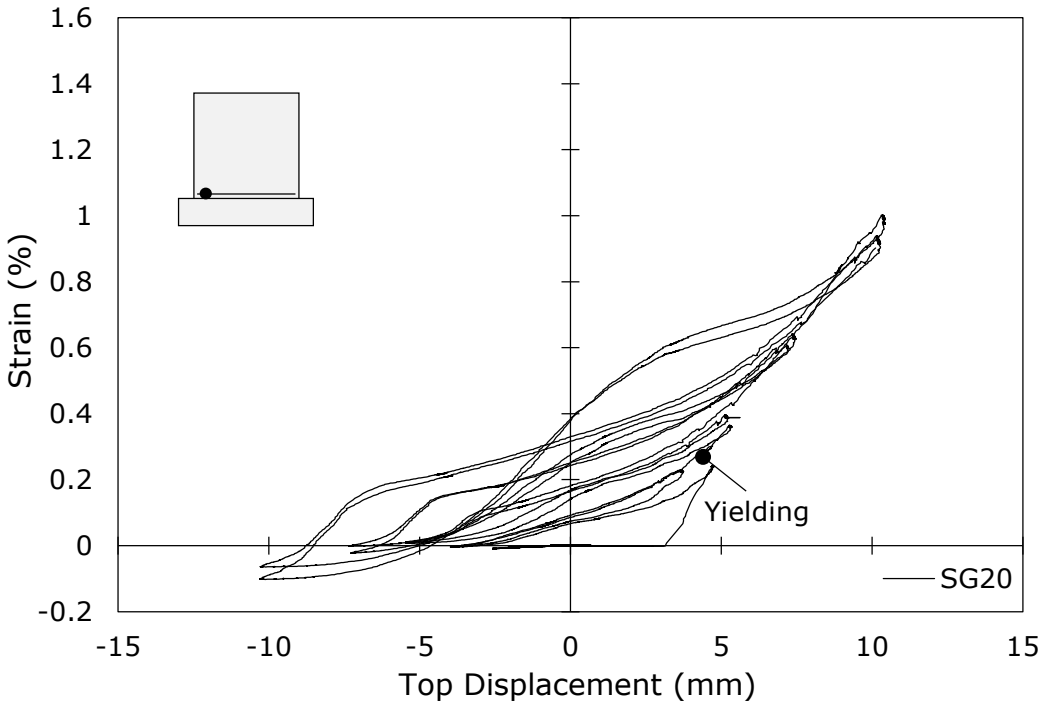


Figure B-84 Strain response of transverse reinforcement, strain gauge 20 in SQ1S

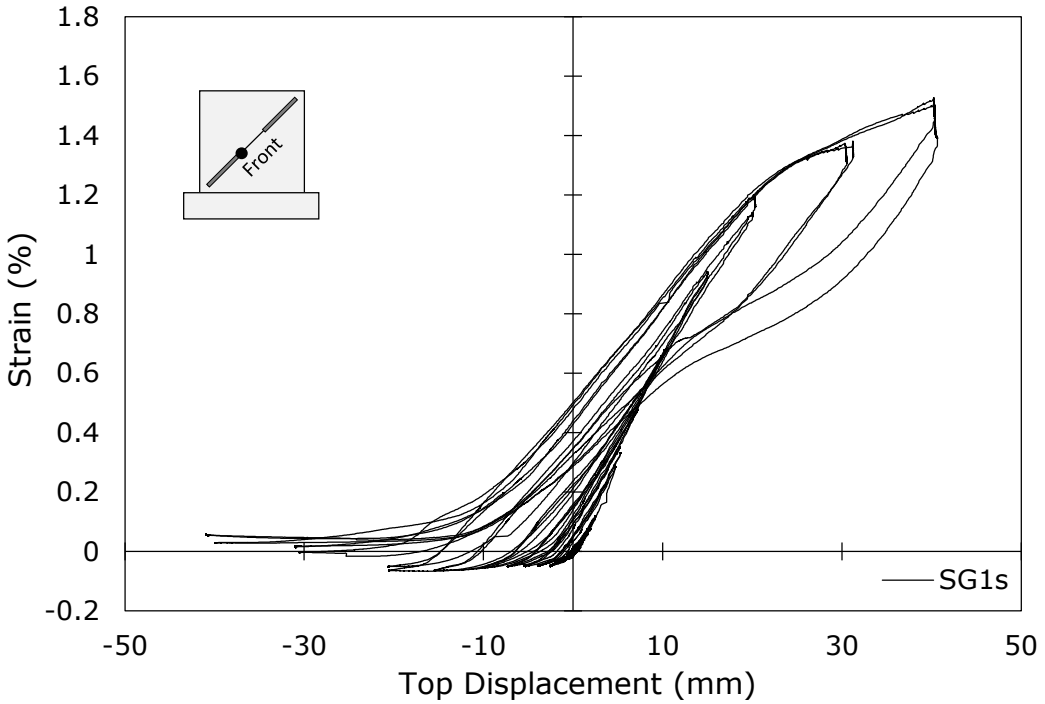


Figure B-85 Strain response of SMA link, strain gauge 1s in front brace in SQ1S

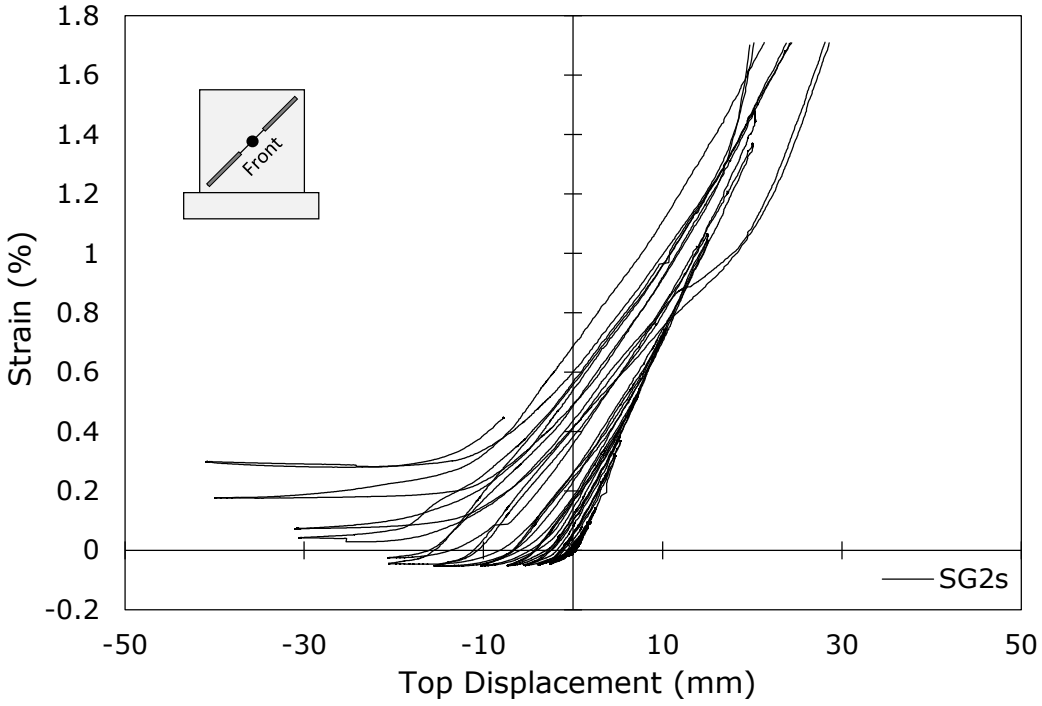


Figure B-86 Strain response of SMA link, strain gauge 2s in front brace in SQ1S

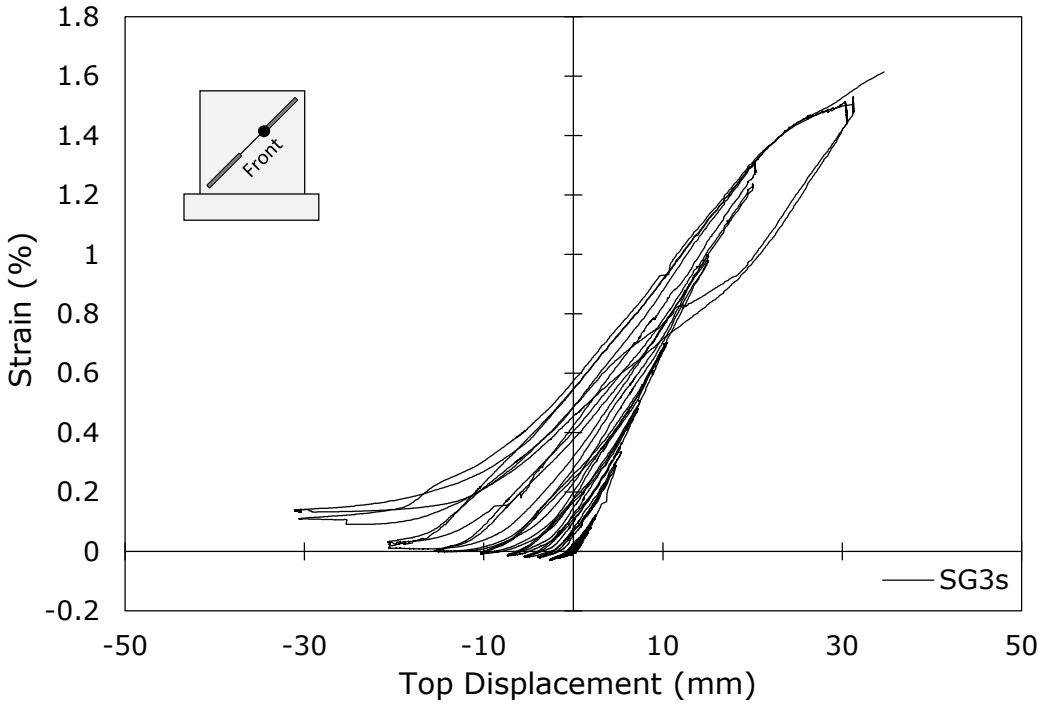


Figure B-87 Strain response of SMA link, strain gauge 3s in front brace in SQ1S

B.6.3.4 Wall SQ2

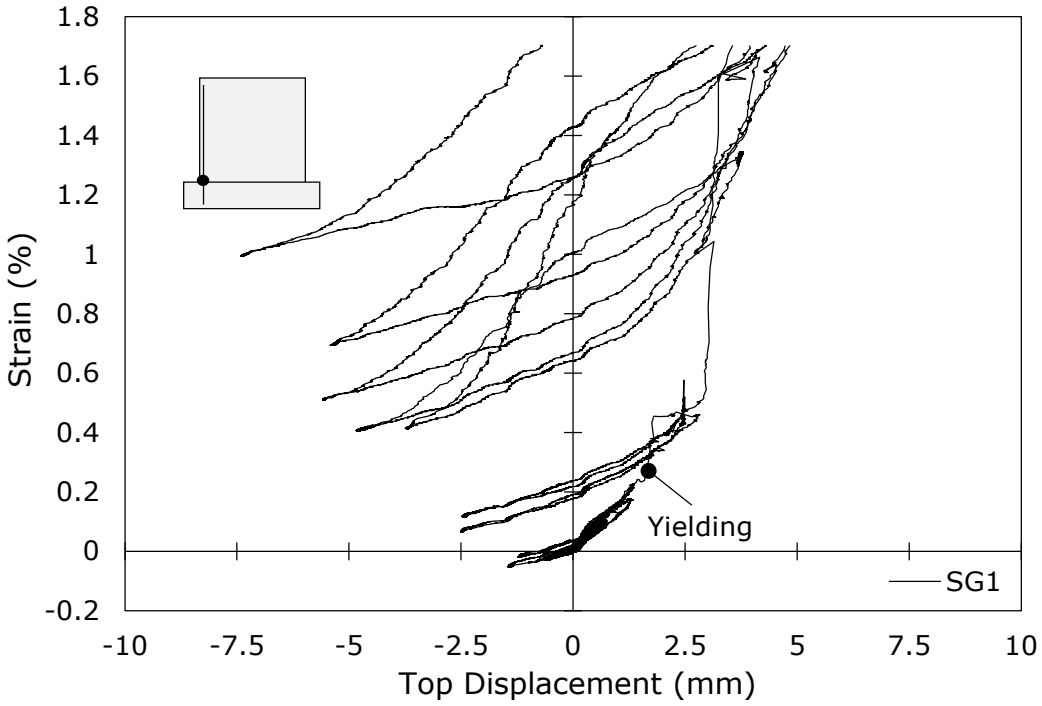


Figure B-88 Strain response of longitudinal reinforcement, strain gauge 1 in SQ2

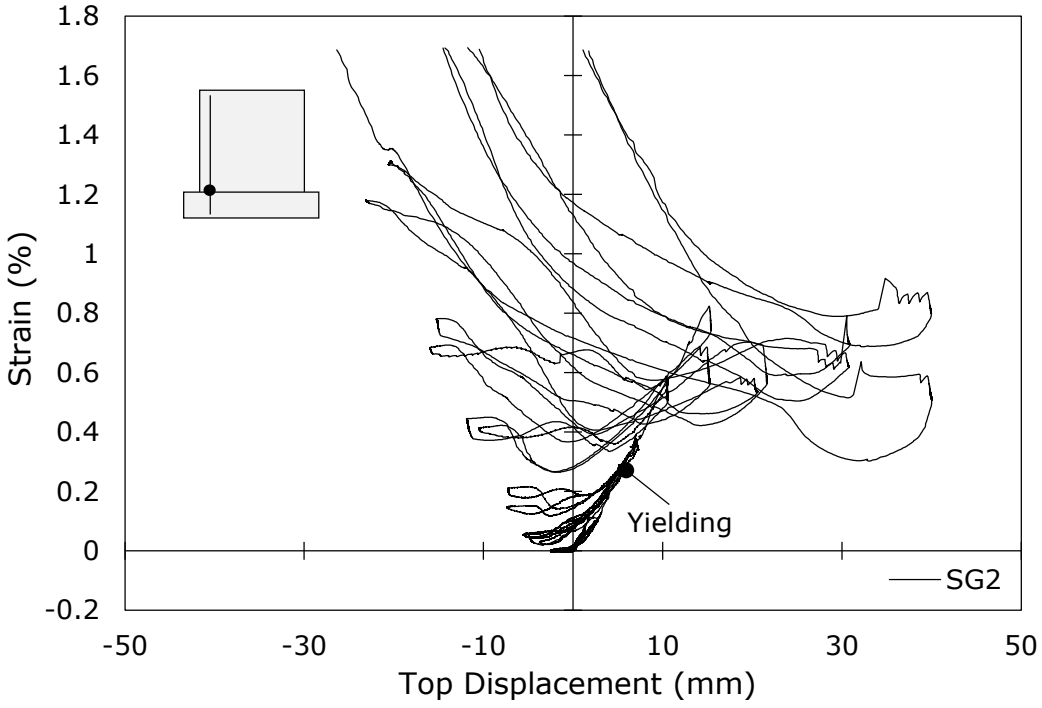


Figure B-89 Strain response of longitudinal reinforcement, strain gauge 2 in SQ2

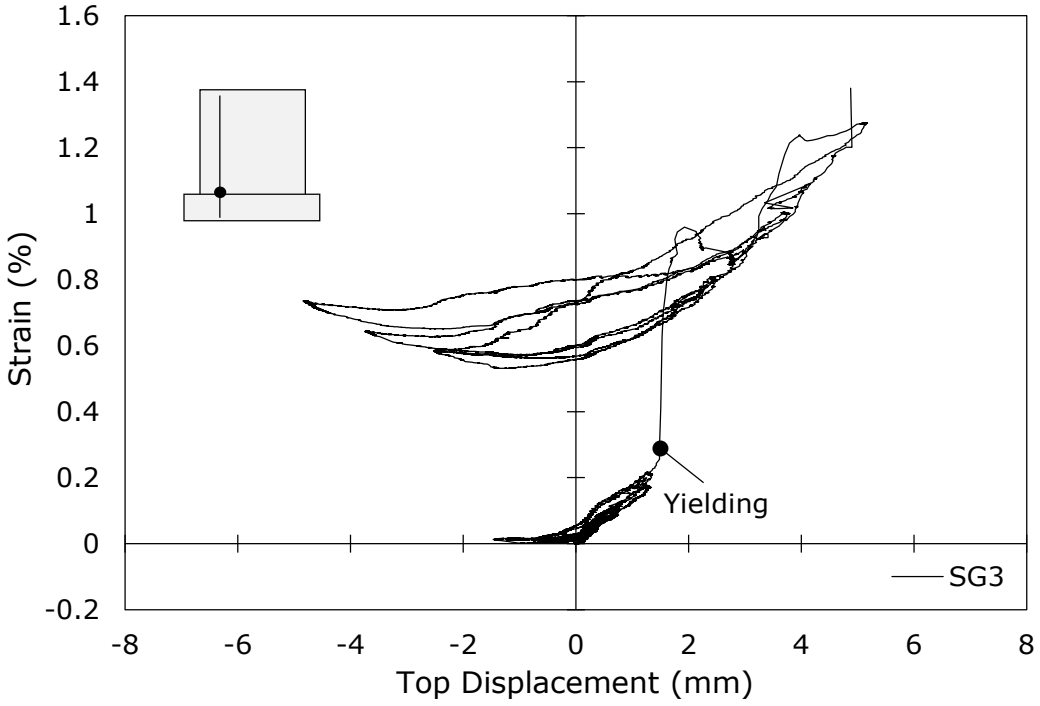


Figure B-90 Strain response of longitudinal reinforcement, strain gauge 3 in SQ2

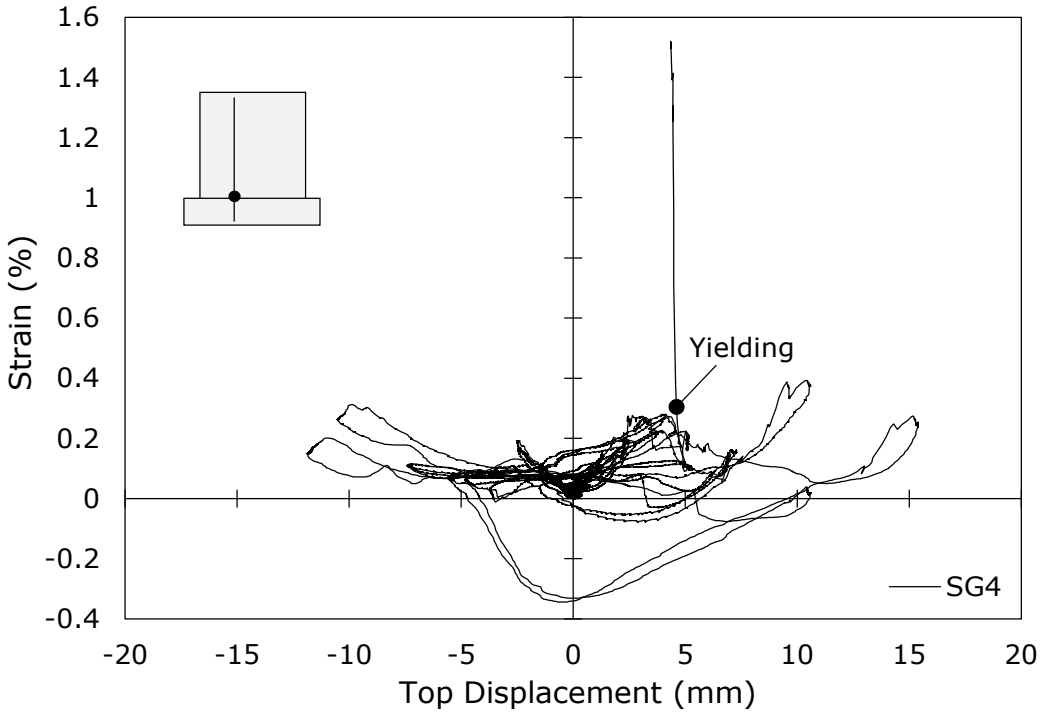


Figure B-91 Strain response of longitudinal reinforcement, strain gauge 4 in SQ2

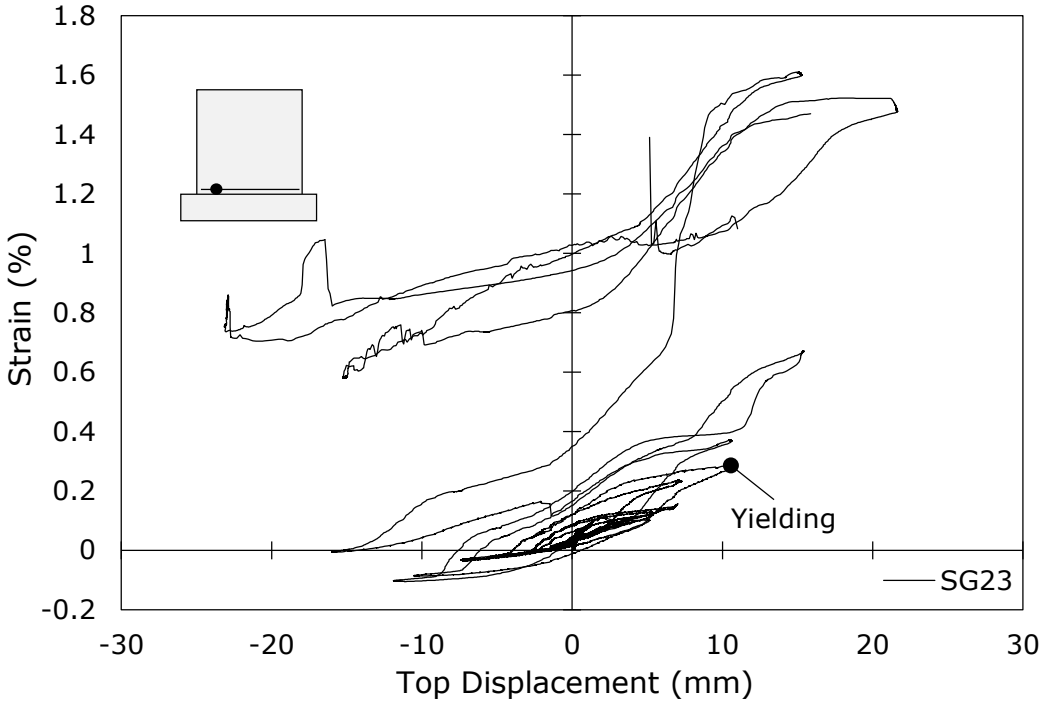


Figure B-92 Strain response of transverse reinforcement, strain gauge 23 in SQ2

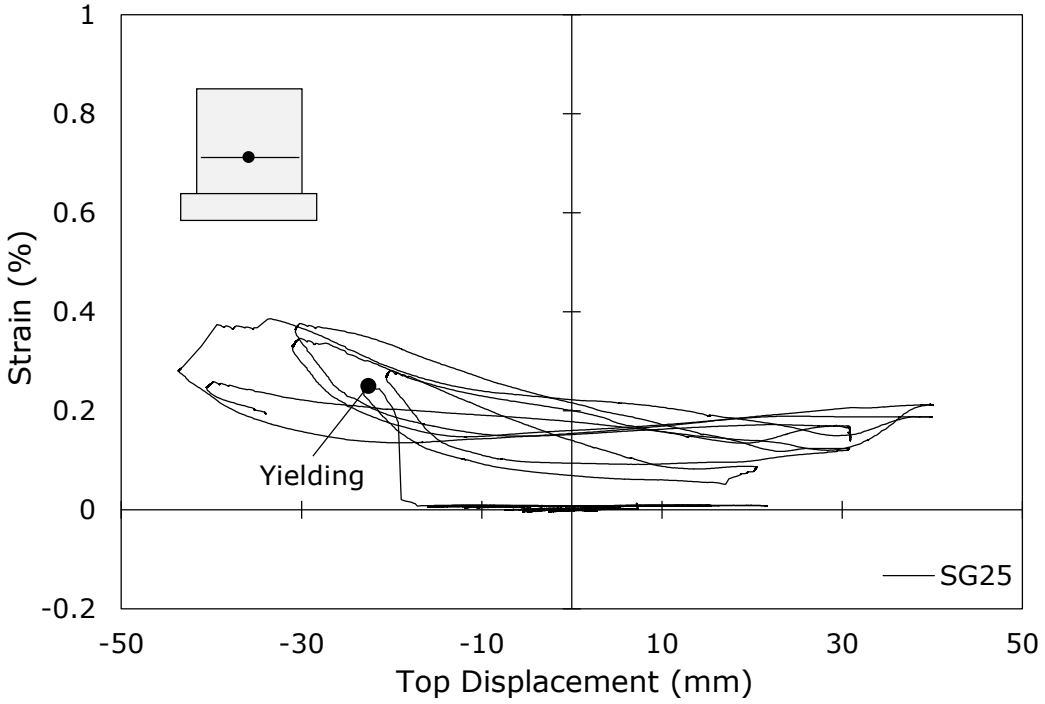


Figure B-93 Strain response of transverse reinforcement, strain gauge 25 in SQ2

B.6.3.5 Wall SQ2S

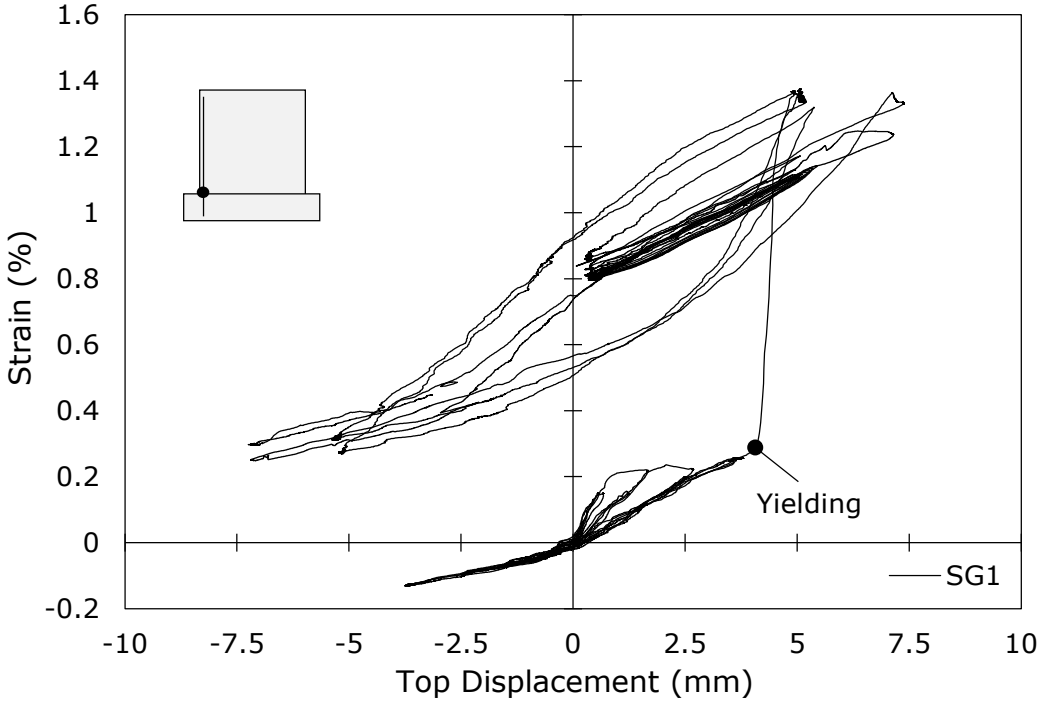


Figure B-94 Strain response of longitudinal reinforcement, strain gauge 1 in SQ2S

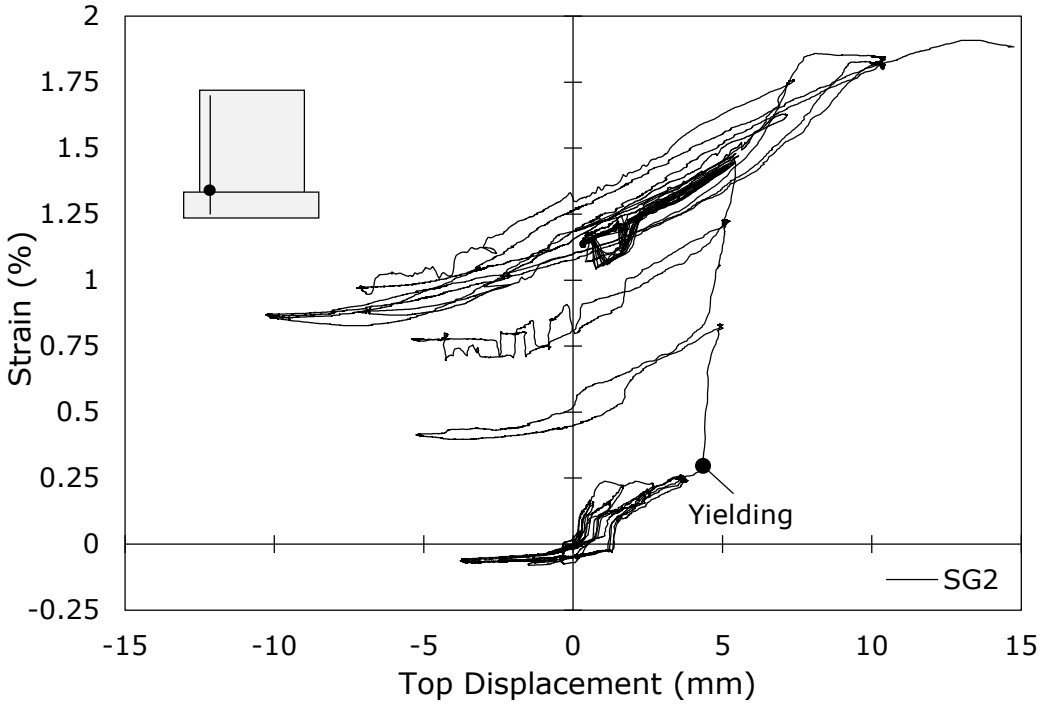


Figure B-95 Strain response of longitudinal reinforcement, strain gauge 2 in SQ2S

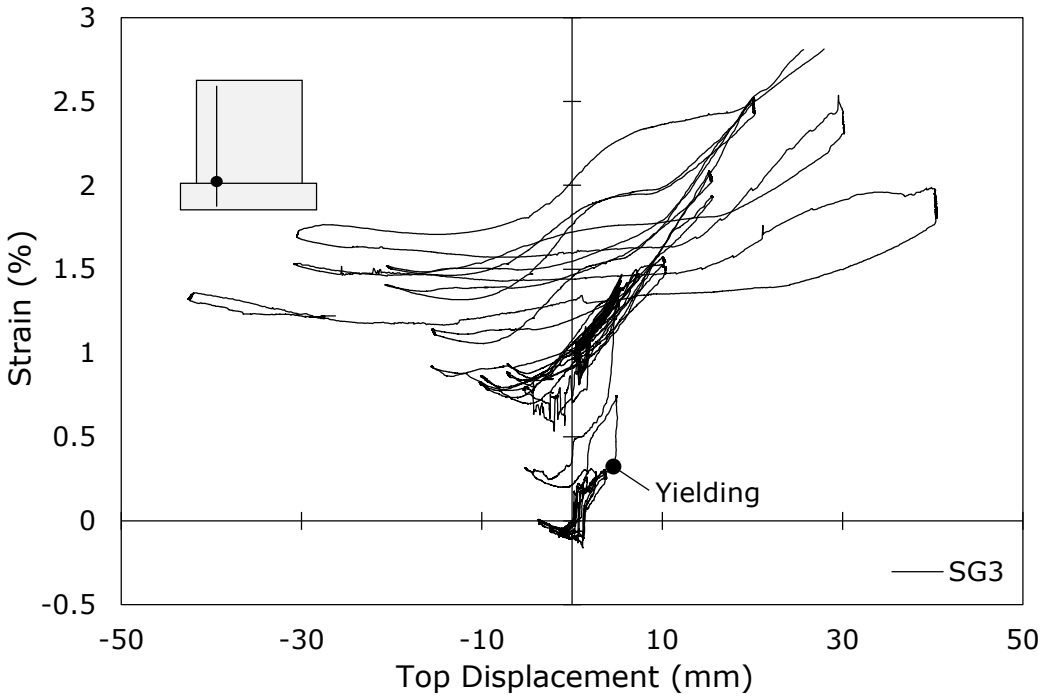


Figure B-96 Strain response of longitudinal reinforcement, strain gauge 3 in SQ2S

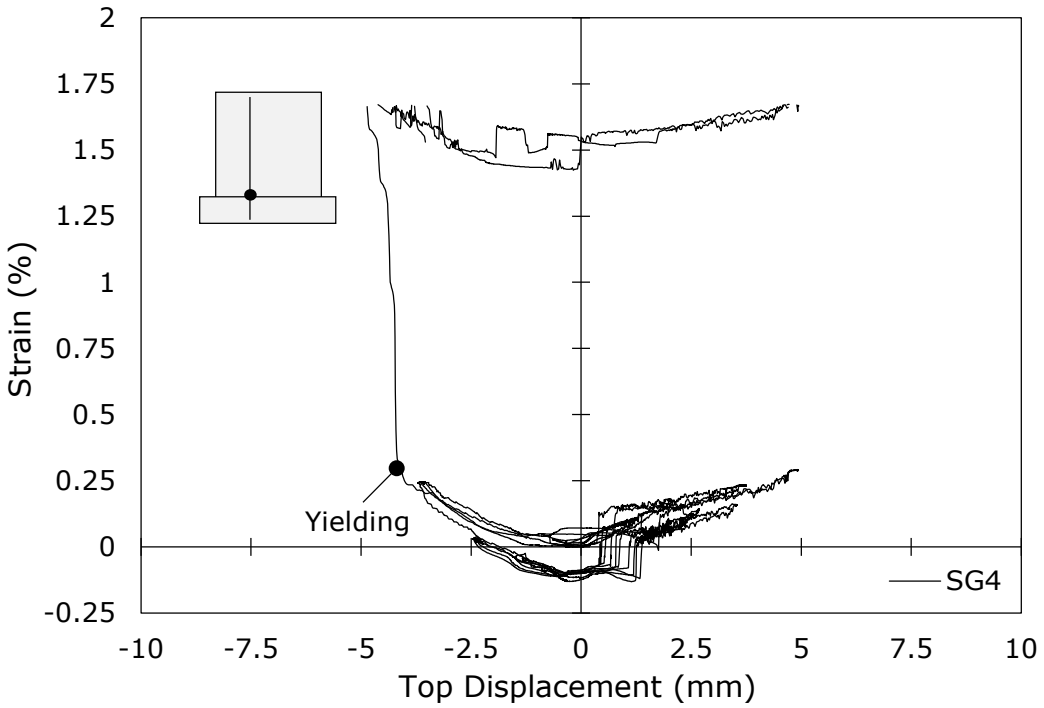


Figure B-97 Strain response of longitudinal reinforcement, strain gauge 4 in SQ2S

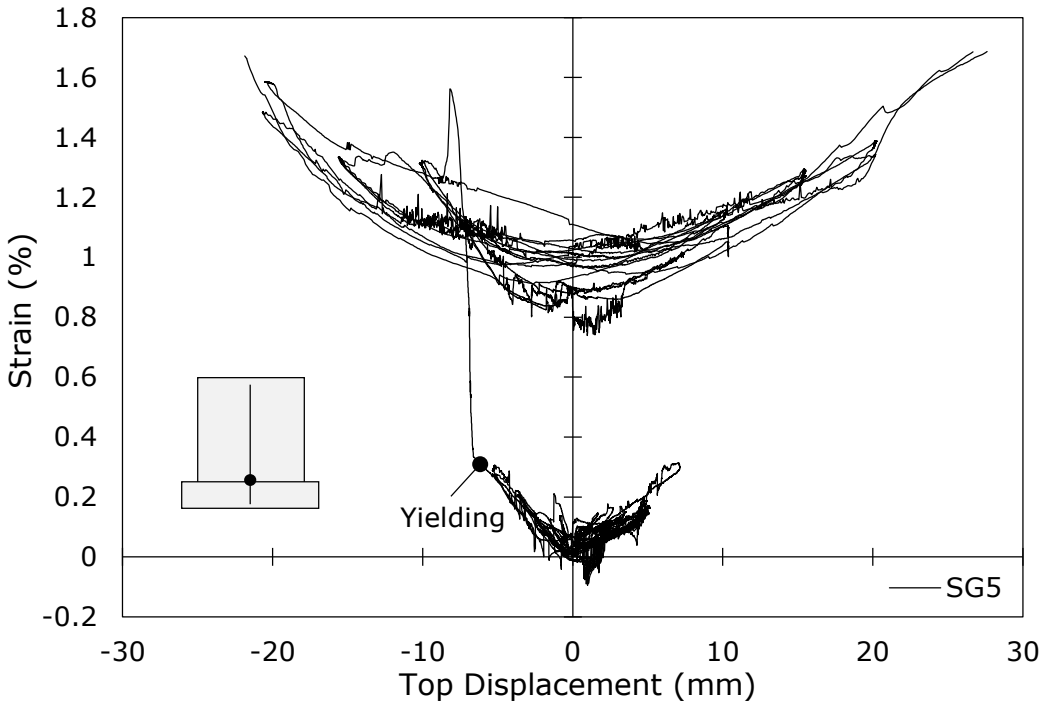


Figure B-98 Strain response of longitudinal reinforcement, strain gauge 5 in SQ2S

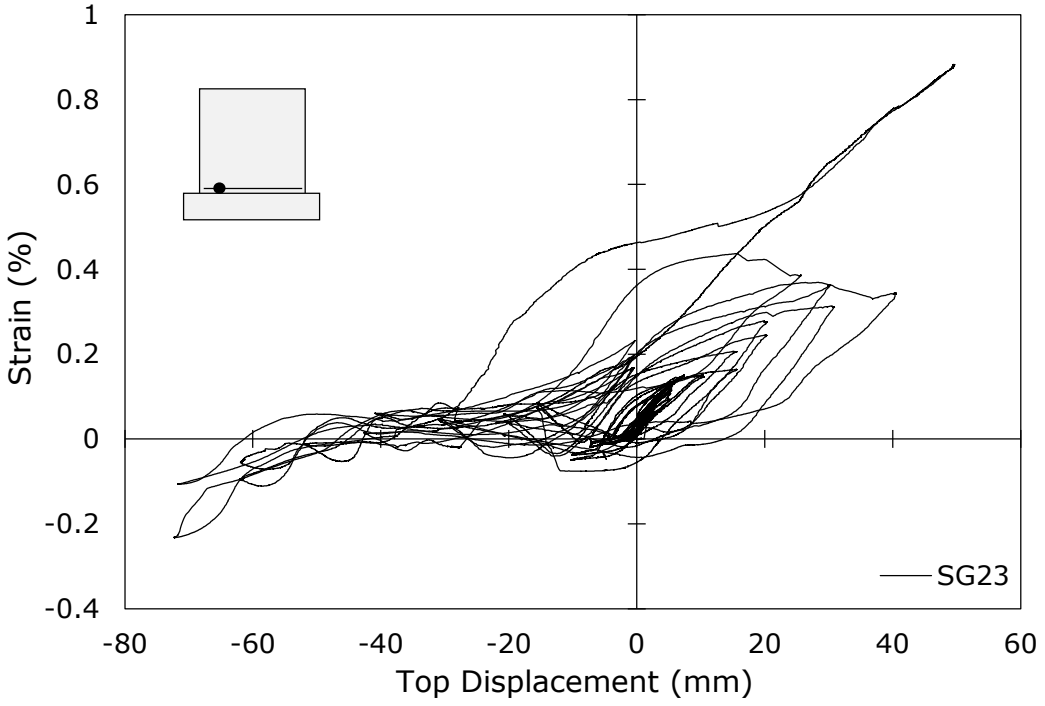


Figure B-99 Strain response of transverse reinforcement, strain gauge 23 in SQ2S

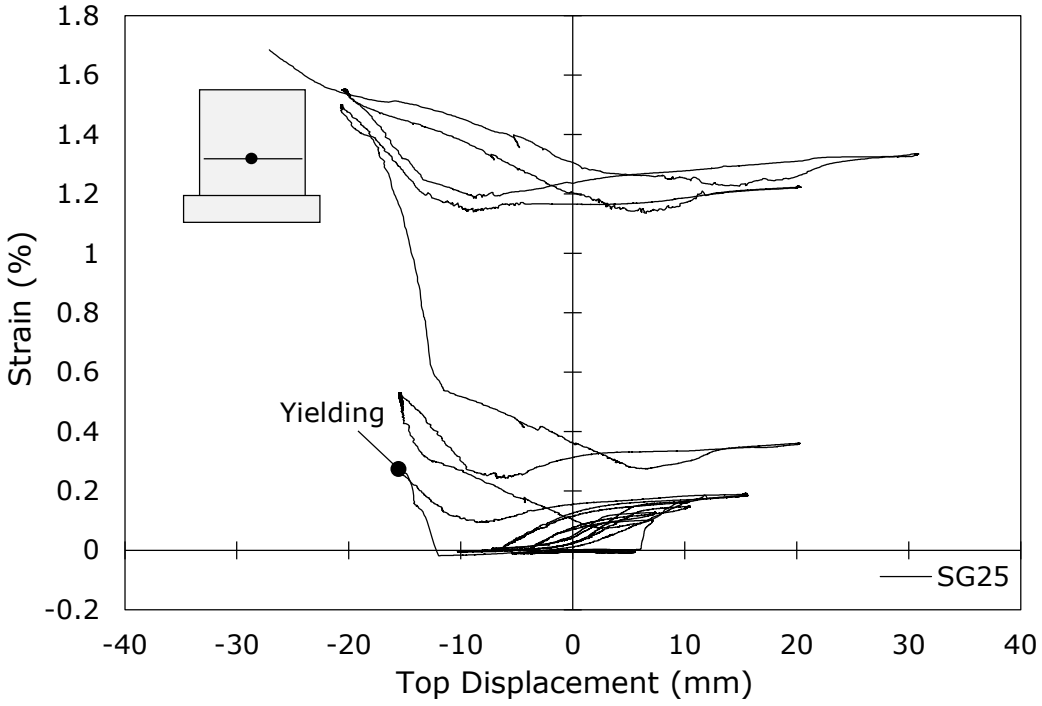


Figure B-100 Strain response of transverse reinforcement, strain gauge 25 in SQ2S

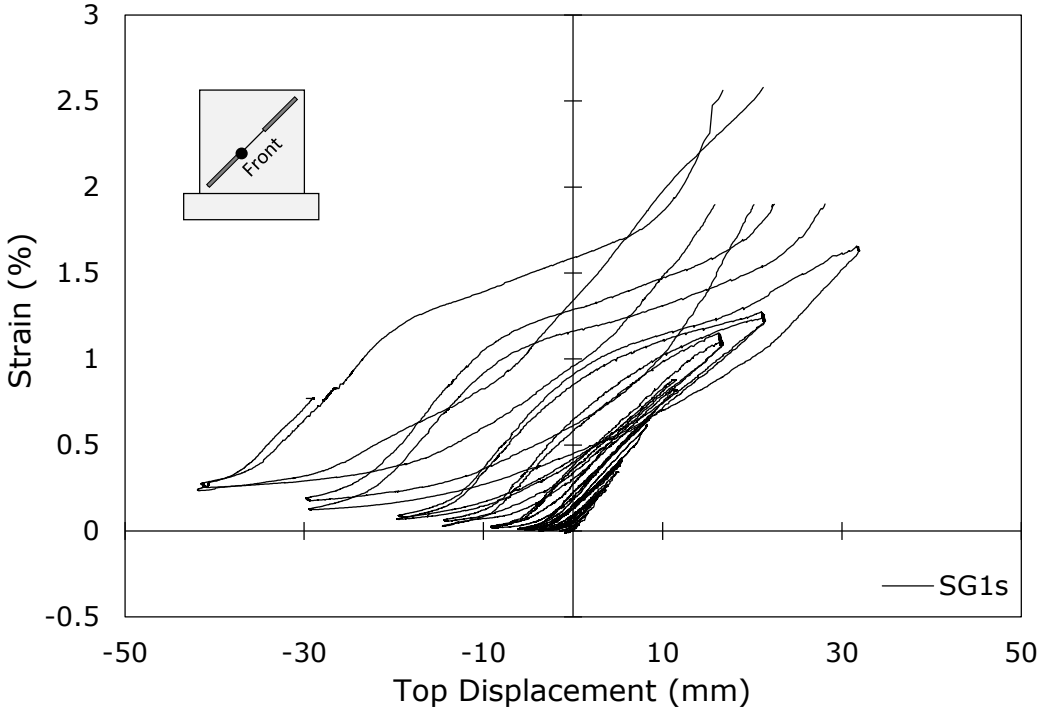


Figure B-101 Strain response of SMA link, strain gauge 1s in front brace in SQ2S

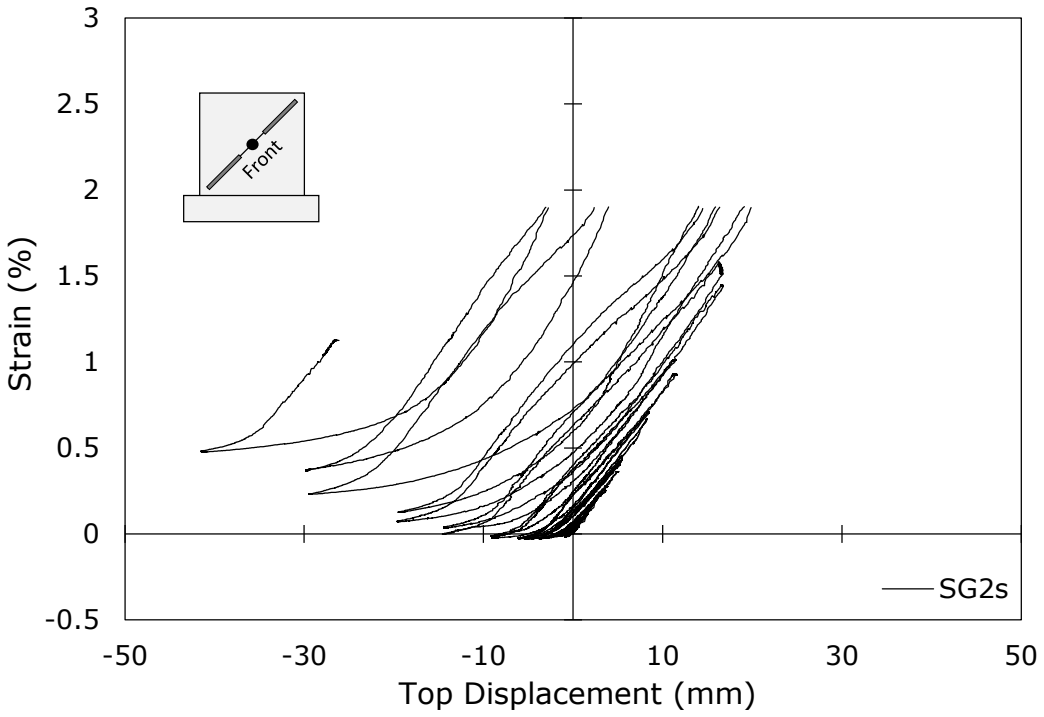


Figure B-102 Strain response of SMA link, strain gauge 2s in front brace in SQ2S

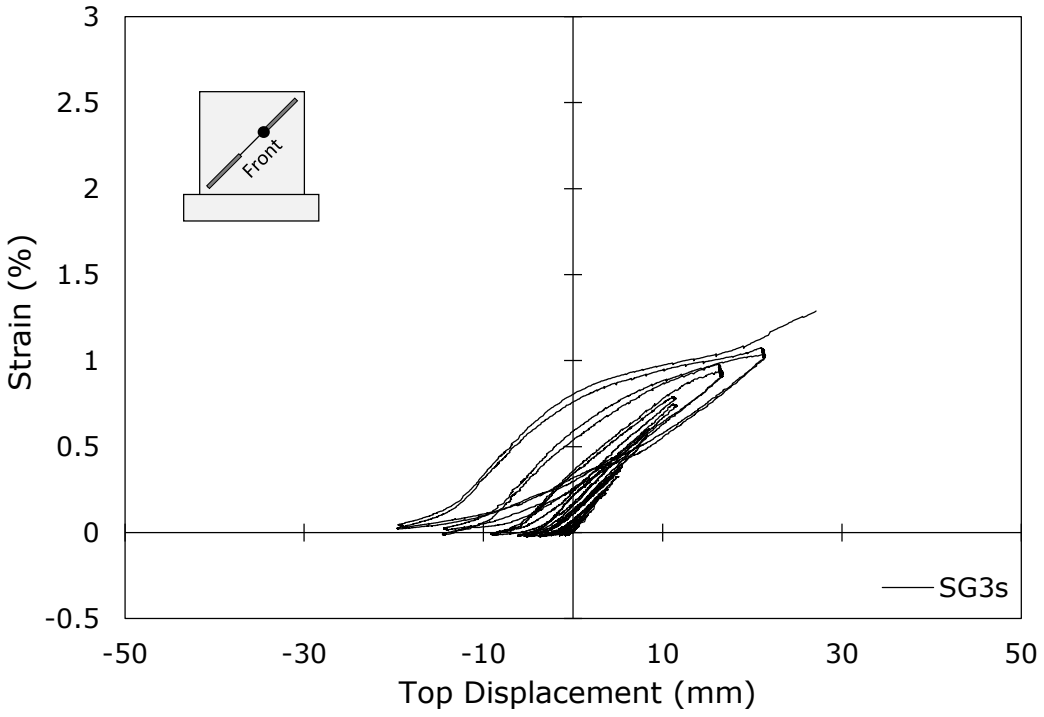


Figure B-103 Strain response of SMA link, strain gauge 3s in front brace in SQ2S

B.7 References

ASTM. (2011). *ASTM C496/C496M-11, Standard test method for splitting tensile strength of cylindrical concrete specimens*. ASTM International, West Conshohocken, PA, USA.

ASTM. (2014). *ASTM F2516-14, Standard test method for tension testing of nickel-titanium superelastic materials*. ASTM International, West Conshohocken, PA, USA.

ASTM. (2016a). *ASTM C39/C39M-16b, Standard test method for compressive strength of cylindrical concrete specimens*. ASTM International, West Conshohocken, PA, USA.

ASTM. (2016b). *ASTM A615/A615M-16, Standard specification for deformed and plain carbon-steel bars for concrete reinforcement*. ASTM International, West Conshohocken, PA, USA.

ATC. (2007). *FEMA 461 Interim testing protocols for determining the seismic performance characteristics of structural and nonstructural components*. Federal Emergency Management Agency, Washington D.C., USA.

SAES Smart Materials. (2012). "Memry a SAES Getter Company, Nitinol." *Memry.com*, <http://www.memry.com/sites/default/files/documents/memry-capabilities-brochure.pdf>.

Appendix C

Modelling of Shear Walls: Supplementary Material

C.1 Modelling of Prototype Walls

The prototype walls were modelled with the nonlinear finite element program VecTor2 (Wong et al. 2013) to assess the retrofitting scheme with SMA braces. The original wall was modelled with three reinforced concrete zones: zone 1 for the web, zone 2 for the slabs, and zone three for the foundation (Figure C-1).

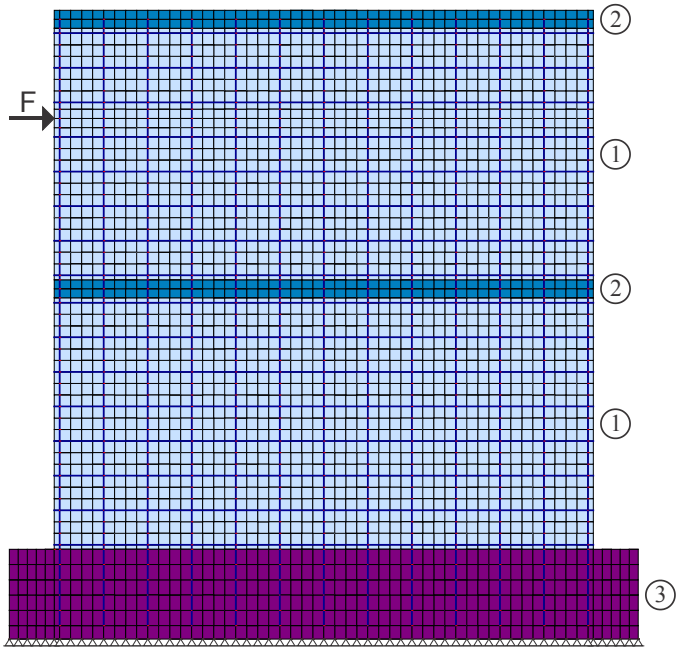


Figure C-1 Finite element model of original wall

The longitudinal and transverse reinforcement in the original wall were modelled with truss elements. Bond-link elements were used to connect the longitudinal reinforcement to the concrete elements. The transverse reinforcement was directly connected to the concrete elements.

The SMA-retrofitted wall was modelled based on the mesh used for the original wall. The SMA braces were modelled with single truss elements with length of 8040 mm (Figure C-2). The truss elements were connected to opposite corners at the base and top of the wall and were assigned an equivalent stress-strain relationship assuming that all deformation would be experienced by the SMA links.

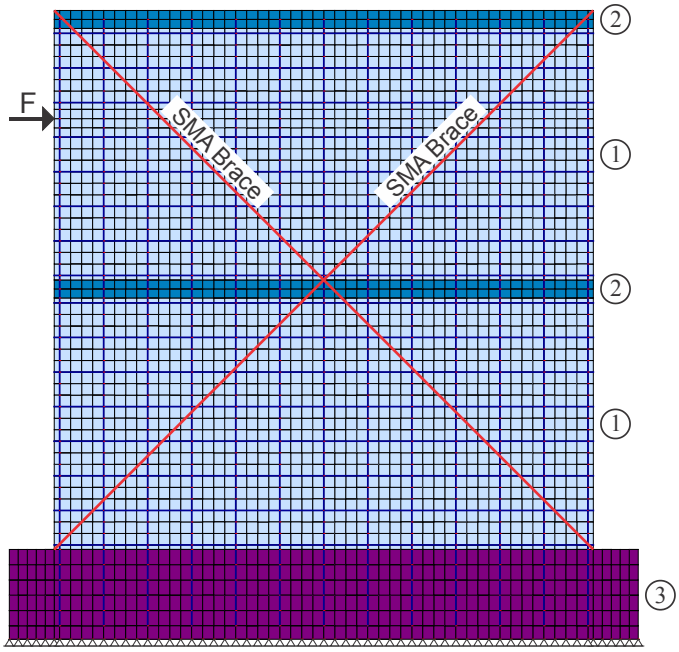


Figure C-2 Finite element model of SMA-retrofitted wall

The Popovics stress-strain relationship for normal strength concrete was employed to model the pre-peak and post-peak response of the concrete in the walls. The other constitutive models that were employed to capture salient features of the response included: Vecchio 1992-A model for compression softening, modified Bentz model for tension stiffening, and Palermo and Vecchio 2002 model for hysteretic behaviour. Steel reinforcement was modelled with a stress-strain relationship defined by an linear-elastic phase, a yield plateau, and a curvilinear strain hardening. The

hysteretic response of the steel was modelled with the Seckin model, which accounts for the Bauschinger effect. Modelling of the SMA braces followed a constitutive model for SMA reinforcement (Figure 5-6) developed by Abdulridha et al. (2013).

Axial loads were distributed along the top row of finite elements corresponding to the top slab, while the lateral seismic load (lateral displacement) was assigned to the nodes located at 4900 mm in height with respect to the base of the wall. The location of the lateral loading corresponded to the shear span, which was calculated based on the overturning moment and the base shear force determined from the equivalent static force procedure. The lateral loading followed a reverse cyclic protocol with two repetitions at each displacement level, which was incremented by a factor of 1.4. The simulation initiated with a cycle to 0.5 mm displacement.

C.2 Calculated Response

Figure C-3 and Figure C-4 illustrate the lateral load-displacement responses of the original and retrofitted walls. The numerical analysis of the original wall predicted peak lateral strength of 1124 kN at a corresponding lateral top displacement of 39 mm (Figure C-3). Concentrated damage along the base of the wall resulted in rocking behaviour (Figure C-5(a)) and rupture of the vertical reinforcement near the edges of the walls at 57 mm of lateral displacement. This failure mechanism is consistent with observations during testing of lightly reinforced squat reinforced concrete shear walls (Taghdi et al. 2000). At ultimate, the residual lateral displacement was approximately 38 mm. The wall retrofitted with the SMA bracing sustained an ultimate strength of 1760 kN at 54 mm (Figure C-4), which represented an increase in strength of approximately 57%. The predicted failure mechanism involved rocking of the shear wall with subsequent rupture of the vertical reinforcement (Figure C-5(b)), similar to that calculated for the original wall. At ultimate, the retrofitted wall experienced a residual lateral displacement of 6 mm, representing approximately 16% of the residual displacement of the original wall.

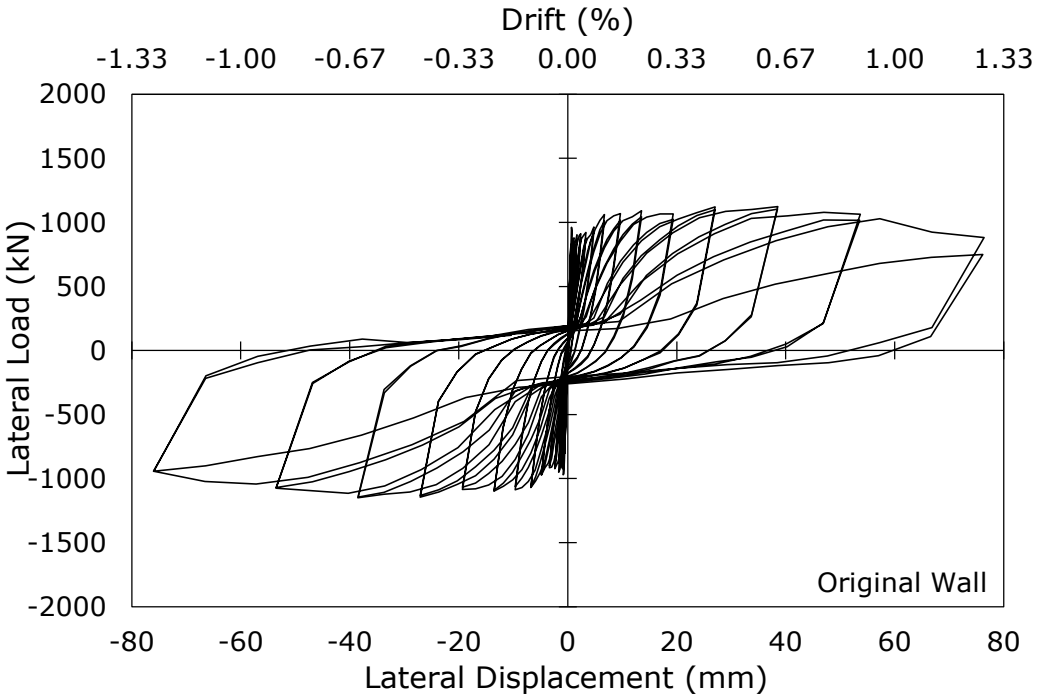


Figure C-3 Predicted response of original wall

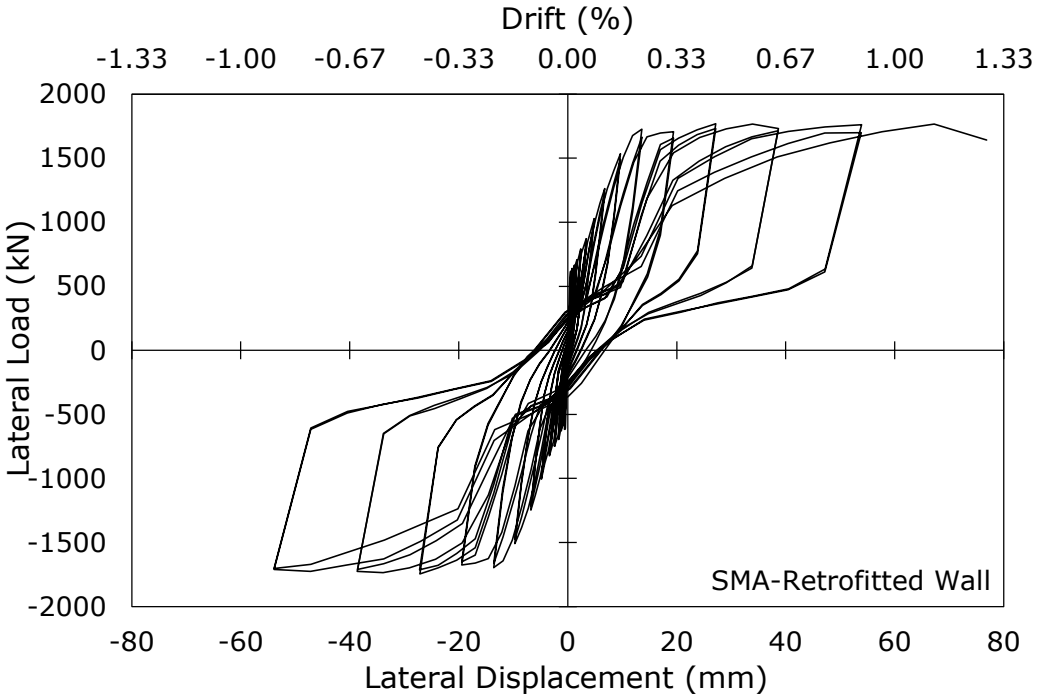
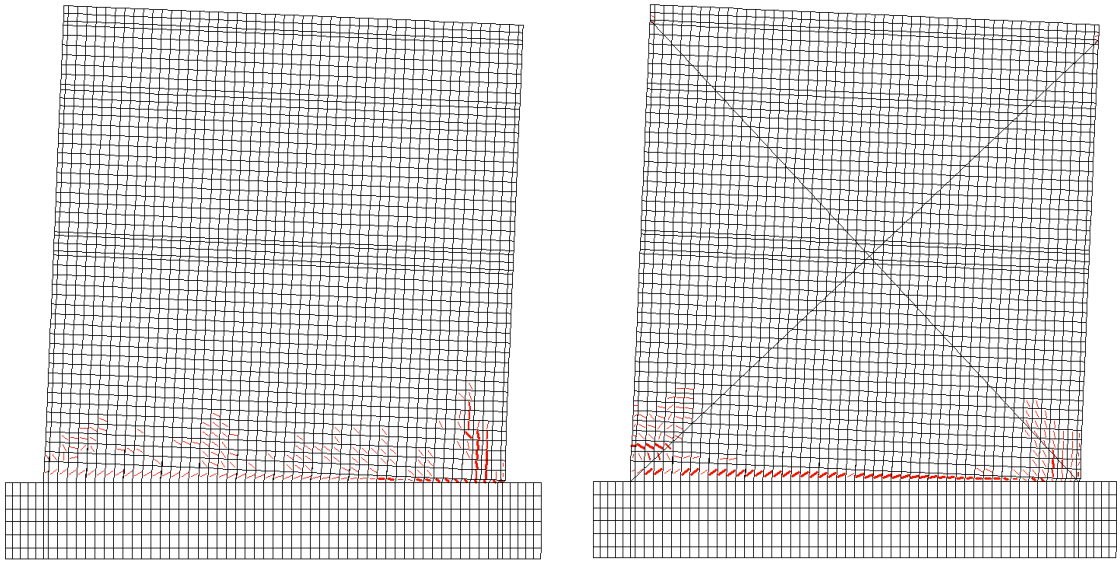


Figure C-4 Predicted response of SMA-retrofitted wall



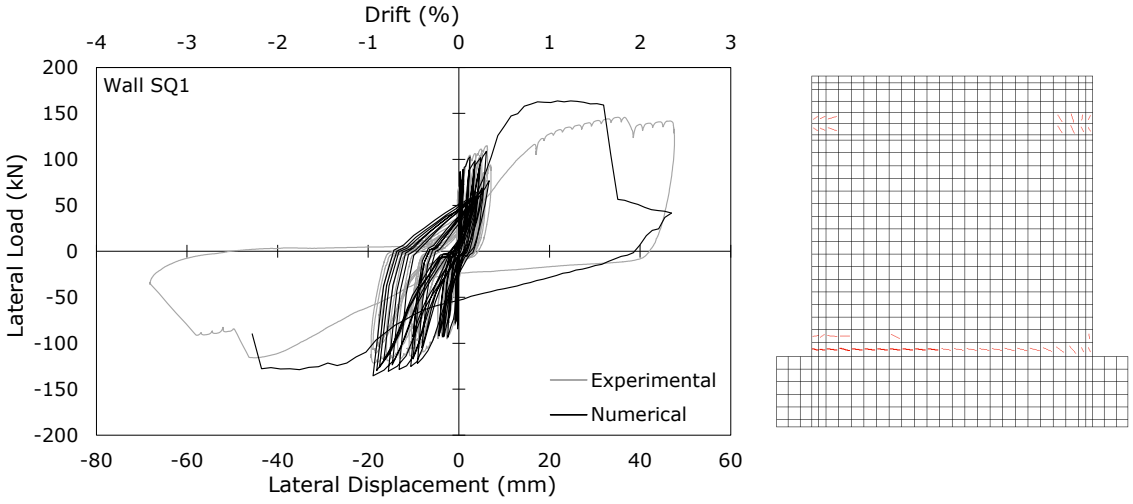
(a) (b)

Figure C-5 Predicted damage of walls: (a) original wall; and (b) SMA-retrofitted wall

C.3 Numerical Analysis of Third-Scale Walls

C.3.1 Sensitivity Study

C.3.1.1 Medium Mesh



(a) (b)

Figure C-6 Response of Wall SQ1, medium mesh: (a) lateral load-displacement response; and (b) damage at 1.5% drift

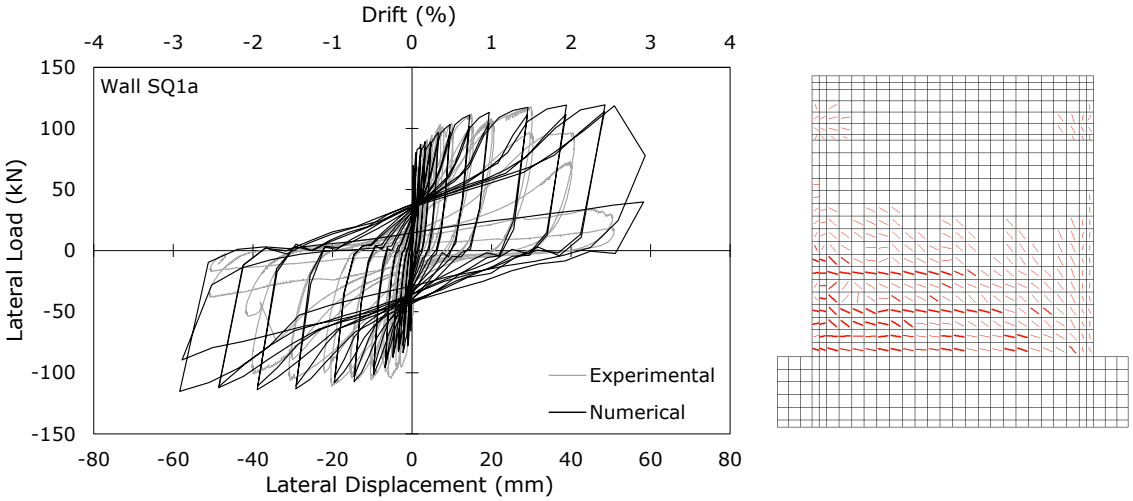


Figure C-7 Response of Wall SQ1a, medium mesh: (a) lateral load-displacement response; and (b) damage at 2% drift

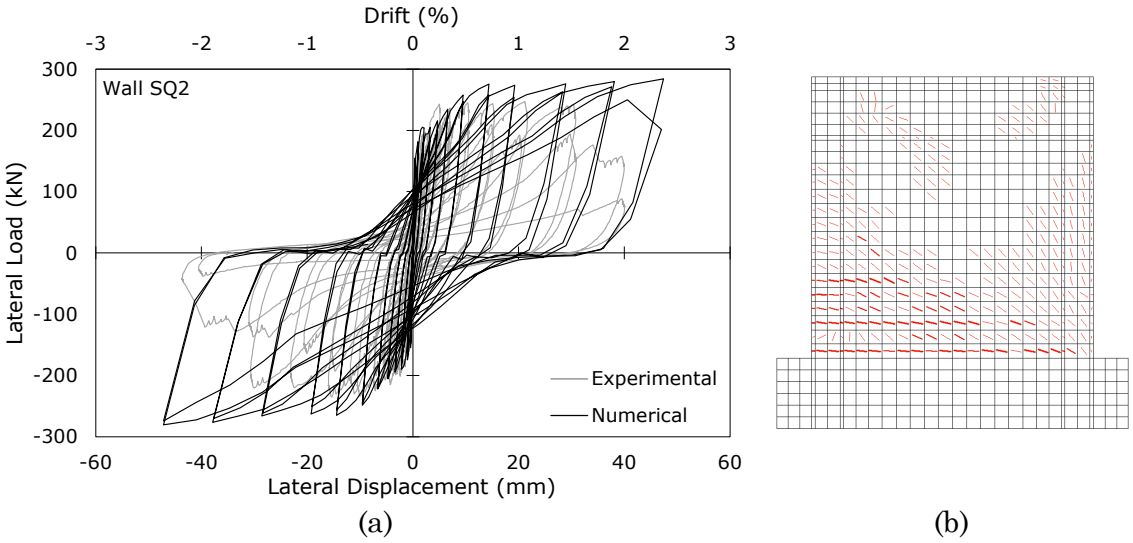


Figure C-8 Response of Wall SQ2, medium mesh: (a) lateral load-displacement response; and (b) damage at 1.5% drift

C.3.1.2 Coarse Mesh

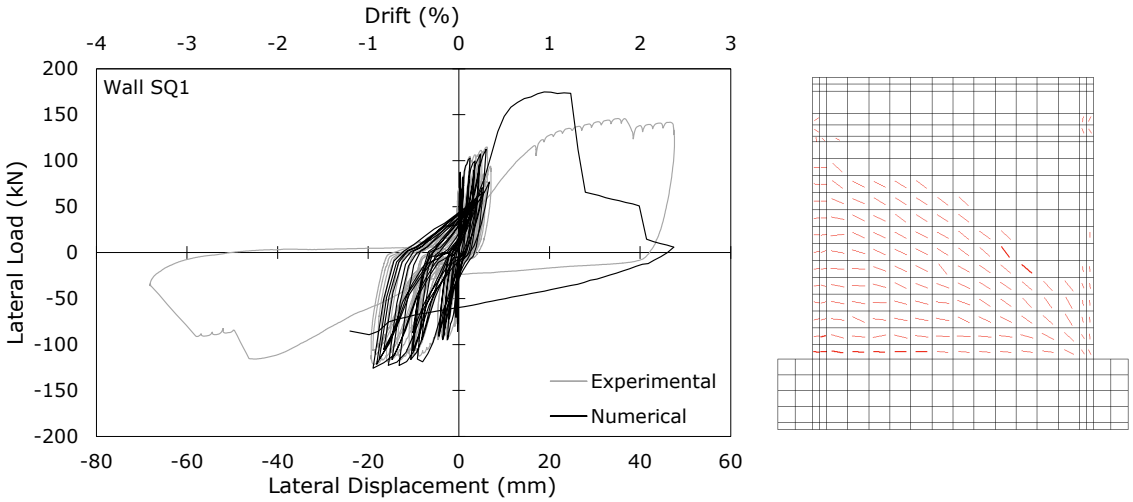


Figure C-9 Response of Wall SQ1, coarse mesh: (a) lateral load-displacement response; and (b) damage at 1.25% drift

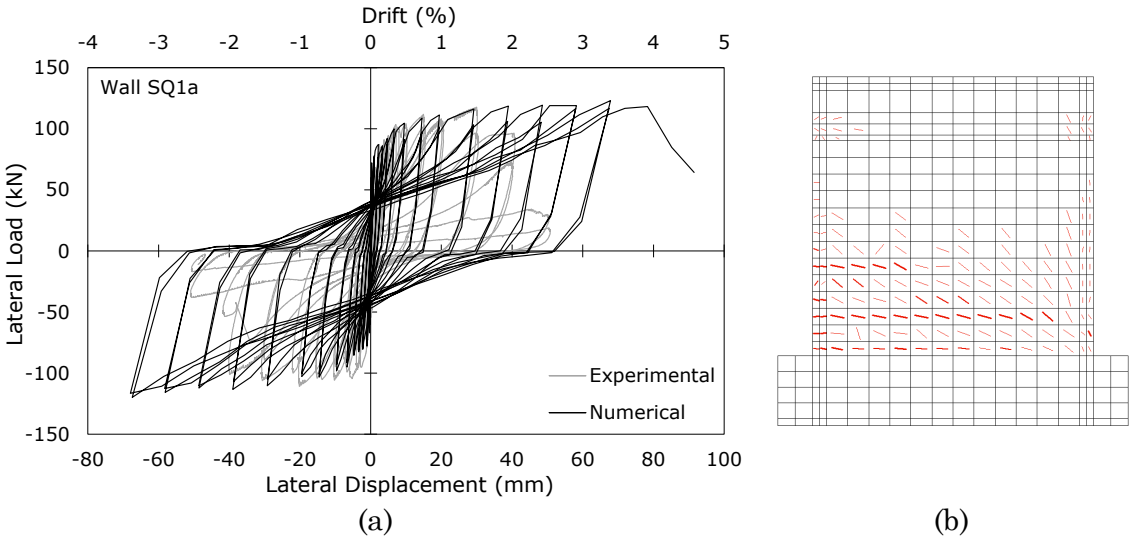


Figure C-10 Response of Wall SQ1a, coarse mesh: (a) lateral load-displacement response; and (b) damage at 2% drift

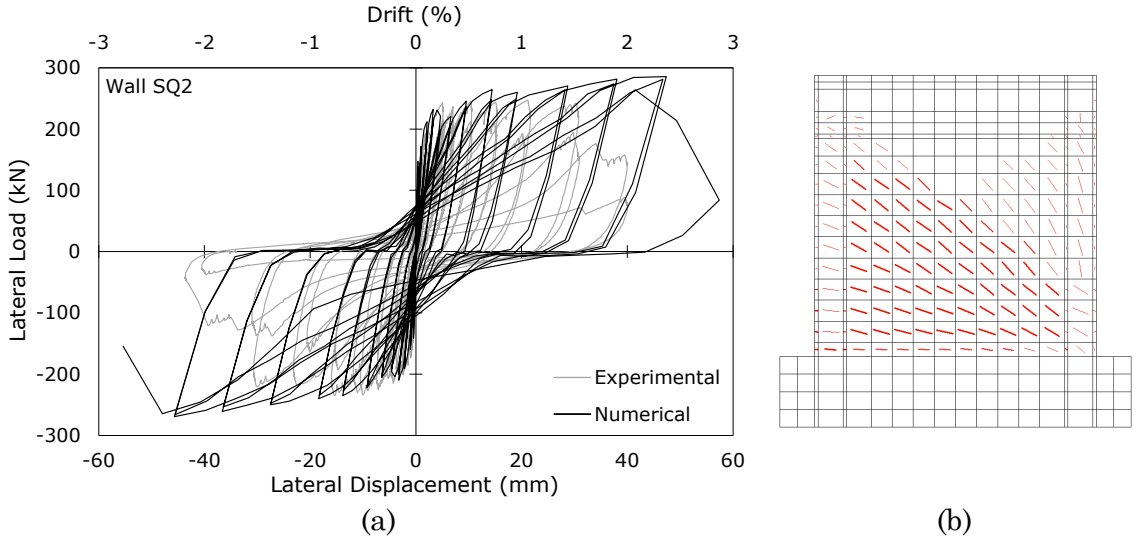


Figure C-11 Response of Wall SQ2, coarse mesh: (a) lateral load-displacement response; and (b) damage at 1.5% drift

C.3.2 Parametric Study

C.3.2.1 Effect of Axial Load, P

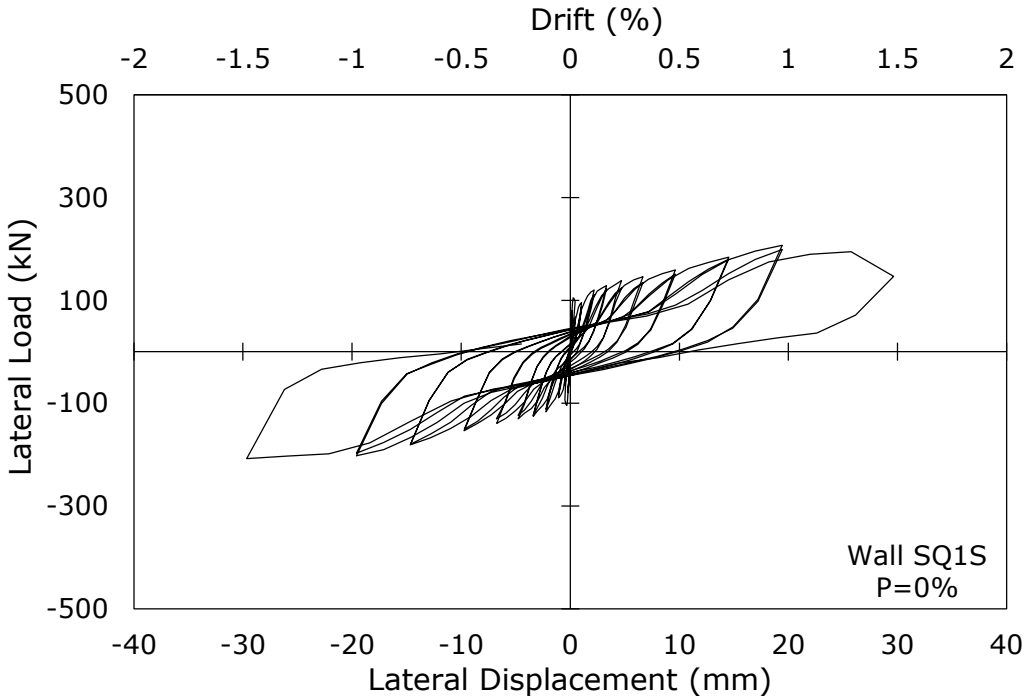


Figure C-12 Lateral load-displacement response of SQ1S, 0% axial load

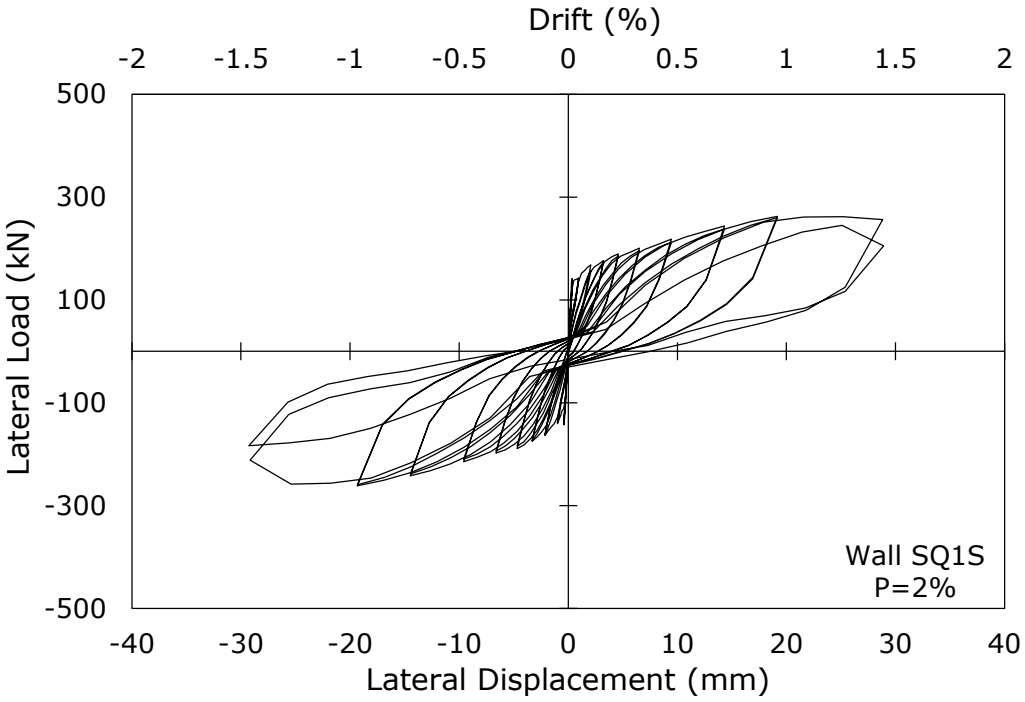


Figure C-13 Lateral load-displacement response of SQ1S, 2% axial load

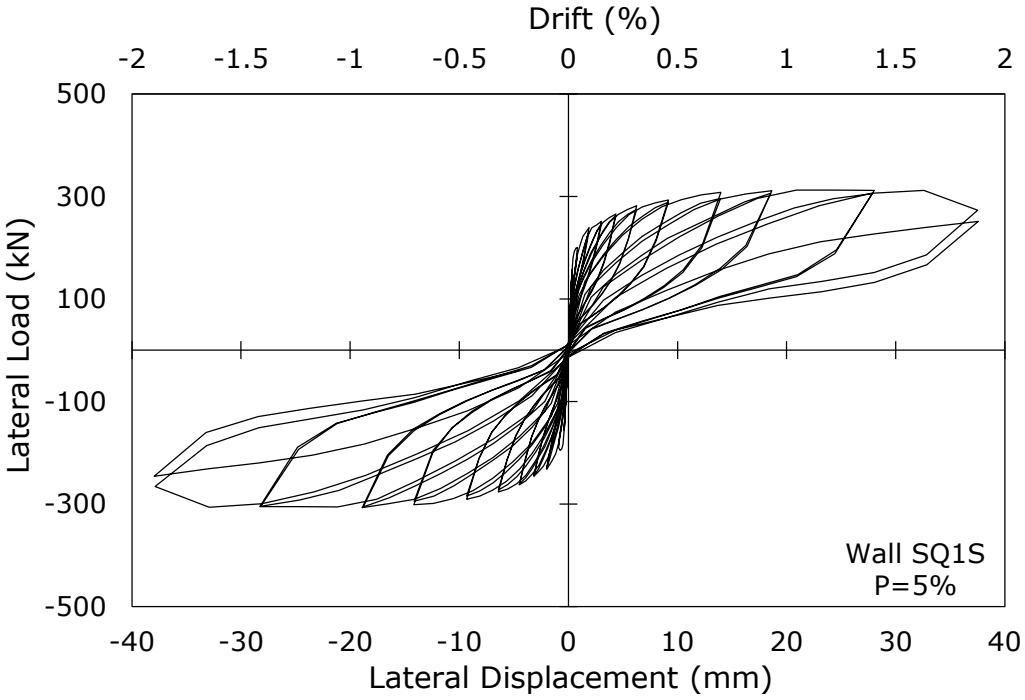


Figure C-14 Lateral load-displacement response of SQ1S, 5% axial load

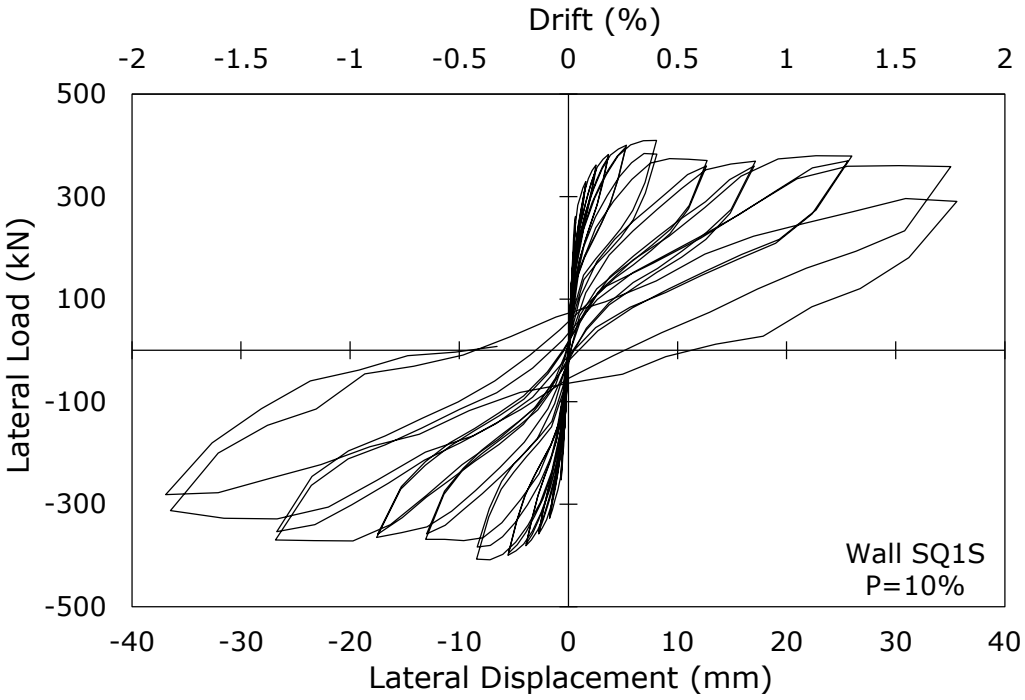


Figure C-15 Lateral load-displacement response of SQ1S, 10% axial load

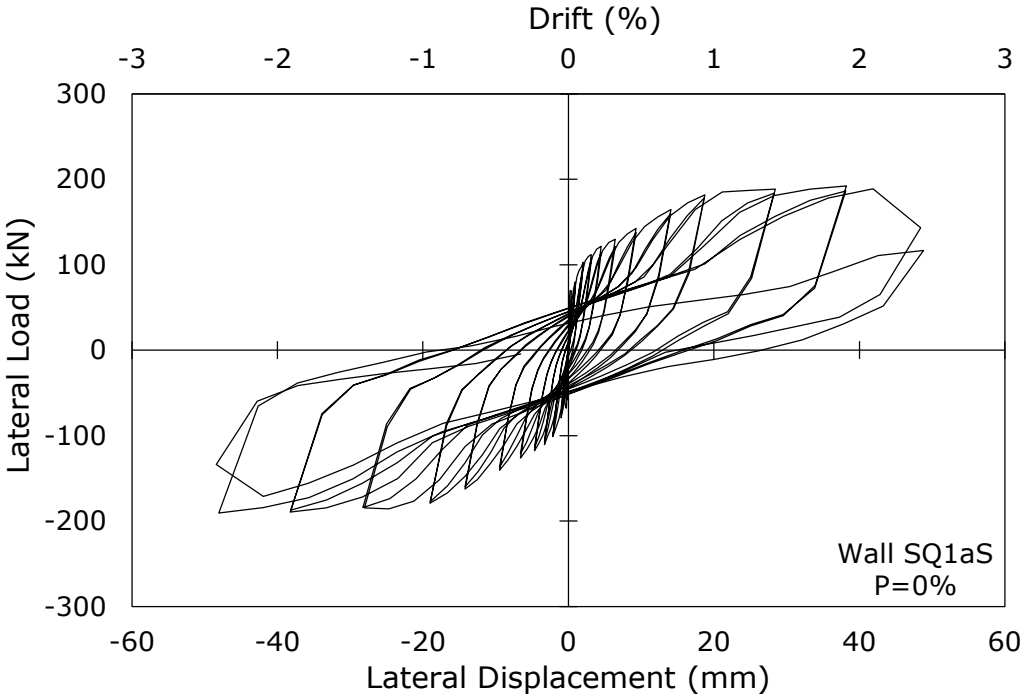


Figure C-16 Lateral load-displacement response of SQ1aS, 0% axial load

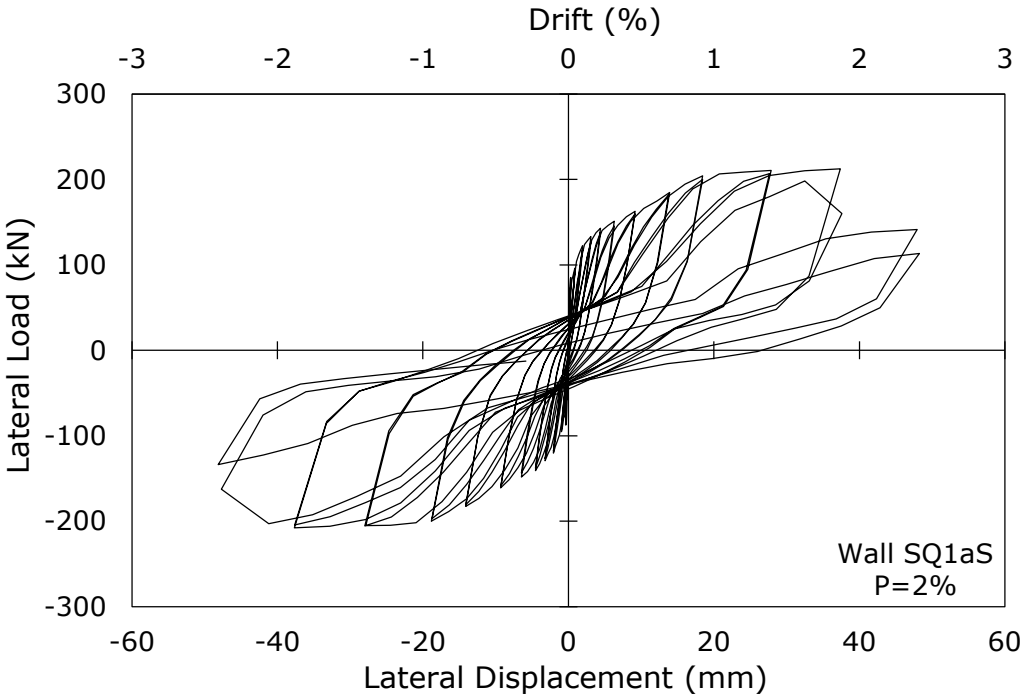


Figure C-17 Lateral load-displacement response of SQ1aS, 2% axial load

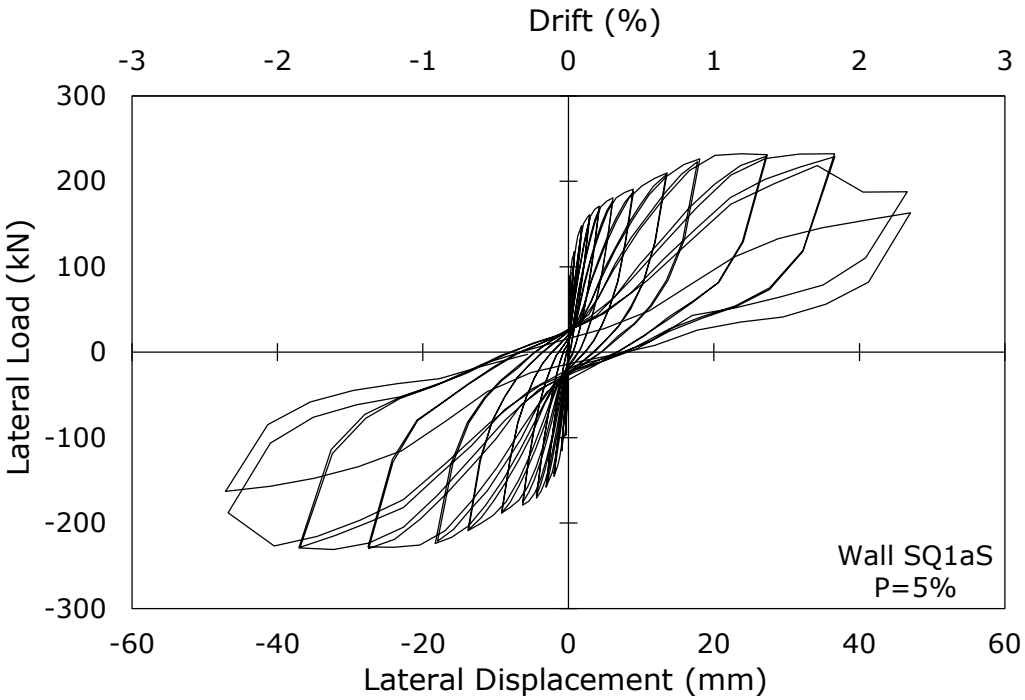


Figure C-18 Lateral load-displacement response of SQ1aS, 5% axial load

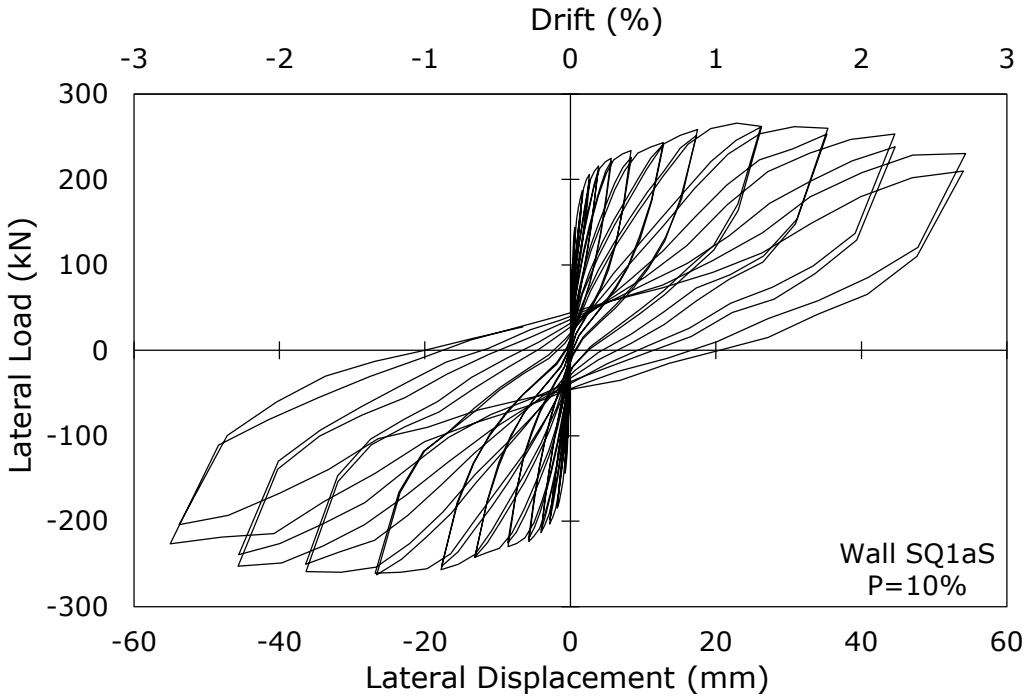


Figure C-19 Lateral load-displacement response of SQ1aS, 10% axial load

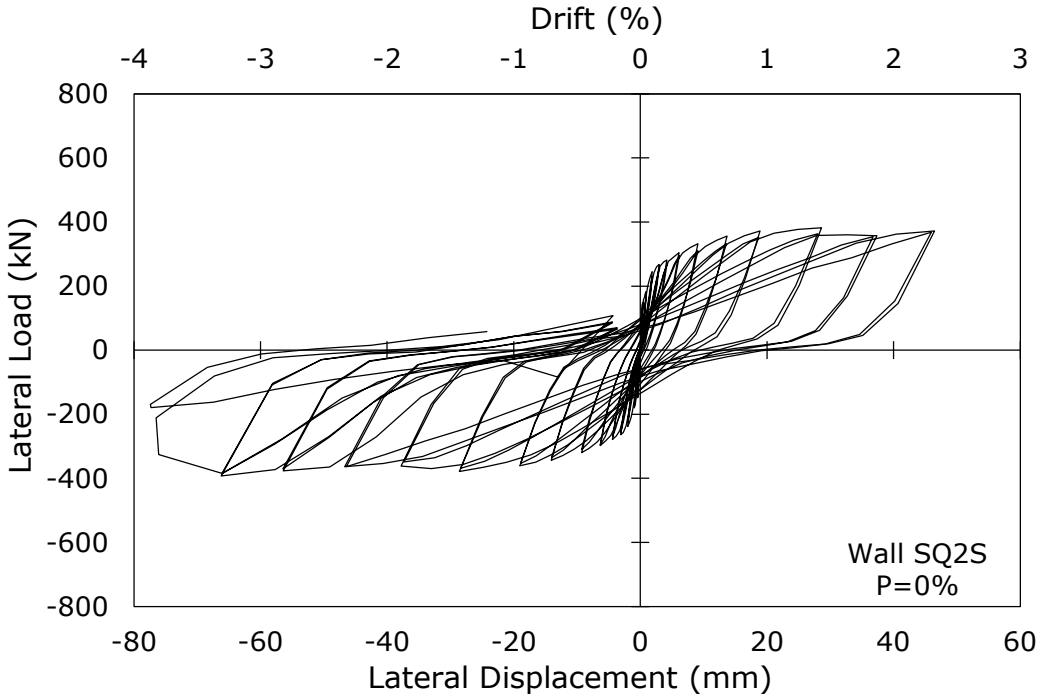


Figure C-20 Lateral load-displacement response of SQ2S, 0% axial load

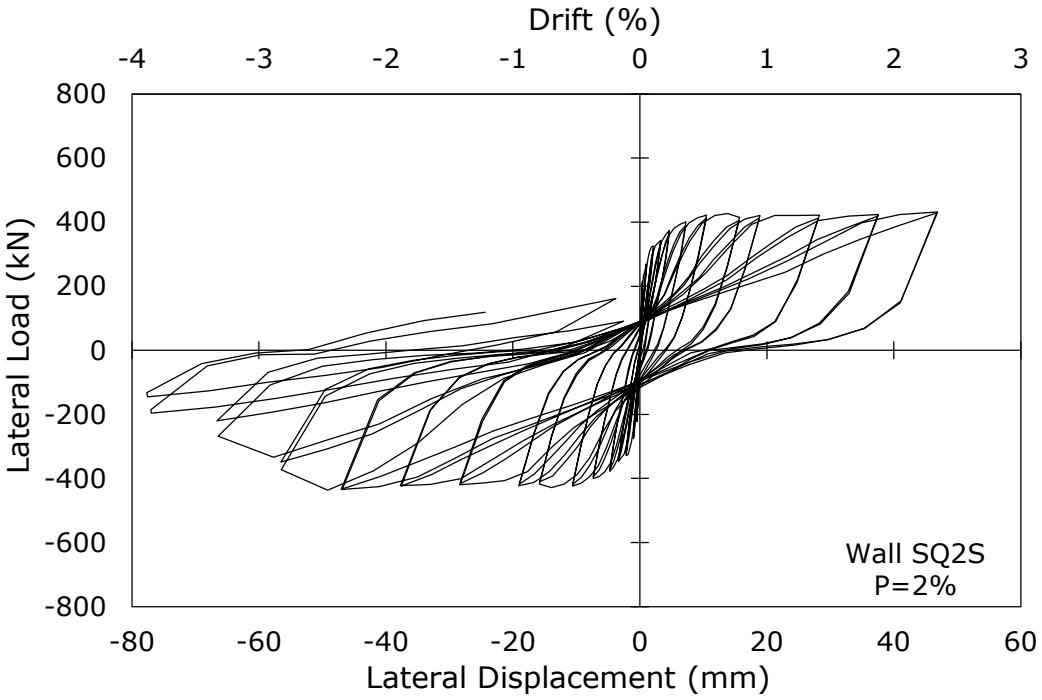


Figure C-21 Lateral load-displacement response of SQ2S, 2% axial load

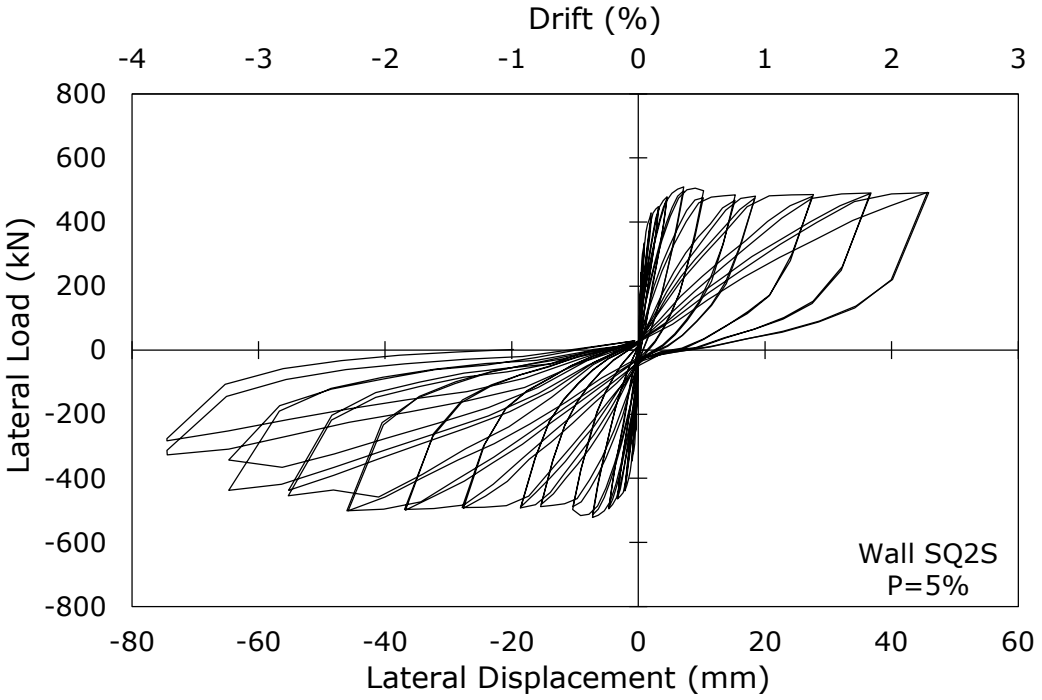


Figure C-22 Lateral load-displacement response of SQ2S, 5% axial load

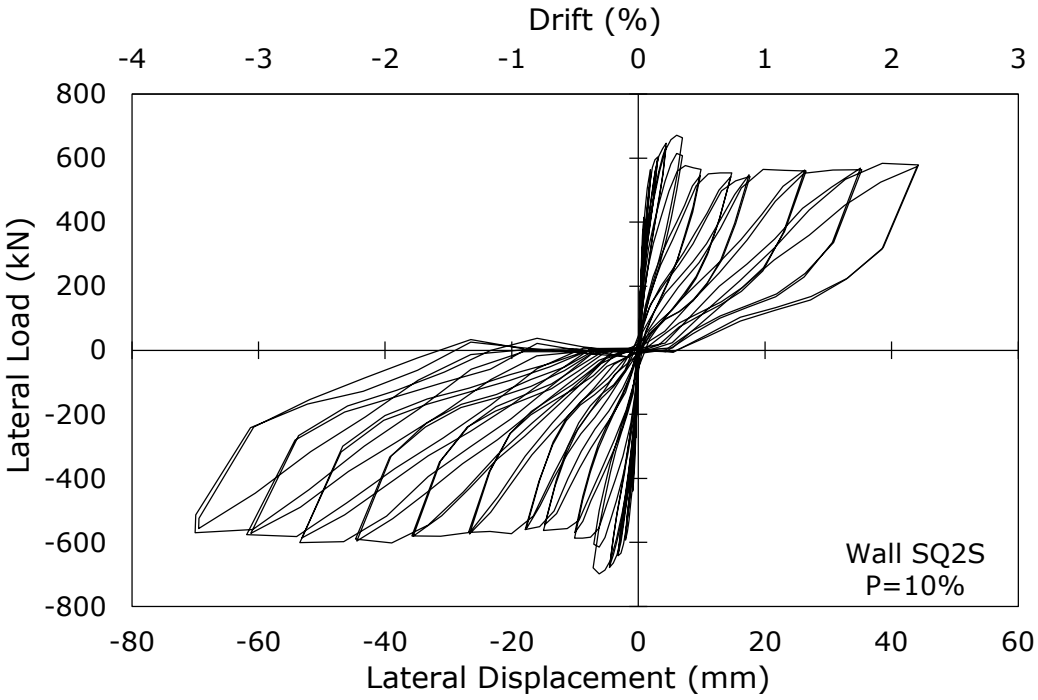


Figure C-23 Lateral load-displacement response of SQ2S, 10% axial load

C.3.2.2 Effect of Size of SMA Links, ϕ

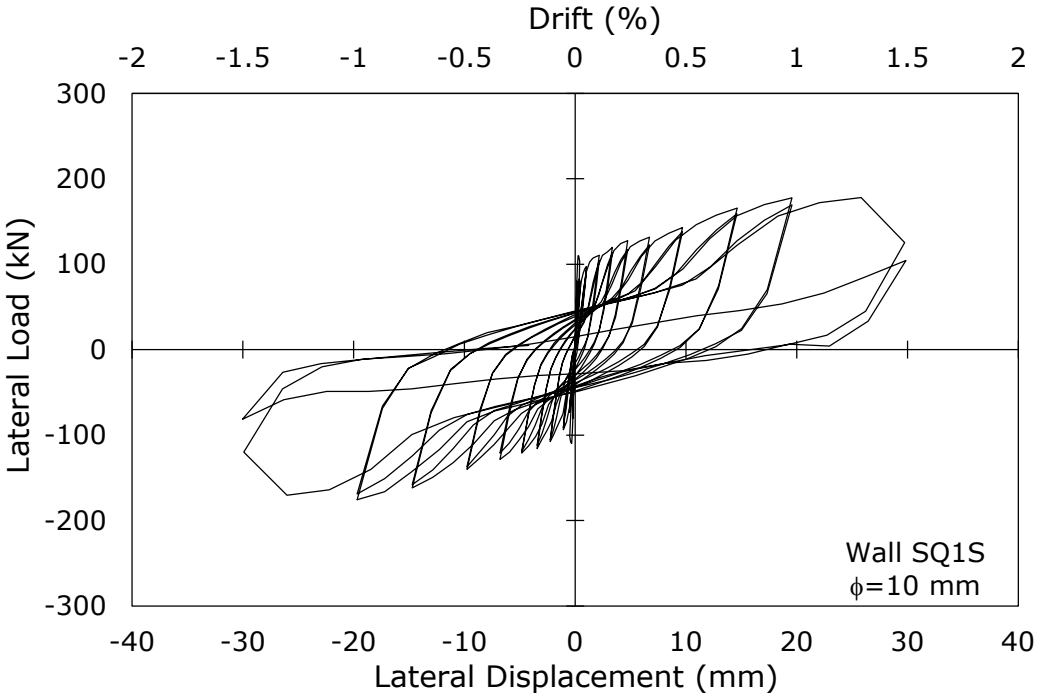


Figure C-24 Lateral load-displacement response of SQ1S, 10-mm SMA link

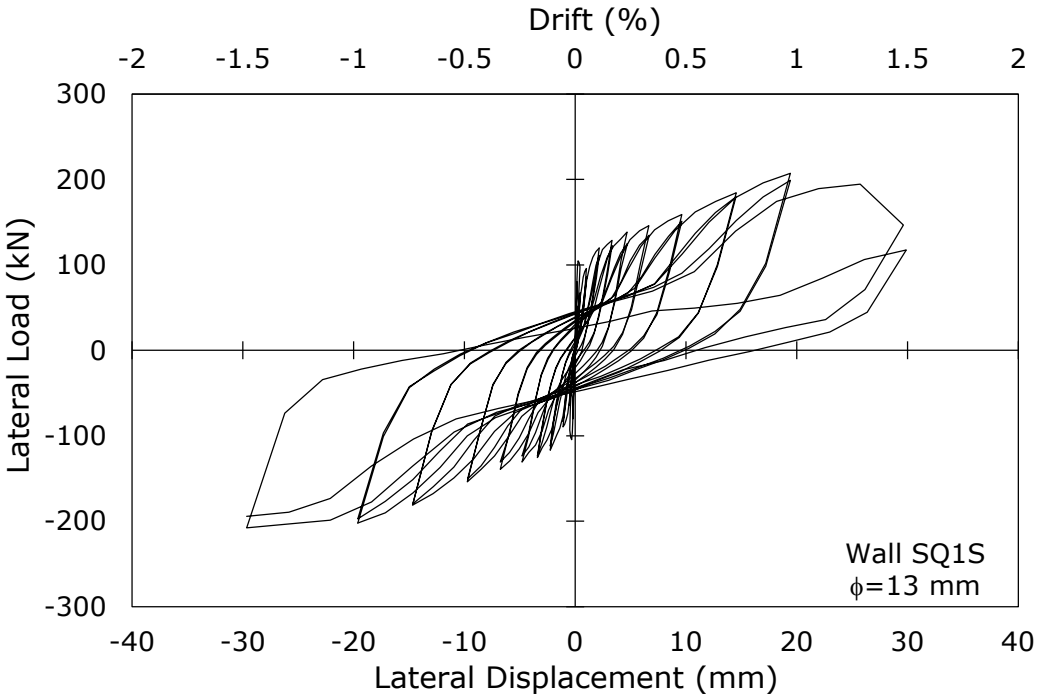


Figure C-25 Lateral load-displacement response of SQ1S, 13-mm SMA Link

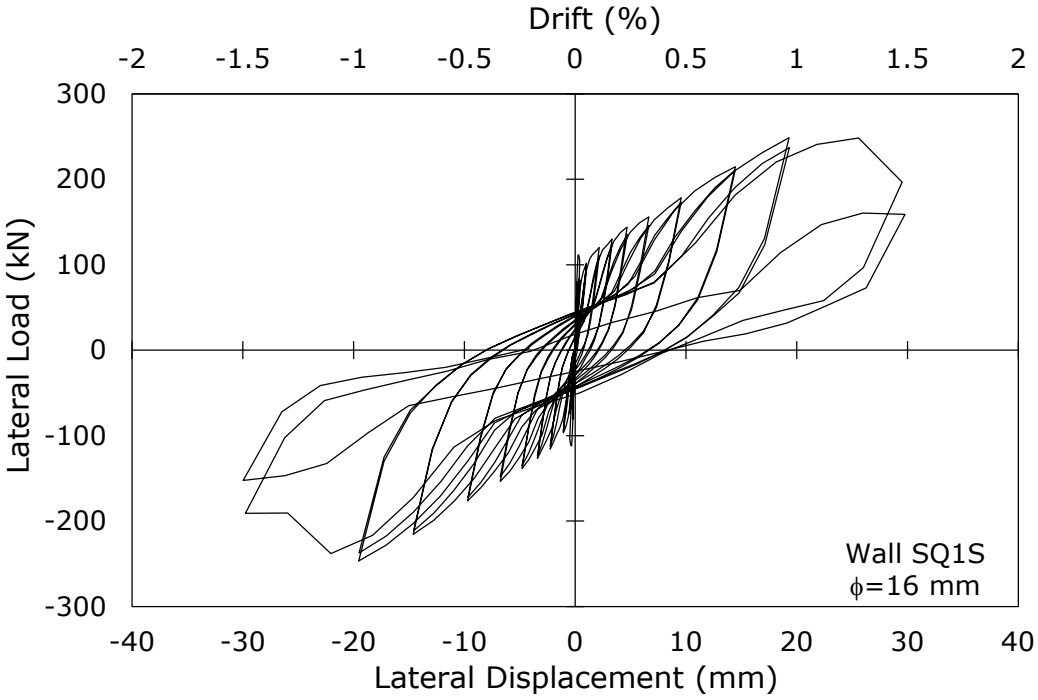


Figure C-26 Lateral load-displacement response of SQ1S, 16-mm SMA Link

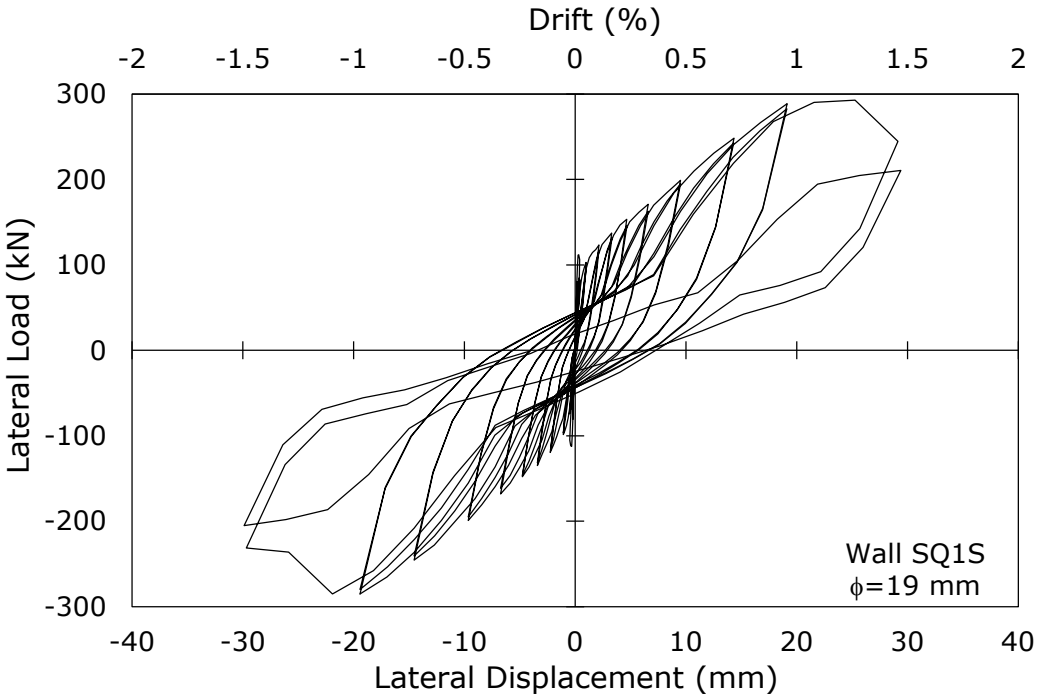


Figure C-27 Lateral load-displacement response of SQ1S, 19-mm SMA Link

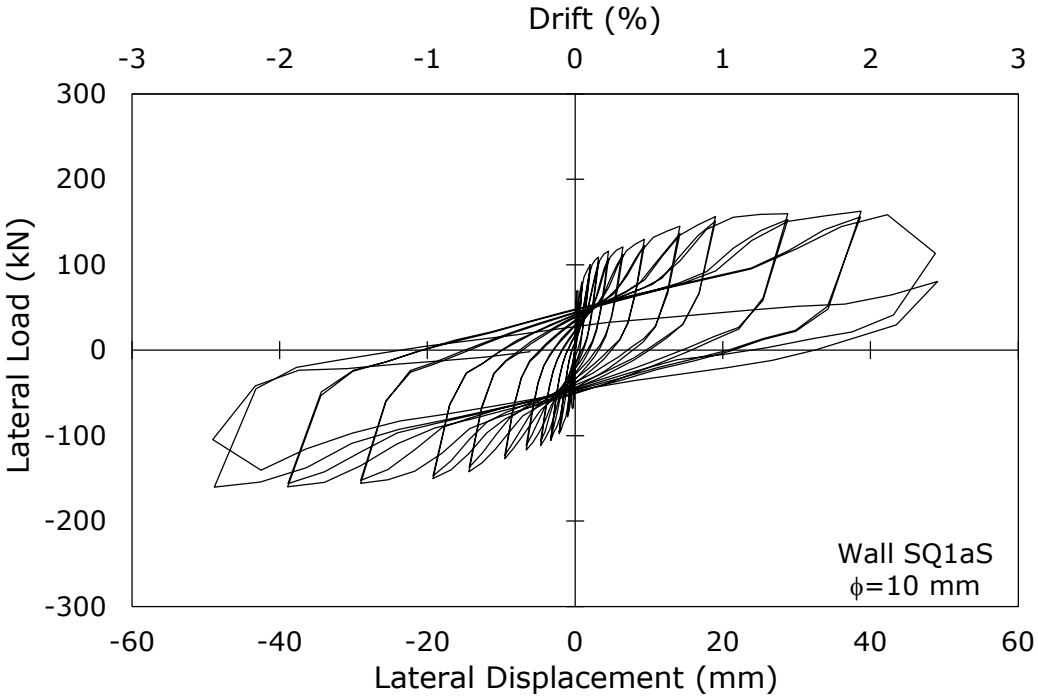


Figure C-28 Lateral load-displacement response of SQ1aS, 10-mm SMA Link

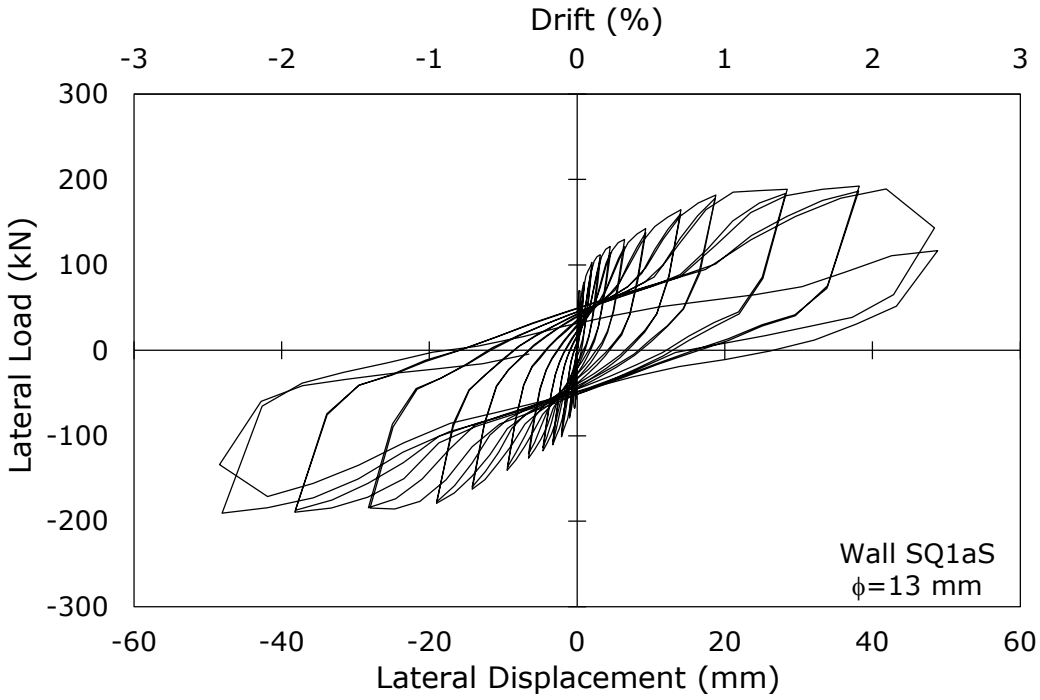


Figure C-29 Lateral load-displacement response of SQ1aS, 13-mm SMA Link

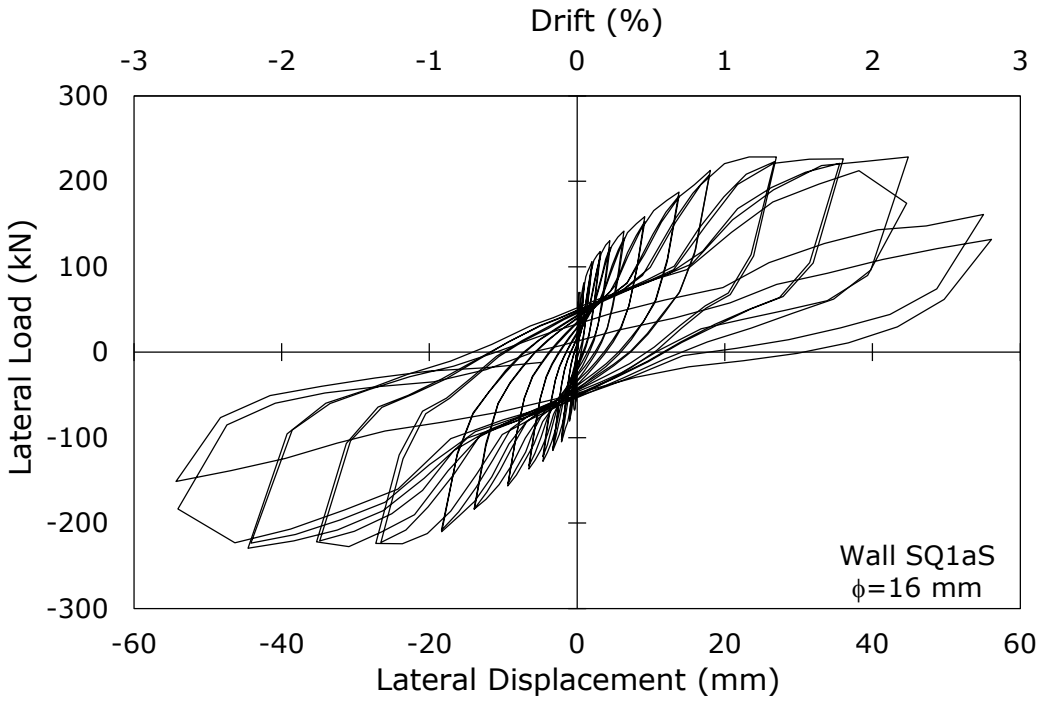


Figure C-30 Lateral load-displacement response of SQ1aS, 16-mm SMA Link

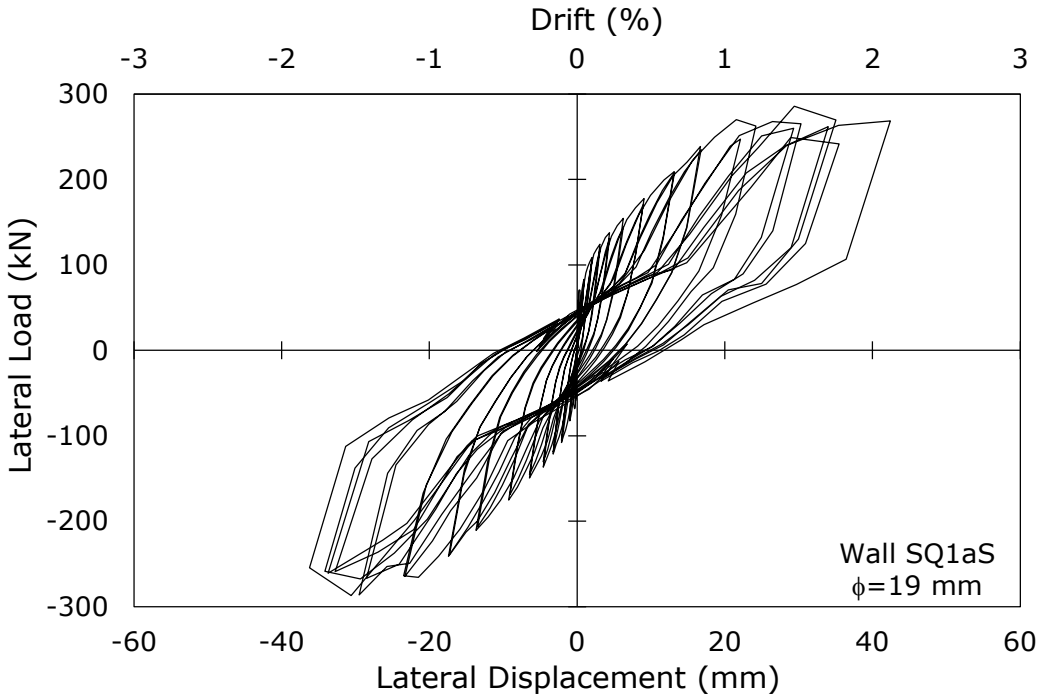


Figure C-31 Lateral load-displacement response of SQ1aS, 19-mm SMA Link

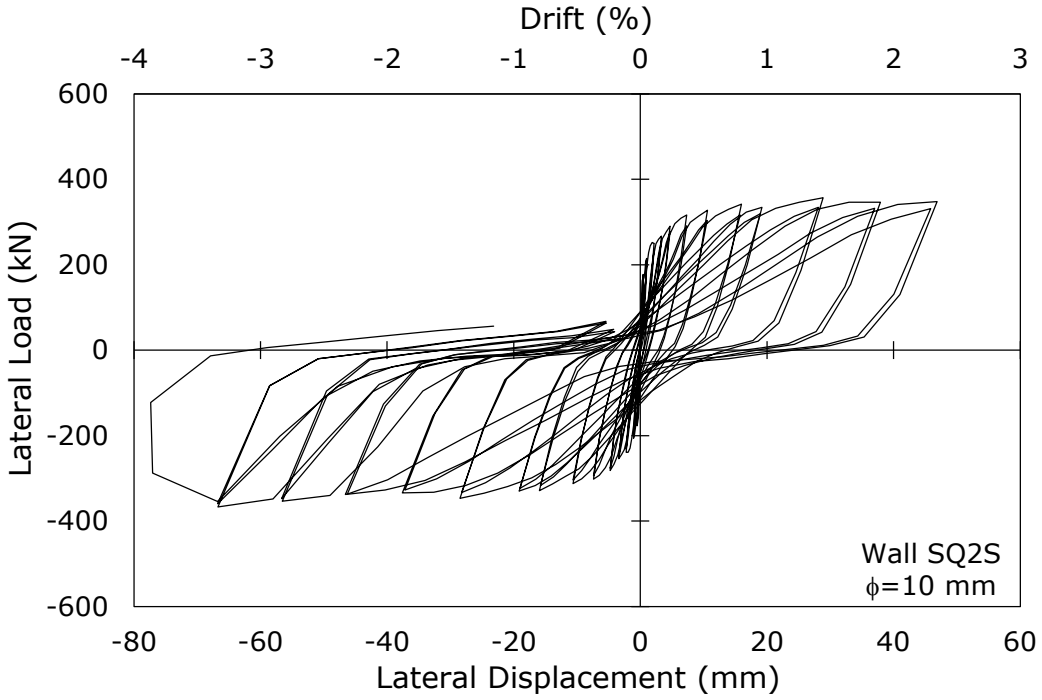


Figure C-32 Lateral load-displacement response of SQ2S, 10-mm SMA Link

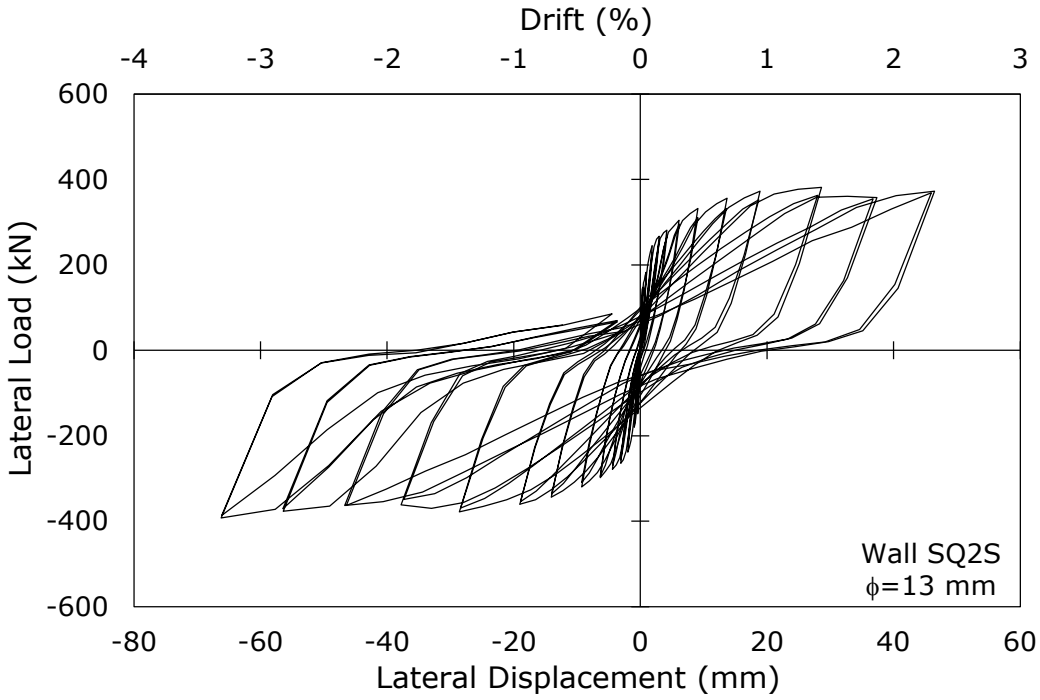


Figure C-33 Lateral load-displacement response of SQ2S, 13-mm SMA Link

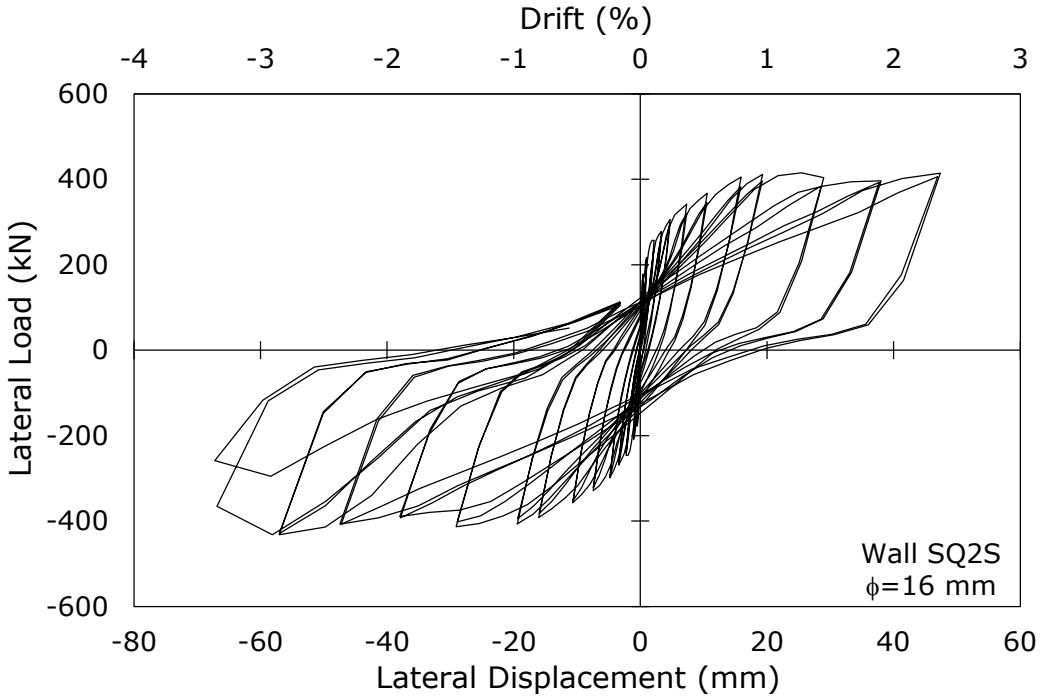


Figure C-34 Lateral load-displacement response of SQ2S, 16-mm SMA Link

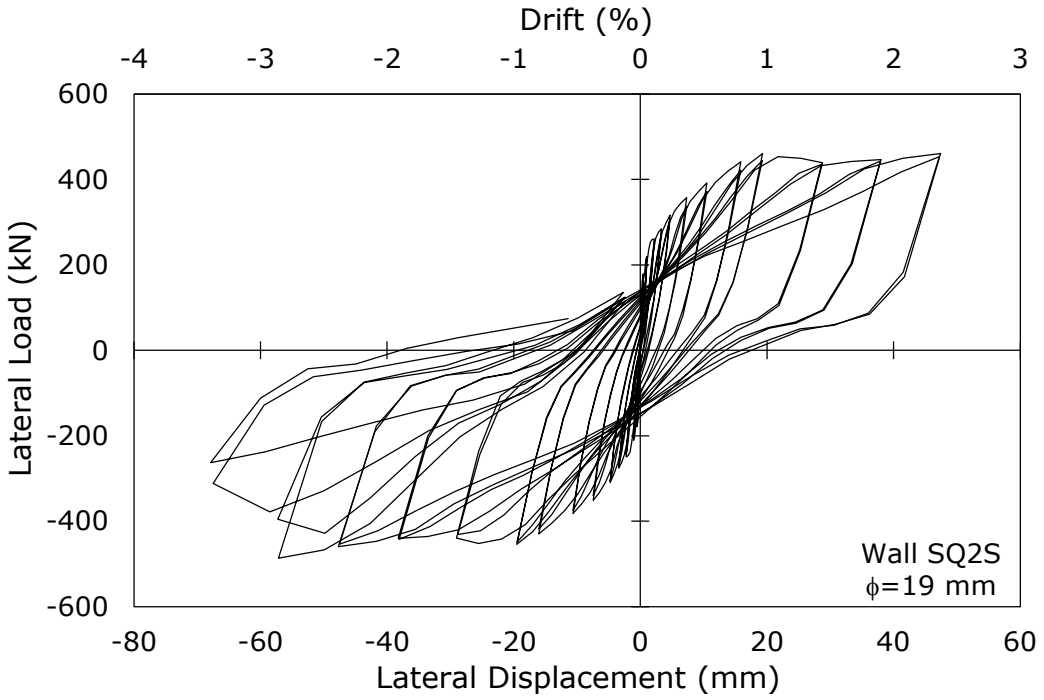


Figure C-35 Lateral load-displacement response of SQ2S, 19-mm SMA Link

C.4 References

Abdulridha, A., Palermo, D., Foo, S., and Vecchio, F. J. (2013). "Behavior and modeling of superelastic shape memory alloy reinforced concrete beams." *Engineering Structures*, 49, 893–904.

Taghdi, M., Bruneau, M., and Saatcioglu, M. (2000). "Seismic retrofitting of low-rise masonry and concrete walls using steel strips." *Journal of Structural Engineering*, 126(9), 1017–1025.

Wong, P. S., Vecchio, F. J., and Trommels, H. (2013). *VecTor2 and Formworks user's manual: second edition*. Manual, Department of Civil Engineering, University of Toronto, Toronto, ON, Canada.